UNIVERSITÀ
DEGLI STUDI
FIRENZE

DOTTORATO DI RICERCA
INTERNATIONAL DOCTORATE IN STRUCTURAL BIOLOGY

CICLO XXIX

COORDINATORE Prof. Claudio Luchinat

Design of chimeric proteins and metalloproteins for the creation of innovative bio-inspired material.

Settore Scientifico Disciplinare CHIM/03

Dottorando
Dott. Alexandra Louka

Tutore
Prof. Marco Fragai

Coordinatore
Prof. Claudio Luchinat

Novembre 2013 - 2016

This thesis has been approved by the University of Florence, the University of Frankfurt and the Utrecht University

Universiteit Utrecht

UNIVERSITÀ
DEGLI STUDI
FIRENZE

DOTTORATO DI RICERCA
INTERNATIONAL DOCTORATE IN STRUCTURAL BIOLOGY

CICLO XXIX

COORDINATORE Prof. Claudio Luchinat

Design of chimeric proteins and metalloproteins for the creation of innovative bio-inspired material.

Settore Scientifico Disciplinare CHIM/03

Dottorando
Dott. Alexandra Louka

Tutore
Prof. Marco Fragai

Coordinatore
Prof. Claudio Luchinat

Novembre 2013 - 2016

This thesis has been approved by the University of Florence, the University of Frankfurt and the Utrecht University

Universiteit Utrecht

CERM Firenze

FRANKFURT AM MAIN

dedicato al mio gatto....

TABLE OF CONTENTS

1. INTRODUCTION 1

1.1 Silica Biomineralization in Diatoms 4

1.2 Enzyme encapsulation in silica matrices: the catalyst choice 6

1.3 Hydroxyapatite 8

Statherin and Dentin matrix protein 1 (DMP1) 9

1.4 Recombinant proteins for biopharmaceuticals applications and drug discovery 10

1.4.1 L-Asparaginase: a biological drug 10

1.4.2. Matrix Metalloproteinases as potential drug targets 13

Collagenases and the elucidation of collagenolytic mechanism 17

Gelatinases 18

1.4.3. Carbonic Anhydrases as potential drug targets 20

1.5. AIMS OF THE PROJECT 23

2. MATERIALS AND METHODS 25

2.1. MOLECULAR CLONING 26

2.1.1 Polymerase Chain Reaction (PCR) 26

2.1.2 Digestion with restriction enzymes & Ligation 26

2.1.3. The choice of expression vector 27

2.1.4. Construction of the pET21a HABP expression vector 28

2.1.5. Cloning of recombinant proteins in the pET21aHABP expression vector and pET21aR5 expression vector 28

2.1.6. Cloning of MT1-MMP and Expression tests 29

2.2. PROTEIN EXPRESSION in *E.coli* 30

2.2.1. Benefits of expression in *E.coli* 30

2.2.2. Bacterial transformation 31

2.2.3. Small Scale Protein Expression 31

2.2.4. Large Scale Protein Expression 32

2.2.5. Laemmli Extraction Method 32

2.2.6. Electrophoresis 32

2.2.6.1. DNA agarose gel 32

2.2.6.2. SDS-PAGE 33

2.2.6.3 Native-page 33

2.3. CELL LYSIS 33

2.3.1. Sonication **33**
2.3.2. Freezing and grinding **34**
2.3.3. Osmotic shock **34**
2.4. PROTEIN PURIFICATION **34**
2.4.1. Metal ion affinity chromatography (IMAC) **34**
2.4.2. Ion-exchange Chromatography **35**
2.4.3. Gel filtration (GF) or Size exclusion chromatography (SEC) **35**
2.4.4. Determination of protein concentrations **36**
2.5. PROTEIN EXPRESSION AND PURIFICATION PROTOCOLS DEVELOPED IN THIS STUDY **36**
2.6. CATALYTIC ACTIVITY ASSAYS **42**
2.6.1. Asparaginase Activity assay **42**
2.6.2. MMPs Activity Assays **42**
2.7. CHARACTERIZATION OF OLIGOMERIZATION STATES **43**
2.7.1. Analytical Gel Filtration Chromatography **43**
2.7.2. Dynamic Light Scattering (DLS) **43**
2.8. PROTEIN CRYSTALIZATION AND X-RAY DIFFRACTION **44**
2.9. BIOMINERALIZATION REACTIONS **44**
2.9.1. Silicification reaction **44**
2.9.2. Biomineralization reaction for the formation of HA **45**
BIBLIOGRAPHY **46**
3. RESULTS **60**
3.1. Atomic-Level Quality Assessment of Enzymes Encapsulated in Bioinspired Silica. **61**
3.2. ^{1}H-detected solid-state NMR of proteins entrapped in bioinspired silica: a new tool for biomaterials characterization. **81**
3.3. A Divalent PAMAM-Based Matrix Metalloproteinase/Carbonic Anhydrase Inhibitor for the Treatment of Dry Eye Syndrome. **88**
3.4. Biomaterial-embedded asparaginase removes asparagine from serum: a route to treat childhood leukemia. **105**
4: CONCLUSIONS - PERSPECTIVES **137**

1. INTRODUCTION

Introduction

Biomineralization processes lead to complex solid structures of inorganic material in biological systems and they are constantly gaining attention in biotechnology and biomedical research. Two outstanding examples of biomineral morphogenesis are the formation of highly elaborate nano-patterned **silica shells by diatoms,** and the formation of **HydroxyApatite** (**HA**) **in hard tissues of vertebrates**. Among the organic macromolecules that have been closely linked to the tightly controlled precipitation of silica in diatoms, **silaffins** play an important role. These proteins typically occur as complex post-translationally modified variants and they are directly involved in the silica deposition process in diatoms. However, even in vitro silaffin-based peptides alone, with and without post-translational modifications, can efficiently mediate biomimetic silica precipitation, leading to silica material with different properties [(1-3)]. **Bone** is another important biomineral material composed of a mineral phase (70% w/w), an organic matrix (~25% w/w), and water (~ 5% w/w). The inorganic phase is mainly consisted by the HA, which is $\mathbf{Ca_5(PO_4)_3(OH)}$ [(4)]. Besides Ca^{2+}, the second major component of the HA is phosphate, which, during bone synthesis, originates from organic phosphate, such as poly- phosphates and β- glycerophosphate. During the past decades the biomineralization process has been widely studied both in vitro and in vivo, trying in this way to shed light upon this complicated mechanism because of its unique biocompatibility [(5)]. Innovative biomaterials inspired by nature can find applications in reconstructive and regenerative medicine, in order to successfully repair or replace hard tissue, or to prepare potential thermostable vaccines [(6)]. Through the last decade, different groups have developed an in situ forming scaffold sequence with a high, inherent propensity for calcium phosphate mineralization by conjugating a self-assembling peptide hydrogel and a combinatorially selected hydroxyapatite (HA) binding peptide (HABP) that regulates the calcium phosphate mineralization [(7)]. Among nucleating peptides, two types of representative nucleators; a phosphate chelating agent (N6p) [(8)] or calcium chelating agents (NWp and W6p) [(9,10)], were selected and genetically engineered on the surface of a virus in order to enhance its capacity to initiate CaP mineralization and thus create a potential thermostable vaccine [(6)].

An interesting application of the biomineralization process is the enzyme immobilization. Enzymes are inherently “green” catalysts that can perform complex chemical tasks under mild conditions in a fully aqueous environment (i.e., under physiological conditions). Enzymes are optimized by natural selection for energy efficiency, time efficiency, and atom economy. Furthermore, they can be prepared under benign biotechnological conditions and are fully biodegradable [(11)]. This makes enzymes the optimal candidates for “green chemistry” applications [(12–14)]. The improvement of immobilization techniques, nowadays, enables us to tackle some drawbacks of the enzymes as catalysts, such as low stability against organic solvents, temperature and pH, inhibition by high

concentration of substrates and products, difficult recovery from reaction mixture, etc [15,16]. Indeed, the introduction of immobilized biocatalysts has improved the performance and the cost-efficiency of industrial processes and finds a wide range of applications in scientific research, medical devices, and industrial processes [16–19].

The **major techniques for enzyme immobilization** include covalent binding, ionic and hydrophobic adsorption, aggregation, entrapment and encapsulation. However, many methods of immobilization and entrapment cause significant structural deformation of the enzyme, leading to reduction in activity. Significant optimization of the immobilization method is therefore often required, and factors such as stability might be sacrificed in favor of increased loading capacity [21, 22].

Among those immobilization techniques enzyme encapsulation and enzyme entrapment, are two distinct techniques widely used in scientific research and industrial processes. **Entrapment** is the confinement of an enzyme in a solid matrix while **encapsulation** refers to the formation of a physical barrier around the enzyme. Encapsulation within a solid matrix offers several advantages over simple adsorption or covalent linking to a matrix surface [20]. Usually, an encapsulated enzyme shows long-term preservation of the structure and catalytic activity, and a larger thermal stability than that of the free enzyme [20].

Porous silica has been widely used as an inert and stable matrix for enzyme immobilization owing to its high specific surface areas and controllable pore diameters, which can be tailored to the dimension of a specific enzyme: that is, micro-porous (<2 nm pore size), meso-porous (2–50 nm pore size) or macro-porous (>50 nm pore size) silica. Because most enzymes are of the order of 3 to 6 nm in diameter, mesoporous materials are most commonly used [23]. Bio-inspired silica occurs under mild natural conditions, based upon those that diatoms and sponges use in order to create highly ordered silica in vivo. Bio-silica demands an extremely easy sample preparation and the reactions are compatible with the functionality of the enzyme, providing a versatile new technology for enzyme immobilization with several inherent advantages [20].

- **Inexpensive:** No need for chemical reagents for laborious synthesis.
- **Rapid:** Immobilization occurs in seconds.
- **Mild:** Formation of the particles occurs at room temperature and neutral pH.
- **Nanosized:** Lower diffusion limitations and higher volumetric activities.
- **Smart:** Matrix can be dissolved to release the entrapped enzyme.
- **Robust:** Physical properties suitable for flow-through applications.
- **Stabilizing:** Numerous enzymes have been stabilized by entrapment in this support.
- **Polymorphous:** Shapes can be tailored by varying the conditions of silica deposition.

1.1 Silica Biomineralization in Diatoms

Diatoms are eukaryotic, unicellular organisms with cell sizes ranging typically from 10 to 200 μm [3], which are ubiquitously found in both marine and fresh water environments in all parts of the world as long as sufficient amounts of nutrients are present. These unicellular microalgae represent the major producers of amorphous silica in aqueous habitats. During their cell cycle, diatoms use special transporter proteins [24] to take up silicon mainly as silicic acid from their marine or fresh water environment. The controlled precipitation of silica takes place in a specialized compartment, the silica deposition vesicle (SDV) in acidic environment where pH ~4.5 [25], and the newly formed silica is finally deposited to build their unique silicified cell walls. The diatom shell is made out of hard plates or valves of silica. As the diatom grows, small plates are added to allow cell growth [26]. Thus, they are able to produce a wide variety of nano-patterned silica structures in a genetically controlled manner. The biological processes underlying the formation of silica structures in diatoms have been extensively investigated. Though many details regarding silica formation in diatoms are still unknown, several groups of proteins and enzymes play key role in the process, with the most important of them being silaffins that have been studied in detail [27, 28].

Silaffins were initially identified from the diatom *C. fusiformis* [29]. They are uniquely modified peptides that have been implicated in the biogenesis of diatom biosilica. Extraction of the silica cell wall with anhydrous Hydrogen Fluoride was used in order to release tightly bound organic material led to isolation of high molecular weight pleuralins and proteins in the mass range of 4, 8 and 17 kDa. Based on their high affinity to silica, these proteins were named **silaffins**. The 4 kDa fraction was denoted silaffin-1A, the 8 kDa fraction was named silaffin-1B and the 17 kDa fraction silaffin-2. The corresponding gene sil1 could be cloned from *C. fusiformis* encoding the precursor protein Sil1p encoding 265 amino acids **(Figure1)**.

Figure 1: Primary structure of the silaffin precursor protein Sil1p. The signal peptide consisting of amino acids 1-19 is shown in italics and the repetitive units R1-R7 in bold. The lysine clusters in the repetitive C-terminal part are highlighted in grey. [29]

The protein contains an *N*-terminal signal sequence for translocation into the endoplasmic reticulum (ER) (amino acids 1–19) followed by an acidic *N*-terminal domain of yet unknown function (amino acids 20–107). The *C*-terminal part is strongly basic and highly repetitive (units R1–R7). Silaffin-1A and silaffin-1B both result from proteolytic processing of Sil1p. Silaffin-1B derives from peptide R1, whereas silaffin-1A can be further subdivided into silaffin-1A1, representing peptides R3–R7, and silaffin-1A2 originating from peptide R2 **(Figure 1)** [27, 29]. The mature forms of silaffin peptides lack the *C*-terminal RRIL- and RRNL-sequences that are present in the repeat units R1–R7 **(Figures 1 and 2)**. Similar to the RXL motif *C*-terminal of the signal sequence in the precursor protein of Sil1p **(Figure 1)**, also in other proteins associated with diatom silica, RXL motifs exist in precursor proteins located at the *C*-terminus of individual repeats, e.g., in frustulins, cingulins or silacidins [30-32]. Thus the RXL-sequence may serve as a general recognition motif for a specific endopeptidase in diatoms that processes precursor polypeptides by cleavage of the RXL motifs and releases the individual peptides.

Extensive analyses were necessary to reveal the complete chemical structure of silaffins due to numerous and extraordinary posttranslational modifications (PTMs) **(Figure 2)** [27-29]. In silaffin-1A1 all lysine ε-amino groups are either di- or trimethylated or alkylated with *N*-methylated oligo-propyleneimine chains [27, 29].

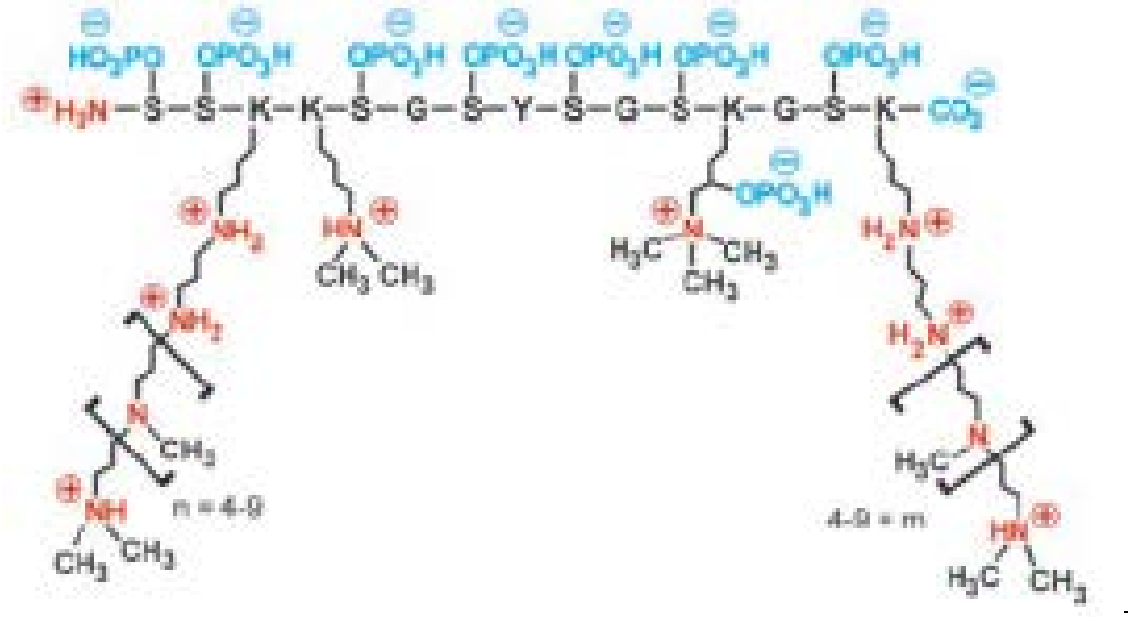

Figure 2: Schematic chemical structure of natSil-1A1. The annotation of charges within the molecule is tentative for a solution around pH 5. Most likely, not all amino groups are protonated, because the basicity of amino groups is reduced due to mutual repulsion of the positive charges within the polyamine chains [(28)].

A method that avoids the harsh anhydrous hydrogen fluoride treatment commonly used to dissolve biosilica allows the extraction of silaffins in their native state. The native silaffins carry further posttranslational modifications in addition to their polyamine moieties. Each serine residue is phosphorylated, and this high level of phosphorylation is essential for the biological activity. The zwitterionic structure of native silaffins enables the formation of supramolecular assemblies [(28)].
Silaffin-based peptides from *C. fusiformis* are capable of precipitating silica from a solution of silicic acid *in vitro* and the amount of precipitated silica is directly proportional to the amount of silaffin in the reaction. Moreover, the silaffin peptides completely co-precipitate with the silica as long as silicic acid is present in excess [(29)]. The **R5 peptide**, a synthetic variant of silaffins with the sequence of the repetitive unit 5 of Sil1p but lacking any PTMs (Figure 3), has no silica precipitation activity below pH 6 [(28, 33)].

1.2 Enzyme encapsulation in silica matrices: the catalyst choice

Initial studies focused on the immobilization of enzymes within biosilica nanoparticles obtained by the reaction of a silicate precursor with a silica-precipitating peptide (R5) [(35)]. As mentioned above, the R5 peptide is a synthetic derivative of a naturally occurring silaffin protein that is found in the silica skeleton of the marine diatom *Cylindrotheca fusiformis* [(34, 36)]. The reaction rapidly forms a network of fused silica nano-spheres with a diameter of about 500 nm that entraps the scaffold

peptide and any other material that is present within the reaction mixture. Preliminary experiments carried out with the R5 peptide showed the successful encapsulation of a range of enzymes, as well as non-biological components such as magnetic cobalt platinum, CdSe/ZnS nanoparticles (quantum dots) and iron oxide nanoparticles. Both enzymes and non-biological components maintain their properties after the biosilification [(35)]. Despite the versatility of the synthetic peptide (R5), subsequent studies demonstrated that silica-formation can also be catalyzed by a wide range of cationic amine-rich molecules, including silica-binding peptides, polymers such as polyethyleneimine (PEI) and poly-L-lysine (PLL), cysteamine and other proteins such as silicatein and lysozyme **(Table 1)**. The latter has been observed to retain the antibacterial activity [(37)]. The mild reaction conditions associated with silica formation are compatible with enzyme immobilization and allow retention of high levels of enzyme activity. As such, the encapsulation of biomolecules within silica nanoparticles using bioinspired silica formation has already been investigated for a wide variety of enzymes. Silica formation catalyzed by the R5 peptide is suitable to encapsulate a wide variety of monomeric and multimeric enzymes

Silica Catalyst	Silica Characteristics
Silaffin and R5 peptide	Spherical particles 500 nm to 700 nm
Poly(EAK)n-R5	Bimodal spheres ~ 83 nm and ~ 463 nm
Lysozyme	Spherical particles ~ 500 nm
Silica-binding peptides	Spherical particles 250nm - 500 nm
Silicateins	Silica sheets along protein filaments
Block co-polypeptides	Various morphologies from spheres to columns depending upon the precursor
Poly-L-lysine	Various morphologies, including nanoparticles (50-100nm), hexagonal platelets (0.5-1μm)
Polyethyleneimine	Various morphologies: spheres, ribbons, nanofibers and platelets
Amine-terminated dendrimers	Spherical particles, size dependent upon reaction conditions
Spermine /Spermidine	Spherical particles 500 nm to 1 μm
Cysteamine	Spherical particles ~ 40-100 nm
Protamine	Spherical particles ~ 25nm

Table 1: Characteristics of silica formation from biological and bioinspired catalysts [(20)]**,** where:

a) R5 sequence n-SSKKSGSYSGSKGSKRRIL-c. b) Poly(EAK)n sequence: n-AEAEAKAKAEAEAKAK-c.

1.3 Hydroxyapatite

Hydroxyapatite ($Ca_{10}(PO_4)_6(OH)_2$, HA) is an important inorganic biomaterial which has attracted the attention of researchers in recent years. Due to its chemical and structural similarity with the mineral phase of bone and teeth, HA is widely used for hard tissue repair. For instance it is used as a coating on orthopedic and dental implants to enhance fixation of the implant to the surrounding bone. This inorganic phosphate has been studied extensively for medical applications in the form of powders, composites or even coatings. In nature, organisms control the nucleation and growth of HA crystals using interfaces such as organic templates. Scientists have been inspired by nature in order to design biomimetic biomaterials and to control the biomineralization process by observing the bone/teeth complex hierarchical structure and other mineralized natural tissues. Mineralized tissue such as bone and dentin are unique bio-composites of a structured organic matrix impregnated with matrix-oriented carbonated apatite crystals. Osteoblasts and odontoblasts, respectively, are the cells responsible for the formation of the bone and dentin matrices [38, 39]. The mineral deposited on the organic framework locally adopts the preferred orientation relative to the matrix surrounding it [40]. The formation, remineralization, and dissolution of hard tissues such as bones and teeth are very complicated processes not only because of the presence of multiple components in the solution media but also because of the numerous calcium phosphate phases that may be involved in the reactions, i.e. amorphous calcium phosphate and octacalcium phosphate **(Table 2)**. Although hydroxyapatite is thermodynamically the most stable form, it does not crystallize spontaneously from physiological calcium and phosphate buffer solutions [40, 41]. De novo hydroxyapatite formation is accelerated by nucleators such as certain specific extracellular matrix macromolecules [39]. It is well documented that acidic non-collagenous proteins play an important role in apatite deposition in vitro [43, 44], whereas dysfunctional non-collagenous proteins may lead to impaired apatite deposition in vivo [45, 46]. Understanding the mechanisms involved in the mineralization process could provide the basis to facilitate synthesis of bone and dentin-like materials for tissue regeneration.

Calcium Phosphate Phases

		Empirical formula	Molar Ca/P ratio
Dicalcium phosphate dihydrate	DCPD	$CaHPO_4 2H_2O$	1.00
Dicalcium phosphate	DCPA	$CaHPO_4$	1.00
Octacalcium phosphate	OCP	$Ca_8H_2(PO_4)_6 5H_2O$	1.33
β-Tricalcium phosphate	TCP	$Ca_3(PO_4)_2$	1.50
Whitlockite	Mg-TCP	$Ca_{3-v}Mg_v(PO_4)_2$ $O \leq v \leq 2$	$3 - v/2$
Amorphous calcium phosphate	ACP	$Ca_9(PO_4)_6 xH_2O$	1.50
Hydroxyapatite	HAP	$Ca_{10}(PO_4)_6(OH)_2$	1.67
Defect apatites		$Ca_{10-y}(HPO_4)_{6-y}(OH)_{2-y}O$ $\leq y \leq 2$	$10 - y/6$
Fluoroapatite	FAP	$Ca_{10}(PO_4)_6F_2$	1.67
Fluorohydroxyapatite	FHAP	$Ca_{10}(PO_4)_6F_z(OH)_{2-z}$ $O \leq z \leq 2$	1.67

Table 2: Calcium phosphate phases.

Statherin and Dentin matrix protein 1 (DMP1) are two human proteins which play an important role in apatite deposition in vivo. **Statherin** is a 43-residue acidic proline- and tyrosine-rich phosphopeptide of unique composition with a high degree of structural and charge asymmetry, present in human parotid and submandibular salivas. Statherin is a multifunctional molecule that possesses a high affinity for calcium phosphate minerals such as HA, maintains the appropriate mineral solution dynamics of enamel, promotes selective initial bacterial colonization of enamel, and functions as a boundary lubricant on the enamel surface [(47)]. In addition, statherin may function in the transport of calcium and phosphate during secretion in the salivary glands [(48)]. Statherin's role in mineral solution dynamics of enamel involves its ability to inhibit spontaneous precipitation and crystal growth from supersaturated solutions of calcium phosphate [(49)]. Structural studies have provided evidence that the N-terminal SN15 fragment has a strong tendency to adopt an ordered helical conformation, whereas the shorter N-terminal sequence, middle, and C-terminal fragments are structurally flexible and prefer to adopt scattered turn structures or unordered random conformations in organic and aqueous solutions. The negative charge density, sequence (1-15), and helical conformation at the N-terminal region of statherin are important for its surface interaction with HA [(50)].

DMP1 is an acidic phosphoprotein of theoretical isoelectric point (pI) of about 3.95 that is present in the matrix of both bone and dentin [(51, 52)]. In situ hybridization analysis demonstrated that initial expression of DMP1 coincides with dentin mineralization [(53, 54)]. Today we know that DMP1 plays an active structural and/or regulatory role during bone and dentin calcification, since apatite

crystallization process can be initiated by DMP1 in vitro [55]. DMP1 can nucleate the formation of hydroxyapatite in vitro in a multistep process that begins when DMP1 binds calcium ions triggering the mineral deposition. The structural characterization of the functional domains of DMP1 demonstrated that intermolecular assembly of acidic clusters into a β-sheet template was essential for the observed mineral nucleation[55] This protein, which is critical for proper mineralization of bone and dentin, is present in diverse cells of bone and tooth tissues. The protein contains a large number of acidic domains, multiple phosphorylation sites, a functional Arg-Gly-Asp cell attachment sequence, and a DNA binding domain. In undifferentiated osteoblasts it is primarily a nuclear protein that regulates the expression of osteoblast-specific genes. During osteoblast maturation the protein becomes phosphorylated and is exported to the extracellular matrix, where it promotes mineralized matrix formation. Mutations in the gene are known to cause autosomal recessive hypophosphatemia, a disease that causes rickets and osteomalacia. The gene structure is conserved in mammals.

1.4 Recombinant proteins for biopharmaceuticals applications and drug discovery

1.4.1 L-Asparaginase: a biological drug

L-Asparaginase (L-ASNase or L-ANS, EC 3.5.1.1) is an enzyme that catalyzes the hydrolysis of the non-essential amino acid L-Asn to L- Asp and ammonia. This enzyme is widely used for the treatment of haematopoetic diseases such as acute lymphoblastic leukaemia (ALL) and lymphomas **(Figure 3A, 3B)**. L-ANSases, in combination with other drugs, are first administered to induce a remission of the disease induction therapy. At a later stage, the continued application of L-ANSase helps to prevent further outbreaks and to maintain therapy [56, 57]. Therapeutic forms of L-ANSase come from different biological sources (primarily *E. coli* and *Erwinia chrysanthemi*) [58a]. It is well established that the various preparations have different biochemical pharmacology properties, and different tendency to induce side-effects. A detailed characterization of the different L-ANSases would allow a better understanding of their catalytic and therapeutic activity, thus enabling more accurate predictions of the behaviour of these enzymes under a variety of therapeutic conditions. In addition, detailed understanding of the catalytic mechanism of L-ANSases might permit the design of new forms of L-ANSases with optimal biochemical properties for clinical applications. The most common asparaginases used in therapy are the type-II bacterial asparaginases (ANSII), in particular from *E.coli* and *E.chrysantemi. E.coli* ANSII is in clinical use since 1967 [59] and, more recently the native ANSII is often replaced by its PEGylated form because this formulation exhibits a lower

immunogenicity and prolonged in vivo lifetime[60]. Nevertheless, also in the PEGylated forms the immunogenicity is decreased but not completely abolished.

E.coli L-ASNII is located in the periplasmic space, between the bacterial plasma membrane and the outer membrane of *E. coli*, due to the presence of a pro domain that post expression is cleaved and has a Km value of 11.5 μM for L-Asn. This type of enzyme can also hydrolyze L-Gln to L-Glu. In the cases where L-Gln is the better substrate, the enzyme is termed glutaminase. Four identical non-cooperative active sites have been identified that are formed at the subunit interfaces: two between subunits A and C and two between B and D. The N- and C-terminal domains of the subunits are involved in the formation of each active site. Thus, L-ANSII is active as a homotetramer of identical subunits (with D2 symmetry), or better described as dimer of two intimate dimers [58 a, 58b] **(Figure 3C)**.

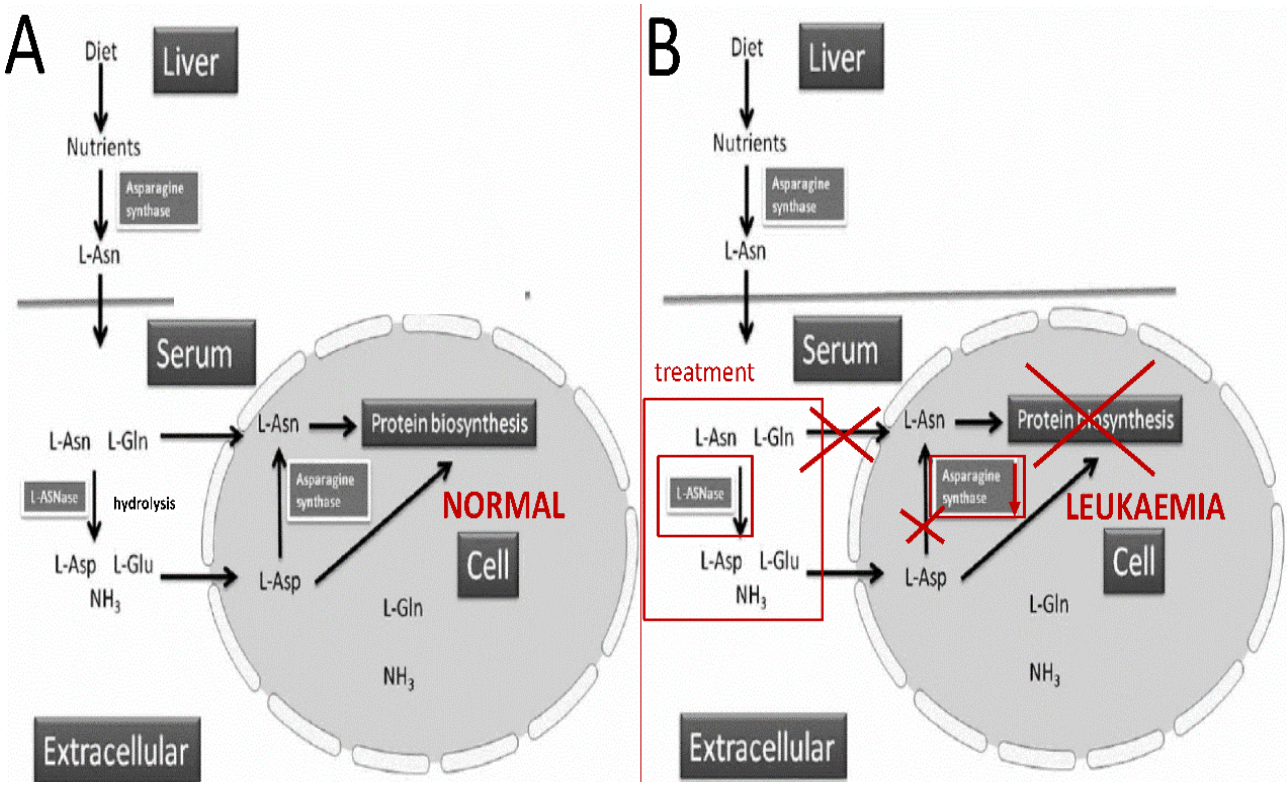

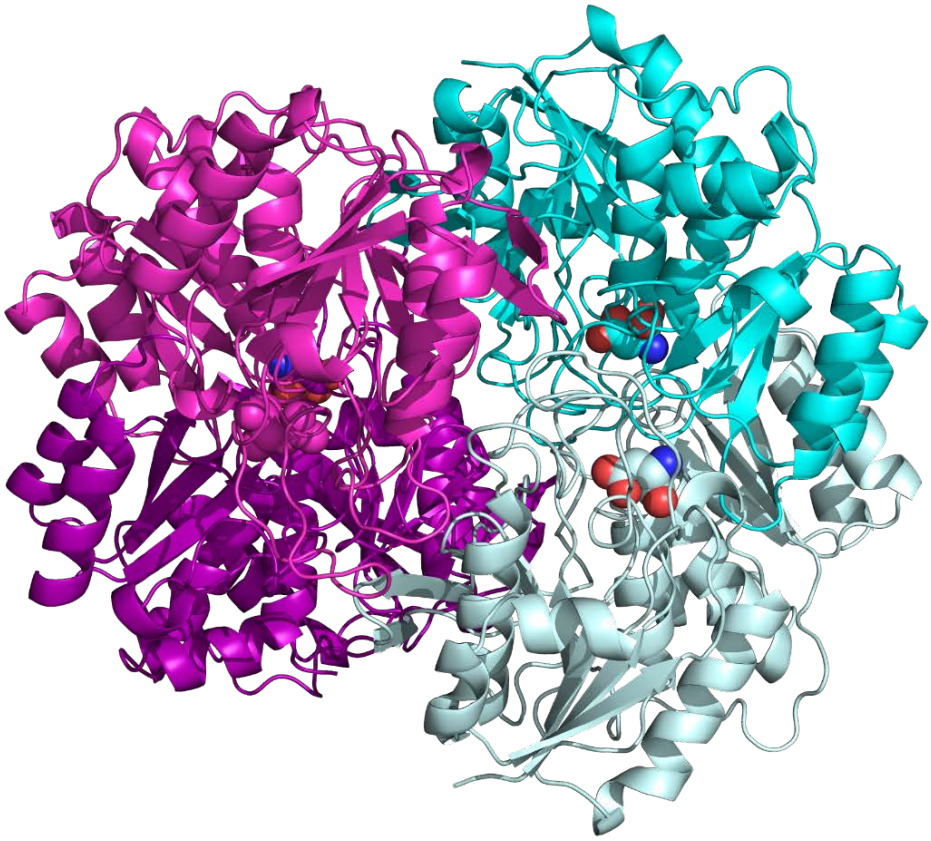

C

Figure 3: **A&B: Mechanism of the anti-tumor activity of L-ANSase.** L-ANSases act extracellularly (e.g. in serum) by depriving tumor cells from the extracellular source of L-Asn and L-Gln. The anti-neoplastic activity results from cellular protein synthesis inhibition due to depletion of the circulating pools of L-Asn by L-ANSase. Contrary to normal cells, malignant leukaemia cells can only synthesize L- Asn slowly, due to downregulation of Asparagine synthetase, and thus their survival depends on an exogenous supply. Rapid depletion of L-Asn and L-Gln in the patients' serum ensures optimal leukemic blast-kill via apoptosis. In contrast, a gradual or incomplete L-Asn or L-Gln depletion may allow the leukemic blasts to adapt and survive (Modified from Labrou N.E. et al. 2010) [(58a)]. **C: Structural representation of *E.coli* L-ANSII (PDB ID: 3ECA)** The two intimate dimers are in magenta and cyan respectively. The aspartate (product of hydrolysis) is displayed in the active site as sphere. [(58b)]

1.4.2. Matrix Metalloproteases as potential drug targets

Matrix metalloproteases (MMPs) are a family of extracellular hydrolytic enzymes in charge of the degradation of the components of the extracellular matrix (ECM). MMPs belong to the metzincin superfamily of metalloproteinases, characterized by the presence of a catalytic zinc atom in the active center and the HEXXHXXGXXH/D zinc binding consensus sequence, followed by a conserved methionine residue. The family of human matrix metalloproteinases includes 24 members, displaying different substrate specificity for the components of the extracellular matrix. The latter is a heterogeneous mixture of well-organized and well-structured proteins, such as collagens, elastines, laminins, fibronectins and proteoglycans, which provides the scaffold on which cells and tissues are anchored. However, extracellular matrix, is not a passive support for cells but acts also as reservoir for embedded cytokines and growth factors [(61)]. An old classification of MMPs[(62)] was performed on the basis of substrate preferences and MMPs were sub-grouped as: i) stromelysins (MMP-3, MMP-10, MMP-11), ii) gelatinases (MMP-2, MMP-9), iii) collagenases (MMP-1, MMP-8, MMP-13), iv) elastases (MMP-12), v) matrylisins (MMP-7, MMP-26) and vi) membrane proteins (MMP-14, MMP-15, MMP-16, MMP-24). However, their selectivity towards these substrates is not high [(64)] and most of them hydrolyze also other extracellular components [(65)], such as extracellular domains of membrane receptors [(66)], and other proteases. Recent classifications are based on bioinformatics and structural analysis, which through sequence and structural alignment allow to identify five main groups: i) non-furin regulated MMPs, ii) gelatinases, iii) transmembrane MMPs, iv) glycosylphosphatidylinositol (GPI)-anchored MMPs and v) others [(66)]. MMPs are involved in several physiological functions such as embryogenesis, tissues growth, development [(67, 68)], wound healing, and cell migration. Because of their potential destructive effect, MMPs activity is strictly regulated in healthy tissues **(Figure 4)** by a tight control of expression, secretion and clearance and by the presence of endogenous tissue inhibitors of metalloproteinases (TIMPs) [(71)]. Moreover, MMPs are produced by the cell as inactive proenzymes thanks to the presence of a pro-domain that prevents the access of the substrates to the active site. The pro-domain is removed by a proteolytic cleavage upon the activation. Some members of the family are involved in the activation of other MMPs. For example the subgroup of stromelysins regulates collagenases function [(72)] and the membrane-type metalloproteinases, such as MMP-14, activate MMP-2[(73)]. An imbalance among inhibition and activation of MMPs is often associated with pathological states such as inflammatory and auto-immune disorders, rheumatoid arthritis, cancer and metastasis [(74)]. Some synthetic inhibitors of MMPs were thus designed as potential drugs [(75)]. Unfortunately, these molecules failed the clinical trials due to side effects and poor pharmacological activities. The main reasons of the

failure of these molecules are related to their poor selectivity [76] and an uncomplete knowledge of the biological activity of the different members of the MMPs family [77]

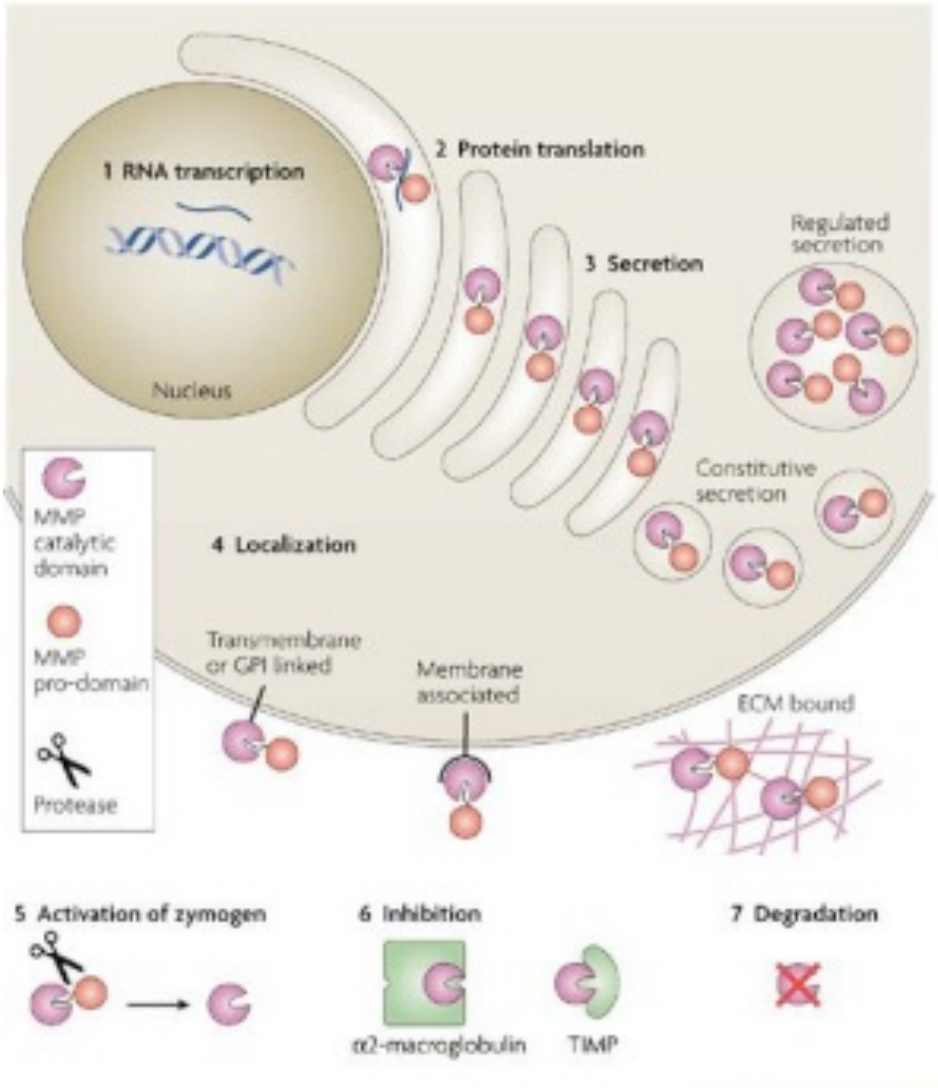

Figure 4: Regulation of MMPs function at various levels. [68]

MMPs are synthesized as zymogens with a signal peptide which leads them to the secretory pathway. Then, they can be secreted outside the cell or can be anchored to the plasma membrane, thereby confining their catalytic activity to the extracellular space or to the cell surface, respectively **(Figure 4)**. However, several MMPs [69, 70, 78] can be found also as intracellular proteins, although their functions inside the cells are still largely unknown. Most of MMPs are constituted by a pro-domain (from 66 to 80 amino acids), a catalytic metalloproteinase domain (of about 160 amino acids) and a hemopexin domain (of about 210 amino acids) connected to the catalytic domain by a linker peptide of variable length (**Figure 5**).The pro-domain maintains the active site inaccessible to substrates through a cysteine switch PRCXXPD consensus sequence, until the proteolytic activation occurs.

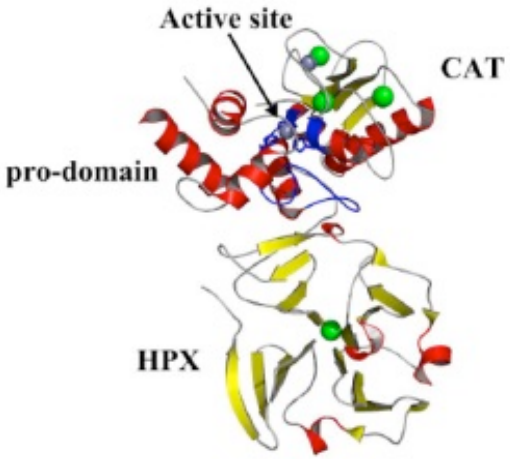

Figure 5: General structural representation of MMPs. The pro-domain, CAT and HPX domains are highlighted in the figure. The active site with the zinc(II) ligands and the loop L8 that flanks the S1' pocket are colored in blue.

The catalytic (CAT) domain is largely conserved in all MMPs and consists of three α- helices, a twisted five-stranded β-sheet and eight intervening loops. In almost all MMPs the CAT domain contains two zinc (II) ions, one responsible for the catalytic activity, and the second with a structural function. Furthermore, in the CAT domain from one to four calcium (II) ions with structural role are present. The catalytic zinc (II) ion is coordinated by three conserved histidines and by one water molecule that is hydrogen bonded to the catalytically relevant glutamate and is, in this way, activated for a nucleophilic attack towards the peptide bond of the substrate, allowing its hydrolysis also at neutral pH [(79)]. The substrate binding groove is constituted by the catalytic zinc ion and several binding pockets. The hydrophobic S1' pocket, delimited by the last loop (L8), represent together with the zinc (II) ion, the preferred site for synthetic inhibitors. In fact, this loop is a region of relatively large variability among MMPs and can be targeted in order to have selectivity [(80)]. The inhibitors bind the active site in a way that resembles the substrate in the transition state, fitting the deep S1' pocket with a lipophilic moiety [(81)].

The hemopexin-like (HPX) domain has the same structural features in all the members of the family and it is constituted by four β-sheets organized in a symmetric four-blade propeller, forming a deep tunnel closed by a calcium ion at the bottom. The folding of HPX domain is stabilized by a disulfide bridge that links the beginning of the first blade with the end of the fourth blade of the propeller. These two domains experience large amplitude motions in correspondence of the loops. Especially the loop flanking the S1' pocket in the CAT domain, mainly involved in the substrate recognition, is characterized by high flexibility in all the members of the family, indicating the importance of conformational heterogeneity in these domains for the hydrolysis of the substrates

[82]. The CAT and the HPX domain are connected together by a proline-rich linker whose length vary among the members of the family (**Figure 6**) ranging from 14 amino acids in collagenases (MMP-1, MMP-8 and MMP-13) to 68 AA in MMP-9 [82]. The linker allows large interdomain flexibility and binding to structurally unrelated substrates with a variety of molecular conformations. It, thus, permits interdomain re-orientation during the explication of the mechanism of these enzymes.

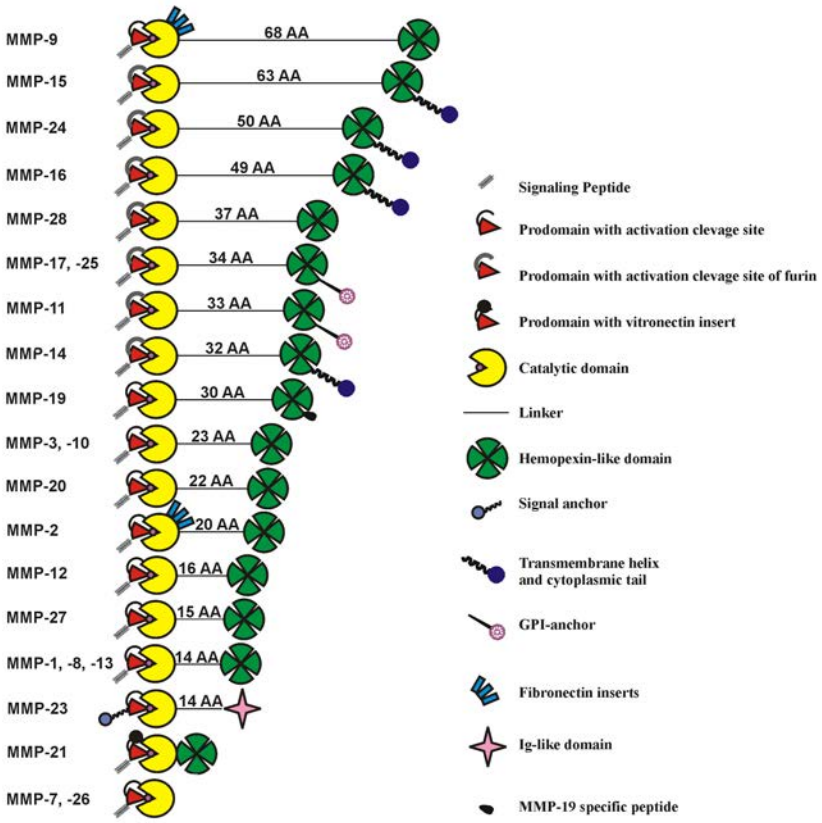

Figure 6: Schematic domain structure of MMPs with the corresponding linker length [82].

Interdomain flexibility of two of the members of the family with the shortest linkers (MMP-1 and MMP-12) [83, 84] has been investigated in the last years by a combination of solution NMR and SAXS measurements. NMR relaxation data indicated that the two domains are not rigidly held to each other but they can experience independent motions. Moreover, the analysis of SAXS data indicated that a good description of the behavior of these proteins in solution can be provided only when ensembles of heterogeneous conformations are taken into account. In fact, the crystallographic structures displaying a closed conformations, when taken alone, fail in the description of experimental data. Instead, when these structures are flanked by a significant amount

of extended conformations in equilibrium with the closed ones, a good agreement with the experimental data is achieved. From these observations it was shown that the two domains can freely reorient among each other. This data can, however, hardly provide a quantitative and detailed description of the conformational heterogeneity of the protein and highlight the most probable conformations sampled in solution, that are necessary to afford hints for the mechanism of collagenolysis.

Collagenases and the elucidation of collagenolytic mechanism

Collagens are the major structural proteins of connective tissues and can be classified in three different types, I, II and III. Interstitial collagens have a unique molecular structure that consist of three α-chains staggered by one residue and constituted by repeating Gly–X–Y triplets, where X and Y are often proline and hydroxyproline, respectively [(85)]. Each α-chain, for the high content of proline and hydroxyproline in the sequence, forms a left-handed poly-Pro II-like helix. The three α-chains are coiled in overall right-handed superhelical conformation[(86)], stabilized by hydrogen bonds among the backbones of three α-chains, that make the structure resistant to many proteases. In vertebrates, the only enzymes that can cleave this very complex triple-helical structure are collagenases of the MMPs family and cathepsin K [(87)] produced by osteoclasts. Collagenolysis, the degradation of collagen, by matrix metalloproteinases (MMPs) occurs during development, wound healing, and major inflammatory diseases. A number of MMP family members possess collagenolytic activity [(88)], which is one of the "committed" steps in ECM turnover. For example, interstitial collagens (types I–III) are hydrolyzed by MMP-1, MMP-2, MMP-8, MMP-13, MMP-14, MMP-18, and MMP-22 [(89-96)]. Conversely, MMP-3 and MMP-9 bind to type I collagen, but do not cleave the native triple helix [(97-99)]. Triple helical collagens are resistant to most proteinases, but collagenases cleave them into specific 3/4 and 1/4 fragments. This process is critical for collagenolysis in the tissue and for tissue damage in degenerative diseases. The rates of collagen hydrolysis differ amongst MMPs. For example, MMP-13 cleaves type II collagen 5–6 times more rapidly than types I and III, [(92)] while MMP-14 is 5–7 fold less efficient at hydrolyzing type I collagen than MMP-1.[(94)] The mechanism of collagenolysis by soluble collagenases, such as MMP-1, has been widely studied and, although its molecular details have not been completely elucidated, it is known that the presence of both catalytic (CAT) and hemopexin-like (HPX) domains as well as their flexibility are prerequisite and crucial. The catalytic domain alone can cleave non-collagen substrates, but for the enzyme to cleave triple-helical fibrillar collagen, the presence of the hemopexin domain is essential [(108-110)]. The catalytic and hemopexin domains cooperate to first locally unwind the triple-helical structure of collagen before cleavage takes place [(101)].

Membrane type 1 matrix metalloproteinase (MT1-MMP) is a transmembrane cell-surface collagenase that mainly confines its activity at the cellular surface. MT1-MMP was the first transmembrane-type MMP to be discovered. It degrades various components of the extracellular matrix on the cell surface, including collagen-I, -II, -III, fibronectin, vitronectin, laminins and aggrecan core protein [105], and also activates pro-MMP2 [106] and pro-MMP13 [107], expanding its proteolytic repertoire on the cell surface. Furthermore, MT1- MMP processes cell-surface molecules, including CD44 [108], syndecan1 [109], aV integrin [110] and low-density lipoprotein receptor- related protein 1 (LRP1) [111], affecting cellular functions, especially cell motility. Among these enzymatic activities, collagenolytic activity has been proposed to be particularly important. MT1-MMP-null mice exhibit several developmental phenotypes, including skeletal abnormality and soft tissue fibrosis, and these phenotypes are, at least in part, due to a lack of pericellular collagen [112, 113]. MT1-MMP is also an essential pericellular collagenase for cancer cells to grow in a collagen- rich environment [114]. MT1-MMP also plays a major role in angiogenesis [115, 116], in migration of smooth muscle cells to the neo-intima of the artery upon injury [117] and in cartilage invasion by rheumatoid synovial tissue [118, 119]. Thus, MT1-MMP plays important roles in invasive processes of different cell types.

Gelatinases

MMP-9, also known as gelatinase B, is a prototypical target in inflammatory diseases, because of its tissue-damaging roles [132-134] and inflammation-promoting processing of soluble proteins, including protease inhibitors [135], chemokines [136], and cytokines [137]. MMP-9 posesses a linker of 66 amino acids which is the longest and most flexible in all protein family (**Figure 6**). This linker has a unique proline rich sequence and is extensively O-glycosylated (OG) [140]. MMP-2 (Gelatinase A) In contrast, MMP-2, or gelatinase A, mainly has anti-inflammatory and homeostatic functions, and it presumably acts by inactivating inflammatory chemokines [141] and by regulating connective tissue turn-over. In fact, the main structural difference between MMP-9 and MMP-2 is the presence of this extensively O-glycosylated (OG) linker-domain[138, 139]. This implies that selective inhibitors, discriminating between these highly similar enzymes, are crucial for efficient anti-inflammatory therapy without side effects.

Homodimerization/multimerization has emerged as an important mechanism for regulating the activation and activity of MMPs, in particular, MT1-MMP **(Figure 7)** and MMP-9 [120, 122, 123]. It was demonstrated that MMP ancillary domains, including the hemopexin, transmembrane, and cytoplasmic domains, are required for MT1-MMP to form a homooligomer complex, which is important for MT1-MMP cell surface activation of pro-MMP-2 [121, 122, 124, 125] and for

collagenolysis [126]. MMP-9 also exists as a monomeric and homodimeric molecule [127], in both its latent and active forms. Both monomeric and dimeric forms of MMP-9 have been identified in a variety of cells (including normal and tumor cells) and in biological fluids and tissues, indicating that both forms are physiologically relevant. More recently, MMP-9 has been shown to be a trimer [167]. Dimerization/multimerization is mediated by the carboxyterminal domains of MMP-9 and occurs intracellularly [123]. The biological functional role of the MMP-9 dimer has not been elucidated.

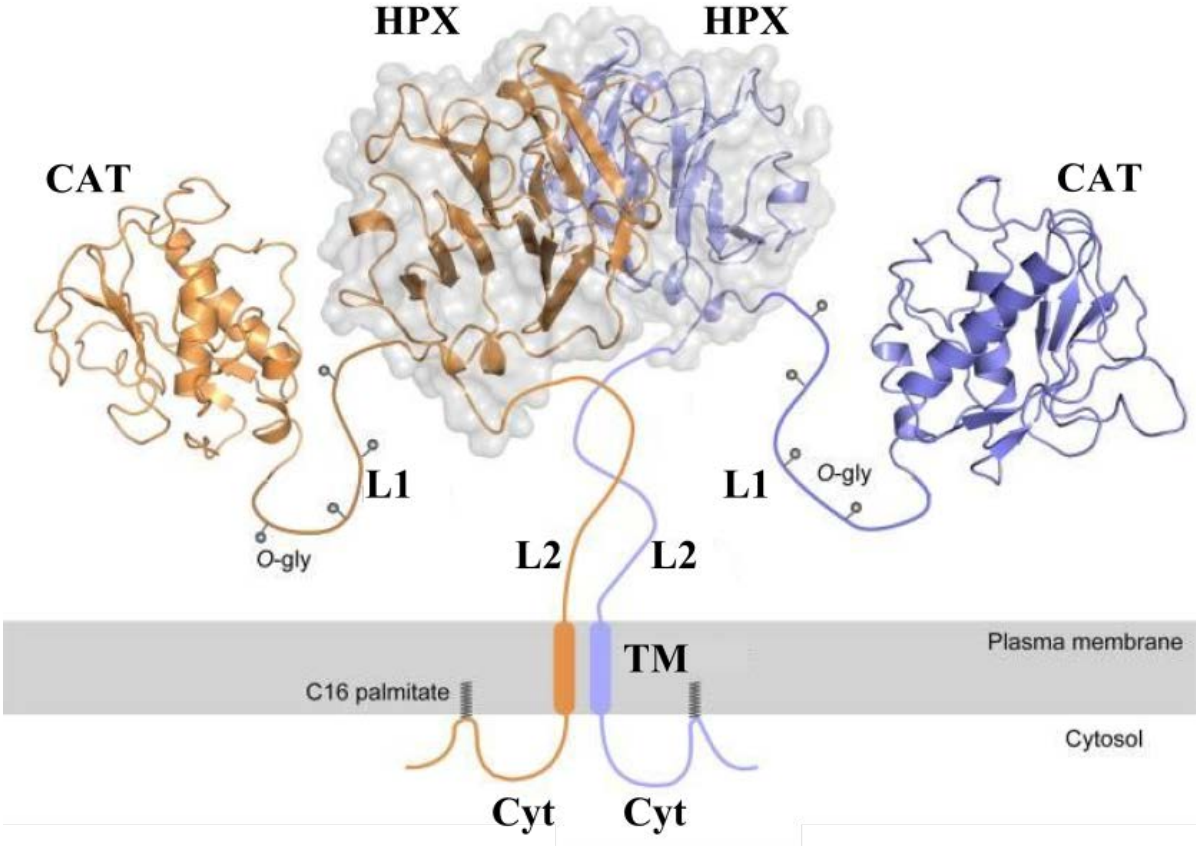

Figure 7: Model of MT1-MMP dimer on the cell surface MT1-MMP forms homodimer through Hpx and transmembrane domains to become a functional enzyme.[104]

Numerous reports emphasize the need for highly selective MMP inhibitors to target MMPs [128, 129]. Inhibition of MT1-MMP, MMP-9 and other MMPs could be useful to treat diseases, such as cancer, arthritis, and other diseases [130]. However, the design of selective inhibitors is a challenge because the high structural similarity of the catalytic domains of these enzymes. In this respect, it is important to remember that, most of the inhibitors designed so far bind the proteins at the catalytic zinc site [131].An alternative strategy to face the poor selectivity of the synthetic inhibitors relies on the use of dendrons and on the topical administration that avoids a systemic spreading of the molecule and minimizes the possible side effects.

1.4.3. Carbonic Anhydrases as potential drug targets

The **carbonic anhydrases** (or carbonate dehydratases, **CA**s EC 4.2.1.1) belong to a superfamily of metallo-enzymes that catalyze the rapid interconversion of carbon dioxide and water to bicarbonate and protons (or vice versa). Although this reaction may occur without a catalyst, at physiological pH values it is too slow to meet metabolic needs. CO_2, a poorly water soluble gas, may damage cellular components (e.g. membranes) if generated in exceedingly high amounts in a cell/tissue, whereas its conversion to water soluble ions (bicarbonate and protons), may interfere with the pH balance of the cell through the generation of an acid (H^+) and a buffering base (HCO_3^-). [142-146] Thus, six genetically diverse CA families have evolved and are known to date, the α-, β-, γ -, δ-, ζ- and η-CAs, which evolved in an astonishing manner: the α-, β-, γ -CAs are probably convergently evolved, whereas δ-, ζ- and η-CAs seem to be highly divergent variants of the β- or α-CAs, constituting however diverse genetic families of their own [146]. Detailed kinetic and X-ray crystallographic studies have allowed a deep understanding of the structure–function relationship in this superfamily of proteins. The α-CAs are present in vertebrates, protozoa, algae, cytoplasm of green plants and in many Gram negative bacteria and 14 different isozymes are known to date. In many organisms these enzymes are involved in crucial physiological processes connected with pH and CO_2 homoeostasis/sensing; biosynthetic reactions, such as gluconeogenesis, lipogenesis and ureagenesis; respiration and transport of CO_2/bicarbonate; electrolyte secretion in a variety of tissues/organs; bone resorption; calcification; tumorigenicity and many other physiological or pathological processes (thoroughly studied in vertebrates and some pathogens) [142-146]. The CA enzymes found in mammals are divided into four broad subgroups, which, in turn consist of several isoforms:

* Cytosolic CAs (CA-I, CA-II, CA-III, CA-VII and CA XIII)
* Mitochondrial CAs (CA-VA and CA-VB)
* Secreted CAs (CA-VI)
* Membrane-associated CAs (CA-IV, CA-IX, CA-XII, CA-XIV and CA-XV)

There are three additional "acatalytic" CA isoforms (CA-VIII, CA-X, and CA-XI) whose functions remain unclear.

Carbonic anhydrase II is a monomeric cytosolic isoenzyme of carbonic anhydrase with no post-translational modification. Its molecular mass is 29 kDa. CA-II is the most ubiquitous and the most studied. Due to its localization it is involved in a lot of biological process; therefore CA-II deficiency is linked to a syndrome that involves more than one organ. [147-148] **CAII** has the highest catalytic activity for physiological functions including electrolyte and water balance; pH homeostasis; CO2 and HCO_3 transport; and production of aqueous humor, cerebrospinal fluid,

gastric acidity and pancreatic secretions. It also assists in metabolic pathways such as gluconeogenesis, lipogenesis, ureagenesis and **bone resorption** and **calcification**. The **CA II structure (Figure 8A)** can be described as a single domain mixed α/β globular protein. The central structural motif is a twisted β-sheet of 8 strands, which is near seven α-helices. The catalytic active site is characterized by a conical cleft that is approximately 15 Å deep with the zinc residing in the interior. The zinc is tetrahedrally coordinated by three histdine ligands (His 94, His 96, and His 119) and a bound water/hydroxyl **(Figure 8B)**. The zinc-ligand distances are all ~2.1 Å including the zinc-bound solvent molecule.There is a hierarchy of zinc ligands in the active site: the first-shell, or direct zinc ligands, are the three histidine residues His 94, His 96, His 119 and a solvent molecule. The second-shell, or indirect ligands, stabilize the direct ligands and help position them for zinc ion coordination. Residue Gln 92 stabilizes His 94, Glu 117 stabilizes His 119, and the backbone carbonyl oxygen of Asp 244 stabilizes His 96, while residue Thr 199 hydrogen bonds with the zinc-bound solvent. Finally a third-shell of stabilization was proposed of a cluster of aromatic residues (Phe 93, Phe 95, and Trp 97) that anchor the β-strand βF that contains His 94 and His 96 [149] .

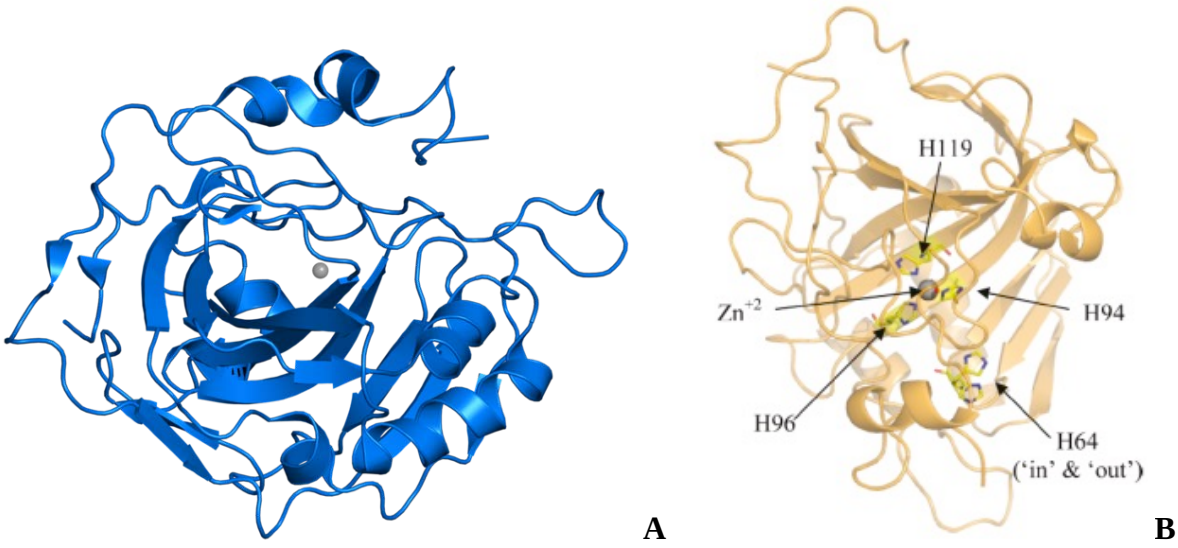

Figure 8: A: Refined X-ray crystal structure of holo human Carbonic Anhydrase II (h CAII) to 1.05 Å resolution. [Fisher SZ, et al (2007) *Biochemistry* (PDB ID: 2ili)] **B:** Overall structure of holo-hCA II. Cartoon depiction of the secondary structural elements are as shown. Structure used was PDB ID 2ILI. The zinc atom is represented as a gray sphere; histidine residues His 94, His 96, His 119, and the dual conformation of His 64 are represented in stick model representation (carbon, yellow; oxygen, red; nitrogen, blue).[149]

CA XII is a transmembrane protein found in normal endometrium, [158] colon, [159] and kidney [160] suggesting an important physiological role for this enzyme in ion transport and fluid concentration.

CA-XII has also been found to be overexpressed in 10% of clear cell renal carcinomas. As mentioned above, it has been observed that many tumors display strong expression of CA XII or co-expression of CA XII and CA IX, mostly in the perinecrotic areas, in accord with the fact that both isozymes are induced by hypoxia. [155-157] Recently, Lerman's group showed that CA XII is highly overexpressed (up to 5 times) in the eyes of glaucoma patients [161], suggesting that this isozyme may be a target for the treatment of glaucoma (up to now the isozymes thought to be involved in aqueous humor secretion within the eye, and thus considered as targets for the development of **antiglaucoma drugs** were CA II and CA IV [152] . Thus, hCA XII is less effective as a catalyst for the CO_2 hydration reaction, as compared to the very rapid isozymes **hCA II** (cytosolic) or **hCA IX** (transmembrane) [152-154], but its catalytic activity seems to be relevant to oncogenesis (acidification of the tumor environment) [153], and its potential as a clinically useful tumor marker clearly merit further investigation, together with the design of inhibitors that may show clinical applications as antitumor drugs.

The protein fold in the diverse CA classes is highly different, as it is the oligomeric state of these enzymes. The **CA activation** and **inhibition** mechanisms of these enzymes are known in detail, with a large number of new inhibitor classes being described in recent years. Besides the zinc binders, which are the classic CAIs known since the 40s (i.e. the primary sulfonamides), some other classes of inhibitors were shown to possess a similar mechanism of action (e.g. carboxylates, hydroxamates, dithiocarbamates and phosphonates). Other classes of inhibitors were shown to anchor to the metal ion coordinated nucleophile binding in a more distant part of the active site cavity compared with the zinc binders. Other inhibitors occlude the entrance of the active site cavity, whereas more recently, compounds binding outside the active site were also described. As CA inhibition has therapeutic applications for drugs acting as diuretics, antiepileptics, antiglaucoma, antiobesity and antitumour agents, the discovery of the new inhibition mechanisms mentioned here may also lead to isoform-selective inhibitors which should possess a better pharmacological profile compared with the first/second generation inhibitors still in clinical use [151]. Recently, targeting of pathogen CAs has also been proposed as a new strategy for designing anti-infectives with a new mechanism of action [162-165]. Successful structure-based drug design campaigns allowed the discovery of highly isoform selective CAIs, which may lead to new generation of drugs targeting these widespread enzymes. Overall, this fascinating field led to important discoveries of several widely used drug classes.

1.5. AIMS OF THE PROJECT

Both biosilica and HA are two inorganic matrices which can be used to produce new biocompatible materials for possible therapeutic/clinical applications and for biofluids processing.

In biosilicified materials the poly-condensation of silisic acid is catalyzed by the presence of a poly-cationic templating molecule or by enzymes. During this doctorate, I have designed and expressed some selected proteins and enzymes, engineered with the bio-silification promoting peptide R5. Then, I have analyzed the differences in terms of enzymatic activity, yield and preservation of the protein structure with respect to the bioinpired material, obtained with the use of external poly-cationic promoters such as poly-L-lysine, lysozyme and R5 peptide.

HA is a major component of hard tissues (e.g. bones, teeth) and provides them with their characteristic stiffness. Therefore, HA is an excellent material to be used as scaffold to regenerate bone and tissues.

Being inspired by recent studies, I have designed an expression vector that hosts two identical hydroxyapatite binding peptides (HABP) and, in the middle of them the sequences for specific restriction enzymes in order to insert the gene encoding the proteins of our interest. The engineered proteins bearing one or two HA peptides (at the N-terminal and C-terminal) have been used to prepare biomineralized materials through a reaction that promotes the hydroxyapatite formation inside the living organisms. These biomaterials have been studied by ssNMR, and characterized with different biophysical and spectroscopic techniques in order to understand if the protein/enzyme retains its structural and functional properties after its immobilization. In this way and by an appropriate selection of a protein, it is possible to create hybrid materials that can upregulate bone formation on the position of interest or be useful for medical purposes.

Concerning the high research interest on MMPs it is widely recognized that the uncontrolled expression of MMPs can lead to severe disorders. Several MMP inhibitors have been reported to suffer from a limited bioavailability and poor selectivity. This relies on the fact that the binding domains of all members of the MMP family share similar structures and can adapt the binding pocket to the ligand shape. Therefore, the undesired side effects and the ineffectiveness observed during the clinical trials have impaired so far the use of synthetic MMPIs in vivo.

Nevertheless, recent structural insights of the catalytic domains of some MMPs in the presence of the aryl sulfonamide inhibitor NNGH has prompted the development of a family of water soluble inhibitors that maintain high affinity for the MMPs. Relying on the properties of the aforementioned inhibitors, we have developed a PAMAM based dendron bearing two aryl sulfonamide scaffolds in the same molecule that can be used for topical administration.

Therefore, this new molecule is a drug candidate designed to be used on diseases such as the Dry Eye Syndrome (DES), where a local

uncontrolled activity of MMPs is present. In particular, this pathology is characterized by an increased expression of MMP-9 that is inhibited by the PAMAM derivative at nanomolar concentrations.

Furthermore, to shed light on the proteolytic mechanism of the membrane-bound MT1-MMP, samples of the its hemopexin-like domain bearing the transmembrane region have been expressed and sedimented in the presence of a membrane mimicking medium for preliminary ssNMR experiments.

2. MATERIALS AND METHODS

2.1. MOLECULAR CLONING

2.1.1Polymerase Chain Reaction (PCR)

PCR is commonly used in molecular biology to amplify a gene sequence of interest by in vitro enzymatic replication assisted by a DNA polymerase. For all the PCR reactions we have used the Thermo Scientific™ Phusion™ Flash High-Fidelity PCR 2x Master Mix in order to amplify our genes of interest. This mastermix contains besides the polymerase, deoxy-ribonucleoside tri-phosphates (dNTPs) and $MgCl_2$. The primers have been designed in order to meet the following criteria:

1. **Melting temperature (Tm)** between 55 and 65°C and Tm difference between forward and reverse primer not higher than 5°C. A Tm over 70°C can lead to secondary priming artifacts and noisy sequences.

2. **GC content** that is between 45 and 65%. GC content is also important as it will affect Tm and the secondary structures possible within a given primer sequence. Strong secondary structures can prevent a primer from binding to its intended target.

3. The **length** of the primers should be at least 18 bases long in order to uniquely bind to their target among a heterogeneous mix of sequences. The length of the primer sequence is mostly be determined by the desired Tm.

4. Lack of secondary priming sites in the template.

All primers were purchased by Eurofins genomics.

For the amplification of all genes were used the following conditions:

1. **Initial denaturation** →98 °C for 30 s (1 cycle)
2. **Denaturation** →98 °C for 30 s
   Annealing →58 °C for 30 s (depending on the Tm of the primers*) (30 cycles)
   Extension →72 °C for 2min (15 s/1 kb)
3. **Final Extension** →72 °C 10 min (1 cycle) & 4 °C for ∞

*For primers >20 nt, anneal for 5 seconds at a Tm +3 °C of the lower Tm primer. For primers ≤20 nt, use an annealing temperature equal to the Tm of the lower Tm primer.

2.1.2 Digestion with restriction enzymes & Ligation

After amplification the genes were purified with PCR DNA extraction kit according to manufacturer's instructions.

Then DNA was quantified using Nano-Drop and digested with the same restriction enzymes as the expression vector that will host the insert. In order to confirm the digestion of the vector and the purity of the insert from unspecific amplifications both of them were loaded to agarose gel and then purified through extraction from the gel with the same kit. Vector and insert were then quantified and ligated overnight at16°C overnight using the T4 DNA ligase according to the following equation:

Insert mass in ng = 3 (or 6) × ($\frac{\text{insert length in bp}}{vector\ length\ in\ bp}$) ×vector mass in ng

The next day the ligation products were transformed in *DH5a E.coli* competent cells, were plated and were left at 37°C for 18 hours. Colonies were afterwards controlled with PCR reaction using 2xTAQ polymerase Blue Master Mix (Giotto Biotech) and the same primers that were used for the amplification of the insert (see figure PCR program with TAQ polymerase). Positive clones were then amplified and the DNA was extracted and sequenced.

First denaturation step	94 °C	5 min	
Denaturation step	94 °C	30 sec	
Annealing step	T_a	30 sec	} 35 cycles
Elongation step	72 °C	1–2 min	
Final elongation step	72 °C	5 min	
End	4 °C	∞	

The annealing temperature (T_a) was set 5 °C below the melting temperature of the primers.

2.1.3. The choice of expression vector

To maximize expression, the cloned gene must be transcribed and translated as efficiently as possible. This is feasible due to the construction of expression vectors, i.e. modified plasmids with useful features which can be propagated and controlled in special hosts (expression systems). Usually, vectors for cloning and expressing target DNA are derived from medium-copy plasmids such as pET. *E.coli* expression systems should meet several criteria including:

(I) Minimal basal expression of the gene to be expressed under repressed conditions,

(II) Fast and uncomplicated induction of a wide variety of genes to a high level of expression,

(III) Easy cloning and DNA manipulation features.

The most common expression system is the T7 expression system derived from bacteriophage T7. The T7 expression system is based on the use of the T7 bacteriophage promoter and RNA polymerase. The T7 RNA polymerase is useful for synthesizing selectively large amounts of RNA because it recognizes only the T7 promoter and not the *E.coli* promoters. Conversely, the *E.coli* RNA polymerase does not recognize the T7 promoter. The T7 RNA polymerase is able to transcribe genes five times faster than the *E.coli* RNA polymerase. The gene encoding the T7 RNA polymerase is inserted into the chromosome of the bacteria used for over expression. Expression of the target gene is induced upon addition of IPTG (isopropyl-ß-D-thiogalactopyranoside) to a growing culture.

The pET-21a (+) vector and pET-28 vector (Invitrogen) were used for expression of all proteins used in this study.

2.1.4. Construction of the pET21a HABP expression vector: A gene that is encoding: a His_6 tail, a TEV cutting site, a HABP, a Thrombin cutting site, a multiple cloning site, a HABP and a stop codon designed and purchased. This gene was then amplified by Polymerase Chain Reaction and was digested with XhoI and XbaI. Then this gene was integrated to the pET21a (+) Invitrogen expression vector, which was digested with XhoI and SalI, by using a T4 DNA ligase. The ligation product was transformed in *E.coli* cells and the DNA extracted from the positive clones was checked by DNA sequencing.

2.1.5. Cloning of recombinant proteins in the pET21aHABP expression vector and pET21aR5 expression vector: The genes of Superoxide Dismutase AS (human), Carbonic Anhydrase II (human), Green Fluorescent Protein, Ubiquitin, Catalytic domain of Matrix Metalloproteinase 12 (human) and L-Asparaginase II (E.coli) have been amplified by Polymerase chain reaction and digested with the same restriction enzymes as the pET21aHABP and pET21aR5. The digested vector was then ligated to the insert by using the T4 DNA ligase and the ligation product was transformed in *E.coli* cells. The DNA extracted from the positive clones was checked by DNA sequencing. (**Figure 9**)

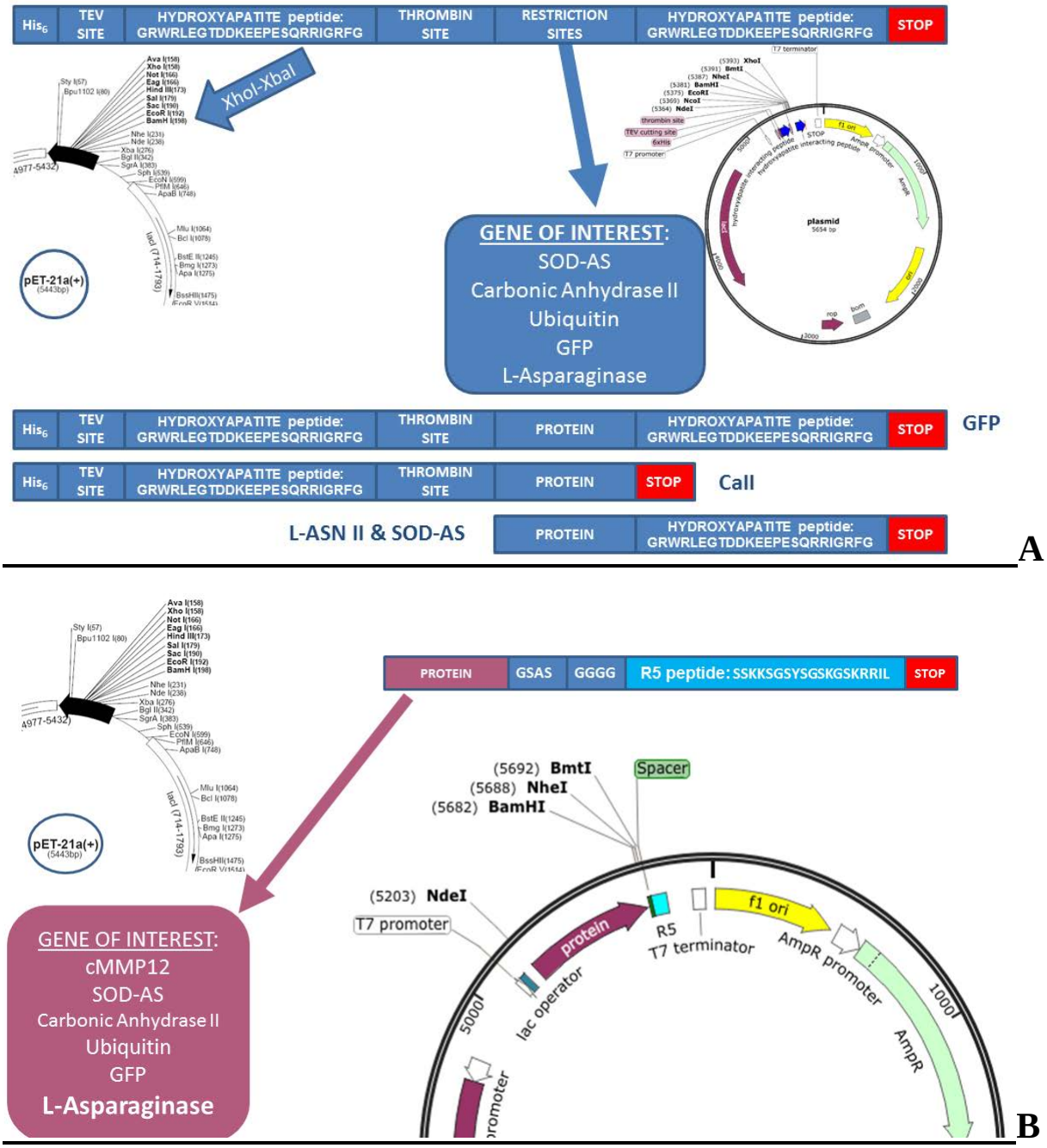

Figure 9: **Schematic representation of vector construction and expression: A)** On the top is represented the encoded gene that was inserted into pET21a between XhoI and SalI and then the constructed vector with the two HABP. On the botom are represented the four different constructs that can be expressed for each protein. **B)** pET21a expression vector constructed to fuse the R5 peptide at the C-terminus of the protein that is clonned between NdeI and BamHI or BmtI.

2.1.6. Cloning of MT1-MMP and Expression tests:

Both full length MT1-MMP encoding amino acids 111 to 582 and ΔCAT MT1-MMP encoding amino acids 316 to 582 have been amplified with Polymerase Chain Reaction **(Figure 10)**. Then

they have been cloned in pET28 expression vector, which co-expresses a 6-His tag at the N-terminal part of the protein for "facilitated" purification. After being sequenced, both constructs have been transformed according to the traditional protocol in several different *E. coli* strains in order to achieve the best expression conditions with the highest purity. Both proteins' expression has been tested in: *BL21DE3, BL21DE3plys, BL21DE3 Gold, BL21DE3 Codon*$^{+}$*, Origami plysS, RIPL, C41 and C43* in temperatures 18-25-30-37^{0}C and with different amounts of IPTG and induction time.

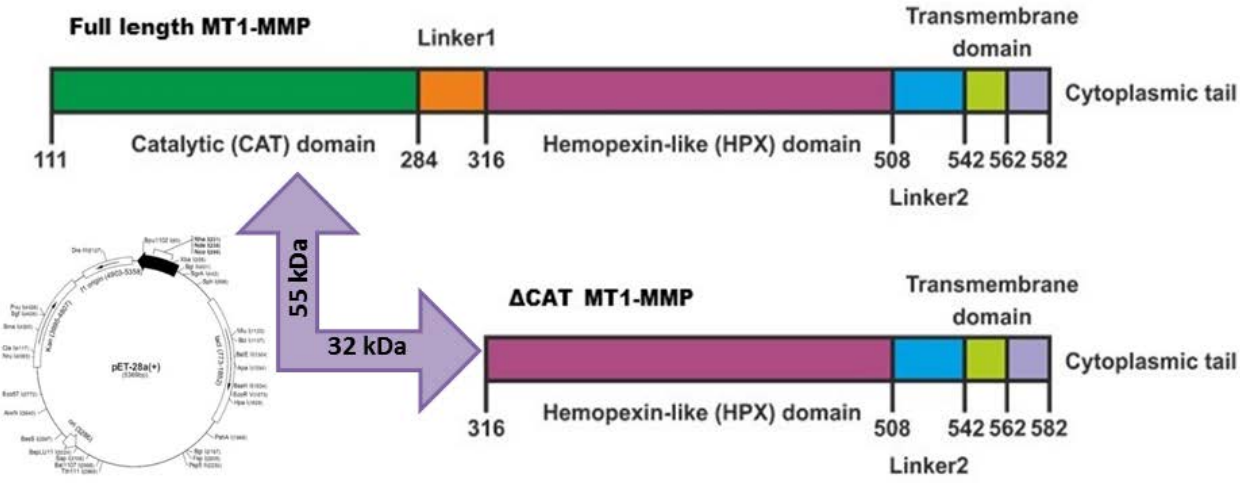

Figure 10: Schematic representation of vector construction and expression for full length MT1-MMP and ΔCAT MT1-MMP in pET28.

2.2. PROTEIN EXPRESSION *E.coli*

2.2.1. Benefits of expression in E.coli

Various host systems can be used in molecular cloning for the proliferation of the gene of interest. In this research, a bacterial host, *E. coli,* was used for gene amplification and expression. Bacterial hosts are often used for production of protein in order to carry out structural analysis or molecular assays. The main advantages of using bacterial host are the simplicity of the cultures, the fact that expression is scalable, and low cost. However, some drawbacks are inherent to this method. The first is that protein solubility can be an issue. Second, though some minor PTMs are possible, glycosylated proteins 43 cannot be produced by this system. And finally, it is often challenging to express functional mammalian proteins. Nevertheless, protein cloning is a method of choice to obtain large quantities of a pure protein at a reasonable cost.

2.2.2. Bacterial transformation

Bacterial transformation is the process of getting the recombinant vector from a reaction mixture or vector solution into *E. coli* cells. To enable the cells to take up circular vector DNA they have to be made competent. There are a number of different types of competent cells that can be used depending on the application. These differences are due to the mutations that have been introduced to make the cells more amenable to transformation. The genotype description can be found in the protocol that accompanies the cells. However, all competent cells have been treated so that they are primed to take up DNA. Competent cells are stored at - 80°C and should never be allowed to warm to room temperature - always thaw cells on ice and keep them cold until ready for transformation. Transformation occurs when the competent cells that take up the plasmid have an altered phenotype, which is typically observed as antibiotic resistance (e.g., ampicillin, kanamycin, or chloramphenicol). Therefore cells that take up the plasmid can be selected using medium containing the appropriate antibiotic. Resistant cells are identified as single colonies on the transformation plate. Because plasmids have their own origin of replication, they are replicated independently of the host cell's chromosome. The plasmid's origin of replication determines the number of copies that are produced within each cell. Most plasmids used in the lab are termed "high-copy number" and may have up to 100 or more copies/cell. On agar plates, each well isolated colony originates from a single cell. Therefore all the cells in the colony are considered to be identical (clones). Several individual clones are generally picked for expansion so that they can be screened for the plasmid. Transformation is an inefficient process and it is important to note that not all cells will actually take up the plasmid. The growth of non-transformed cells that may be on the plate is inhibited by adding the appropriate antibiotic to the medium. If multiple forms of the plasmid are present in the transformation mix, as occurs when cloning, not all clones will be identical. This means selection beyond antibiotic resistance will be required to screen for the clone that contains the correct of the plasmid. This second level of screening is typically carried out using either restriction enzyme digestion or polymerase chain reaction.

2.2.3. Small Scale Protein Expression

After being sequenced, all new constructs were transformed according to the traditional protocol in several different *E. coli* strains in order to achieve the best expression conditions with the highest purity. All proteins' expression has been tested in: *BL21DE3, BL21DE3plys, BL21DE3 Gold, BL21DE3 Codon*$^{+}$*, Origami plysS, RIPL, C41 and C43* in temperatures 18-25-30-37^{0}C and with different amounts of IPTG (0.5–1mM) and induction time (3 hours–5 hours–overnight). The

following day, colonies were picked up on the plate selecting for the expression plasmid, and transferred into 5 mL LB medium and 1 mM of Ampicilin or Kanamycin and the antibiotic selecting for the cell line, usually Chloramphenicol. The cultures were incubated at 37 °C in an incubator shaker. When their OD_{600} reached 0.6 - 0.8, the protein expression was induced by adding 0.5-1 mM IPTG. The cultures were incubated for 3 to 16 h. All culture samples were centrifuged at 10,000 rpm for 1 min. The supernatant was discarded and cell pellets were collected. 1x laemmli sample buffer were added to the samples for SDS PAGE analysis. The strain expressing the highest amount of protein with the highest purity.

2.2.4. Large Scale Protein Expression

A small amount of cells taken from a previously prepared glycerol stock were transferred to a flask containing 50 mL of 25 g/L LB medium and the antibiotic selecting for the expression vector and for the cell line, if necessary. The culture was incubated overnight at 37 °C in a shaker. The following morning, the overnight growth was added to 1 L of 25 g/L LB (rich) media or Minimal Media (M9), the antibiotic selecting for the cell line and the expression vector. The cells were grown at 37 °C in the shaker. When their OD_{600} reached 0.6 - 0.8, the expression was induced by adding 0.5-1 mM IPTG. The culture was left to grow at the selected temperature from the expression tests for three more hours. Then, the cells were harvested by centrifugation (6000 rpm at 4 °C for 20 min) using a Beckman Coulter™ JA-10 centrifuge. The supernatant was discarded. The cell pellet was then recovered and weighed.

2.2.5. Laemmli Extraction Method

E.coli cells, lysates or purified protein samples were resuspended in 1× Laemmli buffer or 2× Laemmli buffer respectively [166]. The samples were briefly vortexed and incubated at 95 ^{0}C for 10 min. Samples were then spun down at 14,000 g for 5 min at RT. The samples were then loaded on an SDS–PAGE gel.

2× Laemmli buffer: 4 % (w/v) SDS, 20 % (v/v) glycerol, 120 mM Tris-HCl pH 6.8, 0.2 M DTT, 0.01 % (w/v) bromophenol blue.

2.2.6. Electrophoresis

2.2.6.1. DNA agarose gel

DNA-agarose gel was used to confirm each step of the cloning process. They were also used as mean to separate the PCR products in order to purify the desired one. The matrix used for DNA

separation was 0.5 to 2% w/v agarose. The solvent used to dissolve the agarose powder was composed of Tris, EDTA and acetic acid (TAE). The samples were prepared with 6x or 10x loading buffer added to the DNA sample. The products of the reactions were confirmed by size comparison with a standard DNA ladder.

2.2.6.2. SDS-PAGE

SDS PAGE was used to confirm the success of protein expression or to estimate the purity of protein preparation. In the case of protein expression, the samples were prepared as follows: 1mL of the cell sample was collected before induction (t = 0 h) and after induction with IPTG (t = 3 h, 5h, overnight), the samples were centrifuged (5 min at 10,000 rpm) and 100 µL 1x laemmli buffer were added to the pellet. To confirm solubility, cells were subjected to sonication 1mL of the lysis mixture was collected and centrifuged for 5 min at 10,000 rpm. The pellet and supernatant were separated and 2x laemmli buffer was added to each. For purified protein, 10 µL of loading buffer were added to 10 µL of concentrated protein sample. Loading of 10 µL was typically used. The samples were loaded onto a 13.5% SDS page gel and run at 200 V for 70 - 90 min. The gel was stained with a solution of Coomasie blue™ (Giotto Biotech) and destained with MilliQ water. The proteins were identified by mass comparison with an unstained protein marker (Thermo Scientific), ranging from 14.4 to 166 kDa.

2.2.6.3. Native-page

For the determination of monomeric or multimeric protein states native page electrophoresis was applied. The gels used for this purpose were precast miniprotean gels from BioRad. Both the loading die and the running buffer did not contain SDS or other denaturing agent and was runned according to manufacturer's instructions. The protein's state was then identified either using Native mark unstained protein ladder for native page or a protein of similar characteristics to the expected of the unknown sample.

2.3.CELL LYSIS

To each gram of cells, 10 mL of lysis buffer were added.

2.3.1. Sonication is the most popular technique for lysing small quantities of cells (1-6 L of cell culture). Cells are lysed by liquid shear and cavitation. DNA is also sheared during sonication, so it is not necessary to add DNase to the cell suspension. The main problem is controlling the temperature. This is addressed by keeping the suspension on ice and using a number of short pulses (5-10 sec) with pauses (10-30 sec) to re-establish a low temperature. For cell quantities larger than

50 g the method is of limited value because of the difficulty in maintaining low temperatures and the long sonication times needed to reach adequate lysis. All sonication has been performed at 4°C and in ice-cold conditions.

2.3.2. Freezing and grinding. An alternative lysis method is to freeze the cells directly in liquid nitrogen and ground the frozen cells to a powder using a mortar and pestle that are chilled with liquid nitrogen. The powder can be stored indefinitely at -80°C and the cell lysate can be prepared by adding the powder to 5 volumes of buffer. This method has been used for expression tests or extraction from eukaryotic cells.

2.3.3. Osmotic shock has been used in order to extract proteins expressed in the periplasmic space of *E.coli*.

2.4. PROTEIN PURIFICATION

Protein purification is a series of processes intended to isolate a single type of protein from a complex mixture and it is vital for the characterization of the structure, function and interactions of the protein of interest. Separating steps exploit differences in protein size, physical-chemical properties and binding affinity.

The location of the expressed protein within the host will affect the choice of methods for its isolation and purification. Bacterial hosts may secret the protein into the growth media, transport it to the periplasmic space, express a cytosolic protein or store it as insoluble inside inclusion bodies within the cytoplasm. In the latter case, the first purification step is the extraction from inclusion bodies with a denaturing buffer (and post purification follow a refolding process); whereas in the other cases proteins are removed by following different extraction conditions in native conditions.

2.4.1. Metal ion affinity chromatography (IMAC)

Histidine tags are widely used because they are small and rarely interfere with the function, activity, or structure of target proteins. Immobilized metal ion affinity chromatography (IMAC) is the most common method for purifying native or denatured histidine-tagged proteins. IMAC chromatography media charged with divalent metal ions, such as nickel, binds selectively histidine-tagged proteins and permits the purification of soluble or insoluble histidine-tagged proteins when denaturing conditions are used. Nickel affinity chromatography gives a high yield of pure and active target protein. Imidazole competes with the poly-histidine tag for binding to the column. Thus, by increasing the concentration of imidazole in the binding and wash buffers, proteins nonspecifically bound to the column are released, while the histidine tagged protein remains bound until the final step of elution. After the affinity purification, the fusion-tag must be removed –if

needed- from the recombinant protein. Indeed, many expression vectors (as well as the vectors designed for this study, see **figure 9**) are engineered to express a protease cleavage site between the fusion-tag and the protein. Tobacco Etch Virus (TEV), Factor Xa and Thrombin are some examples of proteases that are normally used for such cleavage. In this case a second IMAC is necessary in order to separate the fusion from the target native protein.

2.4.2. Ion-exchange Chromatography

A separation method that depends upon the interaction between charged molecules and an oppositely charged chromatography resin. In cation exchange chromatography positively charged protein molecules (when pH < pI) bind to a negatively charged resin. Conversely, in anion exchange chromatography, negatively charged molecules (when pH > pI) bind to a positively charged resin. This method involves in both cases, anionic or cationic exchange, after equilibration the sample containing the target molecule in the same pH and ionic strength as the starting buffer is passing through the resin and the target molecule binds. All unbound molecules are washed out during the washing steps. During elution all biomolecules are released from the resin by changing the ionic strength in the buffer composition, i.e. using an ionic strength up to 1M Sodium Cloride or any other simple salt in order to release the bound proteins. Proteins are released according to the number of charged groups on their surface.

2.4.3. Gel filtration (GF) or Size exclusion chromatography (SEC)

Is the most commonly used purification step if the protein after affinity chromatography is not pure enough. It is the simplest and mildest of all chromatographic techniques. The support for GF chromatography is composed of beads which contain holes, called “pores”, of given sizes. Larger molecules which can’t penetrate the pores, move around the beads and migrate through the spaces which separate the beads themselves faster than the smaller molecules, which may penetrate the pores. Size exclusion can be performed on a “rough” level, separating the components of a sample in major groups to remove for example high or low molecular weight contaminants or to exchange buffers; while high resolution fractionation of biomolecules allows to isolate one or more components of a protein mixture, to separate monomers from aggregates and last but not least to determine molecular weights distribution analysis. Unlike ion exchange chromatography, gel filtration does not depend on any chemical interaction with protein, rather it is based on a physical property of the protein - that being the effective molecular radius (which relates to mass for most globular proteins).

2.4.4. Determination of protein concentrations

Protein concentrations were either estimated from measuring the absorbance at 280 nm (A280). Theoretical molar extinction coefficients were obtained from ProtParam analysis (http://ca.expasy.org/tools/protparam.html

2.5. PROTEIN EXPRESSION AND PURIFICATION PROTOCOLS DEVELOPED IN THIS STUDY

The genes encoding **cMMP12** and **cMMP12 R5** were transformed into competent Escherichia coli BL21 (DE3) strain according to the standard protocol. Bacteria were grown in LB medium containing 50 µg/mL ampicillin in at 37 °C. Protein expression was induced with 0.5 mM IPTG at OD_{600} 0.6, and cell growth was continued for a further 5 h. For expression of 15N and 13C-enriched cMMP-12, the bacteria were grown in minimal medium containing ^{15}N enriched $(NH4)_2SO_4$ and ^{13}C enriched glucose (Cambridge Isotope Laboratories). Cells were harvested by centrifugation and resus- pended in a buffer containing 25% sucrose, 50 mM Tris-HCl (pH 8), 0.1 M NaCl, 0.2 M EDTA, 1 mM DTT. Five to ten milligrams of lysozyme were added to the resulting suspension and stirred for 15-20 min at 4 °C. A buffer containing 2% Triton, 50 mM Tris- HCl (pH 8), 0.1MNaCl, 0.2M EDTA, and 1 mM DTT was added, and the suspension was sonicated (7-8 30 s cycles) and centrifuged at 40 000 rpm for 20 min at 4 °C. The same procedure was followed twice, first with 1M Urea, 50 mM Tris- HCl (pH 8) and then with 2M Urea, 50 mM Tris- HCl (pH 8). The resulting inclusion bodies were finally solubilized in 6 M Urea, 20 mM NaOAc pH 5.5. The insoluble material was removed by ultra-centrifugation at 40 000 rpm for 40 min at 4 °C. Then the protein was further purified using cationic exchange chromatography with a linear NaCl gradient 0-1 M. Fractions containing pure cMMP12 were identified by Coomassie staining 15% SDS-PAGE gels.
The protein was diluted to a final concentration of 0.1 mg/mL in 4 M Urea, 20 mM Tris-HCl (pH 8), 10 mM $CaCl_2$, 0.1 mM $ZnCl_2$ 0.3 M NaCl and dialyzed twice against a buffer containing 2M Urea, 20 mM Tris (pH 7.2), 10 mM $CaCl_2$, 0.1 mM $ZnCl_2$, 0.3 M NaCl. The protein was further dialyzed twice against 20 mM Tris (pH 7.2), 10 mM $CaCl_2$, 0.1 mM $ZnCl_2$, 0.3 M NaCl. The refolded protein solution was concentrated up to 15 mL and purified by size exclusion chromatography using Superdex 75 26/60 (Amersham Biosciences) and eluted with 20 mM Tris pH 7.2, 10 mM $CaCl_2$, 0.1 mM $ZnCl_2$, 0.3 M NaCl, and 0.2 M AHA. The eluted fractions were checked for purity on 15% gel by SDS-PAGE, and those containing the cMMP-12 protein were pooled and concentrated. The **F171D** (mutant for crystallization) and **F171D, E219A** (inactive mutant) mutants of **cMMP-12** were expressed and purified using the same procedure described above. An excess of

NNGH (N-Isobutyl-N-(4-methoxyphenylsulfonyl) glycyl hydroxamic acid) was added to the samples of **cMMP12 R5** to prevent auto-hydrolysis of the protein.

The gene encoding **cMMP14** was transformed into competent Escherichia coli *BL21 (DE3) Gold* strain according to the standard protocol. Bacteria were grown in LB medium containing 50 µg/mL ampicillin in at 37 °C. Protein expression was induced with 0.5 mM IPTG at OD_{600} 0.6, and cell growth was continued for a further 5 h. For expression of 15N and 13C-enriched cMMP-14, the bacteria were grown in minimal medium containing ^{15}N enriched $(NH4)_2SO_4$ and ^{13}C enriched glucose (Cambridge Isotope Laboratories). Cells were harvested by centrifugation and resus-pended in a buffer containing 25% sucrose, 50 mM Tris-HCl (pH 8), 0.1 M NaCl, 0.2 M EDTA, 1 mM DTT. Five to ten milligrams of lysozyme were added to the resulting suspension and stirred for 15-20 min at 4 °C. A buffer containing 2% Triton, 50 mM Tris- HCl (pH 8), 0.1MNaCl, 0.2M EDTA, and 1 mM DTT was added, and the suspension was sonicated (7-8 30 s cycles) and centrifuged at 40 000 rpm for 20 min at 4 °C. The same procedure was followed twice, first with 1M Urea, 50 mM Tris- HCl (pH 8) and then with 2M Urea, 50 mM Tris- HCl (pH 8). The resulting inclusion bodies were finally solubilized in 8 M Urea, 50 mM Tris pH 8.5. The insoluble material was removed by ultra-centrifugation at 40 000 rpm for 40 min at 4 °C. Fractions containing pure cMMP14 were identified by Coomassie staining 15% SDS-PAGE gels.

The protein was diluted to a final concentration of 0.1 mg/mL in 6 M Urea, 50 mM Tris-HCl (pH 8.5) and dialyzed twice against a buffer containing 2M Urea, 50 mM Tris (pH 8.5), 10 mM $CaCl_2$, 0.01 mM $ZnCl_2$, 0.1 M NaCl. The protein was further dialyzed twice against 1M Urea, 50 mM Tris (pH 7.5), 10 mM $CaCl_2$, 0.01 mM $ZnCl_2$, 0.1 M NaCl and three times against 50 mM Tris (pH 7.5), 5 mM $CaCl_2$, 0.001 mM $ZnCl_2$, 0.1 M NaCl. The refolded protein solution was concentrated up to 15 mL and purified by size exclusion chromatography using Superdex 75 26/60 (Amersham Biosciences) and eluted with 20 mM Tris pH 7.5, 5 mM $CaCl_2$, 0.1 M NaCl, and 0.2 M AHA. The eluted fractions were checked for purity on 15% gel by SDS-PAGE, and those containing the cMMP-14 protein were pooled and concentrated.

The gene encoding **Hemopexin MMP14 TMB** was transformed into competent Escherichia coli *C41*strain according to the standard protocol. Bacteria were grown in LB medium containing 50 µg/mL Kanamycin at 37 ^{0}C. Protein expression was induced with 1 mM IPTG at OD_{600} 0.6, and cell growth was continued overnight at 25^{0}C. For expression of 15N and 13C-enriched **HPX-TMB MMP-14**, the bacteria were grown in minimal medium containing ^{15}N enriched $(NH4)_2SO_4$ and ^{13}C enriched glucose (Cambridge Isotope Laboratories). Cells were harvested by centrifugation and resus- pended in a buffer containing 25% sucrose, 50 mM Tris-HCl (pH 8), 0.1 M NaCl, 0.2 M EDTA, 1 mM DTT. Five to ten milligrams of lysozyme were added to the resulting suspension and

stirred for 15-20 min at 4 °C. A buffer containing 2% Triton, 50 mM Tris- HCl (pH 8), 0.1MNaCl, 0.2M EDTA, and 1 mM DTT was added, and the suspension was sonicated (7-8 30 s cycles) and centrifuged at 40 000 rpm for 20 min at 4 °C. The same procedure was followed twice, first with 1M Urea, 50 mM Tris- HCl (pH 8) and then with 2M Urea, 50 mM Tris- HCl (pH 8). The resulting inclusion bodies were finally solubilized in 8 M Urea, 50 mM Tris pH 8.0, 1% SDS. The insoluble material was removed by ultra-centrifugation at 40 000 rpm for 40 min at 4 °C. Fractions containing pure HPX TMB MMP14 were identified by Coomassie staining 13.5% SDS-PAGE gels.

The protein was diluted to a final concentration of 0.1 mg/mL in 6 M Urea, 50 mM Tris-HCl (pH 8.5) and dialyzed twice against a buffer containing 2M Urea, 50 mM Tris (pH 8.5), 10 mM $CaCl_2$, 0.01 mM $ZnCl_2$, 0.1 M NaCl, 5 mM β-mercaptoethanol, 1 mM 2-hydroxy- ethyl disulfide. The protein was further dialyzed twice against 1M Urea, 50 mM Tris (pH 8.5), 10 mM $CaCl_2$, 0.1 mM $ZnCl_2$, 0.1 M NaCl and three times against 50 mM Tris (pH 7.5), 5 mM $CaCl_2$, 0.1 mM $ZnCl_2$, 0.1 M NaCl. The refolded protein solution was concentrated up to 15 mL and purified by size exclusion chromatography using Superdex 75 26/60 (Amersham Biosciences) and eluted with 20 mM Tris pH 7.5, 5 mM $CaCl_2$, 0.1 M NaCl. The eluted fractions were checked for purity on 15% gel by SDS-PAGE, and those containing the HPX TMB MMP-14 protein were pooled and concentrated.

The gene encoding **full length MMP14 with Transmembrane domain** was transformed into competent Escherichia coli *C41p Rosetta* strain according to the standard protocol. Bacteria were grown in LB medium containing 50 µg/mL Kanamycin and 34 µg/mL Chloramphenicol in at 37 °C. Protein expression was induced with 0.5 mM IPTG at OD_{600} 0.6, and cell growth was continued overnight. For expression of 15N and 13C-enriched ffl MMP-14 TMB, the bacteria were grown in minimal medium containing ^{15}N enriched $(NH4)_2SO_4$ and ^{13}C enriched glucose (Cambridge Isotope Laboratories). Cells were harvested by centrifugation and resus- pended in a buffer containing 25% sucrose, 50 mM Tris-HCl (pH 8), 0.1 M NaCl, 0.2 M EDTA, 1 mM DTT. Five to ten milligrams of lysozyme were added to the resulting suspension and stirred for 15-20 min at 4 °C. A buffer containing 2% Triton, 50 mM Tris- HCl (pH 8), 0.1MNaCl, 0.2M EDTA, and 1 mM DTT was added, and the suspension was sonicated (7-8 30 s cycles) and centrifuged at 40 000 rpm for 20 min at 4 °C. The same procedure was followed with 1M Urea, 50 mM Tris- HCl (pH 8), with 2M Urea, 50 mM Tris- HCl (pH 8) and finally with 4M Urea, 50 mM Tris- HCl (pH 8). The resulting inclusion bodies were finally solubilized in 8 M Urea, 50 mM Tris pH 8.0, 1% SDS. The insoluble material was removed by ultra-centrifugation at 40 000 rpm for 40 min at 4 °C. Fractions containing pure ffl MMP14 TMB were identified by Coomassie staining 13.5% SDS-PAGE gels.

The protein was diluted to a final concentration of 0.1 mg/mL in 6 M Urea, 50 mM Tris-HCl (pH 8.5) and dialyzed twice against a buffer containing 2M Urea, 50 mM Tris (pH 8.5), 10 mM $CaCl_2$,

0.01 mM $ZnCl_2$, 0.1 M NaCl, 5 mM β-mercaptoethanol, 1 mM 2-hydroxy- ethyl disulfide. The protein was further dialyzed against 1M Urea, 50 mM Tris (pH 7.5), 10 mM $CaCl_2$, 0.1 mM $ZnCl_2$, 0.1 M NaCl and against 50 mM Tris (pH 7.5), 5 mM $CaCl_2$, 0.1 mM $ZnCl_2$, 0.1 M NaCl. The refolded protein solution was concentrated up to 15 mL and purified by size exclusion chromatography using Superdex 75 26/60 (Amersham Biosciences) and eluted with 20 mM Tris pH 7.5, 5 mM $CaCl_2$, 0.1 M NaCl. The eluted fractions were checked for purity on 13.5% gel by SDS-PAGE, and those containing the protein were pooled and concentrated.

The gene encoding **His_6-GFP** and **His_6-HABP-GFP-HABP** were transformed into Escherichia coli *BL21(DE3)* cells which were subsequently cultured in rich (LB) or ^{13}C,^{15}N-labelled minimal medium (M9). Cells were grown at 37^0C, until OD 0.6–0.8 and subsequently induced with IPTG with a final concentration of 0.75 mM for 5 h at the same temperature and then overnight at 14^0C. The cells were then harvested and then extracted by sonication in 20mM Tris- HCl at pH 8.0, 500mM NaCl. The lysate was ultracentrifuged for 30 min at 40000 rpm at 4^0C and the supernatant was then purified by Ni-NTA affinity chromatography. In the case of **His_6-GFP** the Histidine tag was removed after overnight incubation at room temperature with TEV protease and the protein was subjected to a second Ni-NTA purification in order to remove the protease and the un-digested protein. The protein was then dialyzed against 25mM Tris pH 7.5. In the case of **His_6-HABP-GFP-HABP**, the final purification step includes a Gel Filtration using the Superdex 75 26/60 column in order to exchange the buffer to 25mM Tris pH 7.4.

The gene encoding **GFP-R5** were transformed into Escherichia *BL21(DE3)* cells which were subsequently cultured in rich (LB) or ^{13}C,^{15}N-labelled minimal medium (M9). Cells were grown at 37^0C, until OD 0.6–0.8 and subsequently induced with IPTG with a final concentration of 0.5 mM for 5 h. GFP-R5 was then extracted from harvested cells by sonication and subsequent ultra-centrifugation (40 min, 40000 rpm). The protein was first purified from the crude extract with an anionic exchange column (Q-FF 16/10, A buffer: Tris 50 mM pH 8, B buffer: Tris 50 mM pH 8, NaCl 1 M). The GFP-R5 was finally purified with gel filtration using a Superdex 75 26/60 in Tris 50 mM, NaCl 300 mM, pH 8.

The gene encoding **His_6-HABP-SOD (AS)-HABP** was transformed according to the standard protocol into *BL21(DE3)* Escherichia coli cells for over-expression. The highest expression levels were achieved with 0.75 mM Isopropyl thio-β-D-galactoside and overnight induction at 37^0C. The cells were then harvested and then extracted by sonication in 20mM Tris-HCl at pH 8.0. The lysate was ultracentrifuged for 30 min at 40000 rpm at 4^0C and the suprenatant was then purified with low affinity chromatography, followed by Ni-NTA affinity chromatography. The final purification step

includes a Gel Filtration using the Superdex 75 26/60 column in order to exchange the buffer to 20mM Tris pH8.

The genes encoding **CAII** and **His_6-HABP-CAII** were transformed according to the standard protocol into competent RIPL codon plus Escherichia coli cells for over-expression. 1 Liter of medium was inoculated and incubated at 37^0C overnight, then harvested at 4000 rpm and resuspended in another liter of medium. The highest expression levels were achieved with 1 mM Isopropyl thio-β-D-galactoside and 5 hours of induction at 37^0C. The cells were then harvested and then extracted by sonication in 20mM Tris- HCl at pH 8.0, 500mM NaCl. The lysate was ultracentrifuged for 30 min at 40000 rpm at 4^0C and the supernatant was then purified by Ni-NTA affinity chromatography. The final purification step includes a Gel Filtration using the Superdex 75 26/60 column in order to exchange the buffer to 25mM Tris pH 7.4.

The gene encoding **ANSII** in pET-21a was transformed into Escherichia coli *BL21(DE3)C41* cells which were subsequently cultured in rich (LB) containing ampicillin (0,1 mg/mL). Cells were grown at 37^0C, until A_{600nm} reached 0.6-0.8 and subsequently induced with IPTG (0.75 mM final concentration). Cells were further grown at 25^0C overnight and then harvested by centrifugation at 6500 rpm (JA-10 Beckman Coulter) for 20 min at 4^0C. All the purification procedures were carried out at 4^0C. The pellet was resuspended in 20 mM Tris-HCl, pH 8.6, 15 mM EDTA, 20% sucrose buffer (60 mL per liter of culture) and then kept for 20 min under magnetic stirring. Suspension was centrifuged at 10000 rpm (F15-6x100y Thermo Scientific) for 30 min and supernatant discarded. The pellet was re-suspended in H2O Milli-Q (60 mL per liter of culture) and then kept for 20 min under magnetic stirring. Suspension was centrifuged again at 10000 rpm (F15-6x100y Thermo Scientific) for 30 min. The supernatant was treated with ammonium sulfate from 50% to 90% to precipitate the ANSII protein. Then the protein was re-dissolved in minimal amount of 20 mM Tris-HCl pH 8.6 buffer and dialyzed extensively against the same buffer. The ANSII was further purified by Q-Sepharose column using 20 mM Tris-HCl pH 8.6 buffer with a linear NaCl gradient 0-1 M. Fractions containing pure ANSII HABP were identified by Coomassie staining 13.5% SDS-PAGE gels. The ANSII was further purified by gel filtration using a Superdex 75 26/60 column in 25 mM Tris-HCl pH 7.4 buffer

The gene encoding **ANSII-HABP** in pET-21a-HABP was transformed into Escherichia coli *BL21(DE3)C41* cells which were subsequently cultured in rich (LB) containing ampicillin (0,1 mg/mL). Cells were grown at 37^0C, until A600nm reached 0.6-0.8 and subsequently induced with IPTG (0.75 mM final concentration). Cells were further grown at 25^0C overnight and then harvested by centrifugation at 6500 rpm (JA-10 Beckman Coulter) for 20 min at 4^0C. All the purification procedures were carried out at 4^0C. The pellet was resuspended in 20 mM Tris-HCl, pH 9.5, 15 mM

EDTA, 20% sucrose buffer (60 mL per liter of culture) and then kept for 20 min under magnetic stirring. Suspension was centrifuged at 10000 rpm (F15-6x100y Thermo Scientific) for 30 min and supernatant discarded. The pellet was resuspended in H_2O Milli-Q (60 mL per liter of culture) and then kept for 20 min under magnetic stirring. Suspension was centrifuged again at 10000 rpm (F15-6x100y Thermo Scientific) for 30 min. The supernatant was treated with ammonium sulfate from 30% to 90% to precipitate the ANSII protein. Then the protein was re-dissolved in minimal amount of 20 mM Tris-HCl pH 9.5 buffer and dialyzed extensively against the same buffer. The ANSII was further purified by Q-Sepharose column using 20 mM Tris-HCl pH 9.5 buffer with a linear NaCl gradient 0-1 M. Fractions containing pure ANSII HABP were identified by Coomassie staining 13.5% SDS-PAGE gels. The ANSII was further purified by gel filtration using a Superdex 75 26/60 column in 25 mM Tris-HCl pH 7.4 buffer and concentrated with Amicon ultrafiltration device to a final concentration of 0.4 mM. The overall yield of purified protein is 35 mg/L. The purified protein was analyzed on native PAGE gel (BioRad Mini-PROTEAN Precast Gel) to reveal the molecular mass of the protein assemblies and on a 13.5%SDS-PAGE gel to reveal molecular mass of the monomeric protein.

The gene encoding **ANSII-R5** in pET-21a-R5 was transformed into Escherichia coli *BL21(DE3)C41* cells which were subsequently cultured in rich (LB) containing ampicillin (0,1 mg/mL). 1 Liter of medium was inoculated and incubated at 37^0C overnight, then harvested at 4000 rpm and resuspended in another liter of medium. The highest expression levels were achieved with 0.75 mM Isopropyl thio-β-D-galactoside and overnight induction at 37^0C. Cells were then harvested by centrifugation at 6500 rpm (JA-10 Beckman Coulter) for 20 min at 4^0C. All the purification procedures were carried out at 4^0C. The pellet was resuspended in 20 mM Tris-HCl, pH 9.5, 15 mM EDTA, 20% sucrose buffer (60 mL per liter of culture) and then kept for 20 min under magnetic stirring. Suspension was centrifuged at 10000 rpm (F15-6x100y Thermo Scientific) for 30 min and supernatant discarded. The pellet was resuspended in H_2O Milli-Q (60 mL per liter of culture) and then kept for 20 min under magnetic stirring. Suspension was centrifuged again at 10000 rpm (F15-6x100y Thermo Scientific) for 30 min. The supernatant was treated with ammonium sulfate from 30% to 90% to precipitate the ANSII protein. Then the protein was re-dissolved in minimal amount of 20 mM Tris-HCl pH 9.5 buffer and dialyzed extensively against the same buffer. The ANSII was further purified by Q-Sepharose column using 20 mM Tris-HCl pH 9.5 buffer with a linear NaCl gradient 0-1 M. Fractions containing pure ANSII R5 were identified by Coomassie staining 13.5% SDS-PAGE gels. The ANSII was further purified by gel filtration using a Superdex 75 26/60 column in 25 mM Tris-HCl pH 7.5 buffer. The overall yield of purified protein is 30 mg/L. The purified protein was analyzed on native PAGE gel (BioRad Mini-PROTEAN Precast Gel) to reveal

the molecular mass of the protein assemblies and on a 13.5%SDS-PAGE gel to reveal molecular mass of the monomeric protein.

2.6. CATALYTIC ACTIVITY ASSAYS

2.6.1. Asparaginase Activity assay

Enzymatic activity analysis of ANSII and ANSII HABP were performed according to Sigma Aldrich with slight modifications. The procedure comprises the following steps. A 2ml solution containing 10mM of Asparagine solubilized in 25mMTris buffer pH 8.6 is incubated at 37^0C for 10 minutes. Then an enzyme solution of known concentration or 0.5-6 mg or entrapped enzyme is added and incubated for 30 minutes at 37^0C.The reaction is then stopped by adding TCA to a final concentration of 68mM. Then 0.2 ml of the reaction were added to 4.3 ml of Deionized water and the sample was treated with 1ml of Nessler's reagent. After 1 minute of incubation the optical density was measured at 436nm using a spectrophotometer. The activity values of samples were average of three - repeated measurements.

2.6.2. MMPs Activity Assays

The activity tests for MMPs, as well as binding curves for the evaluation of the binding to new inhibitors were curried out using P126 [Mca-Pro-Leu-Gly-Leu-Dpa-Ala-Arg-NH2 AcOH]. P 126 is a fluorogenic substrate of 1093.2 Da for nearly all matrix metalloproteinase (MMP) enzymes, and ADAM17/TACE. This highly-quenched (99.5%) substrate is useful for inhibitor screening and kinetic analysis. The Mca [(7-methoxycoumarin-4-yl) acetyl] is a fluorophore (Ex.: 328 nm, Em.: 393 nm). When the peptide is bound to the enzyme, the Dpa [N-3-(2,4-dinitrophenyl)-L-a,β-diaminopropionyl] absorbs the fluorescence emitted by the Mca (quencher of fluorescence). The MMPs cleave the bond between Gly-Leu separating Mca from Dpa. In this way, Mca gets excited at 328nm and reemits at a higher wavelength (max 393nm). The peptide has a diverse affinity for the various MMPs, i.e. for MMP14 is 24×10^4 and for MMP12 is 6×10^4. The affinity is expressed from the specificity constant, which is given by the ratio of the catalytic constant (K_{cat}) to the dissociation constant (substrate-enzyme) [$\mathbf{K_{specificity}=K_{cat}\,/\,K_m}$].

K_{cat} is called turn-over number and represents the maximum number of molecules of substrate that are converted to product. K_m is the dissociation constant expressing how much of the substrate is bound to the catalytic site of the enzyme in a unit of time. Hence, the angular coefficient of the line is higher when the ratio K_{cat} / K_m is higher.

An initial stock of 5 to 10 μM of enzyme is diluted to the following duffer solution: 50mM Hepes pH 7, 5mM $CaCl_2$, 0.1mM $ZnCl_2$, Brij-35 0.05% to a final concentration of 5nM to 25nM in the case of the enzyme that is not very active. Just before the start of the experiment 350nM of P126 were added to the cell. In case that we needed to test new MMP inhibitors we have repeated the same procedure titrating each time a different concentration of inhibitor starting from a concentration 7nM in most of the cases. The final concentration depends on the affinity of the inhibitor for the enzyme.

2.7. CHARACTERIZATION OF OLIGOMERIZATION STATES

2.7.1. Analytical Gel Filtration Chromatography shares the same principles with gel filtration. Through a Superdex 200 HR 10/300, connected to ÄKTA pure (25 L), it is feasible to determine the approximate molecular weight of a compound. For the determination of the molecular weight of the protein, the column was calibrated by passing proteins of known molecular weight. Standard proteins used in this study for the calibration were blue dextran, albumin, ovalbumin, alkaline phosphatase, carbonic anhydrase, cytochrome c. Molecules elute depending on their molecular size, i.e. the bigger molecules elute first while smaller molecules elute last. (Molecular size in this technique refers to the effective molecular radius that only in the case of the globular molecules is the molecular mass.) The flow used for this column was 0.5 ml/min and the injection volume 50 ul.

2.7.2. Dynamic Light Scattering (DLS) is based on measuring the time dependent fluctuation of scattered light intensity by macromolecular solution. This light intensity fluctuation can be transformed by non-linear fitting of autocorrelation function into the molecular size distribution. This method gives a possibility of calculating diffusion coefficient, hydrodynamic radius, molecular weight and polydispersity of investigated samples. **Size-exclusion chromatography** (SEC), coupled with **laser light scattering** (LS), **refractive index** (RI), and **ultraviolet** (UV) detection, provides a universal approach for determination of the molar mass and oligomeric state in solution of native proteins as well as glycosylated proteins, PEGylated proteins or membrane proteins solubilized in non-ionic detergents. In the SEC-UV/LS/RI approach, SEC serves solely as a separation /fractionation step, while the responses from the three detectors are utilized to calculate the molar mass for the polypeptide portion of the native or modified protein. The amount of sugar, lipid, or detergent bound to the polypeptide chain can also be estimated from the SEC-UV/LS/RI analysis.

2.8. PROTEIN CRYSTALIZATION AND X-RAY DIFFRACTION

In order to achieve crystallization of the catMMP12 F171D we have used several different PEG based buffers, homemade based upon previous publications with changes and PEG ion crystal screen kits purchased from Hampton Research. Crystallization was carried out with the sitting drop vapor diffusion method at 20°C. Several different pH from 7.2 to 8.5 were used and several different concentrations from 0.8mM up to 2.2mM. For cat MMP12–AHA adduct an aliquot of 2µl of protein solution (10 mM Tris-Cl, 5 mM $CaCl_2$, 0.1 mM $ZnCl_2$, 300 mM NaCl,200 mM AHA, pH 8) was mixed with 2µl of reservoir buffer (0.1 M Tris-HCl, 25% PEG 6000 or 30% PEG 8000, 200 mM AHA, pH 8). The final protein concentration was 1.5 mg/ml. The crystals where afterwards soaked with different inhibitors. The data collection was carried out in-house, using a PX-Ultra copper sealed tube source (Oxford Diffraction) equipped with an Onyx CCD detector. The data set was collected at 100 K and the crystals used for data collection were cryo-cooled using a solution containing 10% ethylene glycol in the mother liquor. The crystals diffracted from 2.0 Å to 3.0 Å resolution.

2.9. BIOMINERALIZATION REACTIONS

2.9.1. Silicification reaction

The samples of catMMP-12 in silica were prepared using Poly L-Lysine as a promoter for the polymerization of silica. MMP-12 (200 µL, 45 mg/mL in buffer A: 20mM Tris, pH 7.2, 50 mM NaCl, 10mM $CaCl_2$,0.1mM $ZnCl_2$, NNGH in excess), Poly L-Lysine (50 µL, 10 mg/mL in H_2O; MW: 4000–15000 Da) were added to 1.5 mL vials and shaken for 10 min. To the resulting solution, a100mm solution of silicic acid (250 µL) in buffer A(freshly prepared from a stock solution of 1M silicic acid obtained by the addition of 1mM HCl (850 µL) to pure tetramethyl orthosilicate (TMOS;150 µL) were added and the mixture was re- acted for 10 min at room temperature. For the sample containing R5 as an external promoter, the same protocol was applied, but with R5 (50 µL, 10 mg/mL) in H2Owith 5mM dithiothreitol (DTT) instead of Poly(L-Lysine). The samples of catMMP12–R5 and GFP-R5 were prepared by using the same protocol, but with water instead of the promoter solution to maintain the same experimental conditions as those used with the external promoters. Samples containing lysozyme and lysozyme+bovine serum albumin (BSA) were prepared as follows: BSA (200 µL, 40 mg/mL) in buffer B: 20mM Tris pH 7.5) and lysozyme (50 µL, 10 mg/mL) in H2O) were added to 1.5 mL vials and shaken for 10 min. To the resulting solution, a100 mM solution of silicic acid (250 mL) in buffer B(freshly prepared from a stock solution of 1m silicic acid obtained from TMOS, see above) were added and the mixture reacted for

10 min at room temperature. For comparison, samples containing lysozyme only were prepared by using the same protocol, but replacing BSA (200 μL) with buffer B (200 μL).After the polycondensation reaction, all samples were centrifuged at 8000 rpm and the supernatant was removed. To remove unreacted TMOS, the precipitates were then washed three times with a buffer containing 20mM Tris (pH 7.2), 10mM $CaCl_2$, and 0.1mM $ZnCl_2$, in the case of catMMP12 and catMMP12–R5, and buffer B, in the case of lysozyme and BSA. The suspension was used to fill the 4mm rotor using an ultracentrifugation device and NMR measurements were performed immediately.

2.9.2. Biomineralization reaction for the formation of HA

To assess the mineralization capabilities of the chimeric proteins co-expressed with the peptides, a mineralization model based on an alkaline phosphatase (ALP) solution was used. The ALP is added to the protein solution to allow the diffusion of Ca^{2+} and the enzymatic hydrolysis of the β-Glycerophosphate ions to the protein. The ALP then releases the PO_4^{3-} groups, which react with the calcium ions to form HA.

The protocol for a successful biomineralization published by Gungormus et al. [7] requires a protein concentration of 0.4 mM in 25 mM Tris-HCl pH 7.4 with 24 mM Ca^{2+} and 14.4 mM β-glycero phosphate with a final concentration of alkaline phosphatase at 1.4 μg/mL. The reaction mixture was then incubated at 310 K for 24 hours, and finally centrifuged at 10000 rpm (Hettich Mikro 200R) for 15 minutes at 273 K. Then, the supernatant of the reaction was removed and the pellet was washed with MilliQ water until all free protein was removed.

BIBLIOGRAPHY:

1.Ravera E., Schubeis T., Martelli T., Marco Fragai M., Parigi G., Luchinat C. (2015) NMR of sedimented, fibrillized, silica-entrapped and microcrystalline (metallo)proteins. Journal of Magnetic Resonance, 253, 60–70

2.Ravera E., Martelli T., Geiger Y., Fragai M., Goobes G., Luchinat C. (2016) Biosilica and bioinspired silica studied by solid-state NMR, Coordination Chemistry Reviews [http://dx.doi.org/10.1016/j.ccr.2016.06.003]

3.Lechner C.C., Becker C.F.W. (2015) Silaffins in Silica Biomineralization and Biomimetic Silica Precipitation Mar. Drugs, 13, 5297-5333.

4.Wang X., Schröder H.C., Müller W.E.G., (2014) Enzyme-based biosilica and biocalcite: biomaterials for the future in regenerative medicine, Trends in Biotechnology, 32(9): 441-447

5.Palmer L.C., Newcomb C.J., Kaltz S.R., Spoerke E.D., Stupp S.I. (2008) Biomimetic systems for hydroxyapatite mineralization inspired by bone and enamel. Chemical Reviews, 108(11):4754–4783.

6.Wang G., Cao R.Y., Chen R., Mo L., Han J.F., Wang X., Xu X., Jiang T., Deng Y.Q., Lyu K., Zhu S.Y., Qin E.D., Tang R., Qin C.F.(2013) Rational design of thermostable vaccines by engineered peptide-induced virus self-biomineralization under physiological conditions. PNAS, 110 (19): 7619-7624

7.Gungormus M., Fong H., Kim I.W., Spencer Evans J., Tamerler C., Sarikaya M. (2008) Regulation of in vitro calcium phosphate mineralization by combinatorially selected hydroxyapatite-binding peptides. Biomacromolecules, 9(3): 966-973.

8.Roy M.D., Stanley S.K., Amis E.J., Becker M.L. (2008) Identification of a highly specific hydroxyapatite-binding peptide using phage display. Advanced Materials, 20(10):610–617.

9.Holt C., Sørensen E.S., Clegg R.A. (2009) Role of calcium phosphate nanoclusters in the control of calcification. FEBS Journal, 276(8):2308–2323.

10.He G., Dahl T., Veis A., George A. (2003) Nucleation of apatite crystals in vitro by self-assembled dentin matrix protein 1. Nature Materials, 2(8):552–558.

11.Anastas P., Warner J. (2000) Green Chemistry: Theory and Practice, Oxford University Press, New York, p.152.

12.Anastas P.T., Kirchhoff M.M. (2002) Origins, current status, and future challenges of green chemistry. Acc. Chem. Res., 35, 686 –694.

13.Sheldon R.A. (2008) E factors, green chemistry and catalysis: an odyssey. Chem. Commun., 29, 3352 –3365.

14.Riva S.(2006) Laccases: blue enzymes for green chemistry. Trends Biotechnol., 24, 219 – 226.

15.Cao L. (2006) Carrier-Bound Immobilized Enzymes: Principles, Application and Design, John Wiley & Sons, Hoboken, NJ.

16.Katchalski- Katzir E.(1993) Immobilized enzymes- learning from past successes and failures. Trends Biotechnol., 11, 471–478.

17.Liang J.F., Li Y.T., Yang V.C. (2000) Biomedical application of immobilized enzymes. J. Pharm. Sci., 89, 979–990.

18.Kandimalla V.B., TripathiV.S., Ju H. (2006) Immobilization of biomolecules in sol-gels: Biological and analytical applications. Crit. Rev. Anal. Chem., 36, 73–106.

19.Nisha A.K.S., Karthick S.A., Gobi N. (2012) A Review on Methods, Application and Properties of Immobilized Enzyme Chem. Sci. Rev. Lett., 1, 148 – 155.

20.Betancor L., Luckarift H.R. (2008) Bioinspired enzyme encapsulation for biocatalysis Trends Biotechnol., 26, 566–572.

21.Mateo C., Palomo J.M., Fernandez-Lorente G., Guisan J.M., Fernandez-Lafuente R. (2007) Improvement of enzyme activity, stability and selectivity via immobilization techniques. Enzyme Microb. Technol., 40,1451–

22.Sheldon R. (2007) Enzyme Immobilization: The quest for optimum performance. Adv. Synth. Catal., 349, 1289–1307

23.Wang Y. and Caruso F. (2004) Enzyme encapsulation in nanoporous silica spheres. Chem. Comm., 1528–1529

24.Hildebrand M., Volcani B.E., Gassmann W., Schroeder J.I. (1997) A gene family of silicon transporters. Nature, 385: 688–689.

25.Pickett-Heaps J., Schmid MM, Edgar LA. (1990) The cell biology of diatom valve formation. In Progress in Phycological Research, Vol. 7, Round FE, Chapman DJ (eds). Biopress: Bristol, 1–169.

26.Poulsen N., Kroger N (2004) Silica Morphogenesis by Alternative Processing of Silaffins in the Diatom Thalassiosira pseudonana. J. Biol. Chem., 279, 42993–42999.

27.Kröger N., Deutzmann R., Sumper M. (2001) Silica-Precipitating peptides from diatoms. The chemical structure of silaffin-1a from *Cylindrotheca fusiformis*. J. Biol. Chem., 276, 26066–26070.

28.Kröger N, Lorenz S, Brunner E, Sumper M. (2002) Self-assembly of highly phosphorylated silaffins and their function in biosilica morphogenesis. Science, 298, 584–586.

29.Kröger N., Deutzmann R., Sumper M. (1999) Polycationic peptides from diatom biosilica that direct silica nanosphere formation. Science, 286, 1129–1132.

30.Kröger N., Bergsdorf C., Sumper M. (2011) Frustulins: Domain conservation in a protein family associated with diatom cell walls. Eur. J. Biochem., 239, 259–264.

31.Scheffel A., Poulsen N., Shian S., Kröger N. (2011) Nanopatterned protein microrings from a diatom that direct silica morphogenesis. Proc. Natl. Acad. Sci. USA, 108, 3175–3180.

32.Wenzl S., Hett R., Richthammer P., Sumper M. (2008) Silacidins: Highly acidic phosphopeptides from diatom shells assist in silica precipitation in vitro. Angew. Chem. Int. Ed., 47, 1729–1732.

33.Senior L., Crump M.P., Williams C., Booth P.J., Mann S., Perriman A.W., Curnow P. (2015) Structure and function of the silicifying peptide R5. J. Mater. Chem. B, 3, 2607–2614.

34.Poulsen N., Sumper M., Kröger N. (2003) Biosilica formation in diatoms: Characterization of native silaffin-2 and its role in silica morphogenesis. Proc. Natl. Acad. Sci. USA, 100, 12075–12080.

35.Luckarift H.R., Spain JC, Naik RR, Stone MO. (2004) Enzyme immobilization in a biomimetic silica support. Nat. Biotechnol., 22, 211–213

36.Kröger N. (2007) Prescribing diatom morphology: toward genetic engineering of biological nanomaterials. Curr. Opin. Chem. Biol., 11, 662–669

37.Luckarift H.R., Dickerson M.B., Sandhage K.H., and Spain J.C. (2006) Rapid, Room-Temperature Synthesis of Antibacterial Bionanocomposites of Lysozyme with Amorphous Silica or Titania. Small, 2, No.5, 640–643

38.Linde A., Lundgren T. (1995) From serum to the mineral phase: The role of the odontoblast in calcium transport and mineral formation. Int. J.Dev. Biol., 39, 213–222.

39.Butler W.T., Ritchie H. (1995) The nature and functional significance of dentin extracellular matrix proteins. Int. J.Dev. Biol., 39, 169–179.

40.Weiner S., Veis A., Beniash E., Arad T., Dillon J.W., Sabsay B., Siddiqui F. (1999) Peritubular dentin formation: crystal organization and the macromolecular constituents in human teeth. J. Struct. Biol., 126, 27–41.

41.Blumenthal N.C., Posner A.S. (1973) Hydroxyapatite: mechanism of formation and properties. Calc. Tiss. Res., 13, 235–243.

42.Eanes E.D., Gillessen I.H. & Posner A.S. (1965) Intermediate states in the precipitation of hydroxyapatite. Nature 208, 365–367.

43.Hunter G.K., Hauschka P.V., Poole A.R., Rosenberg L.C., Goldberg H.A. (1996) Nucleation and inhibition of hydroxyapatite formation by mineralized tissue proteins. Biochem. J., 317, 59–64.

44.Boskey A.L. (1995) Osteopontin and related phosphorylated sialoproteins: effects on mineralization. Ann. NY Acad. Sci., 760, 249–256.

45.Xiao S., Yu C., Chou X., Yuan W., Wang Y., Bu L., Fu G., Qian M., Yang J, Shi Y., Hu L., Han B., Wang Z., Huang W., Liu J., Chen Z., Zhao G., Kong X. (2001) Dentinogenesis imperfecta 1 with or without progressive hearing loss is associated with distinct mutations in DSPP. Nature Genet., 27, 201–204.

46.Kinney J. H., Pople J.A., Driessen C.H., Breunig T.M., Marshall G.W., Marshall S.J. (2001) Intrafibrillar mineral may be absent in dentinogenesis imperfecta type II (DI-II). J. Dent.Res., 80, 1555–1559

47.Douglas W.H., Reeh E.S., Ramasubbu N., Raj P.A., Bhandary K.K., and Levine M.J. (1991) Statherin: A major boundary lubricant of human saliva. Biochem. Biophys. Res. Commun., 180,91-97

48.Bennick A, McLaughlin A.C, Grey A.A, Madapallimattam, G. (1981) The location and nature of calcium-binding sites in salivary acidic proline-rich phosphoproteins. J. Biol. Chem., 256,4741–4746

49.Johnsson M., Richardson C.F., Bergey E.J., Levine M.J., and Nancollas G.H. (1991) The effects of human salivary cystatins and statherin on hydroxyapatite crystallization. Arch. Oral Biol., 36, 631-636

50.Raj P.A., Johnsson M., Levine M.J., Nancollas G.H.(1992) Salivary statherin: Dependence on sequence, charge, hydrogen bonding potency, and helical conformation for adsorption to hydroxyapatite and inhibition of mineralization J. Biol. Chem., Vol 267, 9, 5968-5976

51.George A., Sabsay B., Simonian P.A., Veis A. (1993) Characterization of a novel dentin matrix acidic phosphoprotein. Implications for induction of biomineralization. J. Biol. Chem., 268, 12624–12630.

52.Qin C., Brunn J.C., Jones J., George A., Ramachandran A., Gorski J.P., Butler W.T. (2001) Comparative study of sialic acid-rich proteins in rat bone and dentin. Eur. J. Oral. Sci., 109, 133–141.

53.George A., Silberstein R. & Veis A. (1995) In situ hybridization shows Dmp1 (AG1) to be a developmentally regulated dentin-specific protein produced by mature odontoblasts. Connect. Tissue Res., 33, 67–72.

54. D'Souza R.N., Cavender A., Sunavala G., Alvarez J., Ohshima T., Kulkarni A.B., MacDougall M.(1997) Gene expression patterns of murine dentin matrix protein 1 (Dmp1) and dentin sialophosphoprotein (DSPP) suggest distinct developmental functions in vivo. J. Bone Miner. Res., 12, 2040–2049.

55.He G., Dahl T., Veis A., George A., (2003) Nucleation of apatite crystals in vitro by self-assembled dentin matrix protein 1. Nat Mater., Aug 2 (8):552-8.

56.Apostolidou E., Swords R., Alvarado Y., Giles, F.J. (2007) Treatment of acute lymphoblastic leukaemia: a new era. Drugs, 67, 2153- 2171.

57.Avramis V.I., Martin-Aragon S., Avramis E.V., Asselin B.L. (2007) Pharmacoanalytical assays of Erwinia asparaginase (erwinase) and pharmacokinetic results in high-risk acute lymphoblastic leukemia (HR ALL) patients: simulations of erwinase population PK-PD models. Anticancer Res., 27, 2561-2572.

58.a. Labrou N.E., Papageorgiou A.C. and Avramis V.I. (2010) Structure-Function Relationships and Clinical Applications of L- Asparaginases. Cur. Med. Chem., 17, 2183-2195.

b. Swain A.L., Jaskolski M., Housset D., Manana R.J.K., Wlodawer A.(1993) Crystal structure of Escherichia coli L-asparaginase, an enzyme used in cancer therapy. PNAS, 90, 1474-1478

59.Hill J.M., Roberts J., Loeb E., Khan A., MacLellan A., Hill R.W. (1967) L-asparaginase therapy for leukemia and other malignant neoplasms. Remission in human leukemia. *JAMA*, *202* (9), 882–888.

60.Graham, M. L. (2003) Pegaspargase: a review of clinical studies. *Adv. Drug Deliv. Rev.*, *55* (10), 1293–1302.

*61.*Mott J.D., Werb Z. (2004) Regulation of matrix biology by matrix metalloproteinases. Curr. Opin. Cell Biol., 16, 558–564.

62.Nagase H., Barrett A.J. & Woessner J.F.Jr (1992) Nomenclature and glossary of the matrix metalloproteinases. Matrix Suppl, 1, 421–424.

63.Massova I., Kotra L.P., Fridman R., Mobashery S. (1998) Matrix metalloproteinases: structures, evolution, and diversification. FASEB J, 12, 1075–1095.

64.Fanjul-Fernández M., Folgueras A.R., Cabrera S., López-Otín C. (2010) Matrix metalloproteinases: evolution, gene regulation and functional analysis in mouse models. Biochim. Biophys. Acta, 1803, 3–19.

65.Nesi A., Fragai M. (2007) Substrate Specificities of Matrix Metalloproteinase 1 in PAR-1 Exodomain. Proteolysis. Chem. Bio. Chem., 8, 1367–1369.

66. Andreini C., Banci L., Bertini I., Luchinat C. & Rosato A. (2004) Comparison of Structures and Homology-Models of Matrix Metalloproteinases. J. Proteome Res., 3, 21–31.

67.Aiken A., Khokha R. (2010) Unraveling metalloproteinase function in skeletal biology and disease using genetically altered mice. Biochimica et Biophysica Acta (BBA) – Molecular Cell Research, 1803, 121–132.

68.Page-McCaw A., Ewald A. J. & Werb Z. (2007) Matrix metalloproteinases and the regulation of tissue remodelling. Nature Rev. Mol. Cell Biol., 8, 221–233.

69.Butler G. S., Overall C.M. (2009) Updated Biological Roles for Matrix Metalloproteinases and New 'Intracellular' Substrates Revealed by Degradomics. Biochemistry, 48, 10830–10845.

70.Limb G.A., Matter K., Murphy G., Cambrey A.D., Bishop P.N., Morris G.E., Khaw P.T. (2005) Matrix metalloproteinase-1 associates with intracellular organelles and confers resistance to lamin A/C degradation during apoptosis. Am. J. Pathol., 166, 1555–1563.

71.Visse R. & Nagase H. (2003) Matrix metalloproteinases and tissue inhibitors of metalloproteinases: structure, function, and biochemistry. Circ. Res, 92, 827–839.

72.Barksby H.E., Milner J.M., Patterson A.M., Peake N.J., Hui W., Robson T., Lakey R., Middleton J., Cawston T.E., Richards C.D., Rowan AD. (2006) Matrix metalloproteinase 10 promotion of collagenolysis via procollagenase activation: implications for cartilage degradation in arthritis. Arthritis Rheum. , 54, 3244–3253.

73.Sounni N.E., Noel A. (2005) Membrane type-matrix metalloproteinases and tumor progression. Biochimie, 87, 329–342.

74.Alaaho R., Kähäri V.M. (2005) Collagenases in cancer. Biochimie, 87, 273–286.

75.Puerta D.T., Lewis J.A., Cohen S.M. (2011) New Beginnings for Matrix Metalloproteinase Inhibitors: Identification of High-Affinity Zinc-Binding Groups. J. Am. Chem. Soc., 126, 8388–8389.

76.Konstantinopoulos P.A., Karamouzis M.V., Papatsoris A.G., Papavassiliou, A.G. (2008) Matrix metalloproteinase inhibitors as anticancer agentsInt. J. Biochem. Cell Biol. 40, 1156–1168.

77.Overall C.M., Kleifeld O. (2006) Validating matrix metalloproteinases as drug targets and anti-targets for cancer therapy. Nature Reviews Cancer, 6, 227–239

78.Luo D., Mari B., Stoll I., Anglard P. (2002) Alternative splicing and promoter usage generates an intracellular stromelysin 3 isoform directly translated as an active matrix metalloproteinase. J. Biol. Chem., 277, 25527–25536.

79.Bertini I., Calderone V., Fragai M., Luchinat C., Maletta M., Yeo K.J. (2006) Snapshots of the reaction mechanism of matrix metalloproteinases. Angew. Chem. Int. Ed. Engl., 45, 7952–7955.

80.Maskos K., Bode, W. (2003) Structural basis of matrix metalloproteinases and tissue inhibitors of metalloproteinases. Mol. Biotechnol., 25, 241–266.

81.Grams F., Reinemer P, Powers JC, Kleine T, Pieper M, Tschesche H, Huber R, Bode W. (1995) X-ray structures of human neutrophil collagenase complexed with peptide hydroxamate and peptide thiol inhibitors. Implications for substrate binding and rational drug design. Eur. J. Biochem., 228, 830–841.

82.Bertini I., Fragai M., Luchinat C. (2009) Intra- and interdomain flexibility in matrix metalloproteinases: functional aspects and drug design. Cur. Pharm Des 15(31):3592-605.

83.Bertini I., Fragai M., Luchinat C., Melekian M., Mylonas E., Sarti N., Svergum D. (2009) Interdomain Flexibility in Full-length Matrix Metalloproteinase-1 (MMP-1). J. Biol. Chem., 284, 12821 –12828.

84.Bertini I., Calderone V., Fragai M., Jaiswal R., Luchinat C., Melikian M., Mylonas E., Svergun D.I. (2008) Evidence of Reciprocal Reorientation of the Catalytic and Hemopexin-Like Domains of Full-Length MMP-12. JACS, 130, 7011–7021.

85.Ramachandran, G.N. (1956) Structure of Collagen. Nature 177, 710–711.

86.Orgel J.P.R.O., Irving T.C., Miller A., Wess T.J. (2006) Microfibrillar structure of type I collagen in situ. PNAS, 103, 9001–9005.

87.Garnero P., Borel O., Byrjalsen I., Ferreras M., Drake F.H., McQueney M.S., Foged N.T., Delmas P.D., Delaissé J.M. (1998) The collagenolytic activity of cathepsin K is unique among mammalian proteinases. J. Biol. Chem., 273, 32347–32352.

88.Woessner J.F, Nagase H. (2000) Matrix Metalloproteinases and TIMPs, Oxford University Press, Oxford.

89.Aimes R. T., Quigley J. P. (1995) Matrix metalloproteinase-2 is an interstitial collagenase. Inhibitor-free enzyme catalyzes the cleavage of collagen fibrils and soluble native type I collagen generating the specific 3/4- and 1/4-length fragments. J. Biol. Chem., 270, 5872–5876.

90.Fields G. B. J (1991) A model for interstitial collagen catabolism by mammalian collagenases. Theor Biol, 153, 585–602.

91.Freije J.M.P., Diez-Itza T., Balbin M., Sanchez L.M., Blasco R., Tolivia J., Lopez-Otin C. (1994) Molecular cloning and expression of collagenase-3, a novel human matrix metalloproteinase produced by breast carcinomas. J. Biol. Chem., 269, 16766–16773.

92.Knauper V., Lopez-Otin C., Smith B., Knight G., Murphy G. (1996) Biochemical characterization of human collagenase-3. J. Biol. Chem., 271, 1544–1550.

93.Mitchell P.G., Magna H.A., Reeves L.M., Lopresti-Morrow L.L., Yocum S.A., Rosner P.J., Geoghegan K.F., Hambor J.E. (1996) Cloning, expression, and type II collagenolytic activity of matrix metalloproteinase-13 from human osteoarthritic cartilage. J. Clin. Invest., 97, 761–768.

94.Ohuchi E., Imai K., Fujii Y., Sato H., Seiki M., Okada Y. (1997) Membrane type 1 matrix metalloproteinase digests interstitial collagens and other extracellular matrix macromolecules. J. Biol. Chem., 272, 2446–2451.

95. Stolow M.A., Bauzon D.D., Li J., Sedgwick T., Liang V.C., Sang Q.A., Shi Y.B. (1996) Identification and characterization of a novel collagenase in Xenopus laevis: possible roles during frog development. Mol. Biol. Cell, 7, 1471–1483.

96.Yang M., Kurkinen M. (1998) Cloning and characterization of a novel matrix metalloproteinase (MMP), CMMP, from chicken embryo fibroblasts. CMMP, Xenopus XMMP, and human MMP19 have a conserved unique cysteine in the catalytic domain. J. Biol. Chem., 273, 17893–17900

97.Allan J.A., Hembry R.M., Angal S., Reynolds J.J., Murphy G. (1991) Binding of latent and high Mr active forms of stromelysin to collagen is mediated by the C-terminal domain. J. Cell Sci., 99, 789–795

98.Allan J.A., Docherty A.J.P., Barker P.J., Huskisson N.S., Reynolds J.J., Murphy G. (1995) Binding of gelatinases A and B to type-I collagen and other matrix components. Biochem J., 309, 299–306.

99.Murphy G., Allan J.A., Willenbrock F., Cockett M.I., O'Connell J.P., Docherty A.J.P. (1992) The C- terminal domain in collagenase and stromelysin specificity. J. Biol. Chem., 267, 9612–9618

100.Lauer-Fields J.L., Juska D., Fields G.B. (2002) Matrix metalloproteinases and collagen catabolism. Biopolymers. 66(1):19-32.

101.Chung L., Dinakarpandian D., Yoshida N., Lauer-Fields J.L., Fields G.B., Visse R., Nagase H. (2004) Collagenase unwinds triple-helical collagen prior to peptide bond hydrolysis. EMBO J., 23, 3020–3030.

102.Clark I.M., Cawston T.E. (1989) Fragments of human fibroblast collagenase. Purification and characterization. Biochem. J., 263, 201–206.

103.Murphy G., Allan J.A., Willenbrock F., Cockett M.I., O'Connell J.P., Docherty A.J. (1992) The role of the C-terminal domain in collagenase and stromelysin specificity, J. Biol. Chem. 267, 9612–9618.

104.Tochowicz A., Goettig P., Evans R., Visse R., Shitomi Y., Palmisano R., Ito N., Richter K., Maskos K., Franke D., Svergun D., Nagase H., Bode W., Itoh Y. (2011) The Dimer Interface of the Membrane Type 1 Matrix Metalloproteinase Hemopexin Domain: CRYSTAL STRUCTURE AND BIOLOGICAL FUNCTIONS. J. Biol. Chem., 286, (9) 7587-7600.

105.Ohuchi E., Imai K., Fujii Y., Sato H., Seiki M., Okada Y. (1997). Membrane type 1 matrix metalloproteinase digests interstitial collagens and other extracellular matrix macromolecules. J. Biol. Chem., 272, 2446-2451.

106.Sato H., Takino T., Okada Y., Cao J., Shinagawa A., Yamamoto E. and Seiki M. (1994). A matrix metalloproteinase expressed on the surface of invasive tumour cells. Nature, 370, 61-65.

107.Knauper V., Will H., Lopez-Otin C., Smith B., Atkinson S. J., Stanton H., Hembry R. M. and Murphy G. (1996). Cellular mechanisms for human procollagenase-3 (MMP-13) activation. Evidence that MT1-MMP (MMP-14) and gelatinase a (MMP-2) are able to generate active enzyme. J. Biol. Chem., 271, 17124-17131.

108.Kajita M., Itoh Y., Chiba T., Mori H., Okada A., Kinoh H., Seiki M. (2001). Membrane-type 1 matrix metalloproteinase cleaves CD44 and promotes cell migration. J. Cell Biol., 153, 893-904.

109.Endo K., Takino T., Miyamori H., Kinsen H., Yoshizaki T., Furukawa M. and Sato H. (2003). Cleavage of syndecan-1 by membrane type matrix metalloproteinase-1 stimulates cell migration. J. Biol. Chem., 278, 40764-40770.

110.Ratnikov B.I., Rozanov D.V., Postnova T.I., Baciu P.G., Zhang H., DiScipio R.G., Chestukhina G.G., Smith J.W., Deryugina E.I. and Strongin A.Y. (2002) An alternative processing of integrin alpha(v) subunit in tumor cells by membrane type-1 matrix metalloproteinase. J. Biol. Chem., 277, 7377-7385.

111.Rozanov D. V., Hahn-Dantona E., Strickland D. K., Strongin A. Y. (2004). The low density lipoprotein receptor-related protein LRP is regulated by membrane type-1 matrix metalloproteinase (MT1-MMP) proteolysis in malignant cells. J. Biol. Chem., 279, 4260-4268.

112.Holmbeck K., Bianco P., Caterina J., Yamada S., Kromer M., Kuznetsov S.A., Mankani M., Robey P.G., Poole A.R., Pidoux I., Ward JM, Birkedal-Hansen H. (1999). MT1- MMP-

deficient mice develop dwarfism, osteopenia, arthritis, and connective tissue disease due to inadequate collagen turnover. Cell, 99, 81-92.

113. Zhou Z., Apte S.S., Soininen R., Cao R., Baaklini G. Y., Rauser R. W., Wang J., Cao Y. and Tryggvason K. (2000). Impaired endochondral ossification and angiogenesis in mice deficient in membrane-type matrix metalloproteinase I. Proc. Natl. Acad. Sci. USA, 97, 4052-4057.

114. Hotary K.B., Allen E.D., Brooks P. C., Datta N.S., Long M.W. and Weiss S.J. (2003). Membrane type I matrix metalloproteinase usurps tumor growth control imposed by the three-dimensional extracellular matrix. Cell, 114, 33-45.

115. Chun T. H., Sabeh F., Ota I., Murphy H., McDonagh K.T., Holmbeck K., Birkedal-Hansen H., Allen E.D. and Weiss S.J. (2004). MT1-MMP- dependent neovessel formation within the confines of the three-dimensional extracellular matrix. J. Cell Biol., 167, 757-767.

116. Hiraoka N., Allen E., Apel I.J., Gyetko M.R., Weiss S.J. (1998). Matrix metalloproteinases regulate neovascularization by acting as pericellular fibrinolysins. Cell, 95, 365-377.

117. Filippov S., Koenig G. C., Chun T. H., Hotary K. B., Ota I., Bugge T. H., Roberts J. D., Fay W.P., Birkedal-Hansen H., Holmbeck K., Sabeh F.,Allen E.D.,Weiss S.J. (2005). MT1-matrix metalloproteinase directs arterial wall invasion and neointima formation by vascular smooth muscle cells. J. Exp. Med., 202, 663-671

118. Miller M.C., Manning H.B., Jain A., Troeberg L., Dudhia J., Essex D., Sandison A., Seiki M., Nanchahal J., Nagase H., Itoh Y. (2009). Membrane type 1 matrix metalloproteinase is a crucial promoter of synovial invasion in human rheumatoid arthritis. Arthritis Rheum., 60, 686-697.

119. Sabeh F., Fox D. and Weiss S. J. (2010). Membrane-type I matrix metalloproteinase-dependent regulation of rheumatoid arthritis synoviocyte function. J. Immunol., 184, 6396-6406.

120. Cell Surface Proteases, Academic Press, New York (2003).

121. K. Lehti, J. Lohi, M.M. Juntunen, D. Pei, J. Keski-Oja (2002) Oligomerization through hemopexin and cytoplasmic domains regulates the activity and turnover of membrane-type 1 matrix metalloproteinase. J. Biol. Chem., 277, 8440–8448.

122. Itoh Y., Takamura A., Ito N., Maru Y., Sato H., Suenaga N., Aoki T., Seiki M. (2001) Homophilic complex formation of MT1-MMP facilitates proMMP-2 activation on the cell surface and promotes tumor cell invasion. EMBO J., 20, 4782–4793.

123. Olson M.W., Bernardo M.M., Pietila M., Gervasi D.C., Toth M., Kotra L.P., Massova I., Mobashery S., Fridman R. (2000) Characterization of the monomeric and dimeric forms of

latent and active matrix metalloproteinase-9. Differential rates for activation by stromelysin 1. J. Biol. Chem., 275, 2661–2668.

124.Itoh Y., Ito N., Nagase H., Seiki M. (2008) The second dimer interface of MT1-MMP, the transmembrane domain, is essential for proMMP-2 activation on the cell surface. J. Biol. Chem., 283, 13053–13062.

125.Ingvarsen S., Madsen D.H., Hillig T., Lund L.R., Holmbeck K., Behrendt N., Engelholm L.H. (2008) Dimerization of endogenous MT1-MMP is a regulatory step in the activation of the 72-kDa gelatinase MMP-2 on fibroblasts and fibrosarcoma cells. Biol. Chem., 389, 943–953.

126.Itoh Y., Ito N., Nagase H., Evans R.D., Bird S.A., Seiki M. (2006) Cell surface collagenolysis requires homodimerization of the membrane-bound collagenase MT1-MMP. Mol. Biol. Cell, 17, 5390–5399.

127.Goldberg G.I., Strongin A., Collier E., Genrich L.T., Marmer B.L. (1992) Interaction of 92-kDa type IV collagenase with the tissue inhibitor of metalloproteinases prevents dimerization, complex formation with interstitial collagenase, and activation of the proenzyme with stromelysin. J. Biol. Chem., 267, 4583–4591.

128. Overall C.M., Kleifeld O. (2006) Tumour microenvironment — opinion: validating matrix metalloproteinases as drug targets and anti-targets for cancer therapy. Nat. Rev. Cancer, 6, 227–239.

129.Martin M.D., Matrisian L.M. (2007) The other side of MMPs: protective roles in tumor progression. Cancer Metastasis Rev., 26, 717–724.

130. Aureli L., Gioia M., Cerbara I., Monaco S., Fasciglione G.F., Marini S., Ascenzi P., Topai A., Coletta M. (2008) Structural bases for substrate and inhibitor recognition by matrix metalloproteinases. Curr. Med. Chem., 15, 2192–2222.

131. Overall C.M., Kleifeld O. (2006) Towards third generation matrix metalloproteinase inhibitors for cancer therapy. British J. Cancer, 94, 941–946.

132.Agrawal S., Anderson P., Durbeej M., van Rooijen N., Ivars F., Opdenakker G., Sorokin L.M. (2006). Dystroglycan is selectively cleaved at the parenchymal basement membrane at sites of leukocyte extravasation in experimental autoimmune encephalomyelitis. J. Exp. Med., 203, 1007–1019.

133.Opdenakker G., Nelissen I., Van Damme J. (2003). Functional roles and therapeutic targeting of gelatinase B and chemokines in multiple sclerosis. Lancet Neurol. 2, 747–756.

134.Van den Steen P.E., Proost P., Brand D.D., Kang A.H., Van Damme J., Opdenakker G. (2004). Generation of glycosylated remnant epitopes from human collagen type II by gelatinase B. Biochemistry, 43, 10809–10816.

135.Liu Z., Zhou X., Shapiro S.D., Shipley J.M., Twining S.S., Diaz L.A., Senior R.M., Werb Z. (2000). The serpin a1-proteinase inhibitor is a critical substrate for gelatinase B/MMP-9 in vivo. Cell, 102, 647–655.

136.Van den Steen P.E., Proost P., Wuyts A., Van Damme J., and Opdenakker G. (2000). Neutrophil gelatinase B potentiates interleukin-8 tenfold by aminoterminal processing, whereas it degrades CTAP-III, PF-4, and GRO-a and leaves RANTES and MCP-2 intact. Blood, 96, 2673–2681.

137.Heissig B., Hattori K., Dias S., Friedrich M., Ferris B., Hackett N.R., Crystal R.G., Besmer P., Lyden D., Moore M.A., Werb Z., Rafii S. (2002). Recruitment of stem and progenitor cells from the bone marrow niche requires MMP-9-mediated release of kit-ligand. Cell, 109, 625–637.

138.Opdenakker G., Van den Steen P.E., Van Damme J. (2001). Gelatinase B: a tuner and amplifier of immune functions. Trends Immunol., 22, 571–579.

139.Van den Steen P.E., Van Aelst I., Hvidberg V., Piccard H., Fiten P., Jacobsen C., Moestrup S.K., Fry S., Royle L., Wormald M.R., Wallis R., Rudd P.M., Dwek R.A., Opdenakker G. (2006). The hemopexin and O-glycosylated domains tune gelatinase B/MMP-9 bioavailability via inhibition and binding to cargo receptors. J. Biol. Chem., 281, 18626–18637

140.Rosenblum G., Van den Steen P.E., Sidney R. Cohen S.R., Gunter Grossmann J., Frenkel,Rotem Sertchook J., Slack N., Strange R. W., Opdenakker G., Sagi I (2007) Insights into the Structure and Domain Flexibility of Full-Length Pro-Matrix Metalloproteinase-9/Gelatinase B. Structure, 15, 1227–1236.

141.McQuibban G.A., Gong J.H., Tam E.M., McCulloch C.A., Clark-Lewis I., Overall C.M. (2000). Inflammation dampened by gelatinase A cleavage of monocyte chemoattractant protein-3. Science, 289, 1202–1206.

142.Supuran C.T. (2008) Carbonic anhydrases: novel therapeutic applications for inhibitors and activators. Nat. Rev. Drug Discov., 7, 168–181

143.Smith K.S., Jakubzick C., Whittam T.S. and Ferry J.G. (1999) Carbonic anhydrase is an ancient enzyme widespread in prokaryotes. Proc. Natl. Acad. Sci. U.S.A., 96, 15184–15189

144.Xu Y., Feng L., Jeffrey P.D., Shi Y. and Morel F.M. (2008) Structure and metal exchange in the cadmium carbonic anhydrase of marine diatoms. Nature, 452, 56–61

145. Neri D. and Supuran C.T. (2011) Interfering with pH regulation in tumours as a therapeutic strategy. Nat. Rev. Drug Discov., 10, 767–777

146.Capasso C. and Supuran C.T. (2015) An overview of the alpha-, beta- gamma-carbonic anhydrases from bacteria: can bacterial carbonic anhydrases shed new light on evolution of bacteria? J. Enzyme Inhib. Med. Chem. 30, 325–332

147.Hu P. Y., Ernst A. R., Sly W. S., Venta P. J., Skaggs L. A., & Tashian R. E. (1994). Carbonic anhydrase II deficiency: single-base deletion in exon 7 is the predominant mutation in Caribbean Hispanic patients. Am. J. Hum. Gen., 54(4), 602–608.

148.Bosley T.M., Salih M.A., Alorainy I.A., M. Islam Z., Oystreck D.T., Suliman O.S.M., Al Malki S., Suhaibani A.H., Khiari H., Beckers S., Van Wesenbeeck L., Perdu B., Al Drees A., Elmalik S.A., Van Hul W., Abu-Amero K.K.(2011) The neurology of carbonic anhydrase type II deficiency syndrome. Brain, 134 (12) 3502-3515.

149.Avvaru B. S., Busby S. A., Chalmers M. J., Griffin P. R., Venkatakrishnan B., Agbandje-McKenna M., McKenna R. (2009). Apo-Human Carbonic Anhydrase II Revisited: Implications of the Loss of a Metal in Protein Structure, Stability and Solvent Network. Biochemistry, 48(31), 7365–7372.

150.Supuran C.T. (2016) Structure and function of carbonic anhydrases. Biochem J. Jul 15; 473(14):2023-32.

151.Supuran C.T. and Scozzafava A.,(2000) Carbonic anhydrase inhibitors and their therapeutic potential Expert Opinion On Therapeutic Patents Vol. 10 , Iss. 5

152.(a) Pastorekova S., Parkkila S., Pastorek J., Supuran C. T.(2004) Carbonic anhydrases: current state of the art, therapeutic applications and future prospects., J. Enz. Inhib. Med. Chem., 19, 199–229; (b) Supuran C. T., Vullo D., Manole G., Casini A., Scozzafava A.(2004) Designing of novel carbonic anhydrase inhibitors and activators. Curr. Med. Chem. Cardiovasc. Hematol. Agents, 2, 49–68.

153.Supuran C. T., Scozzafava A., Conway J., (2004) Carbonic Anhydrase—Its Inhibitors and Activators, Eds., CRC: Boca Raton (FL), USA, pp 1–363, and references cited therein.

154. Pastorekova S., Pastorek J.(2004) Cancer-Related Carbonic Anhydrase Isozymes and their Inhibition. In Carbonic Anhydrase—Its Inhibitors and Activators Eds., CRC: Boca Raton (FL),USA, pp 253–280.

155.Tureci O., Sahin U., Vollmar E., Siemer S., Gottert E., Seitz G., Parkkila A. K., Shah G. N., Grubb J. H., Pfreundschuh M., Sly W. S.(1998) Proc. Natl. Acad. Sci. U.S.A., 95, 7608–7613.

156.Ivanov S. V., Kuzmin I., Wei M. H., Pack S., Geil L., Johnson B. E., Stanbridge E. J., Lerman M. I. (1998) Proc. Natl. Acad. Sci. U.S.A., 95, 12596–12601.

157.(a) Wykoff C., Beasley N., Watson P., Turner L., Pastorek J., Wilson G., Turley H., Maxwell P., Pugh C., Ratcliffe P., Harris A.(2000) Cancer Res., 60, 7075– 7083; (b) Ashida S., Nishimori I., Tanimura M., Onishi S., Shuin T. J.(2002) Cancer Res. Clin. Oncol., 128, 561–568.

158.Karhumaa P., Kaunisto K., Parkkila S., Waheed A., Pastorekova S., Pastorek J., Sly W. S., Rajaniemi H.(2000) Mol. Hum. Reprod., 7, 611–616.

159.(a) Kivela A. J., Parkkila S., Saarnio J., Karttunen T. J., Kivela J., Parkkila A. K., Pastorekova S., Pastorek J., Waheed A., Sly W. S., Rajaniemi H.(2000) Expression of transmembrane carbonic anhydrase isoenzymes IX and XII in normal human pancreas and pancreatic tumours. Histochem. Cell Biol., 114, 197–204; (b) Kivela A., Parkkila S., Saarnio J., Karttunen T. J., Kivela J., Parkkila A. K., Waheed A., Sly W. S., Grubb J. H., Shah G., Tureci O., Rajaniemi H. (2000) Expression of a novel transmembrane carbonic anhydrase isozyme XII in normal human gut and colorectal tumors. Am. J. Pathol., 156, 577–584; (c) Kivela A., Parkkila S., Saarnio J., Karttunen T. J., Kivela J., Parkkila A. K., Pastorekova S., Pastorek J., Waheed A., Sly W. S., Parkkila S., Rajaniemi H.(2001) Differential Expression of Cytoplasmic Carbonic Anhydrases, CA I and II, and Membrane-Associated Isozymes, CA IX and XII, in Normal Mucosa of Large Intestine and in Colorectal Tumors Dig. Dis. Sci., 46, 2179–2186.

160.Parkkila S., Parkkila A. K., Saarnio J., Kivela J., Karttunen T., Kaunisto K., Waheed A., Sly W. S., Tureci O., Virtanen I., Rajaniemi H. (2000) J. Histochem. Cytochem., 48, 1601–1608.

161. Liao S. Y., Ivanov S., Ivanova A., Ghosh S., Cote M. A., Keefe K., Coca-Prados M., Stanbridge E.J., Lerman M. I. (2003) J. Med. Genet., 40, 257–261.

162.Capasso C. and Supuran C.T. (2015) An overview of the alpha-, beta- and gamma-carbonic anhydrases from bacteria: can bacterial carbonic anhydrases shed new light on evolution of bacteria? J. Enzyme Inhib. Med. Chem. **30**, 325–332

163.Supuran C.T. (2012) Structure-based drug discovery of carbonic anhydrase inhibitors. J. Enzyme Inhib. Med. Chem. **27**, 759–772

164.Supuran C.T. (2011) Bacterial carbonic anhydrases as drug targets: towards novel antibiotics? Front. Pharmacol. **2**, 34

165.Schlicker C., Hall R.A., Vullo D., Middelhaufe S., Gertz M., Supuran C.T., Muhlschlegel F.A. and Steegborn C. (2009) Structure and inhibition of the CO_2-sensing carbonic

anhydrase Can2 from the pathogenic fungus Cryptococcus neoformans. J. Mol. Biol. **385**, 1207–1220.

166.Laemmli U. K. (1970). Cleavage of structural proteins during the assembly of the head of bacteriophage T4. Nature 227(5259): 680-685.

167. Vandooren J., Born B., Solomonov I., Zajac E., Saldova R., Senske M., … Opdenakker G. (2015). Circular trimers of gelatinase B/matrix metalloproteinase-9 constitute a distinct population of functional enzyme molecules differentially regulated by tissue inhibitor of metalloproteinases-1. The Biochem. J., **465**(2), 259–270.

3. RESULTS

ChemPubSoc Europe

DOI: 10.1002/chem.201503613

CHEMISTRY A European Journal Full Paper

Solid-State NMR Spectroscopy |*Hot Paper*|

Atomic-Level Quality Assessment of Enzymes Encapsulated in Bioinspired Silica

Tommaso Martelli,[a, b, e] Enrico Ravera,[a, b] Alexandra Louka,[a] Linda Cerofolini,[c, f] Manuel Hafner,[d] Marco Fragai,[a, b] Christian F. W. Becker,[d] and Claudio Luchinat*[a, b]

Abstract: Among protein immobilization strategies, encapsulation in bioinspired silica is increasingly popular. Encapsulation offers high yields and the solid support is created through a protein-catalyzed polycondensation reaction that occurs under mild conditions. An integrated strategy is reported for the characterization of both the protein and bioinspired silica scaffold generated by the encapsulation of enzymes with an external silica-forming promoter or with the promoter expressed as a fusion to the enzyme. This strategy is applied to the catalytic domain of matrix metalloproteinase 12. Analysis reveals that the structure of the protein encapsulated by either method is not significantly altered with respect to the native form. The structural features of silica obtained by either strategy are also similar, but differ from those obtained by other approaches. In case of the covalently linked R5–enzyme construct, immobilization yields are higher. Encapsulation through a fusion protein, therefore, appears to be the method of choice.

Introduction

Enzymes are inherently "green" catalysts that can perform complex chemical tasks under mild conditions in a fully aqueous environment (i.e., under physiological conditions). Enzymes are optimized by natural selection for energy efficiency, time efficiency, and atom economy. Furthermore, they can be prepared under benign biotechnological conditions and are fully biodegradable.[1] This makes enzymes the optimal candidates for "green chemistry" applications.[2–4] Immobilized enzymes are used for a wide range of applications in scientific research, medical devices, and industrial processes.[5–7] Encapsulation within a solid matrix offers several advantages over simple adsorption or covalent linking to a matrix surface.[8] Usually, an encapsulated enzyme shows long-term preservation of the structure and catalytic activity, and a larger thermal stability than that of the free enzyme.[9,10] To achieve efficient encapsulation, it is common to resort to the formation of a silica matrix by catalyzing the condensation of silicic acid in a bioinspired process.

In living organisms, the polycondensation of silicic acid is promoted by positively charged proteins that bring the negatively charged monomers close together.[11–16] In vitro the same proteins[11,17–19] or polycationic polypeptides[11,20] can be used to promote biosilicification under mild conditions starting from silicic acid (Scheme 1).

Any protein and enzyme that lacks hydrolytic activity toward the silica can be efficiently entrapped in the silica matrix if it is simply added to the solution before the start of the reaction.[8,19] It has been shown that large amounts of proteins or

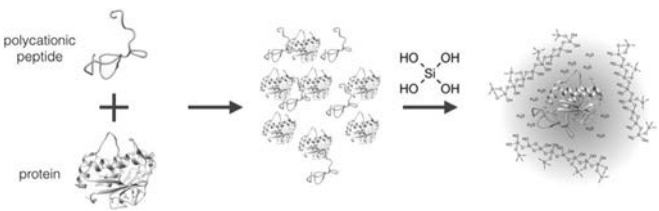

Scheme 1. Protein-templated polycondensation of silicic acid.

[a] *Dr. T. Martelli, Dr. E. Ravera, A. Louka, Prof. M. Fragai, Prof. C. Luchinat*
Magnetic Resonance Center (CERM), University of Florence
Via L. Sacconi 6, 50019 Sesto Fiorentino, FI (Italy)
Fax: (+39) 0554574923
E-mail: claudioluchinat@cerm.unifi.it

[b] *Dr. T. Martelli, Dr. E. Ravera, Prof. M. Fragai, Prof. C. Luchinat*
Department of Chemistry "Ugo Schiff", University of Florence
Via della Lastruccia 3, 50019 Sesto Fiorentino, FI (Italy)

[c] *Dr. L. Cerofolini*
Giotto Biotech S.R.L., Via Madonna del Piano 6
50019 Sesto Fiorentino, FI (Italy)

[d] *M. Hafner, Prof. C. F. W. Becker*
Institute of Biological Chemistry, Department of Chemistry
University of Vienna, Waehringer Str. 38
1090 Vienna (Austria)

[e] *Dr. T. Martelli*
Present address:
Giotto Biotech S.R.L., Via Madonna del Piano 6
50019 Sesto Fiorentino, FI (Italy)

[f] *Dr. L. Cerofolini*
Present address:
Magnetic Resonance Center (CERM)
University of Florence, Via L. Sacconi 6
50019 Sesto Fiorentino, FI (Italy)
and
Department of Chemistry "Ugo Schiff"
University of Florence, Via della Lastruccia 3
50019 Sesto Fiorentino, FI (Italy)

Supporting information and ORCID(s) from the author(s) for this article are available on the WWW under http://dx.doi.org/10.1002/chem.201503613.

enzymes can be properly encapsulated in silica by simply mixing a polycationic molecule with silicic acid and the biomolecule itself. The most characterized of those promoters is a Silaffin-1A-derived peptide called R5.[19] In vivo the R5 peptide is heavily post-translationally modified,[11,12,21] but it has been shown that even unmodified R5 can promote silicification in vitro under ambient conditions and neutral pH.[11,22,23] Additionally, this approach has the potential to manipulate the nanometer-scale architecture of the silica matrix, so that it is possible to obtain a large array of materials with different microscopic characteristics for interesting applications in biomedical or materials science.[6,8,24–26] The efficiency of the encapsulation process strongly depends on the nature of the protein (e.g., its charge and size) and this may result in limited or inefficient encapsulation.[27] Encapsulation mediated by fusion proteins endowed with catalytic activity has been proposed to increase entrapment efficiency.[24,25,27–32] Herein, we specifically study the possible differences between the use of an external polycationic promoter (poly(L-lysine)) and the R5 peptide fused to our target enzyme[27,32–35] as biosilicification-promoting agents. A comparison with the unmodified R5 peptide alone[18] as an external polycationic promoter is also provided.

The materials described above have been characterized in terms of enzymatic activity and electron microscopy.[25,27] The silicic component of the silica samples containing R5-related peptides have been characterized by solid-state (SS) ^{29}Si NMR spectroscopy,[36,37] which is a common approach to study silicic matrices.[38–41] Recently, ^{13}C SSNMR spectroscopy was used to detect the peptidic component,[42] as previously reported for other biomaterials.[43–46]

SSNMR spectroscopy is also proven to be a powerful method for the characterization of protein systems,[47] especially due to theoretical and experimental[47–57] advancements, as well as to improvements in sample preparation.[58–66] Whereas solution NMR spectroscopy becomes more challenging with increasing molecular weight,[67–75] and diffraction methods fall short in structurally characterizing systems that lack long-range order, SSNMR spectroscopy is capable of providing an atomic-level description of systems that are either large or disordered or both.[76–81]

We have also shown that an assessment of the preservation of the native conformation of silica-entrapped enzymes with atomic detail can be achieved by SSNMR spectroscopy.[82] The catalytic domain of matrix metalloproteinases 12 (catMMP-12) and C6A/C111S mutant dimeric human superoxide dismutase (SOD) coprecipitated with poly(L-lysine) provided good-resolution SSNMR spectra, which showed at atomic level that the overall tertiary structure of the two proteins observed in solution and in the crystals was maintained after silica entrapment.[82] We have also shown that the detection limit of such studies can be lowered by means of dynamic nuclear polarization, up to the detection of the silica-templating molecule (hen egg-white lysozyme).[83] Dynamic nuclear polarization was also applied in a recent paper to probe the structural propensity of a silica-forming peptide.[84]

Herein, we apply high-resolution SSNMR spectroscopy to provide the first atomic-level characterization of a further step towards highly efficient immobilization based on the R5 peptide genetically fused to MMP12 (catMMP12–R5), leading to encapsulation of this fusion protein.

Because the encapsulation process is no longer random, but rather directed by the fusion protein, encapsulated samples have a higher protein/silica ratio.[25,27] Thus, such samples are more promising in terms of SSNMR spectroscopy characterization because the higher protein concentration reflects a necessarily higher signal to noise (S/N) ratio.

Experimental Section

SSNMR spectroscopy

All spectra were acquired with a Bruker AvanceII spectrometer operating at 700 MHz ^{1}H larmor frequency, equipped with a 4 mm probe head tuned to ^{1}H–^{13}C–^{15}N with a $\lambda/4$ insert or to ^{1}H–^{29}Si without $\lambda/4$ insert. Samples were packed into Bruker 4 mm zirconia rotors center packed with CRAMPS inserts (50 μL total volume). Pulses were 3.5 μs for ^{1}H, 4.8 μs for ^{13}C, 7 μs for ^{15}N, and 3 μs for ^{29}Si. The optimal interscan delay was 1.6 s for H-start experiments. In 2D ^{13}C–^{13}C dipolar-assisted rotational resonance (DARR) spectroscopy, the magic-angle spinning (MAS) frequency was set to 11.5 kHz, ^{1}H decoupling to 71 kHz, cross-polarization (CP) contact time to 750 μs ($\omega_H = 41.5$ kHz, $\omega_C = 30$ kHz), and mixing time to 25 ms; the number of scans was set to 256 for the catMMP12 sample and 128 for the catMMP12–R5 sample. ^{29}Si spectra were acquired with direct excitation by using a spin-echo sequence with a one rotor-cycle delay; the second delay before acquisition also encompassed the dead time of the probe to avoid baseline distortion. Optimal interscan delays for ^{29}Si were reported along with the spectra. During ^{15}N and ^{13}C evolution/detection, SW$_f$TPPM[85–88] decoupling was applied at 75 kHz, and the optimal decoupling power was chosen based on ^{13}C′ T_2 measured by echo decay.[89]

Solution NMR spectroscopy

All experiments were performed on samples of the ^{13}C,^{15}N isotopically enriched catalytic domain of MMP-12 fused with R5 peptide at a protein concentration of 0.90 mM in aqueous buffer solution (20 mM Tris, pH 7.2, 50 mM NaCl, 0.1 mM $ZnCl_2$, 10 mM $CaCl_2$, 200 mM acetohydroxamic acid (AHA)). The protein was inhibited with *N*-isobutyl-*N*-(4-methoxyphenylsulfonyl)glycyl hydroxamic acid (NNGH) to reproduce the experimental conditions used in previous studies.[82,90–93] All proton-detected NMR spectra were recorded at 298 K on a DRX 500 spectrometer equipped with a triple-resonance CryoProbe; carbon-detected NMR spectra were acquired on a Bruker AVANCE 700 spectrometer with a triple-resonance CryoProbe optimized for ^{13}C-direct detection.[94] Spectra were processed with the Bruker TOPSPIN software packages and analyzed with the program CARA (Computer Aided Resonance Assignment, ETH Zurich).

The 2D ^{1}H–^{15}N HSQC spectrum of catMMP12–R5 was superimposable on the spectrum of catMMP-12 with some additional signals related to the C-terminal tail (Figure S3 in the Supporting Information). Minor shifts of some signals, mainly corresponding to the C-terminal residues, were also visible in the spectrum.

The backbone resonance assignment of the C-terminal tail was obtained by the analysis of 3D HNCA, 3D HNCO, 3D HN(CA)CO, and 3D CBCA(CO)NH spectra.[95–97] The assignment of this unfolded peptide was complemented by the use of direct ^{13}C-detected experiments: 2D CON, 2D CACO, 2D CBCACO, 3D CBCANCO, 3D

CBCACON.[98–100] The assignments of ^{1}H, ^{15}N, and ^{13}C resonances are reported in Table S1 in the Supporting Information.

Protein expression and purification

The catalytic domain of MMP-12 (catMMP12) was expressed as fusion protein with an R5 peptide at the C terminus. DNA coding for the catalytic domain of MMP-12 was cloned into a vector containing DNA coding for the R5 peptide at the C terminus of the protein (sequences are reported in the Supporting Information). The protein was expressed and purified as published for catMMP12.[101]

The NNGH inhibitor was added to the proteins (catMMP12 and catMMP12–R5) used in the preparation of samples for NMR spectroscopy measurements. The inhibitor was not used to prepare samples for activity assays.

Peptide synthesis

The R5 peptide (aa sequence: CSSKKSGSYSGSKGSKRRIL) was synthesized by using 9-fluorenylmethoxycarbonyl (Fmoc) solid-phase peptide synthesis (SPPS)[21,26] on preloaded Wang polystyrene resin[102] and a CEM Liberty Blue automated microwave peptide synthesizer (0.25 mmol scale). To improve the synthetic quality and yield, the pseudo-proline dipeptide, Fmoc-Gly-Ser($\psi^{Me,Me}$pro) was incorporated at two positions.[103] For analysis results, see the Supporting Information.

Silicification reaction

The samples of catMMP-12 in silica were prepared as previously reported[82] by using poly(L-lysine) as a promoter for the polymerization of silica. MMP-12 (200 μL, 45 mg mL^{-1} in buffer A: 20 mM Tris, pH 7.2, 50 mM NaCl, 10 mM $CaCl_2$, 0.1 mM $ZnCl_2$, NNGH in excess), poly(L-lysine) (50 μL, 10 mg mL^{-1} in H_2O; MW: 4000–15000 Da) were added to 1.5 mL vials and shaken for 10 min. To the resulting solution, a 100 mM solution of silicic acid (250 μL) in buffer A (freshly prepared from a stock solution of 1 M silicic acid obtained by the addition of 1 mM HCl (850 μL) to pure tetramethyl orthosilicate (TMOS; 150 μL)) were added and the mixture was reacted for 10 min at room temperature. For the sample containing R5 as an external promoter, the same protocol was applied, but with R5 (50 μL, 10 mg mL^{-1} in H_2O with 5 mM dithiothreitol (DTT)) instead of poly(L-lysine). The samples of catMMP12–R5 were prepared by using the same protocol, but with water instead of the promoter solution to maintain the same experimental conditions as those used with the external promoters.

Samples containing lysozyme and lysozyme + bovine serum albumin (BSA) were prepared as follows: BSA (200 μL, 40 mg mL^{-1} in buffer B: 20 mM Tris pH 7.5) and lysozyme (50 μL, 10 mg mL^{-1} in H_2O) were added to 1.5 mL vials and shaken for 10 min. To the resulting solution, a 100 mM solution of silicic acid (250 μL) in buffer B (freshly prepared from a stock solution of 1 M silicic acid obtained from TMOS, see above) were added and the mixture reacted for 10 min at room temperature. For comparison, samples containing lysozyme only were prepared by using the same protocol, but replacing BSA (200 μL) with buffer B (200 μL).

After the polycondensation reaction, all samples were centrifuged at 8000 rpm and the supernatant was removed. To remove unreacted TMOS, the precipitates were then washed three times with a buffer containing 20 mM Tris (pH 7.2), 10 mM $CaCl_2$, and 0.1 mM $ZnCl_2$, in the case of catMMP12 and catMMP12–R5, and buffer B, in the case of lysozyme and BSA. The suspension was used to fill the 4 mm rotors using an ultracentrifugal device[104] and NMR spectroscopy measurements were performed immediately afterwards.

Enzymatic activity assay

In all samples used for the enzymatic activity assays, the protein was not bound to the nanomolar inhibitor NNGH. Enzyme assays were carried out in 50 mM Hepes buffer, pH 7, 10 mM $CaCl_2$, 0.1 mM $ZnCl_2$, 0.05% Brij-35, with a commercial fluorogenic substrate (Mca-Pro-Leu-Gly-Leu-Dpa-Ala-Arg-NH_2).

All assays were performed in a 1 cm cuvette (total volume 3 mL) at 310 K under stirring conditions. Progress curves were monitored by following the increase in fluorescence at $\lambda = 393$ nm ($\lambda_{ex} = 328$ nm) induced by cleavage of the fluorogenic substrate by the samples. The conditions of a typical experiment were buffer (2 mL), 5 nM of free or immobilized protein, and 245 μM of substrate.

All measurements were performed by using a Varian Cary Eclipse Fluorimeter.

Results

Entrapment yield

In agreement with the standard characterization of immobilized proteins,[27] the yield of encapsulation as a function of protein loading was determined. The yield of the entrapment of catMMP12–R5 is always higher than catMMP12 with poly(L-lysine). The yield of entrapment at 800 μM is 2.56 and 1.55 nmol protein per μmol SiO_2, respectively (Figure 1). Conversely, when R5 is used as an external promoter, the yield of entrapment at 800 μM is 0.42 nmol protein per μmol SiO_2.

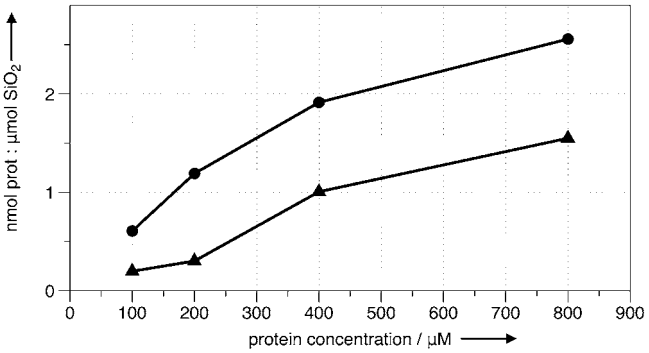

Figure 1. Immobilization yield as a function of protein concentration for unmodified catMMP12 (▲) and catMMP12–R5 (●).

Solution NMR spectroscopy

Amide ^{1}H protons are extremely sensitive reporters of minor variations of their local environment. Such sensitivity is quantitatively analyzed through chemical shift perturbation (CSP) analysis,[105] which shows larger changes for stronger interactions. The CSP is expressed as a combined measure of the change in the chemical shift of both ^{1}H and ^{15}N of the peptide amide [Eq. (1)]:

$$\Delta c.s. = \frac{1}{2}\sqrt{\Delta\delta_H^2 + \left(\frac{\Delta\delta_N}{5}\right)^2} \quad (1)$$

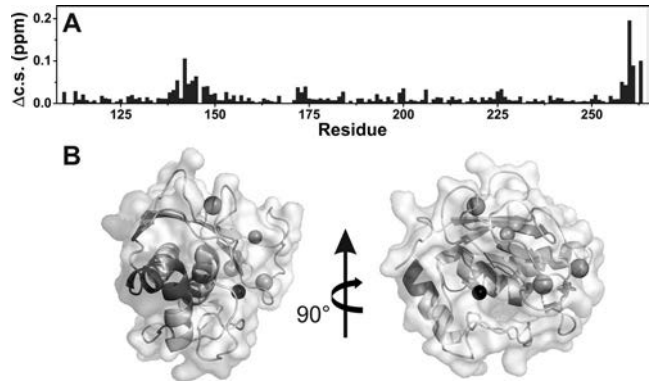

Figure 2. Solution NMR spectroscopy data analysis: A) chemical shift differences between the wild-type catMMP12 and R5-fused construct; B) CSP mapping: the active Zn^{II} ion is shown in black and appears to be far from the region with the largest perturbation, which is shaded in gray.

The CSP analysis performed for catMMP12 with and without the R5 fusion (Figure 2A) shows no sizable effects throughout the sequence, in particular, in the active-site region; this is apparent from the localization of regions with larger perturbation over the 3D structure (Figure 2B). The largest perturbations are found at the C terminus, where the R5 tag is fused and between residues 140–148, which belong to a helix close to the C terminus in the protein fold.

Also, the enzymatic activity of the protein toward a fluorescent substrate peptide in solution is not considerably altered (Figure S4 in the Supporting Information), and the activity of the entrapped R5-fusion protein is almost the same as of the lysine-mediated silica/catMMP12, as shown in Figure S5 in the Supporting Information. Analysis of the progress curves, according to the equations reported in ref. [106] revealed that in the immobilized samples obtained from poly(L-lysine) and R5-fused peptide the value of K_M increased by a factor of about 1.5 with respect to the free enzyme (Table S2 in the Supporting Information). An increase in K_M is usually observed for immobilized enzymes.[107] This effect is ascribed to reduced accessibility to the active site of the enzyme.

The strategy for the entrapment of catMMP12 based on the use of free R5 peptide shows a lower immobilization yield. This can possibly be ascribed to the size of the promoter, which may form a tighter silica network. This hypothesis is supported by SEM data (Figure S6 in the Supporting Information), which show the presence of smaller silica particles when R5 is used as an external promoter with respect to those obtained from the R5 peptide fused with the protein.

^{29}Si SSNMR spectroscopy

We recorded ^{29}Si NMR spectra of catMMP12 entrapped in poly(L-lysine)-mediated silica and encapsulated catMMP12–R5 (Figure 3). ^{29}Si NMR spectra were also acquired on a silica sample obtained with 10 mg mL^{-1} lysozyme as a catalyst[108] with and without the inclusion of 40 mg mL^{-1} BSA. In all spectra, the Q^2 (geminal silanol), Q^3 (silanol) and Q^4 (siloxane) signals are observed. Interestingly, the Q^4/Q^3 ratio, which is a measure of the condensation of silica, is similar for the two samples, and also similar to a sample of silica obtained by the use of lysozyme, but sizably reduced with respect to both the naturally occurring material and silica obtained by another group with lysozyme.[109]

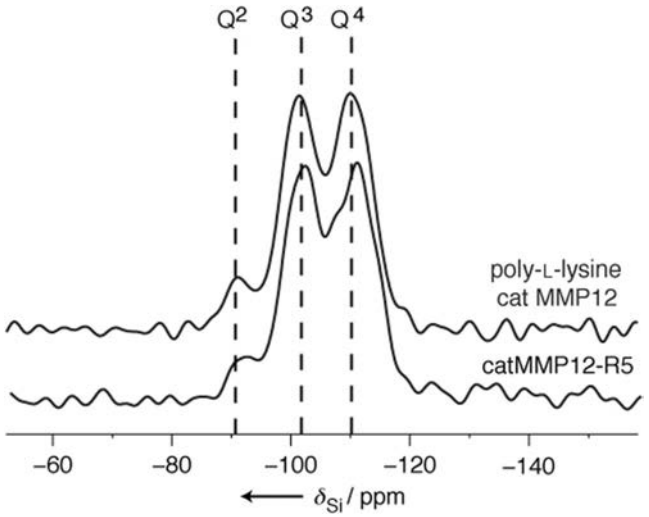

Figure 3. The 1D direct polarization ^{29}Si NMR spectra of the silica matrix of catMMP12 entrapped with poly(L-lysine) (top) and encapsulated catMMP12–R5 (bottom).

The percentage area values of different ^{29}Si NMR spectra are summarized in Table 1.

SSNMR spectroscopy of the protein component

Recently, we demonstrated that high-resolution SSNMR spectroscopy, based on ^{13}C detection, could be applied to observe the spectra of silica-encapsulated enzymes.[82] We thus applied the same protocol to the characterization of both catMMP12 systems. The 1D spectrum of catMMP12–R5 (Figure 4) does not show significant broadening with respect to cat-MMP12 with poly(L-lysine) or with R5. The 2D spectra are shown in Figure 5.

Discussion

NMR spectroscopy measures the behavior of nuclei, which are extremely sensitive reporters of the electronic structure around them (orbital shape and orientation, electrostatics, hydrogen bonding, etc.) and both solution and SSNMR spectroscopy can yield structural information at different levels. First, the information achieved is site specific because each nonequivalent nucleus resonates at a different frequency with respect to the others. At a finer level, the measurement of secondary chemical shifts (i.e., deviation with respect to the random coil chemical shift typical of each amino acid) reveals the presence of secondary-structure elements. Finally, homo- and heteronuclear correlation experiments in which the modulation of the nuclear dipole–dipole interaction is allowed to modulate the signal intensity can be used to calculate the fold of the protein.[113] In SSNMR spectroscopy, this is usually achieved through DARR experiments.[111,112]

Table 1. Percentage area values of different ^{29}Si NMR spectra of silica samples.

Sample	Q^2 *germinal* silanol	Q^3 silanol	Q^4 siloxane	Q^4/Q^3	Ref.
catMMP12/poly(L-lysine)	7	45	48	1.1	this work
catMMP12/R5	0	38	62	1.6	this work
catMMP12–R5	6	44	51	1.2	this work
Cylindrotheca fusiformis (extracted cell walls)	2	26	72	2.8	[36]
synthetic silica gel	2	24	74	3.1	[36]
PL12–silica	6	37	57	1.5	[84]
10 mg mL^{-1} lysozyme, pH 7.5	4	40	56	1.4	this work
10 mg mL^{-1} lysozyme +40 mg mL^{-1} BSA, pH 7.5	6	44	50	1.1	this work

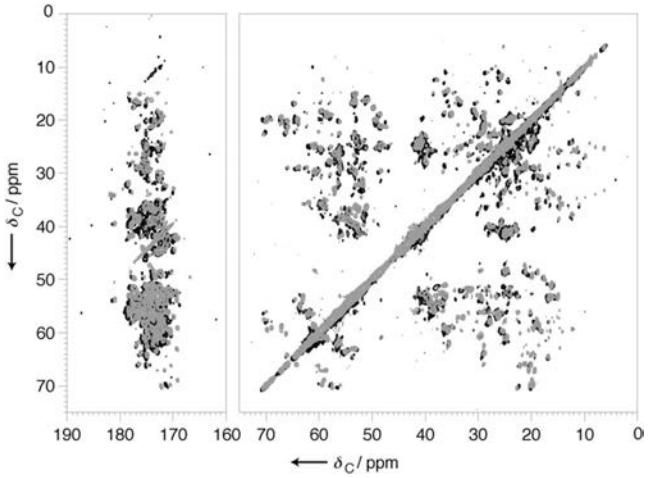

Figure 5. The 2D ^{13}C–^{13}C correlation spectra (DARR[111,112]) of catMMP12 with poly(L-lysine)[82] (gray) and catMMP12–R5 (black).

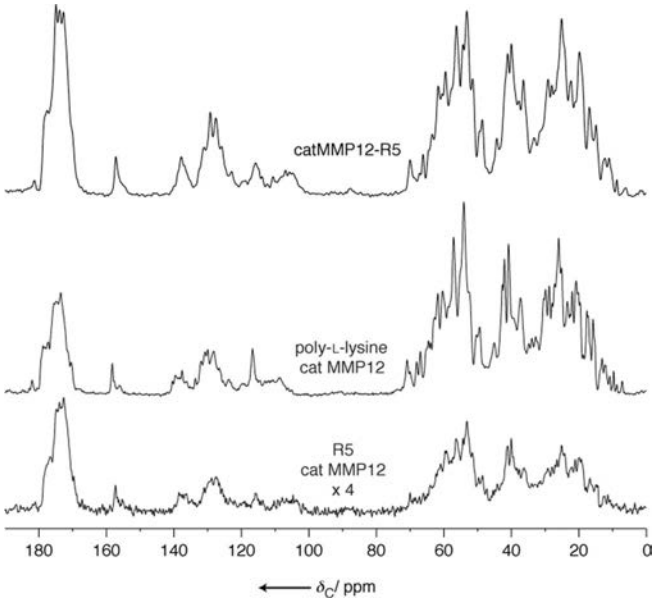

Figure 4. The 1D {^{1}H}–^{13}C CP[110] spectra of R5-mediated silica/catMMP12 (bottom), poly(L-lysine)-mediated silica/catMMP12 (middle), and silica–catMMP12–R5 (top). Spectra were acquired with 1024 scans, and the experimental conditions were the same as those used for the DARR experiments.

We have used NMR spectroscopy both in solution and in the solid state to provide a thorough characterization of the chimeric protein catMMP12–R5. CSP analysis of solution NMR spectroscopy (Figure 2) suggest that the presence of the R5 tail at the C terminus of catMMP12 does not sizably affect the structure of the protein, with perturbations that are rather small and localized at the C terminus of the protein or in its proximity.

The comparison of the 2D ^{13}C–^{13}C correlation spectra presented in Figure 5 reveals the preservation of the fold of the protein because the spectra of catMMP12 and catMMP12–R5 are almost completely superimposable. This is in agreement with the activity data of the immobilized enzymes. The lower entrapment efficiency of catMMP12 in the R5-mediated silica is not surprising, since the size of the promoter is much smaller than the size of the target enzyme, which may result in reduced inclusion of the enzyme in the nascent silica, and directly reflects in the reduced S/N ratio in the NMR spectra (shown with 4× magnification in Figure 4).

By examining the more resolved areas of the spectrum, a number of residues show significant perturbation, mostly in terms of loss of intensity. However, a detailed analysis of the spectra indicates that the alterations are small and widely distributed (Figure S7 in the Supporting Information). The signals belonging to the R5 peptide, which are easily assigned in solution (see the Supporting Information), are not observed in the solid state. This suggests that R5 may adopt different conformations and/or experience a heterogeneous environment; such conditions usually yield severely broadened or dispersed resonances, in agreement with that reported for a R5–silica composite in ref. [42]. Indeed, evidence of biomolecule/silica interactions has recently been provided by the Brunner group,[114] who demonstrated through-space proximity, and also by the joint work of the groups of Goobes and Oschkinat, who probed the proximity of lysines in the silica-forming peptide and the silica matrix.[84] In our case, a standard ^{1}H–^{15}N–^{29}Si NMR spectroscopy experiment did not yield any detectable signals, possibly because of the low sensitivity of ^{29}Si at natural abundance or because of the less efficient double CP pathway.

By comparing the 1D traces extracted from the DARR spectra (examples are given in Figure S8 in the Supporting Information), the linewidth does not seem to be substantially increased, but the cross-peaks seem to be broadened; this may suggest a slightly higher heterogeneity in the catMMP12–R5 sample. However, such a small inhomogeneity is not as extensive as the inhomogeneity reported in ref. [42] for R5 alone.

As a final remark, SSNMR spectroscopic characterization of silica composites has relied upon a description of the silica matrix in terms of ^{29}Si NMR spectroscopy.[36,37,115–117] For instance, extensive characterization of different diatom species has been reported.[36]

The similarity between the catMMP12 samples and the BSA/lysozyme sample can be interpreted in terms of a larger surface area of silica that has to encapsulate bulky proteins. For completeness, we note that the amount of different components in the lysozyme sample reported herein and the one reported in ref. [109] are possibly due to different experimental conditions.

Conclusion

Silica-encapsulated catMMP12–R5 was prepared and characterized by standard enzymatic assays, and compared with catMMP12 encapsulated with poly(L-lysine) and R5 as external promoters. In agreement with reports on other enzymes,[27] we found that the enzymatic activity of catMMP12–R5 in solution remained unaffected with respect to catMMP12, and also that encapsulation of R5-tagged proteins yielded a higher percentage of protein in the silica matrix (2–3 times higher in our case), which confirmed that this was a very promising strategy. To further characterize the obtained material, according to previous spectroscopic studies on silica and biosilica,[36] we also recorded ^{29}Si NMR spectra of the two samples, and found them to be similar under the experimental conditions reported herein: the catMMP12–R5 sample contained slightly fewer condensed siloxane moieties. We also found that silica prepared under our experimental conditions was less condensed with respect to other preparations.[36,115,118]

In addition to the standard methodology for such composites, we applied high-resolution, high-field SSNMR spectroscopy to the characterization of an encapsulated enzyme.[82] The larger encapsulation efficiency with respect to the poly(L-lysine) coprecipitate permitted easier and fast NMR spectroscopic characterization, which reduced the amount of enzyme needed for the analysis. Reports of the spectra of R5 peptide in silica exist, and they appear to be poorly resolved.[42] In contrast, the spectra of the enzyme fused to R5 appeared to be well resolved and, for the first time in such a system, we were able to assess the preservation of the native structure at the atomic level, as probed by SSNMR spectroscopy: the presence of fusion peptides in the protein and interactions with the biomineral did not seem to alter the tertiary structure, as monitored at atomic resolution, and in agreement with the retained enzymatic activity.

We expect this kind of experimental approach to be instrumental in the optimization of heterogeneous catalysts based on encapsulated enzymes.

Acknowledgments

This work has been supported by the Ente Cassa di Risparmio di Firenze, MIUR PRIN 2012K7ASN; EC Contracts pNMR no. 317127, and IDPbyNMR no. 264257; the University of Florence CERM-TT; and Instruct, part of the European Strategy Forum on Research Infrastructures (ESFRI) and supported by national member subscriptions. Specifically, we thank the EU ESFRI Instruct Core Centre CERM, Italy. Prof. Claudio Luchinat holds a share of the company Giotto Biotech S.R.L. The authors report no other conflict of interest.

Keywords: biomaterials · green chemistry · proteins · NMR spectroscopy · silicates

[1] P. Anastas, J. Warner, *Green Chemistry: Theory and Practice*, Oxford University Press, New York, **2000**, p. 152.
[2] P. T. Anastas, M. M. Kirchhoff, *Acc. Chem. Res.* **2002**, *35*, 686 – 694.
[3] R. A. Sheldon, *Chem. Commun.* **2008**, 3352 – 3365.
[4] S. Riva, *Trends Biotechnol.* **2006**, *24*, 219 – 226.
[5] J. F. Liang, Y. T. Li, V. C. Yang, *J. Pharm. Sci.* **2000**, *89*, 979 – 990.
[6] V. B. Kandimalla, V. S. Tripathi, H. Ju, *Crit. Rev. Anal. Chem.* **2006**, *36*, 73 – 106.
[7] A. K. S. Nisha, S. A. Karthick, N. Gobi, *Chem. Sci. Rev. Lett.* **2012**, *1*, 148 – 155.
[8] L. Betancor, H. R. Luckarift, *Trends Biotechnol.* **2008**, *26*, 566 – 572.
[9] R. A. Sheldon, *Adv. Synth. Catal.* **2007**, *349*, 1289 – 1307.
[10] R. M. Blanco, J. J. Calvete, J. Guisán, *Enzyme Microb. Technol.* **1989**, *11*, 353 – 359.
[11] N. Kröger, R. Deutzmann, M. Sumper, *Science* **1999**, *286*, 1129 – 1132.
[12] N. Kröger, R. Deutzmann, M. Sumper, *J. Biol. Chem.* **2001**, *276*, 26066 – 26070.
[13] S. Weiner, P. M. Dove, *Rev. Mineral. Geochem.* **2003**, *54*, 1 – 29.
[14] D. J. Belton, S. V. Patwardhan, V. V. Annenkov, E. N. Danilovtseva, C. C. Perry, *Proc. Natl. Acad. Sci. USA* **2008**, *105*, 5963 – 5968.
[15] D. J. Belton, O. Deschaume, C. C. Perry, *FEBS J.* **2012**, *279*, 1710 – 1720.
[16] L. Senior, M. P. Crump, C. Williams, P. J. Booth, S. Mann, A. Periman, P. Curnow, *J. Mater. Chem. B* **2015**, *3*, 2607 – 2614.
[17] N. Poulsen, M. Sumper, N. Kröger, *Proc. Natl. Acad. Sci. USA* **2003**, *100*, 12075 – 12080.
[18] M. Sumper, N. Kröger, *J. Mater. Chem.* **2004**, *14*, 2059 – 2065.
[19] H. R. Luckarift, J. C. Spain, R. R. Naik, M. O. Stone, *Nat. Biotechnol.* **2004**, *22*, 211 – 213.
[20] K. M. Roth, Y. Zhou, W. Yang, D. E. Morse, *J. Am. Chem. Soc.* **2005**, *127*, 325 – 330.
[21] C. C. Lechner, C. F. W. Becker, *J. Pept. Sci.* **2014**, *20*, 152 – 158.
[22] M. R. Knecht, D. W. Wright, *Chem. Commun.* **2003**, 3038 – 3039.
[23] C. W. P. Foo, J. Huang, D. L. Kaplan, *Trends Biotechnol.* **2004**, *22*, 577 – 585.
[24] C. W. P. Foo, S. V. Patwardhan, D. J. Belton, B. Kitchel, D. Anastasiades, J. Huang, R. R. Naik, C. C. Perry, D. L. Kaplan, *Proc. Natl. Acad. Sci. USA* **2006**, *103*, 9428 – 9433.
[25] W. D. Marner, A. S. Shaikh, S. J. Muller, J. D. Keasling, *Biomacromolecules* **2008**, *9*, 1 – 5.
[26] C. C. Lechner, C. F. W. Becker, *Chem. Sci.* **2012**, *3*, 3500 – 3504.
[27] W. D. Marner II, A. S. Shaikh, S. J. Muller, J. D. Keasling, *Biotechnol. Prog.* **2009**, *25*, 417 – 423.
[28] S. Zhou, W. Huang, D. J. Belton, L. O. Simmons, C. C. Perry, X. Wang, D. L. Kaplan, *Acta Biomater.* **2015**, *15*, 173 – 180.
[29] D. J. Belton, A. J. Mieszawska, H. A. Currie, D. L. Kaplan, C. C. Perry, *Langmuir* **2012**, *28*, 4373 – 4381.
[30] L. L. S. Canabady-Rochelle, D. J. Belton, O. Deschaume, H. A. Currie, D. L. Kaplan, C. C. Perry, *Biomacromolecules* **2012**, *13*, 683 – 690.
[31] A. J. Mieszawska, L. D. Nadkarni, C. C. Perry, D. L. Kaplan, *Chem. Mater.* **2010**, *22*, 5780 – 5785.
[32] C. C. Lechner, C. F. W. Becker, *Biomater. Sci.* **2015**, *3*, 288 – 297.
[33] D. H. Nam, J.-O. Lee, B.-I. Sang, K. Won, Y. H. Kim, *Appl. Biochem. Biotechnol.* **2013**, *170*, 25 – 31.
[34] D. H. Nam, K. Won, Y. H. Kim, B. I. Sang, *Biotechnol. Prog.* **2009**, *25*, 1643 – 1649.
[35] C. C. Lechner, C. F. W. Becker, *Bioorg. Med. Chem.* **2013**, *21*, 3533 – 3541.
[36] R. Bertermann, N. Kröger, R. Tacke, *Anal. Bioanal. Chem.* **2003**, *375*, 630 – 634.
[37] A. Gendron-Badou, T. Coradin, J. Maquet, F. Fröhlich, J. Livage, *J. Non-Cryst. Solids* **2003**, *316*, 331 – 337.
[38] A. Lesage, M. Lelli, D. Gajan, M. Caporini, V. Vitzhum, P. Mieville, J. Alauzun, A. Roussey, C. Thieuleux, A. Mehdi, G. Bodenhausen, C. Coperet, L. Emsley, *J. Am. Chem. Soc.* **2010**, *132*, 15459 – 15461.

[39] A. J. Rossini, A. Zagdoun, M. Lelli, A. Lesage, C. Copéret, L. Emsley, *Acc. Chem. Res.* **2013**, *46*, 1942 – 1951.
[40] M. Lelli, D. Gajan, A. Lesage, M. A. Caporini, V. Vitzthum, P. Miéville, F. Héroguel, F. Rascón, A. Roussey, C. Thieuleux, M. Boualleg, L. Veyre, G. Bodenhausen, C. Coperet, L. Emsley, *J. Am. Chem. Soc.* **2011**, *133*, 2104 – 2107.
[41] W. R. Grüning, A. J. Rossini, A. Zagdoun, D. Gajan, A. Lesage, L. Emsley, C. Copéret, *Phys. Chem. Chem. Phys.* **2013**, *15*, 13270 – 13274.
[42] A. Roehrich, G. Drobny, *Acc. Chem. Res.* **2013**, *46*, 2136 – 2144.
[43] G. Goobes, R. Goobes, O. Schueler-Furman, D. Baker, P. S. Stayton, G. P. Drobny, *Proc. Natl. Acad. Sci. USA* **2006**, *103*, 16083 – 16088.
[44] R. Goobes, G. Goobes, W. J. Shaw, G. P. Drobny, C. T. Campbell, P. S. Stayton, *Biochemistry* **2007**, *46*, 4725 – 4733.
[45] W. J. Shaw, *Solid State Nucl. Magn. Reson.* **2015**, *70*, 1 – 14.
[46] G. Goobes, *Isr. J. Chem.* **2014**, *54*, 113 – 124.
[47] L. Emsley, I. Bertini, *Acc. Chem. Res.* **2013**, *46*, 1912 – 1913.
[48] R. Tycko, *J. Magn. Reson.* **2015**, *253*, 1.
[49] M. Bjerring, S. Jain, B. Paaske, J. M. Vinther, N. C. Nielsen, *Acc. Chem. Res.* **2013**, *46*, 2098 – 2107.
[50] J. R. Lewandowski, *Acc. Chem. Res.* **2013**, *46*, 2018 – 2027.
[51] S. Yan, C. L. Suiter, G. Hou, H. Zhang, T. Polenova, *Acc. Chem. Res.* **2013**, *46*, 2047 – 2058.
[52] M. Tang, G. Comellas, C. M. Rienstra, *Acc. Chem. Res.* **2013**, *46*, 2080 – 2088.
[53] M. J. Knight, I. C. Felli, R. Pierattelli, L. Emsley, G. Pintacuda, *Acc. Chem. Res.* **2013**, *46*, 2108 – 2116.
[54] M. Hong, K. Schmidt-Rohr, *Acc. Chem. Res.* **2013**, *46*, 2154 – 2163.
[55] A. Loquet, B. Habenstein, A. Lange, *Acc. Chem. Res.* **2013**, *46*, 2070 – 2079.
[56] I. Sengupta, P. S. Nadaud, C. P. Jaroniec, *Acc. Chem. Res.* **2013**, *46*, 2117 – 2126.
[57] S. Parthasarathy, Y. Nishiyama, Y. Ishii, *Acc. Chem. Res.* **2013**, *46*, 2127 – 2135.
[58] A. Böckmann, C. Gardiennet, R. Verel, A. Hunkeler, A. Loquet, G. Pintacuda, L. Emsley, B. H. Meier, A. Lesage, *J. Biomol. NMR* **2009**, *45*, 319 – 327.
[59] A. Mainz, S. Jehle, B. J. van Rossum, H. Oschkinat, B. Reif, *J. Am. Chem. Soc.* **2009**, *131*, 15968 – 15969.
[60] I. Bertini, C. Luchinat, G. Parigi, E. Ravera, B. Reif, P. Turano, *Proc. Natl. Acad. Sci. USA* **2011**, *108*, 10396 – 10399.
[61] C. Gardiennet, A. K. Schütz, A. Hunkeler, B. Kunert, L. Terradot, A. Böckmann, B. H. Meier, *Angew. Chem. Int. Ed.* **2012**, *51*, 7855 – 7858; *Angew. Chem.* **2012**, *124*, 7977 – 7980.
[62] A. Mainz, T. L. Religa, R. Sprangers, R. Linser, L. E. Kay, B. Reif, *Angew. Chem. Int. Ed.* **2013**, *52*, 8746 – 8751; *Angew. Chem.* **2013**, *125*, 8909 – 8914.
[63] S. Asami, B. Reif, *Acc. Chem. Res.* **2013**, *46*, 2089 – 2097.
[64] M. Fragai, C. Luchinat, G. Parigi, E. Ravera, *J. Biomol. NMR* **2013**, *57*, 155 – 166.
[65] I. Bertini, C. Luchinat, G. Parigi, E. Ravera, *Acc. Chem. Res.* **2013**, *46*, 2059 – 2069.
[66] E. Ravera, *Concepts Magn. Reson. Part A* **2014**, *43*, 209 – 227.
[67] K. Pervushin, R. Riek, G. Wider, K. Wüthrich, *Proc. Natl. Acad. Sci. USA* **1997**, *94*, 12366 – 12371.
[68] M. Czisch, R. Boelens, *J. Magn. Reson.* **1998**, *134*, 158 – 160.
[69] V. Tugarinov, P. M. Hwang, L. E. Kay, *Annu. Rev. Biochem.* **2004**, *73*, 107 – 146.
[70] A. Grishaev, V. Tugarinov, L. E. Kay, J. Trewhella, A. Bax, *J. Biomol. NMR* **2008**, *40*, 95 – 106.
[71] C. Guo, D. Zhang, V. Tugarinov, *J. Am. Chem. Soc.* **2008**, *130*, 10872 – 10873.
[72] A. Eletsky, A. Kienhofer, K. Pervushin, *J. Biomol. NMR* **2001**, *20*, 177 – 180.
[73] R. Sprangers, L. E. Kay, *J. Am. Chem. Soc.* **2007**, *129*, 12668 – 12669.
[74] M. Matzapetakis, P. Turano, E. C. Theil, I. Bertini, *J. Biomol. NMR* **2007**, *38*, 237 – 242.
[75] L. E. Kay, *J. Magn. Reson.* **2011**, *210*, 159 – 170.
[76] J.-X. Lu, W. Qiang, W.-M. Yau, C. D. Schwieters, S. C. Meredith, R. Tycko, *Cell* **2013**, *154*, 1257 – 1268.
[77] I. Bertini, L. Gonnelli, C. Luchinat, J. Mao, A. Nesi, *J. Am. Chem. Soc.* **2011**, *133*, 16013 – 16022.
[78] M. Huber, O. Y. Ovchinnikova, A. K. Schütz, R. Glockshuber, B. H. Meier, A. Böckmann, *Biomol. NMR Assign.* **2015**, *9*, 7 – 14.
[79] B. Habenstein, L. Bousset, Y. Sourigues, M. Kabani, A. Loquet, B. H. Meier, R. Melki, A. Böckmann, *Angew. Chem. Int. Ed.* **2012**, *51*, 7963 – 7966; *Angew. Chem.* **2012**, *124*, 8087 – 8090.
[80] Y. Su, C. J. Sarell, M. T. Eddy, G. T. Debelouchina, L. B. Andreas, C. L. Pashley, S. E. Radford, R. G. Griffin, *J. Am. Chem. Soc.* **2014**, *136*, 6313 – 6325.
[81] E. Barbet-Massin, C.-T. Huang, V. Daebel, S.-T. D. Hsu, B. Reif, *Angew. Chem. Int. Ed.* **2015**, *54*, 4367 – 4369; *Angew. Chem.* **2012**, *127*, 4441 – 4444.
[82] M. Fragai, C. Luchinat, T. Martelli, E. Ravera, I. Sagi, I. Solomonov, Y. Udi, *Chem. Commun.* **2014**, *50*, 421 – 423.
[83] E. Ravera, V. Michaelis K., T.-C. Ong, E. G. Keeler, T. Martelli, M. Fragai, R. G. Griffin, C. Luchinat, *ChemPhysChem* **2015**, *16*, 2751 – 2754.
[84] Y. Geiger, H. E. Gottlieb, Ü. Akbey, H. Oschkinat, G. Goobes, *J. Am. Chem. Soc.* **2015**, DOI: 10.1021/jacs.5b07809.
[85] R. S. Thakur, N. D. Kurur, P. K. Madhu, *Chem. Phys. Lett.* **2006**, *426*, 459 – 463.
[86] R. S. Thakur, N. D. Kurur, P. K. Madhu, *Magn. Reson. Chem.* **2008**, *46*, 166 – 169.
[87] R. S. Thakur, N. D. Kurur, P. K. Madhu, *J. Magn. Reson.* **2008**, *193*, 77 – 88.
[88] P. K. Madhu, *Isr. J. Chem.* **2014**, *54*, 25 – 38.
[89] W. P. Rothwell, J. S. Waugh, *J. Chem. Phys.* **1981**, *74*, 2721 – 2732.
[90] I. Bertini, V. Calderone, M. Cosenza, M. Fragai, Y.-M. Lee, C. Luchinat, S. Mangani, B. Terni, P. Turano, *Proc. Natl. Acad. Sci. USA* **2005**, *102*, 5334 – 5339.
[91] S. Balayssac, I. Bertini, K. Falber, M. Fragai, S. Jehle, M. Lelli, C. Luchinat, H. Oschkinat, K. J. Yeo, *ChemBioChem* **2007**, *8*, 486 – 489.
[92] I. Bertini, A. Bhaumik, G. De Paepe, R. G. Griffin, M. Lelli, J. R. Lewandowski, C. Luchinat, *J. Am. Chem. Soc.* **2010**, *132*, 1032 – 1040.
[93] C. Luchinat, G. Parigi, E. Ravera, M. Rinaldelli, *J. Am. Chem. Soc.* **2012**, *134*, 5006 – 5009.
[94] I. Bertini, L. Duma, I. C. Felli, M. Fey, C. Luchinat, R. Pierattelli, P. R. Vasos, *Angew. Chem. Int. Ed.* **2004**, *43*, 2257 – 2259.
[95] L. E. Kay, G. Y. Xu, T. Yamazaki, *J. Magn. Reson. Ser. A* **1994**, *109*, 129 – 133.
[96] S. Grzesiek, A. Bax, *J. Biomol. NMR* **1993**, *3*, 185 – 204.
[97] S. Grzesiek, A. Bax, *J. Magn. Reson.* **1992**, *96*, 432 – 440.
[98] W. Bermel, I. Bertini, I. C. Felli, R. Kümmerle, R. Pierattelli, *J. Magn. Reson.* **2006**, *178*, 56 – 64.
[99] W. Bermel, I. Bertini, I. C. Felli, Y.-M. Lee, C. Luchinat, R. Pierattelli, *J. Am. Chem. Soc.* **2006**, *128*, 3918 – 3919.
[100] W. Bermel, I. Bertini, L. Duma, L. Emsley, I. C. Felli, R. Pierattelli, P. R. Vasos, *Angew. Chem. Int. Ed.* **2005**, *44*, 3089 – 3092.
[101] I. Bertini, M. Fragai, C. Luchinat, M. Melikian, C. Venturi, *Chem. Eur. J.* **2009**, *15*, 7842 – 7845.
[102] E. Atherton, R. C. Sheppard, *Solid Phase Peptide Synthesis: A Practical Approach*, Oxford University Press, Oxford, **1989**.
[103] M. Mutter, A. Nefzi, T. Sato, X. Sun, F. Wahl, T. Wöhr, *Pept. Res.* **1995**, *8*, 145 – 153.
[104] I. Bertini, F. Engelke, L. Gonnelli, B. Knott, C. Luchinat, D. Osen, E. Ravera, *J. Biomol. NMR* **2012**, *54*, 123 – 127.
[105] S. Grzesiek, A. Bax, G. M. Clore, A. M. Gronenborn, J. S. Hu, J. Kaufman, I. Palmer, S. J. Stahl, P. T. Wingfield, *Nat. Struct. Biol.* **1996**, *3*, 340 – 345.
[106] M. O. Palmier, S. R. Van Doren, *Anal. Biochem.* **2007**, *371*, 43 – 51.
[107] L. Cao, *Carrier-Bound Immobilized Enzymes: Principles, Application and Design*, Wiley-VCH, Weinheim (Germany), **2006**.
[108] H. R. Luckarift, M. B. Dickerson, K. H. Sandhage, J. C. Spain, *Small* **2006**, *2*, 640 – 643.
[109] X. Song, Z. Jiang, L. Li, H. Wu, *Front. Chem. Sci. Eng.* **2014**, *8*, 353 – 361.
[110] A. Pines, M. G. Gibby, J. S. Waugh, *J. Chem. Phys.* **1973**, *59*, 569 – 590.
[111] K. Takegoshi, S. Nakamura, T. Terao, *Chem. Phys. Lett.* **2001**, *344*, 631 – 637.
[112] K. Takegoshi, S. Nakamura, T. Terao, *J. Chem. Phys.* **2003**, *118*, 2325 – 2341.
[113] K. Wüthrich, *NMR of Proteins and Nucleic Acids*, Wiley, New York, **1986**.
[114] D. Wisser, S. I. Brückner, F. M. Wisser, G. Althoff-Ospelt, J. Getzschmann, S. Kaskel, E. Brunner, *Solid State Nucl. Magn. Reson.* **2015**, *66 – 67*, 33 – 39.

[115] S. C. Christiansen, N. Hedin, J. D. Epping, M. T. Janicke, Y. del Amo, M. Demarest, M. Brzezinski, B. F. Chmelka, *Solid State Nucl. Magn. Reson.* **2006**, *29*, 170 – 182.
[116] M. Sumper, E. Brunner, *ChemBioChem* **2008**, *9*, 1187 – 1194.
[117] C. Gröger, K. Lutz, E. Brunner, *Prog. Nucl. Magn. Reson. Spectrosc.* **2009**, *54*, 54 – 68.
[118] J. N. Cha, K. Shimizu, Y. Zhou, S. C. Christiansen, B. F. Chmelka, G. D. Stucky, D. E. Morse, *Proc. Natl. Acad. Sci. USA* **1999**, *96*, 361 – 365.

Received: September 9, 2015
Published online on December 2, 2015

CHEMISTRY
A European Journal

Supporting Information

Atomic-Level Quality Assessment of Enzymes Encapsulated in Bioinspired Silica

Tommaso Martelli,[a, b, e] Enrico Ravera,[a, b] Alexandra Louka,[a] Linda Cerofolini,[c, f] Manuel Hafner,[d] Marco Fragai,[a, b] Christian F. W. Becker,[d] and Claudio Luchinat*[a, b]

chem_201503613_sm_miscellaneous_information.pdf

SEQUENCE, EXPRESSION & PURIFICATION

pET-21a constructs encoding catMMP12 and catMMP12-R5 were transformed into Escherichia coli BL21(DE3) cells which were subsequently cultured in rich (LB) or ^{13}C,^{15}N-labelled minimal medium (M9). Cells were grown at 310 K, until OD 0.6–0.8 and subsequently induced with IPTG (isopropyl 1-thio-β-D-galactopyranoside) with a final concentration of 0.5 mM for 5 h.

catMMP12 and catMMP12-R5 were then extracted, purified and also refolded, using the methods already reported for catMMP12.[1]

The proteins were finally purified with gel filtration using a Superdex 75 26/60 in Tris 20 mM, $CaCl_2$ 10 mM, $ZnCl_2$ 0.1 mM, NaCl 150 mM, acetohydroxamic acid (AHA) 200 mM, pH 7.2.

An excess of NNGH (N-Isobutyl-N-(4-methoxyphenylsulfonyl)glycyl hydroxamic acid) was added to the samples to prevent auto-hydrolysis of the protein.

```
  1 MGPVWRKHYI TYRINNYTPD MNREDVDYAI RKAFQVWSNV TPLKFSKINT
 51 GMADILVVFA RGAHGDFHAF DGKGGILAHA FGPGSGIGGD AHFDEDEFWT
101 THSGGTNLFL TAVHEIGHSL GLGHSSDPKA VMFPTYKYVD INTFRLSADD
151 IRGIQSLYGG SASGGGGSSK KSGSYSGSKG SKRRIL
```

Scheme S1. - Sequence of the catMMP12-R5. In black the sequence of the catMMP12 (G106-G263), in red a linker that connect the protein to the R5 peptide, and in green the R5 sequence (S201-L220 from sil1P from *C. fusiformis*).

R5 CHARACTERIZATION

R5 (H-CSSKKSGSYSGSKGSKRRIL–OH) synthesis was verified via HPLC and ESI-MS using a Waters LC-MS System and a Dionex ultimate 3000 HPLC system with a C18 column, and a 0.1% TFA / Acetonitrile gradient.[2] Amino acids highlighted in red have been incorporated as pseudo-proline building blocks.

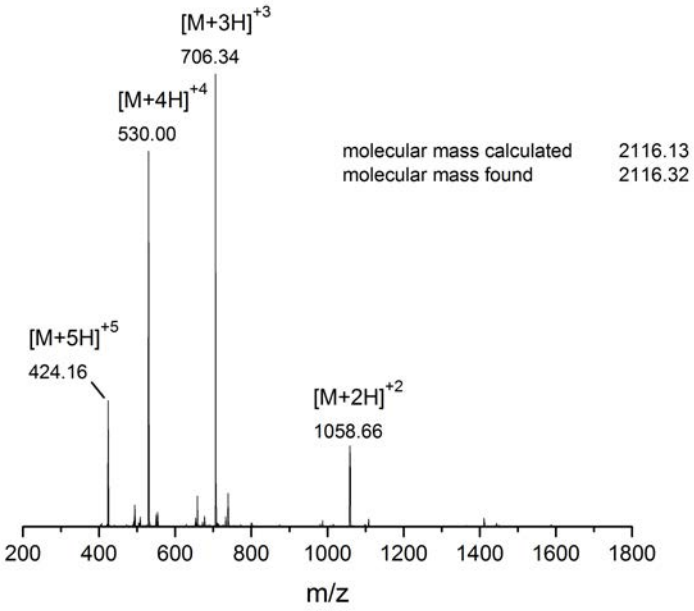

Figure S1. ESI MS spectrum of R5 peptide

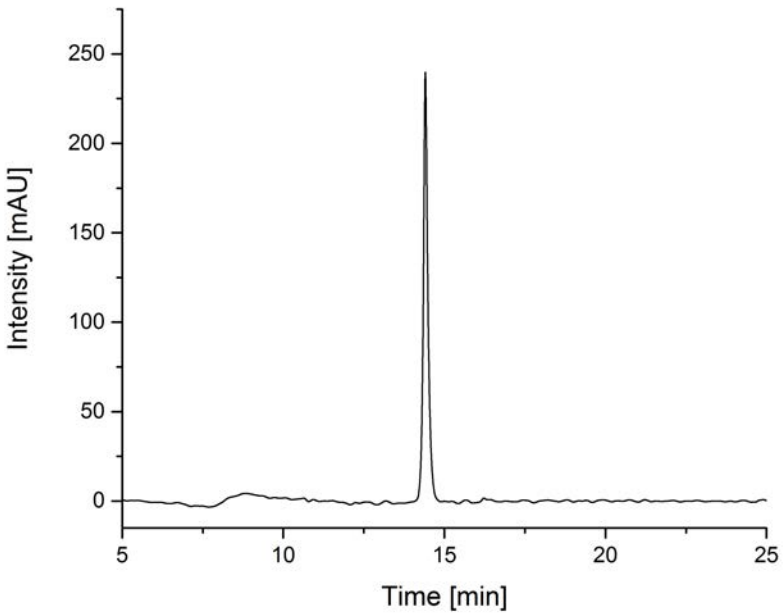

Figure S2. C18 HPLC analysis (UV detection, λ = 214 nm) of R5 using a 5-65% ACN gradient over 30 minutes.

SOLUTION NMR CHARACTERIZATION OF R5-catMMP12

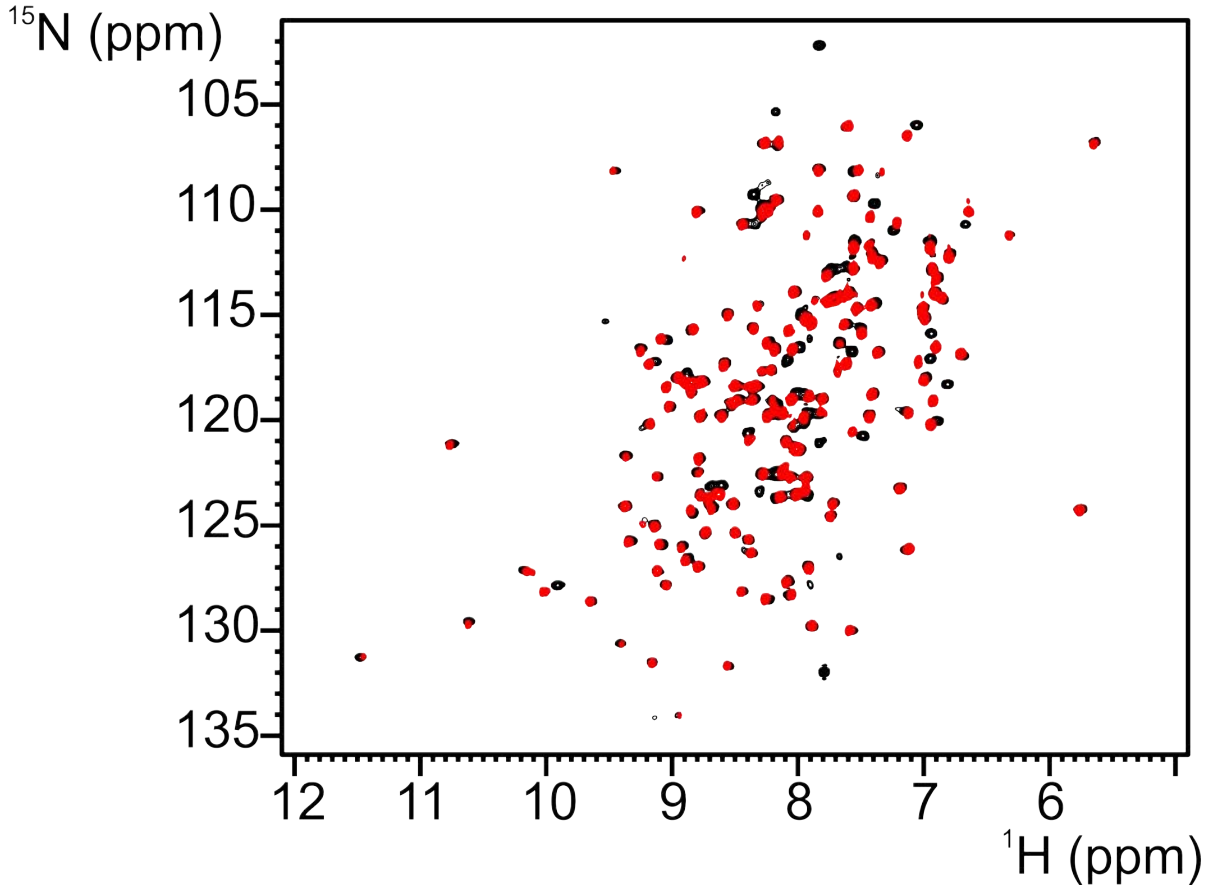

Figure S3. Superimposition of 2D ^{1}H ^{15}N HSQC spectra of catMMP12 (red) and catMMP12-R5 (black).

Table S1 Assignment of ^{1}H ^{15}N ^{13}C resonances of the C-terminal tail of catMMP12-R5 by solution NMR.

	H^N	N	C	Cα	Cβ
GLY	7.90	102.26	174.72	44.28	
SER	7.81	112.86	174.94	58.30	63.85
ALA	8.51	126.20	177.96	52.60	19.15
SER	8.27	114.96	175.22	58.47	63.88
GLY	8.39	110.79	174.95	45.37	
GLY	8.38	108.96		45.11	
GLY			174.84	45.44	
GLY	8.32	108.82	174.48	45.35	
SER	8.27	115.60	174.81	58.40	63.82
SER			174.43	58.40	63.86
LYS			176.62	56.10	32.76
LYS	8.31	122.64	176.69	56.24	32.82
SER	8.35	117.22	175.01	58.37	63.90
GLY		110.85		45.27	
SER			174.19	58.14	63.90
TYR	8.27	122.52	175.97	57.96	38.76
SER			174.77	58.17	63.84
GLY		110.38		45.15	
SER			174.97	58.14	63.72
LYS			177.21	56.53	32.64
GLY	8.37	109.78	174.12	45.35	
SER	8.16	115.51	174.61	58.25	63.91
LYS	8.27	123.19	176.41	56.24	32.81
ARG	8.25	122.46	175.89	56.40	30.81
ARG	8.38	123.47	175.71	56.03	30.86
ILE	8.24	123.78	175.13	61.13	38.32
LEU	7.86	132.05	182.17	56.74	43.19

ACTIVITY TEST

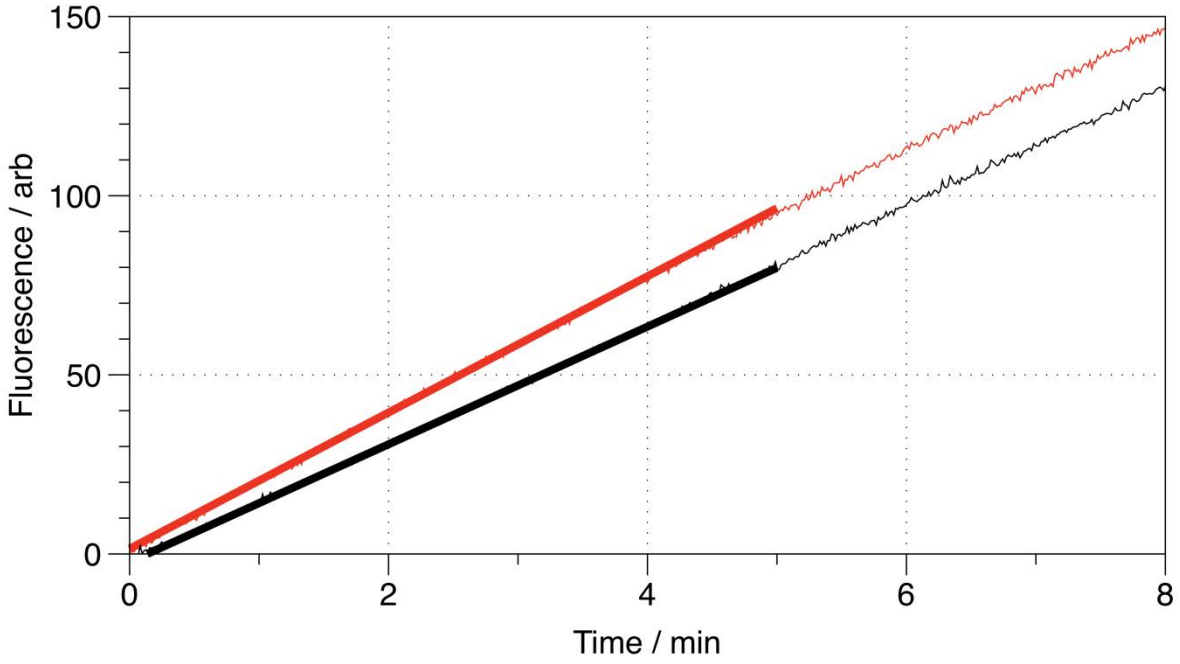

Figure S4. Kinetics curves of free catMMP12 (red) and free catMMP12-R5 (black) with the respective fittings of the initial slopes.

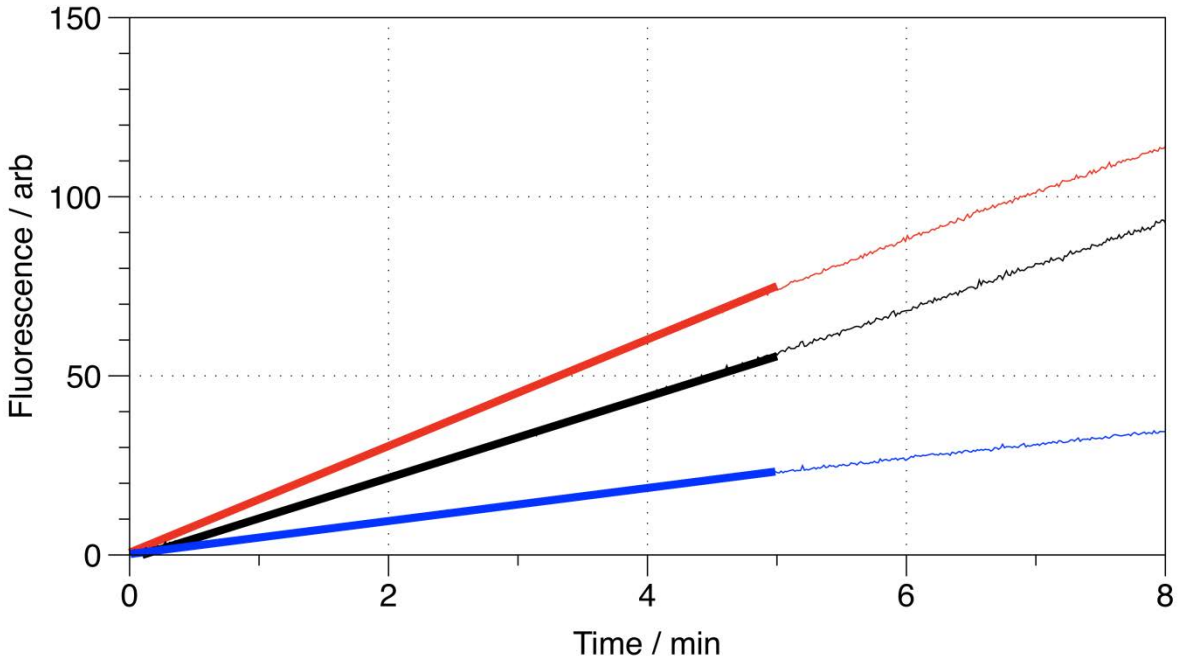

Figure S5. Kinetics curves of poly-L-lysine mediated silica/catMMP12 (red), R5 mediated silica/ catMMP12 (blue) and silica-catMMP12-R5 (black) with the respective fittings of the initial slopes. The curves are normalized to the same protein concentration.

Table S2. K_M values obtained from the analysis of the progress curves of Figures S4 and S5, according to the equations reported in [3].

Sample	K_M (μM)
free catMMP12	480
free catMMP12-R5	480
poly-L-lysine mediated silica/catMMP12	760
silica-catMMP12-R5	690

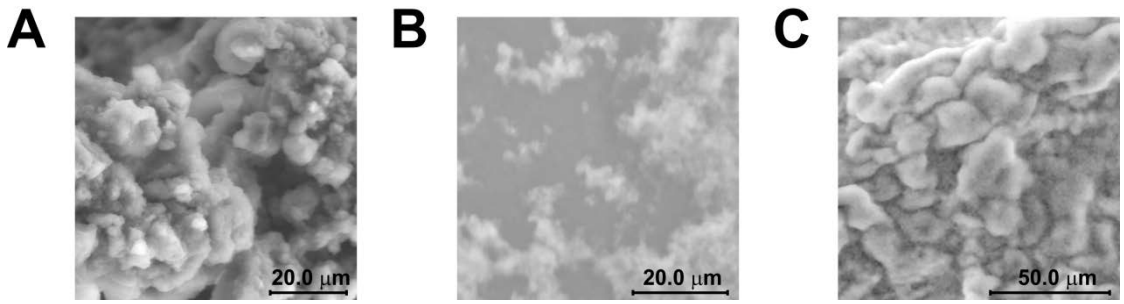

Figure S6. SEM images of poly-L-lysine mediated silica/catMMP12 (A), R5 mediated silica/catMMP12 (B) and silica-catMMP12-R5 (C).

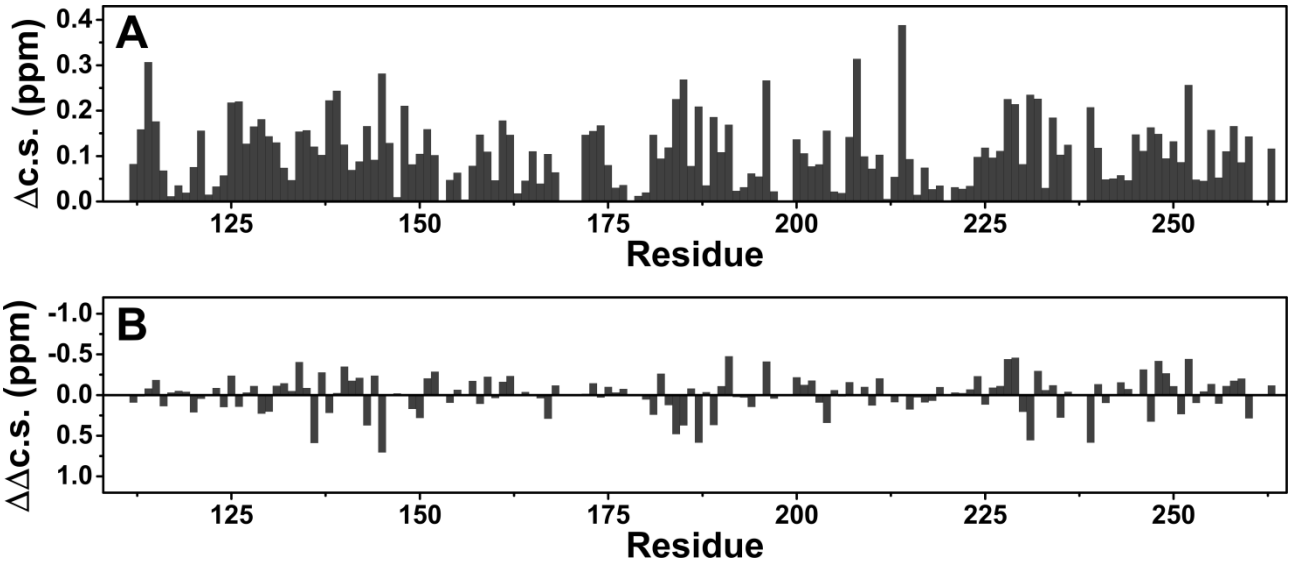

Figure S7. Chemical shift perturbation (panel A) and perturbation of the secondary chemical shifts of C_α and C_β nuclei (panel B) obtained from the analysis of 2D ^{13}C-^{13}C DARR spectra of catMMP12 in poly-L-lysine and catMMP12-R5 samples. The chemical shift perturbation is expressed as a combined measure of the change in the chemical shift of both C_α and C_β according to the formula $\Delta c.s. = \frac{1}{2}\sqrt{\Delta\delta_{C\alpha}^2 + \Delta\delta_{C\beta}^2}$. The perturbation of the secondary chemical shifts of C_α and C_β nuclei is instead expressed by the formula $\Delta\Delta c.s. = \left(C_\alpha - C_\beta\right)_{catMMP12-R5} - \left(C_\alpha - C_\beta\right)_{catMMP12}$.
Of note, no significant change in the secondary structure propensity is observed.

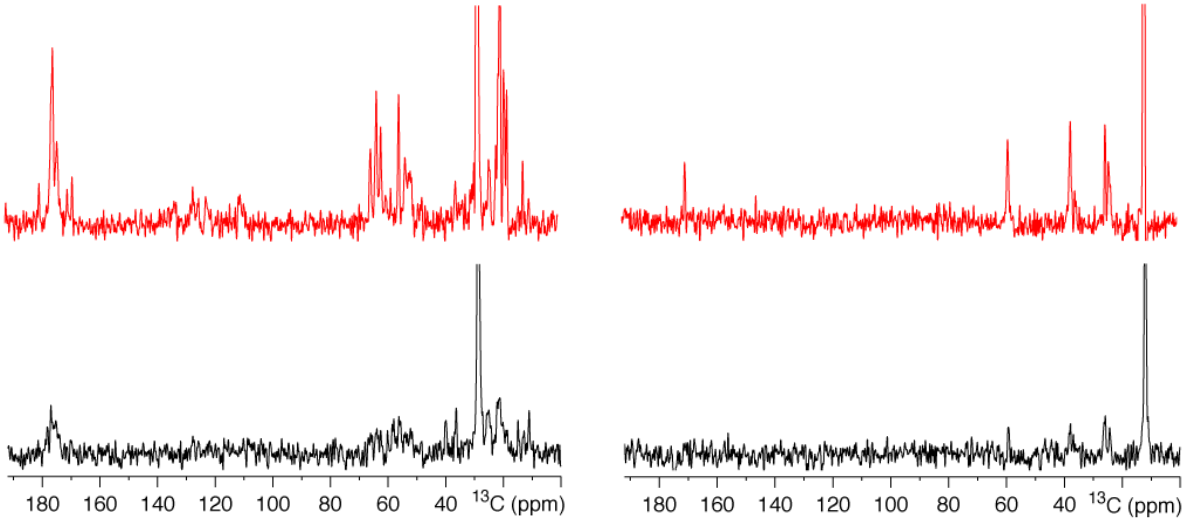

Figure S8. 1D traces from 2D ^{13}C-^{13}C DARR spectra of catMMP12 in poly-L-lysine (red) and catMMP12-R5 (black). The spectra show the effect of local heterogeneity in the broadening of the crosspeaks with respect to the diagonal signal (the signal with highest intensity).

Supporting References:

[1] I. Bertini, V. Calderone, M. Fragai, R. Jaiswal, C. Luchinat, M. Melikian, E. Mylonas, D. Svergun, *J. Am. Chem. Soc.* **2008**, *130*, 7011–7021.
[2] C. C. Lechner, C. F. W. Becker, *J. Pept. Sci.* **2014**, *20*, 152–158.
[3] M. O. Palmier, S. R. Van Doren, *Anal. Biochem.* **2007**, *371*, 43–51.

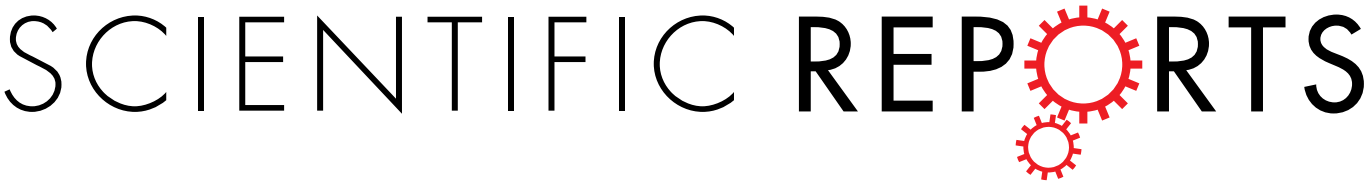

OPEN

^{1}H-detected solid-state NMR of proteins entrapped in bioinspired silica: a new tool for biomaterials characterization

Received: 07 March 2016
Accepted: 24 May 2016
Published: 09 June 2016

Enrico Ravera[1], Linda Cerofolini[1,2], Tommaso Martelli[3], Alexandra Louka[1], Marco Fragai[1,2] & Claudio Luchinat[1,2,3]

Proton-detection in solid-state NMR, enabled by high magnetic fields (>18 T) and fast magic angle spinning (>50 kHz), allows for the acquisition of traditional ^{1}H-^{15}N experiments on systems that are too big to be observed in solution. Among those, proteins entrapped in a bioinspired silica matrix are an attractive target that is receiving a large share of attention. We demonstrate that ^{1}H-detected SSNMR provides a novel approach to the rapid assessment of structural integrity in proteins entrapped in bioinspired silica.

It is the future strategy in biotechnology to use the processes of nature and not only those of chemistry to create biomaterials. The advantage of natural processes is that they occur under physiological conditions, i.e.: in aqueous environment, around neutral pH and at room temperature and ambient pressure. In this light, such processes are promising candidates for a green-based industry. One interesting class of biomaterials is bio-inspired silica, where the polycondensation of silicic acid is directed by the presence of a polycationic templating molecule or by enzymes[1–6]. *In vitro*, large amounts of proteins can be properly encapsulated in silica by simply mixing cationic catalyst with the silicic acid and the protein itself[7] or, to increase the immobilization yield, the protein can be fused to a biosilica-promoting peptide[8–14]. The materials obtained by such natural processes can be easily tuned into different morphologies by the use of slight perturbations of the experimental conditions[10,15], and can be easily endowed with peculiar chemical properties, such as fluorescence or catalytic activity by the incorporation of proteins[9]. In turn, proteins that are entrapped in a silicic matrix become more stable and easily reusable[16,17]. Despite such a vast applicability, the atomic-level structural characterization of such systems is still far from being routine; indeed, the first solid-state nuclear magnetic resonance (SSNMR) spectra of a biosilica entrapped enzyme were published by us only recently[18]. However, such approach relies on ^{13}C detection and thus is intrinsically sensitivity-limited, requiring several milligrams of material for a thorough characterization[19]. We have demonstrated that sensitivity can be dramatically improved by means of Dynamic Nuclear Polarization; and in spite of the sizable reduction in spectral resolution intrinsic of DNP at low temperature, it was possible to observe signals of the properly-folded protein[20]. Of note, in a recent paper, DNP was used to detect the signals from the biosilica-forming peptide PL12, also detecting correlation of silica with lysine sidechains[21]. Another recent paper used DNP to study the proteic component of the biosilica of intact diatoms[22].

Yet, another option is available for increasing the sensitivity in the detection of enzymes entrapped in bioinspired-silica, and this strategy also has the intrinsic advantage of a more informative chemical shift distribution: the acquisition of ^{1}H-detected experiments on ^{15}N-labelled samples. Indeed, the development of fast MAS (>50 kHz) and the development of high-field magnets (>18T) allows for proton-detected techniques, because the frequency of the dipolar interaction stays constant but its effect is mitigated by high field and fast MAS is able to accomplish their averaging. This brings into SSNMR[23–36] many of the procedures for assignment and collection of structural restraints routinely applied in solution NMR since several years[37]. Higher fields and faster spinning made it even possible to record ^{1}H-^{1}H correlation experiments[38]. Recently, ^{1}H-detection based experiments were

[1]Magnetic Resonance Center (CERM), University of Florence, and Interuniversity Consortium for Magnetic Resonance of Metalloproteins (CIRMMP), Via L. Sacconi 6, 50019 Sesto Fiorentino (FI), Italy. [2]Department of Chemistry "Ugo Schiff", University of Florence, Via della Lastruccia 3, 50019 Sesto Fiorentino (FI), Italy. [3]Giotto Biotech S.R.L., Via Madonna del Piano 6, 50019 Sesto Fiorentino (FI), Italy. Correspondence and requests for materials should be addressed to E.R. (email: ravera@cerm.unifi.it) or C.L. (email: claudioluchinat@cerm.unifi.it)

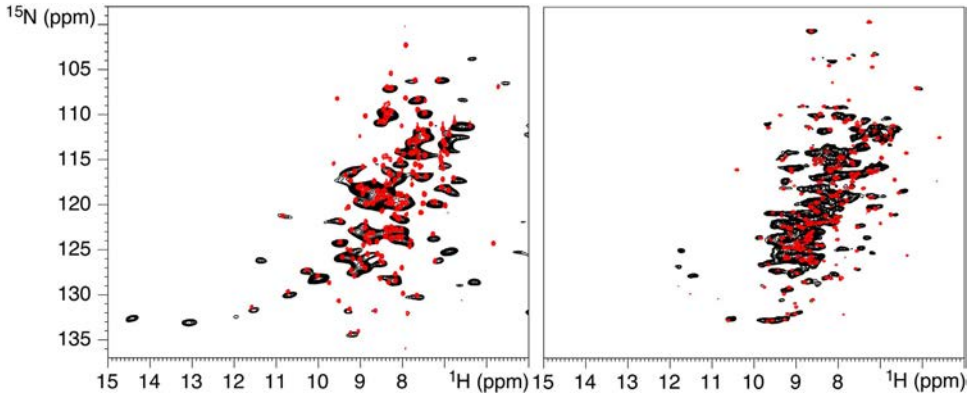

Figure 1. 2D ^{1}H-^{15}N HSQC spectra of catMMP12-R5 (left) and GFP-R5 (right) showing the comparison between the solid-state spectrum (black) and the solution-state spectrum (red). ^{1}H-linewidths are about 240 Hz for catMMP12-R5 and 140 Hz for GFP-R5.

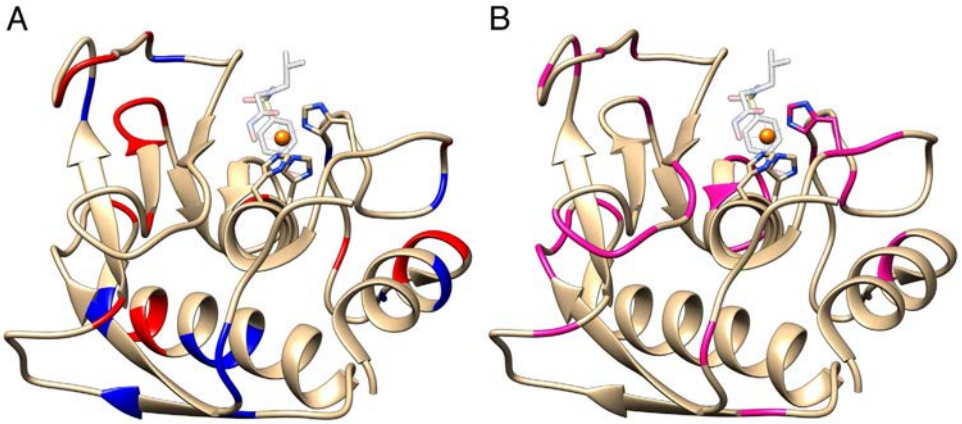

Figure 2. (**A**) The X-ray structure of catMMP12 (1RMZ[42], which does not carry the R5 fusion) showing the charged residues in blue (positive) and red (negative). (**B**) The structure of catMMP12 with the residues showing no signals shown in magenta. Apparently, they tend to cluster close to loops or in proximity of charged residues, which can interact with the biosilica matrix.

applied to the study of bone[39]. It is important to remark that even though ^{1}H-detection has been introduced in solid state NMR already since several years[23,24], it is relevant to understand which samples are amenable for its application. Herein, we demonstrate that proton-detected solid-state NMR, enabled by fast magic angle spinning (60 kHz) and high magnetic field (20 T), is feasible for bioinspired-silica-entrapped proteins. In particular, we show that basic ^{1}H-^{15}N correlation spectra[29,40] can be acquired in fully protonated, ^{15}N-labelled, samples of two proteins, namely green fluorescent protein (GFP) and the catalytic domain of matrix metalloproteinase 12 (catMMP12), both in fusion with the biosilica-promoting R5 peptide (SSKKSGSYSGSKGSKRRIL) at the C-terminus[41].

Results and Discussion

The solid state NMR 2D ^{1}H-^{15}N HSQC spectra of fully protonated GFP-R5 and catMMP12-R5 (Fig. 1) could be acquired in 4 h 34′ and 10 h 36′ respectively on 3 mg of sample, including the bioinspired-silica matrix. The comparison with solution state 2D ^{1}H-^{15}N HSQC is immediate and reveals that the vast majority of resonances is preserved, confirming the preservation of the structural integrity of the protein (Fig. 1).

An interesting observation is that a number of resonances could not be observed for MMP12 in the solid state NMR spectrum (Fig. 2 and Table 1). These resonances cluster at, or near to, loops and charged residues. This can be due to two extreme possibilities, i.e.: static disorder or mobility. The first causes heterogeneous broadening of the resonances, the second makes the dipolar-based polarization transfer inefficient. The negligible INEPT-based signal observed previously[18], suggests that the prevailing effect is static disorder induced by charge interactions with the silica matrix, or by conformational freezing of loops induced by the the presence of the amorphous matrix. This conclusion is further supported by the observation that the residues with missing resonances in the ^{1}H-detected experiments are always found (with the only exception of L147) in the ^{13}C-based experiment. F237 is not observed in the ^{13}C-based strategy, but is observed in the ^{1}H-based strategy, whereas its neighboring M236 is not. Finally, residues D171 and T205, which flank missing stretches in the ^{1}H-based strategy are even not observed in solution-NMR ^{13}C-detected experiments. Taken together, these observations suggest that there is no correlation in the disappearence of peaks between the ^{1}H-detection strategy and the ^{13}C-detection strategy,

Residue No.	Residue Type	Flanking sequences	Secondary structure Element
110	R	RKH	Loop
119	N	RINNY	Loop
121	Y	NNYTP	Loop
122	T	NYTPD	Loop
124	D	TPDMN	Loop
147	L	TPLKF	Loop
157	A	GMADI	Loop
166	G	ARGAH	Loop
168	H	GAHGD	Loop
172	H	DFHAF	Loop
176	G	FDGKG	Loop
185	F	HAFGP	Loop
186	G	AFGPG	Loop
188	G	GPGSG	Loop
189	S	PGSGI	Loop
190	G	GSGIG	Loop
201	F	EDEFW	Loop
206	H	TTHSG	Loop
207	S	THSGG	Loop
208	G	HSGGT	Loop
209	G	SGGTN	Loop
211	N	GTNLF	Loop
213	F	NLFLT	Helix
228 (active site ligand)	H	LGHSS	Loop
229	S	GHSSD	Loop
236	M	AVMFP	Loop
241	K	TYKYV	Loop
254	D	ADDIR	Helix

Table 1. Residues with missing NH resonances in the catMMP12-R5 ^{1}H-^{15}N solid state NMR experiment. The resonances assignment reported in the bmrb under the accession code 6444[42] has been used for the interpretation of the spectra. Also for GFP some resonances could not be observed, again maily in proximity of charged residues and loops (Fig. 3 and Table 2).

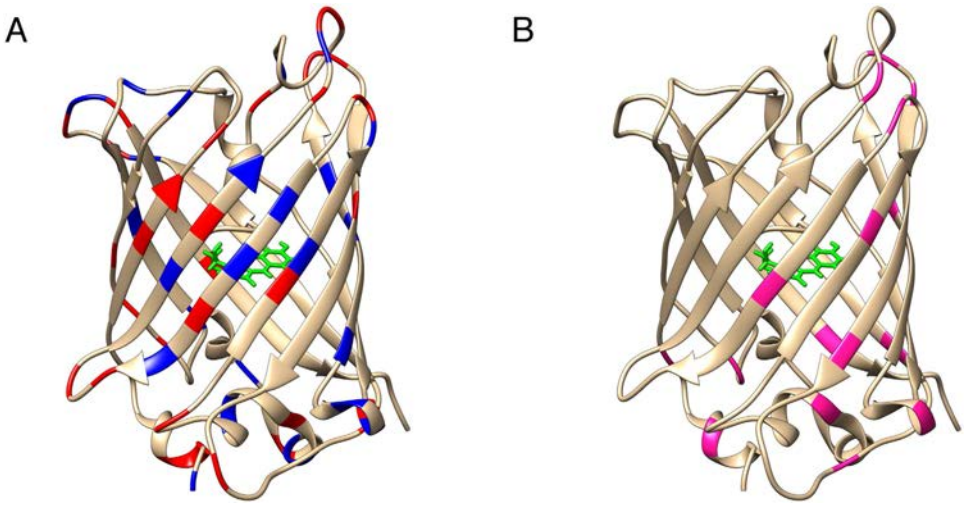

Figure 3. (**A**) The X-ray structure of GFP (2WUR[43], which does not carry the R5 fusion) showing the charged residues in blue (positive) and red (negative). (**B**) The structure of GFP with the residues showing no signals shown in magenta.

and they support the hypothesis that static disorder is sensed to a lesser extent by ^{13}C with respect to ^{1}H nuclei. Some resonances, which are in substantial overlap with others, are not clearly identifiable as missing, but their absence can in be inferred on a structural basis. Some additional peaks appear in the solid state NMR spectrum

Residue No.	Residue Type	Flanking sequences	Secondary structure Element
7	L	EE**L**FT	Helix
37	A	GD**A**TY	Loop
83	F	HD**F**FK	Helix
97	T	ER**T**IS	Strand
104	G	DD**G**NY	Loop
110	A	TR**A**EV	Strand
129	D	GI**D**FK	Loop
130	F	ID**F**KE	Loop
157	Q	DK**Q**KN	Helix
167	I	FK**I**RH	Strand
173	D	IE**D**GS	Loop
175	S	DG**S**VQ	Loop
185	N	QQ**N**TI	Strand
194	L	GV**L**LD	Loop
200	Y	NH**Y**LS	Strand

Table 2. Residues with missing NH resonances in the GFP-R5 ^{1}H-^{15}N solid state NMR experiment. The resonances assignment reported in the bmrb under the accession code 5666[44] has been used for the interpretation of the spectra.

of catMMP12-R5, which are not present in the solution NMR spectrum, at proton/nitrogen chemical shifts of 11.4/126.2, 13.1/ 133.1, 14.4/132.6 ppm respectively. These are ^{15}N-aliased signals (unaliased 15N chemical shift values are 166.0, 172.8 and172.5, respectively), which belong to the Hδ1 (or Hε2) of the histidine residues coordinating the two zinc ions. These protons are very weak in intensity in the solution NMR because of exchange with water. Two further signals at proton/nitrogen chemical shifts of 6.3/128.6 and 6.9/125.2 ppm, respectively, that are present in the solid state NMR spectrum, can be related instead to the protons of lysines or arginines side-chains, that are lost in the solution NMR spectrum for the same reason.

It is interesting to observe that, in line with a previous observation, the R5 tail does not appear in the spectrum, most probably because it is disordered and thus extremely broad, as observed by the Drobny's group[45]. As a remark, while it is possible to observe it for the catMMP12-R5, the R5 tail could not be observed in GFP-R5 solution, under the experimental conditions at which assignment of the WT protein is available, i.e.: pH = 8 and T = 310 K, whereas it reappears at lower temperature, indicating exchange with the solvent in line with previous reports on intrinsically disordered proteins[46,47].

The resolution between the two proteins varies quite significantly (240 Hz and 140 Hz ^{1}H-linewidth for catMMP12-R5 and GFP-R5 respectively). On the one hand, this may suggest that the residual mobility of the entrapped protein is different in the two cases, yielding a different averaging of the dipolar interaction; on the other hand this could reflect different degrees of static disorder or different anisotropic bulk magnetic susceptibility as caused by different silica particle size[48]. However it is important to observe that resolution is in a practically useful range even if the protein is completely protonated. This is an observation of remarkable importance because, on the one hand, ^{1}H-detection based methods have been proven applicable and successful on a rather vast range of substrates[33], also when fully protonated[40,31,19]; but, on the other hand, perdeuteration with more or less extensive back exchange is usually necessary to yield decoupling of the ^{1}H dipolar network[33,49]. Thus, the remarkably sharp lines observed in the present study on fully protonated proteins guarantees, at least for a preliminary step, to use a relatively inexpensive sample, instead of resorting to the more expensive deuterated samples.

Overall, the present approach presents a number of advantages with respect to the approach based on the comparison of ^{13}C-^{13}C correlation maps. Brilliant discussion of the advantages of moving to smaller volumes[50] and ^{1}H detection[33] has been provided, and the solid-state NMR rotor technology is progressing fast[38], so we will only briefly recapitulate the specific advantages in the present case. First of all, the amount of sample needed is far smaller, yielding a reduction in the sample cost. The comparison here reported is based on the catMMP12-R5 sample, which has an encapsulation efficiency of 1.2 nmol of protein per μmol of silica[41]. The total amount of sample for the current work is 3 mg, corresponding to the 1.7 μl of the rotor active volume of a 1.3 mm Bruker rotor; whereas for a 4 mm rotor with CRAMPS inserts, the amount of sample needed to fill a 50 μl volume was over 80 mg[41]. As we are referring to a protein composite, it is rather more instructive to compare the starting protein solutions. The starting protein solution for the sample used in the present work was 400 μl at 45 mg/mL concentration of ^{15}N-labeled protein (estimated cost 100 €, not including manpower), whereas the protein solution used for the sample preparation in reference[41] was 2 mL at 45 mg/mL concentration of $^{13}C^{15}N$ protein (estimated cost 900 €, not including manpower), which corresponds to an order of magnitude difference in sample cost.

Another important point is the amount of measurement time that is needed: a ^{1}H-start/^{1}H detect experiment is expected to be roughly a factor 2.5 more sensitive than a ^{1}H-start-^{13}C detect experiment, neglecting relaxation effects and assuming 100% efficiency in each transfer step; the amount of experiments to be acquired in the indirect detection is about a factor 6 smaller and the full-rotor sensitivity of a solenoid coil (including the higher

efficiency but also the reduction of sample) on passing from a 4 mm to a 1.3 mm rotor is roughly reduced by a factor 9.5 [51,50], which would yield about a factor 2 increase in sensitivity, corresponding to about a factor 4 reduction in experiment time, thus in experiment price. These consideration are qualitatively reflected in the present case, as we find that the ^{1}H-^{15}N HSQC experiment could be acquired in 10 h 36′ for catMMP12-R5 in the current setup, whereas the ^{13}C-^{13}C DARR experiment reported in reference[41] was acquired in 45 h 31′. Considering the price of access to high-field NMR solid-state instrumentation, the ^{1}H-detection-based approach is about 80% cheaper than the ^{13}C-detection based approach.

It is of remarkable importance that the ^{13}C-^{13}C transfers is likely to be differently efficient between the solution and the solid, resulting in a less straightforward interpretation of the spectral fingerprint of the molecule. Finally, ^{1}H is much more sensitive to changes in the local environment.

In conclusion, we here demonstrate that enzymes entrapped in bioinspired silica can be studied by ^{1}H-detected solid-state NMR, using a total sample of about 3 mg (including the silica matrix), as compared to previous studies where a larger amount of protein was used; and we were able to show that structural integrity is maintained.

It is expected that a) this approach will make it easier to screen for reaction conditions and/or substrates on a lower amount of sample and in a shorter time, and b) that the use of extensive deuteration will make it possible to perform assignment and structure calculations on a single SSNMR sample, without resorting to solution NMR, although at the price of increased sample production costs.

Methods

Solid-state NMR spectroscopy. All spectra were acquired with a Bruker AvanceIII spectrometer operating at 850 MHz ^{1}H larmor frequency, equipped with a 1.3 mm probehead tuned to ^{1}H-^{29}Si-^{15}N. Samples were packed into Bruker 1.3 mm zirconia rotors, centerpacked with KFM inserts (3 μl total volume) to avoid dehydration. Sample packing was performed with a ultracentrifugal device (courtesy of Bruker Biospin)[52]. Sample rotation was regulated to 60 kHz via a commercial Bruker MAS II pneumatic unit, and temperature was regulated to 240 K at stator inlet, roughly corresponding to 300 K at the sample. Pulses were 2.5 μs for ^{1}H, 3.5 μs ^{15}N. Optimal interscan delays are reported along with the spectra. During ^{15}N evolution SW$_f$TPPM[53–56] decoupling was applied at 25 kHz. Water suppression was achieved by a 300 ms MISSISSIPPI pulse train at 25 kHz applied during a z-filter period when the magnetization is stored on ^{15}N[29,57]. In the solid state HSQC experiment[29], the polarization transfer steps between different nuclei is accomplished via cross-polarization (CP)[58]. The first CP step, which drives the magnetization from all protons to the nitrogen spins is 1.2-15 ms long; the second step, which must be as short as possible to be specific and not dominated by spin-diffusion, was kept at 300 μs.

Solution-state NMR spectroscopy. Experiments were performed on samples of the ^{15}N isotopically enriched catalytic domain of MMP-12 fused with R5 peptide (catMMP12-R5) at protein concentration of 0.90 mM in water buffered solution (20 mM Tris, pH 7.2, 50 mM NaCl, 0.1 mM $ZnCl_2$, 10 mM $CaCl_2$, 200 mM AHA). The protein was inhibited with NNGH (N-Isobutyl-N-(4-methoxyphenylsulfonyl)glycyl hydroxamic acid) to reproduce the experimental conditions used in previous studies[18,42,59–61]. The same experiments were performed on GFP fused with R5 peptide (GFP-R5) at protein concentration of 0.35 mM in water buffered solution (50 mM Tris, pH 8, 300 mM NaCl). The spectrum of catMMP12-R5 was recorded on a Bruker DRX 500 spectrometer equipped with triple-resonance CryoProbe, and temperature was set to 298 K. The spectrum of GFP-R5 was recorded on a Bruker AVANCE 600 spectrometer equipped with a triple resonance room temperature probe, and temperature was set to 310 K. Spectra were processed with the Bruker TOPSPIN software packages and analyzed with the program CARA (Computer Aided Resonance Assignment, ETH Zurich).

Protein expression and purification. The catalytic domain of MMP-12 (catMMP12) has been expressed as fusion protein with a R5 peptide at the C-terminus as already described[62].

pET-21a constructs encoding GFP-R5, sequence given below, were transformed into Escherichia coli BL21(DE3) cells which were subsequently cultured in ^{15}N-labelled minimal medium (M9). Cells were grown at 310 K, until OD 0.6–0.8 and subsequently induced with IPTG (isopropyl 1-thio-β-D-galactopyranoside) with a final concentration of 0.5 mM for 5 h.

GFP-R5 was then extracted from harvested cells by sonication and subsequent ultra-centrifugation (40 min, 40000 rpm). The protein was first purified from the crude extract with an anionic exchange column (Q-FF 16/10, A buffer: Tris 50 mM pH 8, B buffer: Tris 50 mM pH 8, NaCl 1 M). The GFP-R5 was finally purified with gel filtration using a Superdex 75 26/60 in Tris 50 mM, NaCl 300 mM, pH 8. The concentrations of NaCl was reduced to 50 mM for the preparation of entrapped samples for ssNMR experiments.

The sequence of the GFP-R5 is:

1 MGKVSKGEEL FTGVVPILVE LDGDVNGHKF SVSGEGEGDA TYGKLTLKFI
51 CTTGKLPVPW PTLVTTFGYG LQCFARYPDH MKQHDFFKSA MPEGYVQERT
101 IFFKDDGNYK TRAEVKFEGD TLVNRIELKG IDFKEDGNIL GHKLEYNYNS
151 HNVYIMADKQ KNGIKVNFKI RHNIEDGSVQ LADHYQQNTP IGDGPVLLPD
201 NHYLSTQSAL SKDPNEKRDH MVLLEFVTAA GITLGMDELY K(GSASGGGGS)
251 [SKKSGSYSGS KGSKRRIL]

brackets indicate a linker that connects the protein to the R5 peptide, square brackets denote the R5 sequence (S201-L220 from sil1P from *C. fusiformis*).

References

1. Kröger, N., Deutzmann, R. & Sumper, M. Polycationic peptides from diatom biosilica that direct silica nanosphere formation. *Science* **286,** 1129–1132 (1999).
2. Kröger, N., Deutzmann, R. & Sumper, M. Silica-precipitating Peptides from Diatoms THE CHEMICAL STRUCTURE OF SILAFFIN-1A FROM CYLINDROTHECA FUSIFORMIS. *J. Biol. Chem.* **276,** 26066–26070 (2001).
3. Weiner, S. & Dove, P. M. An Overview of Biomineralization Processes and the Problem of the Vital Effect. *Rev. Mineral. Geochem.* **54,** 1–29 (2003).
4. Belton, D. J., Patwardhan, S. V., Annenkov, V. V., Danilovtseva, E. N. & Perry, C. C. From biosilicification to tailored materials: Optimizing hydrophobic domains and resistance to protonation of polyamines. *Proc. Natl. Acad. Sci. USA*. **105,** 5963–5968 (2008).
5. Belton, D. J., Deschaume, O. & Perry, C. C. An overview of the fundamentals of the chemistry of silica with relevance to biosilicification and technological advances. *FEBS J.* **279,** 1710–1720 (2012).
6. Senior, L. *et al.* Structure and function of the silicifying peptide R5. *J. Mater. Chem. B* (2015). doi: 10.1039/C4TB01679C.
7. Luckarift, H. R., Spain, J. C., Naik, R. R. & Stone, M. O. Enzyme immobilization in a biomimetic silica support. *Nat. Biotechnol.* **22,** 211–213 (2004).
8. Foo, C. W. P. *et al.* Novel nanocomposites from spider silk–silica fusion (chimeric) proteins. *Proc. Natl. Acad. Sci.* **103,** 9428–9433 (2006).
9. Marner, W. D., Shaikh, A. S., Muller, S. J. & Keasling, J. D. Enzyme immobilization via silaffin-mediated autoencapsulation in a biosilica support. *Biotechnol. Prog.* **25,** 417–423 (2009).
10. Marner, W. D., Shaikh, A. S., Muller, S. J. & Keasling, J. D. Morphology of artificial silica matrices formed via autosilification of a silaffin/protein polymer chimera. *Biomacromolecules* **9,** 1–5 (2008).
11. Zhou, S. *et al.* Control of silicification by genetically engineered fusion proteins: Silk-silica binding peptides. *Acta Biomater.* **15,** 173–180 (2015).
12. Belton, D. J., Mieszawska, A. J., Currie, H. A., Kaplan, D. L. & Perry, C. C. Silk-silica composites from genetically engineered chimeric proteins: materials properties correlate with silica condensation rate and colloidal stability of the proteins in aqueous solution. *Langmuir ACS J. Surf. Colloids* **28,** 4373–4381 (2012).
13. Canabady-Rochelle, L. L. S. *et al.* Bioinspired silicification of silica-binding peptide-silk protein chimeras: comparison of chemically and genetically produced proteins. *Biomacromolecules* **13,** 683–690 (2012).
14. Mieszawska, A. J., Nadkarni, L. D., Perry, C. C. & Kaplan, D. L. Nanoscale control of silica particle formation via silk-silica fusion proteins for bone regeneration. *Chem. Mater. Publ. Am. Chem. Soc.* **22,** 5780–5785 (2010).
15. Lechner, C. C. & Becker, C. F. W. Silaffins in Silica Biomineralization and Biomimetic Silica Precipitation. *Mar. Drugs* **13,** 5297–5333 (2015).
16. Sheldon, R. A. Enzyme Immobilization: The Quest for Optimum Performance. *Adv. Synth. Catal.* **349,** 1289–1307 (2007).
17. Blanco, R. M., Calvete, J. J. & Guisán, J. Immobilization-stabilization of enzymes; variables that control the intensity of the trypsin (amine)-agarose (aldehyde) multipoint attachment. *Enzyme Microb. Technol.* **11,** 353–359 (1989).
18. Fragai, M. *et al.* SSNMR of biosilica-entrapped enzymes permits an easy assessment of preservation of native conformation in atomic detail. *Chem. Commun.* **50,** 421–423 (2013).
19. Ravera, E. *et al.* NMR of sedimented, fibrillized, silica-entrapped and microcrystalline (metallo) proteins. *J. Magn. Reson.* **253,** 60–70 (2015).
20. Ravera, E. *et al.* Biosilica-Entrapped Enzymes Studied by Using Dynamic Nuclear-Polarization-Enhanced High-Field NMR Spectroscopy. *ChemPhysChem* **16,** 2751–2754 (2015).
21. Geiger, Y., Gottlieb, H. E., Akbey, Ü., Oschkinat, H. & Goobes, G. Studying the Conformation of a Silaffin-Derived Pentalysine Peptide Embedded in Bioinspired Silica using Solution and Dynamic Nuclear Polarization Magic-Angle Spinning NMR. *J. Am. Chem. Soc.* **138,** 5561–5567 (2016).
22. Jantschke, A. *et al.* Insight into the Supramolecular Architecture of Intact Diatom Biosilica from DNP-Supported Solid-State NMR Spectroscopy. *Angew. Chem. Int. Ed.* **54,** 15069–15073 (2015).
23. Reif, B. & Griffin, R. G. 1H detected 1H,15N correlation spectroscopy in rotating solids. *J. Magn. Reson. San Diego Calif 1997* **160,** 78–83 (2003).
24. Chevelkov, V. *et al.* 1H Detection in MAS Solid-State NMR Spectroscopy of Biomacromolecules Employing Pulsed Field Gradients for Residual Solvent Suppression⊥. *J. Am. Chem. Soc.* **125,** 7788–7789 (2003).
25. Chevelkov, V., Rehbein, K., Diehl, A. & Reif, B. Ultrahigh resolution in proton solid-state NMR spectroscopy at high levels of deuteration. *AngewChem IntEd Engl* **45,** 3878–3881 (2006).
26. Zhou, D. H. *et al.* Proton-detected solid-state NMR spectroscopy of fully protonated proteins at 40 kHz magic-angle spinning. *J. Am. Chem. Soc.* **129,** 11791–11801 (2007).
27. Linser, R., Bardiaux, B., Higman, V., Fink, U. & Reif, B. Structure calculation from unambiguous long-range amide and methyl 1H-1H distance restraints for a microcrystalline protein with MAS solid-state NMR spectroscopy. *J. Am. Chem. Soc.* **133,** 5905–5912 (2011).
28. Linser, R. *et al.* Proton-Detected Solid-State NMR Spectroscopy of Fibrillar and Membrane Proteins. *Angew. Chem. Int. Ed.* **50,** 4508–4512 (2011).
29. Knight, M. J. *et al.* Fast resonance assignment and fold determination of human superoxide dismutase by high-resolution proton-detected solid state MAS NMR spectroscopy. *Angew.Chem.Int.Ed.* **50,** 11697–11701 (2011).
30. Knight, M. J. *et al.* Structure and backbone dynamics of a microcrystalline metalloprotein by solid-state NMR. *Proc.Natl.Acad.Sci. USA* **109,** 11095–11100 (2012).
31. Marchetti, A. *et al.* Backbone Assignment of Fully Protonated Solid Proteins by ^{1}H Detection and Ultrafast Magic-Angle-Spinning NMR Spectroscopy. *Angew. Chem. Int. Ed.* **51,** 10756–10759 (2012).
32. Knight, M. J., Felli, I. C., Pierattelli, R., Emsley, L. & Pintacuda, G. Magic Angle Spinning NMR of Paramagnetic Proteins. *Acc. Chem. Res.* **46,** 2108–2116 (2013).
33. Barbet-Massin, E. *et al.* Rapid Proton-Detected NMR Assignment for Proteins with Fast Magic Angle Spinning. *J. Am. Chem. Soc.* **136,** 12489–12497 (2014).
34. Zhang, R., Pandey, M. K., Nishiyama, Y. & Ramamoorthy, A. A Novel High-Resolution and Sensitivity-Enhanced Three-Dimensional Solid-State NMR Experiment Under Ultrafast Magic Angle Spinning Conditions. *Sci. Rep.* **5,** 11810 (2015).
35. Zhang, R. & Ramamoorthy, A. Selective excitation enables assignment of proton resonances and 1H-1H distance measurement in ultrafast magic angle spinning solid state NMR spectroscopy. *J. Chem. Phys.* **143,** 034201 (2015).
36. Zhang, R. & Ramamoorthy, A. Dynamics-based selective 2D 1H/1H chemical shift correlation spectroscopy under ultrafast MAS conditions. *J. Chem. Phys.* **142,** 204201 (2015).
37. Bertini, I., McGreevy, K. S. & Parigi, G. *NMR in systems biology*. (Wiley, 2012).
38. Pandey, M. K. *et al.* 1020 MHz single-channel proton fast magic angle spinning solid-state NMR spectroscopy. *J. Magn. Reson.* **261,** 1–5 (2015).
39. Mroue, K. H. *et al.* Proton-Detected Solid-State NMR Spectroscopy of Bone with Ultrafast Magic Angle Spinning. *Sci. Rep.* **5,** 11991 (2015).
40. Zhou, D. H., Shah, G., Mullen, C., Sandoz, D. & Rienstra, C. M. Proton-Detected Solid-State NMR Spectroscopy of Natural-Abundance Peptide and Protein Pharmaceuticals. *Angew. Chem.* **121,** 1279–1282 (2009).

41. Martelli, T. *et al.* Atomic level quality assessment of enzymes encapsulated in bio-inspired silica. *Chem. - Eur. J.* **4,** 425–432 (2016).
42. Bertini, I. *et al.* Conformational variability of matrix metalloproteinases: Beyond a single 3D structure. *Proc. Natl. Acad. Sci. USA*. **102,** 5334 –5339 (2005).
43. Shinobu, A., Palm, G. J., Schierbeek, A. J. & Agmon, N. Visualizing Proton Antenna in a High-Resolution Green Fluorescent Protein Structure. *J. Am. Chem. Soc.* **132,** 11093–11102 (2010).
44. Khan, F., Stott, K. & Jackson, S. 1H, 15N and 13C backbone assignment of the green fluorescent protein (GFP). *J. Biomol. NMR* **26,** 281–282 (2003).
45. Roehrich, A. & Drobny, G. Solid-State NMR Studies of Biomineralization Peptides and Proteins. *Acc. Chem. Res.* **46,** 2136–2144 (2013).
46. Gil, S. *et al.* NMR Spectroscopic Studies of Intrinsically Disordered Proteins at Near-Physiological Conditions. *Angew. Chem. Int. Ed.* **52,** 11808–11812 (2013).
47. Croke, R. L., Sallum, C. O., Watson, E., Watt, E. D. & Alexandrescu, A. T. Hydrogen exchange of monomeric α-synuclein shows unfolded structure persists at physiological temperature and is independent of molecular crowding in Escherichia coli. *Protein Sci. Publ. Protein Soc.* **17,** 1434–1445 (2008).
48. Earl, W. L. & Vanderhart, D. L. Measurement of 13C chemical shifts in solids. *J. Magn. Reson. 1969* **48,** 35–54 (1982).
49. Asami, S. & Reif, B. Proton-Detected Solid-State NMR Spectroscopy at Aliphatic Sites: Application to Crystalline Systems. *Acc. Chem. Res.* **46,** 2089–2097 (2013).
50. Demers, J. P., Chevelkov, V. & Lange, A. Progress in correlation spectroscopy at ultra-fast magic-angle spinning: basic building blocks and complex experiments for the study of protein structure and dynamics. *Solid State NuclMagnReson* **40,** 101–113 (2011).
51. McNeill, S. A., Gor'kov, P. L., Struppe, J., Brey, W. W. & Long, J. R. Optimizing ssNMR experiments for dilute proteins in heterogeneous mixtures at high magnetic fields. *Magn. Reson. Chem.* **45,** S209–S220 (2007).
52. Bertini, I. *et al.* On the use of ultracentrifugal devices for sedimented solute NMR. *J.Biomol.NMR* **54,** 123–127 (2012).
53. Thakur, R. S., Kurur, N. D. & Madhu, P. K. Swept-frequency two-pulse phase modulation for heteronuclear dipolar decoupling in solid-state NMR. *Chem. Phys. Lett.* **426,** 459–463 (2006).
54. Thakur, R. S., Kurur, N. D. & Madhu, P. K. An experimental study of decoupling sequences for multiple-quantum and high-resolution MAS experiments in solid-state NMR. *Magn. Reson. Chem.* **46,** 166–169 (2008).
55. Thakur, R. S., Kurur, N. D. & Madhu, P. K. An analysis of phase-modulated heteronuclear dipolar decoupling sequences in solid-state nuclear magnetic resonance. *J. Magn. Reson.* **193,** 77–88 (2008).
56. Madhu, P. K. Heteronuclear Spin Decoupling in Solid-State Nuclear Magnetic Resonance: Overview and Outlook. *Isr. J. Chem.* **54,** 25–38 (2014).
57. Zhou, D. H. & Rienstra, C. M. High-performance solvent suppression for proton detected solid-state NMR. *J. Magn. Reson.* **192,** 167–172 (2008).
58. Pines, A., Gibby, M. G. & Waugh, J. S. Proton enhanced NMR of dilute spins in solids. *J Chem Phys* **59,** 569–590 (1973).
59. Balayssac, S. *et al.* Solid-state NMR of matrix metalloproteinase 12: an approach complementary to solution NMR. *ChemBioChem* **8,** 486–489 (2007).
60. Bertini, I. *et al.* High-Resolution Solid-State NMR Structure of a 17.6 kDa Protein. *J. Am. Chem. Soc.* **132,** 1032–1040 (2010).
61. Luchinat, C., Parigi, G., Ravera, E. & Rinaldelli, M. Solid state NMR crystallography through paramagnetic restraints. *J. Am. Chem. Soc.* **134,** 5006–5009 (2012).
62. Bertini, I., Fragai, M., Luchinat, C., Melikian, M. & Venturi, C. Characterisation of the MMP-12-Elastin Adduct. *Chem. - Eur. J.* **15,** 7842–7845 (2009).

Acknowledgements

This work has been supported by Ente Cassa di Risparmio di Firenze, MIUR PRIN 2012SK7ASN, EC Contracts iNext No. 653706, Bio-NMR No. 261863, pNMR No. 317127 and IDPbyNMR No. 264257, and Instruct, part of the European Strategy Forum on Research Infrastructures (ESFRI), through its Core Centre CERM, Italy. ER holds a FIRC triennial fellowship "Gino Mazzega and Guglielmina Locatello" (17941).

Author Contributions

E.R., C.L. and M.F. designed the research; E.R., L.C., T.M. and A.L. performed the experiments; E.R., L.C., M.F. and C.L. interpreted the data; all authors wrote the manuscript.

Additional Information

Competing financial interests: C.L. holds a share of the company GiottoBiotech.

How to cite this article: Ravera, E. *et al.* ^{1}H-detected solid-state NMR of proteins entrapped in bioinspired silica: a new tool for biomaterials characterization. *Sci. Rep.* **6**, 27851; doi: 10.1038/srep27851 (2016).

ChemPubSoc Europe

DOI: 10.1002/chem.201504355

CHEMISTRY A European Journal Full Paper

Drug Development

A Divalent PAMAM-Based Matrix Metalloproteinase/Carbonic Anhydrase Inhibitor for the Treatment of Dry Eye Syndrome

B. Richichi+,[a] V. Baldoneschi,[a] S. Burgalassi,[b] M. Fragai+,[a, c] D. Vullo,[a] A. Akdemir,[d] E. Dragoni,[a] A. Louka,[c] M. Mamusa,[a] D. Monti,[b] D. Berti,[a] E. Novellino,[e] G. De Rosa,[e] C. T. Supuran,*[f] and C. Nativi*[a, c]

Abstract: Synthetic sulfonamide derivatives are a class of potent matrix metalloproteinase inhibitors (MMPI) that have potential for the treatment of diseases related to uncontrolled expression of these enzymes. The lack of selectivity of the large majority of such inhibitors, leading to the inhibition of MMPs in tissues other than the targeted one, has dramatically reduced the therapeutic interest in MMPIs. The recent development of efficient drug delivery systems that allow the transportation of a selected drug to its site of action has opened the way to new perspectives in the use of MMPIs. Here, a PAMAM-based divalent dendron with two sulfonamidic residues was synthesized. This nanomolar inhibitor binds to the catalytic domain of two MMPs as well as to the transmembrane human carbonic anhydrases (hCAs) XII, which is present in the eye and considered an antiglaucoma target. In the animal model of an experimental dry eye, no occurrence of dotted staining in eyes treated with our inhibitor was observed, indicating no symptoms of corneal desiccation.

Introduction

The widespread family of matrix metalloproteinases (MMPs) is constituted by calcium-dependent zinc-containing peptidases that are also known as matrixins.[1] MMPs exert fundamental physiological roles, such as tissue remodeling and cellular matrix degradation, but, if pathologically over-expressed, trigger a variety of severe disorders including atherosclerosis, heart failure, and cancer.[2]

[a] *Dr. B. Richichi,+ V. Baldoneschi, Prof. M. Fragai,+ Dr. D. Vullo, Dr. E. Dragoni, M. Mamusa, Prof. D. Berti, Prof. C. Nativi*
Department of Chemistry "Ugo Schiff", University of Florence
via della Lastruccia 3—13, 50019 Sesto Fiorentino (Italy)
E-mail: cristina.nativi@unifi.it

[b] *Prof. S. Burgalassi, Dr. D. Monti*
Department of Pharmacy, University of Pisa
via Bonanno 33, 56126 Pisa (Italy)

[c] *Prof. M. Fragai,+ A. Louka, Prof. C. Nativi*
CERM, University of Florence
via Sacconi 6, 50019 Sesto Fiorentino (Italy)

[d] *Dr. A. Akdemir*
Department of Pharmacy
Faculty of Pharmacy, Bezmialem Vakif University
Vatan Caddesi, 34093, Fatih, Istanbul (Turkey)

[e] *Prof. E. Novellino, Prof. G. D. Rosa*
Department of Pharmacy, University of Napoli "Federico II"
via Montesano 49, 80131 Napoli (Italy)

[f] *Prof. C. T. Supuran*
NEUROFARBA Department, University of Florence
via U. Schiff 6, Sesto Fiorentino (Italy)

[+] *These authors contributed equally to the present work.*

Supporting information for this article is available on the WWW under http://dx.doi.org/10.1002/chem.201504355.

For many years, the development of synthetic inhibitors (MMPIs) of MMPs represented an eagerly pursued strategy to regulate the abnormal expression of MMPs; however, the disappointing outcomes of the clinical trials convinced researchers to reconsider this approach.

Similar binding domains, showing the common property of adapting the binding pocket to the ligand shape, characterize all MMPs within the family. In addition, the large majority of the inhibitors reported to present feature low bioavailability and reduced solubility in physiological media. These hallmarks, which lead to a lack of selectivity of all the inhibitors developed so far and for the induction of undesired in vivo side effects, made MMPs unreliable pharmaceutical targets and impaired the development of synthetic MMPIs as drugs.

Recently, structural insights into the X-ray structure of the catalytic domain of MMP-12 in the presence of the nanomolar inhibitor NNGH[3] enabled structural modifications of the skeleton of NNGH to be performed to obtain a new family of non-toxic MMPIs, **A**, that are soluble in water and that maintain high affinity versus MMPs[4,5] (Figure 1).

Relying on the properties of these attracting molecules, we tried to overcome the drawbacks presented by the lack of selectivity of synthetic MMPIs, focusing our attention on diseases mediated by the local uncontrolled activity of MMPs, which could be treated with topical administration of selected inhibitors.

In the uncontrolled breakdown of extracellular matrix, MMPs play a harmful role in the onset and continuous damage of the ocular surface.[6] In particular, the gelatinase MMP-9 is the most important MMP on the ocular surface; its concentration is notably high in tears of patients with dry eye syndrome (DES),

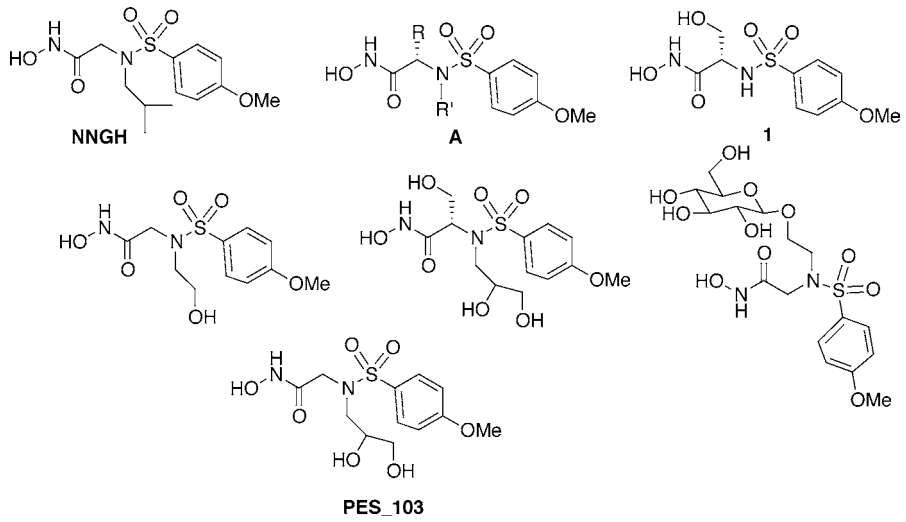

Figure 1. Structure of NNGH and of water-soluble MMPIs.

also known as keratoconjunctivitis sicca (KCS).[6] DES is a multifunctional disorder in which inflammation plays a relevant role[7] and includes aqueous tear deficiency and excessive tear evaporation. Ocular stress due to desiccation was demonstrated to increase the expression of MMP-9 in a murine model.[8] MMP-9 is active in degrading the components of the corneal epithelial basement membrane, greatly compromising the corneal epithelial desquamation.[9]

For the treatment of DES and of ocular diseases in general, the topical administration of drugs remains the easiest route and the preferred one by patients. Symptomatic remedies are largely used for the treatment of DES; alternatively, nonspecific anti-inflammatories can be administered.[10] Recently,[11] we developed a nonsymptomatic approach for the treatment of DES that relies on the inhibition of MMP-9 by a water-soluble small molecule, namely PES 103.[5] In vitro and in vivo tests demonstrated both the efficacy of PES 103 in the treatment of DES on a mice model of reduced lacrimation, and the lack of corneal cytotoxicity.[11]

To develop an effective treatment for DES, it is mandatory to take into account that the absorption of drugs that are applied topically on the eyes is generally very poor because of anatomical and physiological barriers.[10] In particular: 1) the epithelium (the outermost layer of the cornea) hampers drug penetration, and 2) lacrimation (induced by standard application of eye drops on the eye surface) causes dilution of the drug and drainage.

Successful delivery systems that are specifically designed for topical ocular administration have recently been reviewed.[12,13] Among them, PAMAM dendrimers[14] have been evaluated, and preliminary results showed that PAMAM complexes increased the residence time and corneal penetration of ocular drugs such as pueranin[15] in rabbit animal models with respect to the free drug solutions. Other promising data referring to dendrimers as suitable ophthalmic vehicles, also showing their bioadhesive properties on corneal surface,[16] convinced us to chemically link the nanomolar, water-soluble inhibitor **1** (see Figure 1) to the PAMAM-based dendron (G0) **2** with the aim of obtaining a potential new drug for DES treatment (Figure 2).

In this paper, we report on the synthesis of the PAMAM-based divalent inhibitor **3**, and on its binding affinity versus MMP-9 and -12 (macrophage elastase) and on its efficacy for the nonsymptomatic treatment of DES in a rabbit model. In addition, derivative **3**, presenting two residues of the MMPs' inhibitor **1**, also prompted the investigation of a possible simultaneous interaction with the catalytic binding site of two MMPs to form a ternary complex. Given the strong structural similarity among MMPs and carbonic anhydrases (CAs, EC 4.2.1.1), which are metalloenzymes that are physiologically expressed in the eye, we also assessed the binding properties of **3** to all catalytically active human (h) CA isoforms hCA I–XIV.

Results and Discussion

Preparation of the PAMAM-based inhibitor 3

Inhibitor **1** (see Figure 1) is an analogue of PES 103, which is structurally simpler but preserves the nanomolar affinity for an array of MMPs.[5] To obtain the desired PAMAM-based inhibitor **3**, a linker of nine atoms (10 Å length) was introduced on the sulfonamidic nitrogen of **1** to allow the inhibitor to correctly reach the binding pocket of the selected MMP. The serine methyl ester **4**, presenting the hydroxyl group of the lateral chain protected as a *tert*-butyl ether, was thus reacted with 4-methoxybenzensulfonyl chloride and catalytic 4-(*N*,*N*-dimethylamino)pyridine (DMAP), at room temperature in dichloromethane as solvent, to give the corresponding sulfonamide **5** (90%). The latter was then reacted with N-Cbz-ethanolamine **6** under Mitzunobu conditions. After one night at room temperature, compound **7** was isolated in 82% yield. Subsequent removal of the *tert*-butyl protecting group (trifluoroacetic acid, 2 h, RT, **8**, 85%) and of the Cbz group (H_2, Pd/C, 2 h, RT) afforded **9** in 90% yield, which, in turn, was reacted with the linker **10** (see the Supporting Information). The reaction was run in

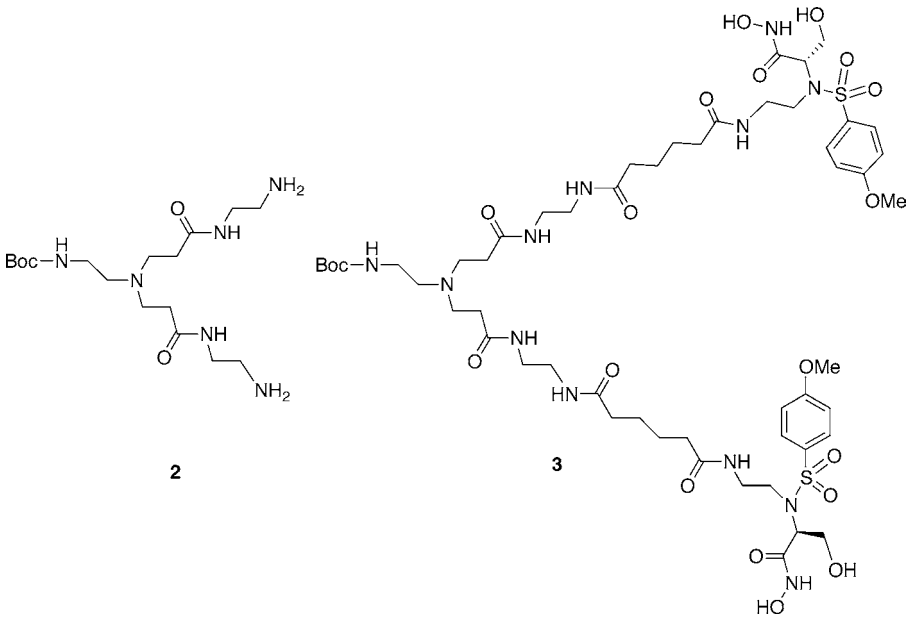

Figure 2. Structure of the PAMAM-based dendron (G0) **2** and the divalent inhibitor **3**.

anhydrous *N*,*N*-dimethylformamide (DMF) as solvent at room temperature and in the presence of *N*-methylmorpholine (NMM) to give sulfonamide **11**, suitably activated to react with the PAMAM-based dendron (G0) **2** (see the Supporting Information). A solution of **11** in DMF was treated at room temperature with **2** and NMM; after two hours, the divalent derivative **12** was isolated and purified by column chromatography on silica gel (72%). Final treatment of **12** with hydroxylamine at 60 °C for two hours afforded, after purification by HPLC, the desired PAMAM-based divalent inhibitor **3** in 30% yield.

Binding assay

MMPs

The affinity of the PAMAM-based divalent inhibitor **3** toward MMP-9 was first evaluated by conducting a fluorimetric assay. The K_i value obtained for **3** against MMP-9 was 289 nM (±53 nM), which is satisfactory, albeit in the high nanomolar range. We then investigated the ability of dendron **3** to bind simultaneously the catalytic domains of two distinct MMPs. In NMR experiments the chemical shift of signals is a sensitive indicator of protein–ligand interactions; therefore, NMR binding studies were run by using the catalytic domain of MMP-12 as a model to evaluate the binding mode of **3** with this widely studied and fully characterized member of the family of MMPs. The identification of the binding site was accomplished by analyzing the chemical shift perturbation of the protein resonances in the ^{1}H-^{15}N HSQC spectrum after the addition of the bifunctional ligand **3** (Figure 3). As expected, the pattern of signal shifts mainly concerns the residues of the active site (Figure 4), including some amino acids forming the S1′ cavity. Given the binding of the catalytic domains of two MMPs to each hydroxamic residue of the divalent dendron **3** could be expected to occur upon the addition of a half equivalent of

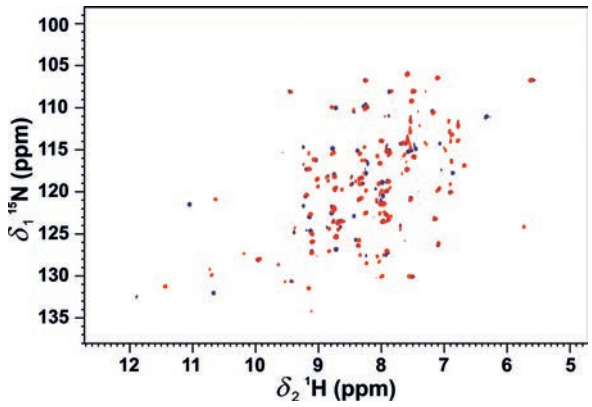

Figure 3. ^{1}H-^{15}N HSQC spectrum of the catalytic domain of MMP-12 (blue), and the same domain in the presence of the PAMAM-based divalent inhibitor **3** (red).

the inhibitor to the protein solution, NH resonances were also considered as possible probes to investigate the formation of a dendron-mediated MMP dimer. However, the addition of the PAMAM-based divalent inhibitor **3** did not produce a significant broadening of the NH resonances, despite the large molecular weight of the expected complex (MW > 35 kDa). This puzzling result has tentatively been ascribed to the length of the dendron's arms, which enables the two proteins to move independently in solution.[17,18] This hypothesis was supported by analysis of the hydrodynamic radius of the catalytic domain of MMP-12 measured by dynamic light scattering analysis in solutions either in the presence or absence of a half equivalent of dendron **3**. Indeed, the small angle X-ray scattering (SAXS) value (see the Supporting Information) of 24 nm found for the radius of gyration of the protein–ligand complex was in good agreement with the expected value of 22 nm calculated with

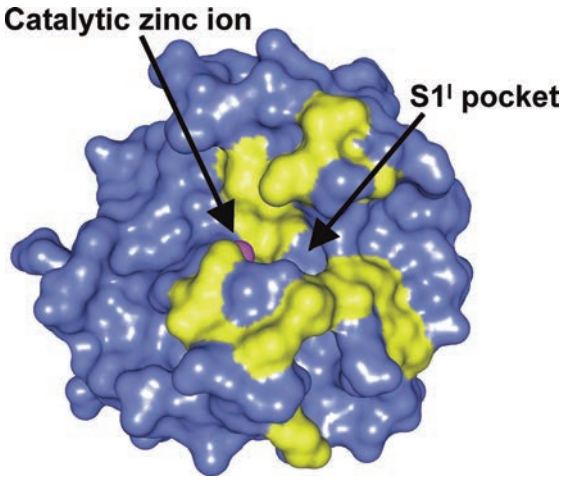

Figure 4. Surface representation of the catalytic domain of MMP-12. The residues showing significant chemical shift perturbation upon the addition of the PAMAM-based divalent inhibitor **3** (V162, D175, G178, I180, A182, H183, H196, D198, E199, A216, H218, E219, H228, S229, K233, F237, T239, Y240, Y241) are highlighted in yellow.

Table 1. Binding studies of hydroxamate **3** versus hCAs.

Isoform	K_i [nM][a] **3**	Acetazolamide
hCA I	>10000[b]	250
hCA II	>10000[c]	12
hCA III	3735	2000
hCA IV	845	74
hCA VA	74.5	63
hCA VI	65.3	11
hCA VII	>10000[d]	2.5
hCA IX	28.9	25
hCA XII	65.1	5.7
hCA XIII	24.7	17
hCA XIV	338	41

[a] Errors in the range of ±10% of the reported values (data not shown, from three assays). [b] At 10 μM an inhibition of 60% was registered. [c] At 10 μM an inhibition of 66% was registered. [d] At 10 μM an inhibition of 54% was registered.

the HydroNMR program[19] for the dimeric structural model composed of two MMP-12 catalytic domains placed in tight contact.

Carbonic anhydrase

Hydroxamates were reported to act as CA inhibitors (CAIs) and to bind to the Zn^{II} ion within the enzyme active site in a different manner compared with their binding to MMPs.[20] Thus, investigations into the interactions of this type of compound with CAs is indeed of interest, especially considering the recent report that dendrimers functionalized with sulfonamide moieties are highly effective CAIs that also show anti-glaucoma effects in an animal model of the disease.[21] Here, we investigated the interaction between hydroxamate **3** and all the catalytically active CA isoforms[22] by using a stopped flow CO_2 hydrase assay (Table 1) as well as using molecular docking of the inhibitor within several CA isoform active sites (Figure 5 and Figure 6).

Data presented in Table 1 (in which the clinically used sulfonamide acetazolamide (AAZ) was used as standard) show that hydroxamate **3** did not inhibit three cytosolic isoforms, namely the widely spread hCA I, II and the brain-associated CA VII, whereas the remaining eight hCAs were all inhibited, with inhibition constants ranging between 24.7 nM to 3.73 μM. Isoforms hCA III (muscle isoform) and the membrane-associated hCA IV and hCA XIV were less sensitive to this inhibitor (K_i values of 338–3735 nM), whereas all the remaining isoforms were inhibited with K_i values below 100 nM. Thus, the mitochondrial hCA VA, the secreted isoform (in saliva and milk) hCA VI, and the transmembrane hCA XII (present in the eye and considered as an antiglaucoma target),[23] were inhibited with K_i values in the range of 65.1–74.5 nM. The tumor-associated hCA IX and the cytosolic hCA XIII were the two isoforms with the highest sensitivity to **3**, with K_i values of 24.7–

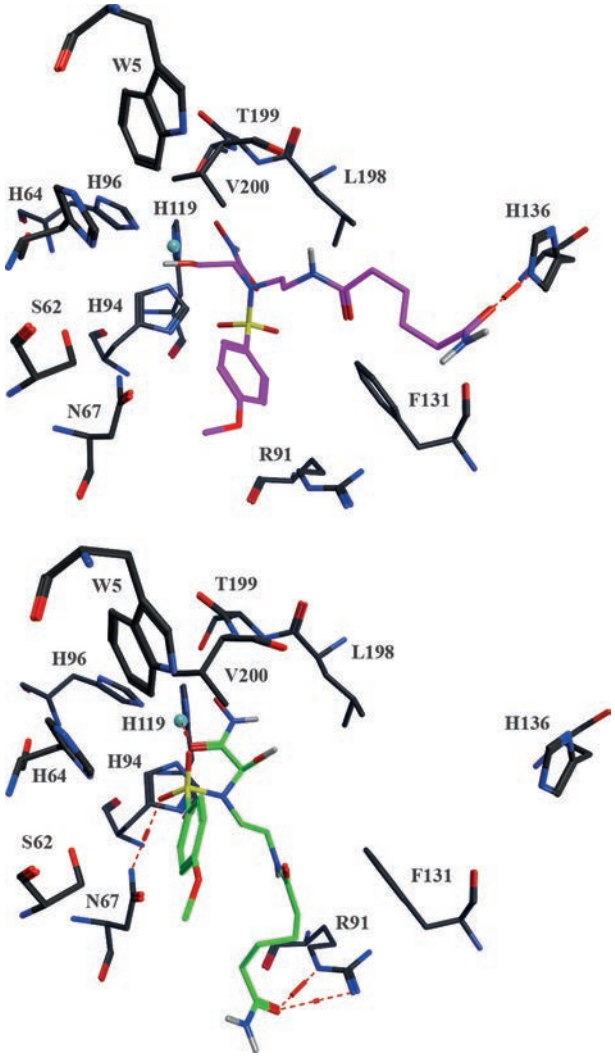

Figure 5. Docked pose of compound **3** in the binding pocket of hCA XIII (**A**, **B**). Hydrogen bonds and the interactions to the Zn^{2+} ion are indicated with red dashed lines. The Zn^{2+} ion is indicated with a turquoise sphere.

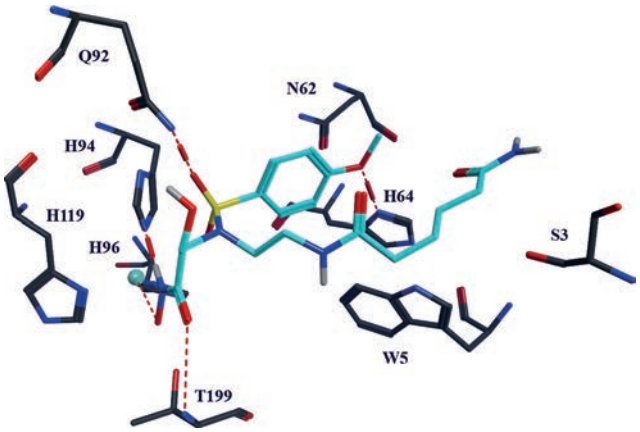

Figure 6. Docked pose of compound **3** in the binding pocket of hCA IX. Hydrogen bonds and the interactions to the Zn^{2+} ion are indicated with red dashed lines. The Zn^{2+} ion is indicated with a turquoise sphere.

28.9 nM. Although **3** is generally less effective than the sulfonamide AAZ, the fact that it does not inhibit the widely spread hCA I and II (present in high amounts in blood, gastrointestinal tract and kidneys, and considered the main offtarget isoforms responsible for the side effects of these drugs), may be considered as a very favorable and salient feature of **3** as a CAI.[24–27]

To rationalize the data presented in Table 1, we also performed docking studies of **3** within the active sites of several isoforms. Compound **3** showed the highest inhibition for hCA XIII (24.7 nM) and hCA IX (28.9 nM), as detailed above. We expected that the hydroxamate nitrogen atom would interact with the Zn^{2+} ion; therefore, we assigned a negative charge to the oxygen atom (R-CONHO$^-$). Two poses have been identified for hCA XIII (Figure 5). The negatively charged oxygen atom approaches the Zn^{2+} ion (distance less than 2.5 Å) and could thus be able to participate in a coordinative interaction with the metal ion. The first pose forms a hydrogen bond between its hexanamide tail and the side chain of His136 (Figure 5 A). The ligand hydrophobic phenyl group and hexanamide tail are located close to Phe131, and additional hydrophobic interactions are formed with Ala135, Leu141, Leu198, and Leu204. The second pose orients its negatively charged oxygen atom in a location that is similar to that of the first pose but the hydroxamate carbonyl group forms an additional interaction with the Zn^{2+} ion (Figure 5 B). One of the sulfonamide oxygen atoms forms a hydrogen bond to the side chain of Asn67 and hydrophobic interactions are formed mainly with Phe131.

Docking studies of **3** into the active site of hCA IX suggest that the hydroxamate group forms extensive contacts with the protein (Figure 6). The negatively charged oxygen atom interacts with the Zn^{2+} ion, the adjacent nitrogen atom forms a hydrogen bond to the side chain of His94, and the carbonyl group forms a hydrogen bond to Thr199. One of the sulfonamide oxygen atoms forms a hydrogen bond with the side chain of Gln92, and the methoxy group forms a hydrogen bond with the side chain of His64. The hexanamide tail is flexible and exposed to water.

In vivo tests

To assess the effectiveness of the PAMAM-based divalent inhibitor **3** to treat DES, an experimental dry eye on rabbits was induced by atropine sulfate (AS) solution ocular instillations. The Schirmer test scores (reported as millimeters of wet strip 3 min after insertion) obtained before (basal values) and after (dry eye) treatment with AS, and relevant to the treatment with the formulation under test, are reported in Figure 7. Decreased

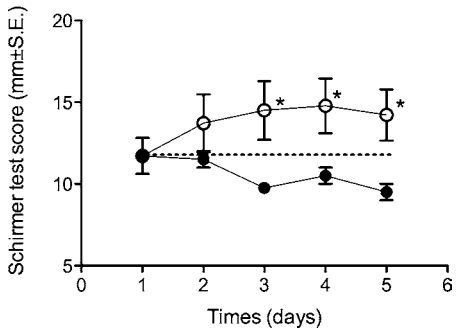

Figure 7. Schirmer test scores obtained by using a solution of **3** in the rabbit dry eye model ($n=7$). ○ = compound **3**; ● = control dry eyes; ----- = baseline (normal eyes). *Significantly different from control dry eye ($p<0.05$, unpaired t test with Welch's correction).

tear production ($p<0.05$, unpaired t test with Welch's correction) was observed starting from the third day after beginning AS treatment: at this time the average Schirmer test score in dry eyes was reduced from 11.72 ± 1.10 mm (basal value) to 9.75 ± 0.25 mm. Eyes treated with **3** showed greater scores with respect to control dry eyes at all experimental times, with values of approximately 14.5 mm, and with statistically significant differences on the 3rd, 4th, and 5th days of treatment ($p<0.05$, unpaired t test with Welch's correction). The slit-lamp examination of the fluorescein-stained corneas revealed no occurrence of dotted staining in treated eyes, indicating no symptom of corneal desiccation. Topical ocular administration of atropine causes the animals a few typical effects of antimuscarinic drugs such as mydriasis and cycloplegia, without producing significant side effects. Depression of saliva and tear production is usually the first sign of adverse systemic reaction and, as a result, leads to the rapid onset of dry eye conditions. The effect is dose-related and it is maximized in albino eyes because loss of drug through binding to the iris pigments does not occur.[28] Decreased tear production (evidenced by lower Schirmer test scores) and occurrence of dry spots on the corneal surface were observed on the second day of treatment, and remained constant (or increased, in the case of dry spots) over the five days of observation time.[29]

Furthermore, anticholinergic-induced dry eye conditions are accompanied by increases in MMP-9 expression;[30] this model can therefore be usefully employed to evaluate the activity of **3**. Notably, this investigation points to **3** as an interesting new compound for artificial tear formulations that are able to re-

store normal hydration levels to the surface of the cornea from the third day of treatment.

Conclusion

The dramatic effects of the uncontrolled expression of MMPs justify the development of new approaches to the use of MMPIs in therapy. Recently, the development of efficient drug delivery systems that allow the transportation of a selected drug to its site of action has represented an important achievement for the administration of pharmaceutically active compounds. The size-modulating and chemical–physical properties of compounds such as PAMAM dendrimers make these macromolecules extremely attractive as ophthalmic drug delivery carrier. In an effort to overcome the undesirably large spectrum of action of many effective MMPs inhibitors, including compound **1**, we linked two residues of the nanomolar MMP inhibitor **1** to the dendron **2** through the use of a suitable spacer, thus affording divalent inhibitor **3**. Merging the unique properties of the PAMAM architecture with the water solubility and high affinity of **1** led to a remarkable topical activity that was accompanied by a reduced systemic absorption for the resulting dendron **3**. The affinity, which was in the high nanomolar range, of **3** versus MMP-9 was assessed and we could also demonstrate that the divalent inhibitor **3** simultaneously links the catalytic domains of two MMPs. This is the first example of a synthetic divalent inhibitor that binds, with nanomolar affinity, the catalytic domain of two different MMPs. Reasoning that the sulfonamidic residues characterizing **3** could also bind CAs, the affinity of **3** versus hCAs was also evaluated. Our data showed that hydroxamate **3** did not inhibit three cytosolic isoforms, among which were the widely spread hCA I, II, and the brain-associated CA VII, whereas the remaining eight hCAs were all inhibited, including transmembrane hCA XII, which is present in the eye and which is considered as an antiglaucoma target. Although **3** is generally less effective than the positive control, AAZ, the fact that it does not inhibit the widely spread hCA I and II appears to be a very favorable and unique feature of **3** as a CAI.

The in vivo effectiveness and the therapeutic potential of the PAMAM-based inhibitor **3** was clearly demonstrated by treating DES on rabbits, in an experimental model of dry eye that was accompanied by an increase in MMP-9 expression. Eyes treated with **3** showed greater scores with respect to control dry eyes at all experimental times. Furthermore, corneas revealed no occurrence of damage in treated eyes, indicating no symptoms of corneal desiccation. This investigation points to **3** as an interesting new compound for artificial tear formulations that can restore normal levels of hydration to the surface of the cornea from the third day of treatment.

Finally, although the administration of high doses of drugs with high molecular weight is generally necessary to reach therapeutic concentrations, in the case of the divalent dendron **3**, the two residues of hydroxamic acid halves the amount of compound that is needed to be applied to the eyes. The divalence of the dendron, however, does not enhance the binding affinity versus the selected MMP, which remains in the high nanomolar range towards the single catalytic domain. Further studies to evaluate specific formulations, such as muco-adhesive gel, to improve the performance of **3**, are ongoing.

Experimental Section

Synthesis of the inhibitor 3: A solution of **2** (0.5 mmol, 194 mg) and NMM (2.0 mmol, 0.220 mL) in anhydrous DMF (5 mL) was added to a stirred solution of **8** (1.0 mmol, 581 mg) in anhydrous DMF (5.0 mL) and the mixture was stirred at RT for 2 h then concentrated to dryness. The crude product was purified by flash column chromatography on silica gel (CH_2Cl_2/MeOH, 8:1 to 4:1) to give **9** (0.72 mmol, 72%). A suspension of KOH (630 mg, 11.2 mmol) in MeOH (2.3 mL) and a suspension of $NH_2OH{\cdot}HCl$ (670 mg, 9.64 mmol) in MeOH (4.5 mL) were separately stirred for 10 min at 70 °C, then the solution of KOH was added to the solution of $NH_2OH{\cdot}HCl$ and the mixture was stirred at 60 °C for 10 min. Compound **9** (50 mg, 0.04 mmol) was dissolved in the freshly obtained suspension of NH_2OH (0.680 mL). The mixture was stirred at RT for 3 h then diluted with MeOH (5 mL) and the solid was filtered off. The filtrate was concentrated to dryness to give the crude product (65 mg), which was purified by HPLC (column Zorbax 300SB-C18; 9.4×250, 5 μm; H_2O/MeOH, 50:50) to give **3** (0.012 mmol, 30%) as a glassy solid (see the Supporting Information for full characterization).

Protein expression and purification: The cDNA encoding the G106–G263 construct of the catalytic domain of MMP-12 was generated by a polymerase chain reaction (PCR) from an IMAGE consortium clone using two synthetic oligonucleotides as primers. The cDNA obtained was cloned into pET21a (Novagen) by using the restriction enzymes Nde I and Xho I (New England BioLabs). The expression vector encoding for wild-type cat-MMP-12 was transformed into competent *Escherichia coli* BL21, and colonies were selected for Ampicillin resistance. Bacteria were grown in LB medium containing ampicillin (100 $\mu g\,mL^{-1}$) in a shaker flask at 37 °C. Protein expression was induced with 0.5 mM IPTG at an $OD_{600}=0.6$, and cell growth was continued for a further 5 h. For expression of ^{15}N cat-MMP-12 proteins, the bacteria were grown in minimal medium containing ^{15}N enriched $(NH_4)_2SO_4$. Following expression, the enzyme was accumulated in the fraction of inclusion bodies. Cells were harvested by centrifugation and suspended in a buffer containing 25% sucrose, 50 mM Tris-HCl (pH 8), 0.1 M NaCl, 0.2 M EDTA, and 1 mM DTT. Lysozyme (5–10 mg) was added to the resulting suspension, which was stirred for 15–20 min at 4 °C. Buffer containing 2% Triton, 50 mM Tris-HCl (pH 8), 0.1 M NaCl, 0.2 M EDTA, and 1 mM DTT was added and the suspension was sonicated (7–8 cycles of 30 s each) and centrifuged at 40000 rpm for 20 min at 4 °C. The pellet was resuspended in 6 M Urea, 20 mM Tris-HCl (pH 8) and centrifuged. The resulting inclusion bodies, containing the protein, were solubilized in a buffered solution with 20 mM Tris-HCl and 8 M urea at pH 8. The protein was then purified with a cation exchange column Mono-S (Pharmacia) using a linear gradient of NaCl up to 0.5 M. The protein was refolded by using multistep dialysis against solution containing 50 mM Tris-HCl (pH 7.2), 10 mM $CaCl_2$, 0.1 mM $ZnCl_2$, and 0.3 M NaCl, and decreasing concentration of urea (from 4 M up to 2 M). The last two dialysis steps were performed against a solution containing 20 mM Tris-HCl (pH 7.2), 10 mM $CaCl_2$, 0.1 mM $ZnCl_2$, 0.3 M NaCl, and 200 mM of hydroxamic acid. The protein solution was concentrated to 5 mL and purified by size-exclusion chromatography using a High LoadTM 16/60 SuperdexTM 75 (Amersham Biosciences) and eluted with 20 mM Tris pH 7.2, 10 mM $CaCl_2$, 0.3 M NaCl, AHA 0.2 M. The eluted

fractions were checked for purity on 15% gel by SDS-PAGE, and those containing the cat-MMP-12 protein were pooled and concentrated.

CA inhibition assay: An Applied Photophysics stopped-flow instrument was used to assay the CA catalyzed CO_2 hydration activity.[31] Phenol red (0.2 mM) was used as indicator, working at the absorbance maximum of 557 nm, with 20 mM Hepes (pH 7.5) as buffer, and 20 mM Na_2SO_4 (to maintain a constant ionic strength), following the initial rates of the CA-catalyzed CO_2 hydration reaction for a period of 10–100 s. The CO_2 concentrations ranged from 1.7 to 17 mM for the determination of the kinetic parameters and inhibition constants. At least six traces of the initial 5–10% of the reaction were recorded for each inhibitor to determine the initial velocity. The uncatalyzed rates were determined in the same manner and subtracted from the total observed rates. Stock solutions of inhibitor (0.1 mM) were prepared in distilled deionized water and dilutions up to 0.01 nM were performed thereafter with the assay buffer. Inhibitor and enzyme solutions were preincubated together for 15 min at RT prior to assay to allow for the formation of the E-I complex. Inhibition constants were obtained by nonlinear least-squares methods using PRISM 3, as reported earlier for other dendrimers,[21] and represent the mean from at least three different determinations. All CA isoforms were recombinant ones obtained in-house as reported earlier.[32–34]

In vivo tests

Animals: Non-anaesthetised, male, New Zealand albino rabbits, weighing 2.5–3.0 Kg (Pampaloni Rabbitry, Fauglia, Italy) were used and treated as prescribed in the publication "Guide for the Care and Use of Laboratory Animals".[35] All experiments conformed with the ARVO Resolution on the Use of Animals in Research: they were carried out under veterinary supervision, and after approval of the protocols by the Ethical-Scientific Committee of the University of Pisa. The animals were housed singly in standard cages in a room with controlled lighting, at 19±1 °C and 50±5% R.H., with no restriction of food or water. During the experiments, the rabbits were placed in restraining boxes to which they had been habituated, in a room with dim lighting; they were allowed to move their heads freely, and their eye movements were not restricted.

Induction and treatment of dry eye conditions: The animals were preliminarily submitted to the Schirmer I test[36] and to slit-lamp examination of the corneal surface to verify the integrity of the corneal epithelium and the function of lachrymal system; then seven of them were treated as reported.[29] Briefly, the animals received in the lower conjunctival sac of both eyes 50 μL of 1% atropine sulfate solution (AS) at 08:00, 13:00, and 18:00. Five minutes after each administration of AS, the subjects received in one eye 50 μL of the formulation under study, while vehicle alone was administered in the control eye. All treatments were discontinued after five days. The Schirmer I test[36] was performed two, three, four, and five days after the first administration of AS, at 10:00. The test was performed on both eyes (non-anaesthetized) of all animals, by maintaining for 3 min a standardized test strip (Alfa Intes, Casoria, Italy) into the external third of the lower conjunctival fornix. The wetted length in millimeters of the strip was taken as the test score. After staining with fluorescein (Fluorets, Smith & Nephew Pharmaceuticals Ltd, Romford, UK), the corneal surface was observed by slit-lamp biomicroscope fitted with a blue filter. The test was performed at 14:00, three, four, and five days after the first administration of AS. The occurrence of dotted staining, revealing the presence of dry spots on the ocular surface, was considered as a symptom of corneal desiccation.

Acknowledgements

We thank Ente Cassa di Risparmio di Firenze for financial support. Elettra Synchrotron is acknowledged for providing access to the SAXS beamline, and Heinz Amenitsch and Barbara Sartori (Elettra Synchrotron) are thanked for their technical support. The authors are grateful to the COST Action CM 1102.

Keywords: dendrimers · drug delivery · drug discovery · inhibitors · metalloproteins

[1] J. Cathcart, A. Pulkoski-Gross, J. Cao, *Gene Dis.* **2015**, *2*, 26, and references cited therein.
[2] J. W. Skiles, N. C. Gonnella, A. Y. Jeng, *Curr. Med. Chem.* **2001**, *8*, 425 and refs cited therein.
[3] I. Bertini, V. Calderone, M. Cosenza, M. Fragai, Y.-M- Lee, C. Luchinat, S. Mangani, B. Terni, P. Turano, *Proc. Natl. Acad. Sci. USA* **2005**, *102*, 5334.
[4] V. Calderone, M. Fragai, C. Luchinat, C. Nativi, B. Richichi, S. Roelens, *ChemMedChem* **2006**, *1*, 598.
[5] E. Attolino, V. Calderone, E. Dragoni, M. Fragai, B. Richichi, C. Luchinat, C. Nativi, *Eur. J. Med. Chem.* **2010**, *45*, 5919.
[6] C. S. De Paiva, R. M. Corrales, A. L. Villarreal, W. J. Farley, D.-Q. Li, M. E. Stern, S. C. Pflugfelder, *Exp. Eye Res.* **2006**, *83*, 526.
[7] Definition and Classification Subcommittee of the *International Dry Eye Workshop*, **2007**.
[8] C. S. De Paiva, S. Chotikavanich, S. B. Pangelinan, J. D. Pitcher 3rd, B. Fang, X. Zheng, P. Ma, W. J. Farley, K. F. Siemasko, J. Y. Niederkon, M. E. Stern, D. Q. Li, S. C. Plugfelder, *Mucosal Immunol.* **2009**, *2*, 243.
[9] P. Aragona, M. A. Aguennouz, L. Rania, E. Postorino, M. S. Sommario, A. M. Roszkowska, M. G. De Pasquale, A. Pisani, D. Puzzolo, *Ophtalmology* **2015**, *122*, 62.
[10] J. G. Souza, K. Dias, T. Aparecida Pereira, D. Spuri Bernardi, R. F. V. Lopez, *J. Pharm. Pharmacol.* **2014**, *66*, 507.
[11] M. Mori, E. De Lorenzo, E. Torre, M. Fragai, C. Nativi, C. Luchinat, A. Arcangeli, *Basic Clin. Pharmacol. Toxicol.* **2012**, *111*, 289.
[12] J. Vandervoort, A. Ludwig, *Nanomedicine* **2007**, *2*, 11.
[13] S. K. Sahoo, F. Dilnawaz, S. Krishnakumar, *Drug Discovery Today* **2008**, *13*, 144.
[14] E. Abbasi, S. F. Aval, A. Akbarzadeh, M. Milani, H. T. Nasrabadi, S. W. Joo, Y. Hanifehpour, K. Nejati-Koshki, R. Pashaei-Asl, *Nanoscale Res. Lett.* **2014**, *9*, 247.
[15] T. F. Vandamme, L. Brobeck, *J. Controlled Release* **2005**, *102*, 23.
[16] N. K. Jain, U. Gupta, *Exp. Opin. Drug Metabolism Toxicol.* **2008**, *4*, 1035.
[17] I. Bertini, M. Fragai, C. Luchint, M. Melikian, E. Mylonas, N. Sarti, D. I. Svergun, *J. Biol. Chem.* **2009**, *284*, 12821.
[18] I. Bertini, V. Calderone, M. Fragai, R. Jaiswal, C. Luchinat, M. Melikian, E. Mylonas, D. I. Svergun, *J. Am. Chem. Soc.* **2008**, *130*, 7011.
[19] J. Garcia de La Torre, M. L. Huertas, B. Carrasco, *J. Magn. Reson.* **2000**, *147*, 138.
[20] A. Di Fiore, A. Maresca, C. T. Supuran, G. De Simone, *Chem. Commun.* **2012**, *48*, 8838.
[21] B. F. Carta, S. M. Osman, D. Vullo, A. Gullotto, J. Y. Winum, Z. AlOthman, E. Masini, C. T. Supuran, *J. Med. Chem.* **2015**, *58*, 4039.
[22] C. T. Supuran, *Nat. Rev. Drug Discovery* **2008**, *7*, 168.
[23] F. Fabrizi, F. Mincione, T. Somma, G. Scozzafava, F. Galassi, E. Masini, F. Impagnatiello, C. T. Supuran, *J. Enzyme Inhib. Med. Chem.* **2012**, *27*, 138.
[24] F. Carta, C. T. Supuran, *Expert Opin. Ther. Pat.* **2013**, *23*, 681.
[25] C. T. Supuran, *Expert Opin. Ther. Pat.* **2013**, *23*, 677.
[26] A. Scozzafava, C. T. Supuran, F. Carta, *Expert Opin. Ther. Pat.* **2013**, *23*, 725.
[27] E. Masini, F. Carta, A. Scozzafava, C. T. Supuran, *Expert Opin. Ther. Pat.* **2013**, *23*, 705.
[28] S. D. Jaanus, J. H. Carter in *Clinical Ocular Pharmacology* (Eds.: J. D. Bartlett, S. D. Jaanus), Butterworth-Heinemann, St. Louis (USA), **1995**, pp. 167–182.
[29] S. Burgalassi, L. Panichi, P. Chetoni, M. F. Saettone, E. Boldrini, *Ophthalmic Res.* **1999**, *31*, 229.

[30] B. Xiao, Y. Wang, P. S. Reinach, Y. Ren, J. Li, S. Hua, H. Lu, W. Chen, *PLoS ONE* 10(1): e0115333 DOI: 10.1371/journal.pone.0115333.
[31] R. G. Khalifah, *J. Biol. Chem.* **1971**, *246*, 2561.
[32] A. Maresca, C. Temperini, H. Vu, N. B. Pham, S. A. Poulsen, A. Scozzafava, R. J. Quinn, C. T. Supuran, *J. Am. Chem. Soc.* **2009**, *131*, 3057.
[33] A. Maresca, C. Temperini, L. Pochet, B. Masereel, A. Scozzafava, C. T. Supuran, *J. Med. Chem.* **2010**, *53*, 335.
[34] J.-Y. Winum, A. Maresca, F. Carta, A. Scozzafava, C. T. Supuran, *Chem. Commun.* **2012**, *48*, 8177.
[35] NIH Publication No. 92–93, revised **1985**.
[36] O. Schirmer, *Arch. Klin. Ophthalmol* **1903**, *56*, 197.

Received: October 29, 2015
Published online on December 22, 2015

CHEMISTRY
A European Journal

Supporting Information

A Divalent PAMAM-Based Matrix Metalloproteinase/Carbonic Anhydrase Inhibitor for the Treatment of Dry Eye Syndrome

B. Richichi[+],[a] V. Baldoneschi,[a] S. Burgalassi,[b] M. Fragai[+],[a, c] D. Vullo,[a] A. Akdemir,[d] E. Dragoni,[a] A. Louka,[c] M. Mamusa,[a] D. Monti,[b] D. Berti,[a] E. Novellino,[e] G. De Rosa,[e] C. T. Supuran,*[f] and C. Nativi*[a, c]

chem_201504355_sm_miscellaneous_information.pdf

Supporting Information

Synthesis of compound **4**	Pag.	S2
Synthesis of compound **5**		S2
Synthesis of compound **6**		S3
Synthesis of compound **7**		S3
Synthesis of compound **8**		S4
Synthesis of compound **9**		S4
Synthesis of compound **10**		S5
In vivo tests – Formulation		S6
SAXS Experiments		S6
References and Notes		S8

Synthesis of compound 4

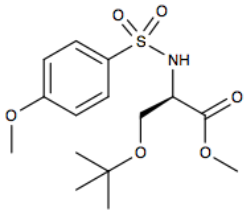

To a stirred solution of H-D-Ser(tBu)-OMe hydrochloride (2 g, 9.45 mmol) in CH_2Cl_2 (20.0 mL), TEA (3.95 mL, 28.35 mmol) was added at 0°C. After 30 min at rt, the mixture was cooled to 0°C and DMAP (0.115 g, 0.94 mmol) and 4-methoxybenzenesulfonyl chloride (1.95 g, 9.45 mmol) were added. The mixture was stirred at rt for 4 h. After this time, the reaction mixture was diluted with CH_2Cl_2 (300 mL) and washed with a saturated solution of NH_4Cl (3 x 30 mL) and with a saturated solution of NaCl (2 x 30 mL). The organic phase was dried over Na_2SO_4 and concentrated to dryness to give **4** (3.21 g, 99%) as a yellow solid. Mp: 65-67°C; ESI-MS 344.14 $[M-H]^-$; ^1H NMR (500 MHz, $CDCl_3$): □ 7.79-7.76 (AA' part of an AA'MM' system, J_{AM} = 4.7 Hz, 2H), 6.96-6.93 (MM' part of an AA'MM' system, J_{MA} = 4.7 Hz, 2H), 5.39-5.38 (bs, 1H), 4.08-4.05 (m, 1H, C<u>H</u>CH_2OtBu), 3.85 (s, 3H, $PhOCH_3$), 3.68 (A part of an ABX system, J_{AB} = 8.9 Hz, J_{AX} = 3.2 Hz, CHC<u>H</u>$_2$OtBu), 3.55 (s, 3H, $COOCH_3$), 3.52 (B part of an ABX system, J_{BA} = 8.9 Hz, J_{BX} = 3.6 Hz, CHC<u>H</u>$_2$OtBu), 1.07 (s, 9H, tBu). ^{13}C NMR (125 MHz, $CDCl_3$): □ 170.3 (Cq), 162.9 (Cq), 131.9 (Cq), 129.3 (CH Ar), 114.1 (CH Ar), 73.6 (Cq), 63.0 (CH<u>C</u>H_2OtBu), 56.3 (<u>C</u>HCH$_2$OtBu), 55.6 ($PhOCH_3$), 52.4 ($COOCH_3$), 27.2 (tBu).

Synthesis of compound 5

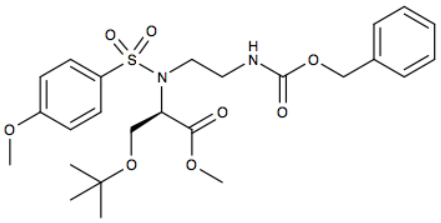

To a stirred solution of **4** (860 mg, 2.49 mmol), N-Z-ethanolamine (584 mg, 2.99 mmol) and PPh_3 (784 mg, 2.99 mmol) in dry THF (45.0 mL), DIAD (2.99 mmol, 0.589 mL) was slowly added. The mixture was stirred overnight at rt then concentrated to dryness. 15 mL of a mixture EtOAc:Petroleum Ether 1:8 were added and the suspension was stirred for 30' at room temperature. The white solid was filtered off and the filtrate was concentrated to dryness. The crude product was purified by flash column chromatography on silica gel (CH_2Cl_2:acetone 40:1) to give **5** (2.05 mmol, 82%) as a yellow oil. $[\alpha]_D^{25}$ +22.5 (c 0.6, $CHCl_3$); ESI-MS 1067.03 $[2M+Na]^+$; ^1H NMR (500 MHz, $CDCl_3$): □ 7.77 (AA' part of an AA'MM' system, J_{AM} = 8.8 Hz, 2H), 7.37-7.30 (m, 5H, Bn), 6.94 (MM' part of an AA'MM' system, J_{MA} = 8.8 Hz, 2H), 5.81 (bs, NH), 5.12 (A part of a AB system, J_{AB} = 12.3 Hz, 1H, CH_2Ph), 5.07 (B part of a AB system, J_{BA} = 12.3 Hz, 1H, CH_2Ph), 4.67 (X part of a ABX system, Jx_A = 3.8 Hz, Jx_B = 3.8 Hz, 1H, C<u>H</u>CH_2OtBu), 3.85 (s, 3H, $PhOCH_3$), 3.83-3.74 (m, 2H, NCH_2CH_2NH), 3.64 (s, 3H, $COOCH_3$), 3.52-3.39 (m, 2H, NCH_2CH_2NH), 1.13 (s, 3H, tBu). ^{13}C NMR (125 MHz, $CDCl_3$): □ 170.1 (Cq), 162.9 (Cq), 156.5 (Cq), 136.8 (Cq), 131.4 (Cq), 129.6 (CH Ar), 128.4 (CH Ar, Bn), 128.0 (CH Ar, Bn), 127.9 (CH Ar, Bn), 114.0 (CH Ar), 66.5 (CH_2Ph), 60.8 (CH<u>C</u>H_2OtBu), 60.7 (<u>C</u>HCH$_2$OtBu), 55.6 ($PhOCH_3$), 52.3 ($COOCH_3$), 46.2 (NCH_2CH_2NH), 40.8 (NCH_2CH_2NH), 27.2 (tBu).

Synthesis of compound 6

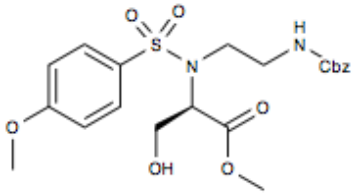

To a stirred solution of **5** (530 mg, 1.01 mmol) in CH_2Cl_2 (15.0 mL), TFA (40.4 mmol, 3.1 mL) was added and the mixture was stirred at rt for 2 h. After this time the solvent was evaporated under reduced pressure to obtain a crude which was purified by flash column chromatography on silica gel (CH_2Cl_2:acetone 12:1) to give **6** (0.86 mmol, 85%) as a colorless oil. $[\alpha]_D^{25}$ +31.27 (c 0.55, $CHCl_3$); ESI-MS 489.50 $[M+Na]^+$, 955.07 $[2M+Na]^+$; ^1H NMR (500 MHz, $CDCl_3$): □ 7.74 (AA' part of an AA'MM' system, J_{AM} = 8.8 Hz, 2H), 7.37-7.31 (m, 5H, Bn), 6.96 (MM' part of an AA'MM' system, J_{MA} = 8.8 Hz, 2H), 5.52 (bs, NH), 5.12 (A part of a AB system, J_{AB} = 12.2 Hz, 1H, CH_2Ph), 5.09 (B part of a AB system, J_{BA} = 12.3 Hz, 1H, CH_2Ph), 4.60 (X part of an ABX system, J_{XA} = 4.1 Hz, J_{XB} = 4.2 Hz, 1H, C<u>H</u>CH_2OH), 4.07-3.98 (m, 2H, CHC<u>H_2</u>OH), 3.86 (s, 3H, $PhOCH_3$), 3.55 (s, 3H, $COOCH_3$), 3.53-3.47 (m, 2H, NCH_2CH_2NH), 3.44-3.38 (m, 2H, NCH_2CH_2NH). ^{13}C NMR (125 MHz, $CDCl_3$): □ 169.7 (Cq), 163.1 (Cq), 157.1 (Cq), 136.3 (Cq), 130.6 (Cq), 129.6 (CH Ar), 128.5 (CH Ar), 128.1 (CH Ar), 128.1 (CH Ar), 114.1 (CH Ar), 67.0 (CH_2Ph), 62.0 (CH<u>C</u>H_2OH), 55.6 ($PhOCH_3$), 52.3 ($COOCH_3$), 45.2 (NCH_2CH_2NH), 41.5 (NCH_2CH_2NH).

Synthesis of compound 7

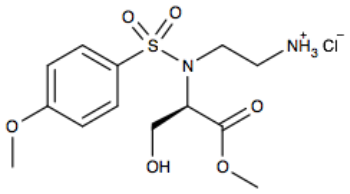

$Pd(OH)_2/C$ (20% Pd content, 225 mg) was added to a stirred solution of **6** (500 mg, 1.07 mmol) and HCl 12M (0.178 mL) in a mixture EtOAc:MeOH 3:1 (12.0 mL). The mixture was stirred at rt for 2 h under a H_2 atmosphere then filtered through a pad of Celite. The filtrate was concentrated to dryness to give **7** (1.02 mmol, 95%) as a glassy solid. $[\alpha]_D^{25}$ +25.0 (c 0.5, CH_3OH); ESI-MS 333.01 $[M+H]^+$; ^1H NMR (500 MHz, CD_3OD): □ 7.80 (AA' part of an AA'MM' system, J_{AM} = 7.4 Hz, 2H), 7.11 (MM' part of an AA'MM' system, J_{MA} = 7.3 Hz, 2H), 4.77-4.72 (m, 1H, C<u>H</u>CH_2OH), 4.03-3.96 (m, 1H, CHC<u>H_2</u>OH), 3.90 (s, 3H, $PhOCH_3$), 3.88-3.86 (m, 1H, CHC<u>H_2</u>OH), 3.70-3.63 (m, 2H, NCH_2CH_2NH), 3.61 (s, 3H, $COOCH_3$), 3.34-3.21 (m, 2H, NCH_2CH_2NH); ^{13}C NMR (125 MHz, CD_3OD): □ 170.4 (Cq), 163.7 (Cq), 130.0.5 (Cq), 129.5 (CH Ar), 114.2 (CH Ar), 61.9 (<u>C</u>HCH_2OH), 60.4 (CH<u>C</u>H_2OH), 55.2 ($PhOCH_3$), 51.9 ($COOCH_3$), 43.4 (NCH_2CH_2NH), 39.7 (NCH_2CH_2NH)

Synthesis of compound 8

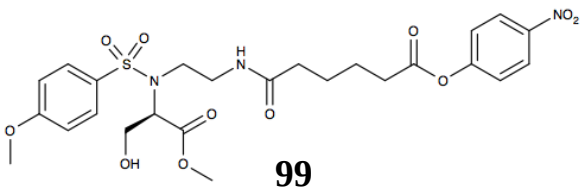

To a stirred solution of the *para* nitro phenyl ester of the butyric acid (1.54 g, 3.96 mmol) and NMM (0.272 mL, 2.44 mmol) in dry DMF (4.0 mL), a solution of **7** (364 mg, 0.99 mmol) in dry DMF (10.0 mL) was added. The mixture was stirred at rt for 4 h then concentrated to dryness. The crude product was purified by column flash chromatography on silica gel (EtOAc:Petroleum Ether 10:1) to give **8** (0.73 mmol, 74%) as a colorless oil. $[\alpha]_D^{25}$ +30.92 (c 0.65, $CHCl_3$); ESI-MS 604.11 $[M+Na]^+$; ^1H NMR (500 MHz, $CDCl_3$): □ 8.26 (AA' part of an AA'MM' system, J_{AM} = 9.0 Hz, 2H), 7.72 (A part of an AA'MM' system, J_{AM} = 8.8 Hz, 2H), 7.30 (MM' part of an AA'MM' system, J_{MA} = 8.9 Hz, 2H), 6.97 (MM' part of an AA'MM' system, J_{MA} = 8.8 Hz, 2H), 6.58-6.48 (bs, NH), 4.61 (X part of an ABX system, J_{XA} = 3.9 Hz, J_{XB} = 3.9 Hz, 1H, $CHCH_2OH$), 4.08-4.00 (m, 2H, CH_2OH), 3.88 (s, 3H, $PhOCH_3$), 3.70-3.65 (m, 1H, NCH_2CH_2NH), 3.58-3.53 (m, 1H, NCH_2CH_2NH), 3.54 (s, 3H, $COOCH_3$), 3.48-3.43 (m, 1H, NCH_2CH_2NH), 3.41-3.40 (m, 1H, NCH_2CH_2NH), 2.65 (at, 2H, $CH_2COOPhNO_2$), 2.31 (at, 2H, $NHCOCH_2$), 1.82-1.80 (m, 4H, $-CH_2CH_2-$); ^{13}C NMR (125 MHz, $CDCl_3$): □ 173.7 (Cq), 171.0 (Cq), 169.6 (Cq), 163.2 (Cq), 155.5 (Cq), 145.3 (Cq),130.6 (Cq), 129.5 (CH Ar), 125.2 (CH Ar), 122.5 (CH Ar), 114.1 (CH Ar), 62.1 ($CHCH_2OH$), 61.9 ($CHCH_2OH$), 55.6 ($PhOCH_3$), 52.3 ($COOCH_3$), 45.7 (NCH_2CH_2NH), 39.8 (NCH_2CH_2NH), 35.9 ($NHCOCH_2$), 34.0 ($CH_2COOPhNO_2$), 24.6 ($-CH_2CH_2-$) , 24.2 ($-CH_2CH_2-$).

Synthesis of compound 9

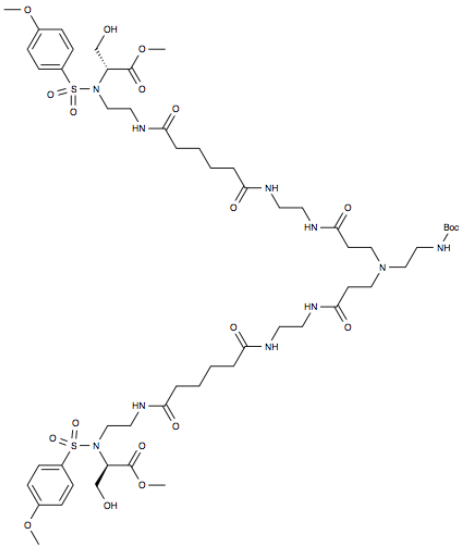

To a stirred solution of **8** (1.0 mmol, 581 mg) in dry DMF (5.0 mL), a solution of **2** (0.5 mmol, 194 mg) and NMM (2.0 mmol, 0.220 mL) in dry DMF (5 mL) was added. The mixture was stirred at rt for 2 h then concentrated to dryness. The crude product was purified by column flash chromatography on silica gel (CH_2Cl_2:MeOH 8:1 to 4:1) to give **9** (0.72 mmol, 72%). $[\alpha]_D^{25}$ +26.8 (c 0.75, $CHCl_3$); ESI-MS 648.23 $[M+H+Na]^+$, 659.33 $[M+2Na]^+$, 1273.15 $[M+H]^+$, 1295.17 $[M+Na]^+$; ^1H NMR (500 MHz, CD_3OD): □ 7.78 (AA' part of an AA'MM' system, J_{AM} = 9.0 Hz, 4H), 7.08 (MM' part of an AA'MM' system, J_{MA} = 9 Hz, 4H), 4.62 (X part of an ABX system, J_{XA} = 5.1 Hz, J_{XB} = 5.1 Hz, 2H, $CHCH_2OH$), 3.97-3.93 (m, 4H, CH_2OH), 3.89 (s, 6H, $PhOCH_3$), 3.55 (s, 6H, $COOCH_3$), 3.53-3.36 (m, 2x2H, NCH_2CH_2NH), 3.43-3.36 (m, 2x2H, NCH_2CH_2NH), 3.31 (s, 8H, $HNCH_2CH_2NH$), 3.15 (t, J = 6.5 Hz, 2H, NCH_2CH_2NHBoc), 2.78 (t, J =

6.7 Hz, 4H, HNCOCH$_2$C$\underline{H}_2$N), 2.57 (t, *J* = 6.4 Hz, 2H, NC$\underline{H}_2$CH$_2$NHBoc), 2.37 (t, *J* = 6.6 Hz, 4H, HNCOC$\underline{H}_2$CH$_2$N), 2.24-2.20 (m, 8H, OCC$\underline{H}_2$CH$_2$CH$_2$C$\underline{H}_2$CO), 1.65-1.62 (m, 8H, OCCH$_2$C$\underline{H}_2$C$\underline{H}_2$CH$_2$CO), 1.44 (s, 9H, tBu); ^{13}C NMR (125 MHz, CD$_3$OD): □ 174.7 (Cq), 174.6 (Cq), 173.9 (Cq), 170.0 (Cq), 163.4 (Cq), 156.9 (Cq), 130.9 (Cq), 129.4 (CH Ar), 113.9 (CH Ar), 62.0 (C$\underline{H}$CH$_2$OH), 60.6 (CH$\underline{C}$H$_2$OH), 54.9 (PhOCH$_3$), 52.08 (N$\underline{C}$H$_2$CH$_2$NHBoc), 51.3 (COOCH$_3$), 49.5 (HNCOCH$_2$$\underline{C}H_2$N), 44.9 (NCH$_2$$\underline{C}H_2$NH), 39.5 (N$\underline{C}H_2CH_2$NH), 38.7 (HNCH$_2CH_2$NH), 37.8 (NCH$_2$$\underline{C}H_2$NHBoc), 35.4-35.3 (OC$\underline{C}H_2CH_2CH_2$$\underline{C}H_2$CO), 33.1 (HNCO$\underline{C}H_2CH_2$N), 27.4 (tBu), 25.1-24.9 (OCCH$_2$$\underline{C}H_2$$\underline{C}H_2CH_2$CO).

Synthesis of compound 3

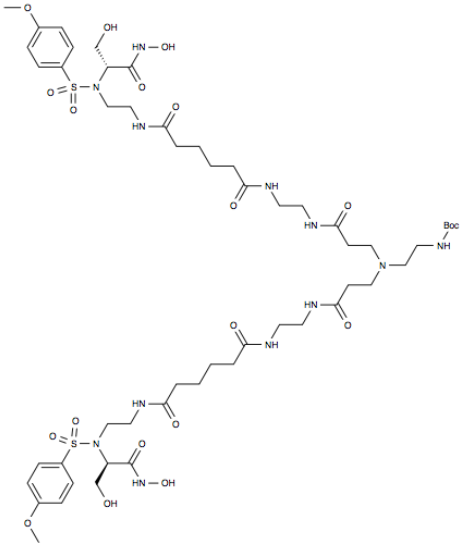

A suspension of KOH (630 mg, 11.2 mmol) in MeOH (2.3 mL) and a suspension of NH$_2$OH·HCl (670 mg, 9.64 mmol) in MeOH (4.5 mL) were separately stirred for 10' at 70°C. Then the solution of KOH was added to the solution of NH$_2$OH·HCl and the mixture was stirred at 60°C for 10'. Then **9** (50 mg, 0.04 mmol) was dissolved in 0.680 mL of the freshly obtained suspension of NH$_2$OH. The mixture was stirred at rt for 3 h then diluted with MeOH (5 mL) and the solid was filtered off. The filtrate was concentrated to dryness to give 65 mg of crude product, which was purified by HPLC (column Zorbax 300SB-C18, 9.4x250, 5 um, H$_2$O:MeOH 50:50) to give **3** (0.012 mmol, 30%) as a glassy solid. ESI-MS 649.31 [M+H+Na]$^+$, 660.53 [M+2Na]$^+$, 1275.33 [M+H]$^+$, 1297.40 [M+Na]$^+$; ^{1}H NMR (500 MHz, CD$_3$OD): □ 7.81 (AA' part of an AA'MM' system, J_{AM} = 8.8 Hz, 4H), 7.06 (MM' part of an AA'MM' system, J_{MA} = 8.8 Hz, 4H), 4.37 (at, 2H, C$\underline{H}$CH$_2$OH), 3.89 (s, 6H, PhOCH$_3$), 3.86-3.82 (m, 1x2H, CHC$\underline{H}_2$OH), 3.76-3.72 (m, 1x2H, CHC$\underline{H}_2$OH), 3.69-3.63 (m, 1x2H, NC$\underline{H}_2$CH$_2$NH), 3.60-3.39 (m, 2x2H, NCH$_2$C$\underline{H}_2$NH), 3.41-3.35 (m, 1x2H, NC$\underline{H}_2$CH$_2$NH), 3.31 (s, 8H, HNCH$_2$CH$_2$NH), 3.14 (t, *J* = 6.4 Hz, 2H, NCH$_2$C$\underline{H}_2$NHBoc), 2.77 (t, *J* = 6.2 Hz, 4H, HNCOCH$_2$C$\underline{H}_2$N), 2.55 (t, *J* = 6.2 Hz, 2H, NC$\underline{H}_2$CH$_2$NHBoc), 2.36 (t, *J* = 6.3 Hz, 4H, HNCOC$\underline{H}_2$CH$_2$N), 2.27-2.19 (m, 8H, OCC$\underline{H}_2$CH$_2$CH$_2$C$\underline{H}_2$CO), 1.68-1.60 (m, 8H, OCCH$_2$C$\underline{H}_2$C$\underline{H}_2$CH$_2$CO), 1.44 (s, 9H, tBu); ^{13}C NMR (125 MHz, CD$_3$OD): □ 174.8 (Cq), 174.6 (Cq), 173.9 (Cq), 166.9 (Cq), 163.3 (Cq), 156.9 (Cq), 130.9 (Cq), 129.3 (CH Ar), 113.9 (CH Ar), 60.0 (CH$\underline{C}$H$_2$OH), 59.4 (C$\underline{H}$CH$_2$OH), 54.8 (PhOCH$_3$), 52.1 (N$\underline{C}$H$_2$CH$_2$NHBoc), 49.5 (HNCOCH$_2$$\underline{C}H_2$N), 43.9 (N$\underline{C}H_2CH_2$NH), 39.6 (NCH$_2$$\underline{C}H_2$NH), 38.7 (HNCH$_2CH_2$NH), 37.9 (NCH$_2$$\underline{C}H_2$NHBoc), 35.4-35.3 (OC$\underline{C}H_2CH_2CH_2$$\underline{C}H_2$CO), 33.1 (HNCO$\underline{C}H_2CH_2$N), 27.4 (tBu), 25.0-24.9 (OCCH$_2$$\underline{C}H_2$$\underline{C}H_2CH_2$CO).

In vivo test

Formulation. A 157 μM solution of compound **3** (1 mg/5 ml, in NaCl 0.9 % physiological solution) was used for in vivo test. The formulation was sterilized by filtration (0.22 μm, Minisart, Sartorius SpA, Florence, Italy) and did not contain preservatives since it was used immediately after opening the vials.

SAXS Experiments

Small Angle X-ray Scattering (SAXS) experiments were carried out at the SAXS beamline of Elettra Synchrotron (Basovizza, Trieste, Italy) with the following experimental parameters: E = 8 keV, λ = 1.54 Å, sample-to-detector distance = 1.3 m, available Q-range = 0.0067 - 0.46 $Å^{-1}$. The samples were enclosed in a quartz capillary of 1 mm exact thickness, and the measurements were performed at room temperature and ambient pressure. Data collected by the 2D detector were circularly integrated using the freeware program FIT2D. Standard correction procedures were applied for sample volume, detector efficiency and background signal subtraction. Ten acquisitions (of 20 seconds each) were averaged for each sample. Data treatment and analysis were performed using Wavemetrics's software "Igor Pro" and the macros provided by the NIST.[S1]

The samples MMP_**3** and MMP_NNGH, both at the concentration of 8 mg/mL, were analysed by means of small-angle x-ray scattering (SAXS). Fig. S1 presents the SAXS spectra obtained for the two samples, after subtraction of the background (the buffer), where the scattered intensity I(Q) is plotted as a function of the scattering vector Q, defined as $4\pi\sin(\theta)/\lambda$, with 2θ the scattering angle. A first inspection of the spectra reveals a different structure at the nanoscale for the two samples.

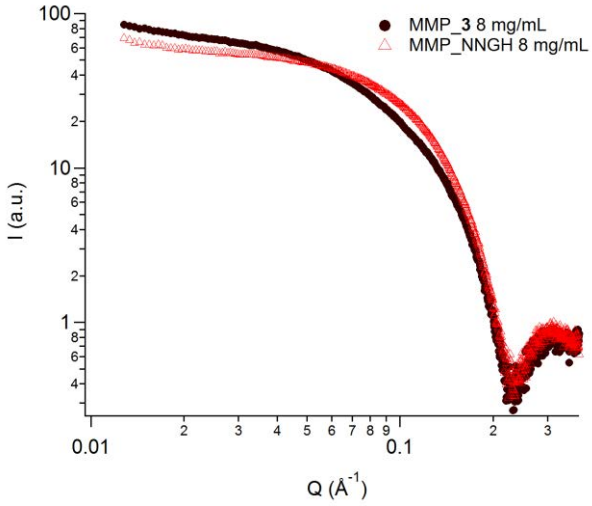

Figure S1. SAXS spectra for the samples MMP_**3** and MMP_NNGH, both at the concentration of 8 mg/mL.

The scattered intensity I(Q) can be written as:

$$I(Q) = NV^2\Delta\rho^2P(Q)S(Q) \qquad \text{Eq. A}$$

with N the number density of the scattering objects, V their volume, $\Delta\rho^2$ the contrast (difference of electron density) between scatterer and solvent. P(Q) is the intraparticle structure factor, also called Form Factor, and S(Q) the interparticle structure factor, which is assumed equal to 1 for dilute non interacting samples.

The spectra were interpreted assuming a pure form factor contribution P(Q). The fitting procedure was performed using the NIST macros for Wavemetrics Igor Pro.[S1] The fixed parameters were the

scattering length densities (SLDs) of the protein (1.23 10^{-6} Å^{-2})[S2] and the solvent (9.36 10^{-6} Å^{-2}), as well as the background level, while the other parameters were inferred from a fitting of the experimental data.

The curve for sample MMP_NNGH was easily modelled as a form factor of ellipsoids (Fig. S2), yielding 14.82 ± 0.09 Å for the two identical semi-minor axes, and 21.70 ± 0.05 Å for the semi-major axis (oblate ellipsoid of revolution). The spectrum of MMP_**3** was more adequately fitted by a form factor of cylinders with polydisperse length (Fig. S3), yielding 15.38 ± 0.04 Å for the radius and an average length 56.8 ± 0.5 Å (35% polydispersity). The results for MMP_**3** are in agreement with an object of similar shape but twice the size as in sample MMP_NNGH.

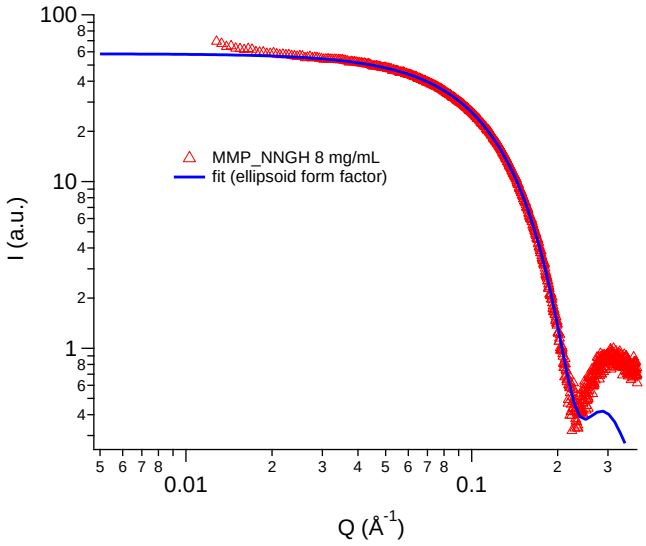

Fig. S2. Fitting of the SAXS spectrum of MMP_NNGH with a form factor of ellipsoids

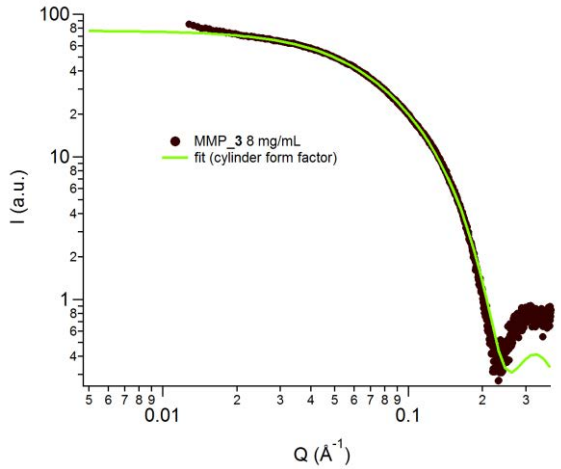

Fig. S3. Fitting of the SAXS spectrum of MMP_**3** with a form factor of cylinders

In both cases we were able to adequately fit the experimental data and estimate a radius of gyration for the two samples thanks to a Guinier linearization in the low-Q region, according to:[S3]

$$Ln[I(Q)] = Ln[I_0] - \frac{Q^2 R_g^2}{3} \qquad \text{Eq. B}$$

By plotting Ln[I(Q)] *vs.* Q^2, it was possible to extract R_g from the slope $R_g^2/3$ (Figs. S4 and S5). The radii of gyration thereby obtained were 15.2 ± 1.7 Å for MMP_NNGH and 23.8 ± 1.2 Å for MMP_**3**. In both cases, the condition $QR_g < 1$ was respected

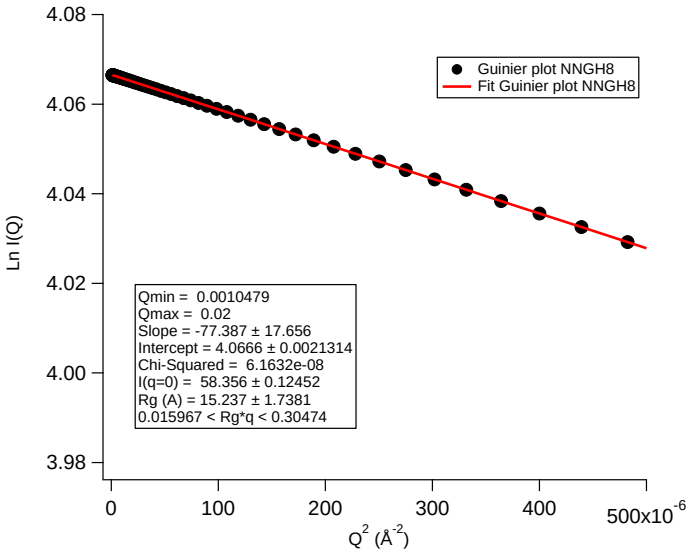

Fig. S4. Guinier plot for sample MMP_NNGH

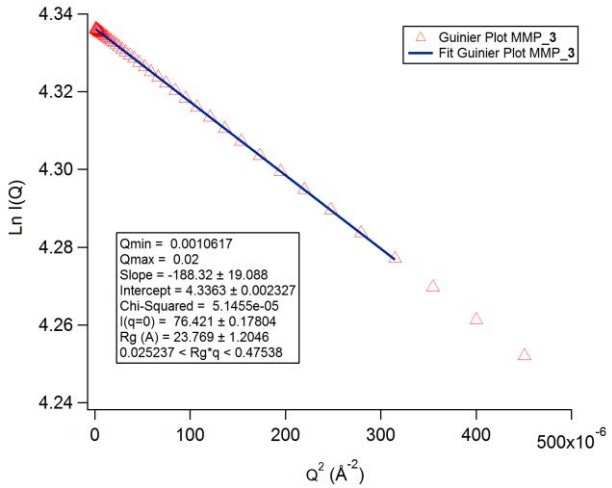

Fig. S5. Guinier plot for sample MMP_**3**

References and Notes

S1 S. R. Kline, *Journal of Applied Crystallography*, 2006, **39**, 895-900.

S2 "Misbehaving proteins. Protein (Mis)Folding, Aggregation, and Stability" Edited by Regina Murphy, Amos Tsai. Springer 2006.

S3 O. Spalla, *General theorems in small-angle scattering*. In Neutrons, X-Rays and Light: Scattering Methods Applied to Soft Condensed Matter. Lindner and Zemb, North-Holland, Elsevier edition, 2002.

Title: Biomaterial-embedded L-asparaginase removes L-asparagine from serum: a route to treat childhood leukemia

Authors: Alexandra Louka[1,2], Irina Matlahov[3], Stefano Giuntini[1,2], Linda Cerofolini[2], Andrea Cavallo[4], Enrico Ravera[2]*, Marco Fragai[1,2]*, Ayyalusamy Ramamoorthy[5,6], Gil Goobes[3], Claudio Luchinat[1,2]*

1. Department of Chemistry, University of Florence, Via della Lastruccia 3, 50019 Sesto Fiorentino, Italy

2. Magnetic Resonance Center (CERM), University of Florence and Consorzio Interuniversitario Risonanze Magnetiche di Metallo Proteine (CIRMMP), Via L. Sacconi 6, 50019 Sesto Fiorentino, Italy

3. Department of Chemistry, Bar-Ilan University, Ramat Gan 52900, Israel

4. CERTEMA, Multidisciplinary technology laboratory, S.P. del Cipressino km 10, 58044 Cinigiano, Grosseto, Italy

5. Biophysics and Department of Chemistry, University of Michigan, Ann Arbor, MI 48109-1055, USA

6. Institute for Advanced Studies, Technical University of Munich, Garching, Munich, Germany

*Corresponding Authors:
Marco Fragai, Claudio Luchinat and Enrico Ravera:

Magnetic Resonance Center (CERM) and Department of Chemistry,

University of Florence

and Consorzio Interuniversitario Risonanze Magnetiche di Metallo Proteine (CIRMMP),

Via L. Sacconi 6, 50019 Sesto Fiorentino, Italy

fax: +390554574923

Marco Fragai: fragai@cerm.unifi.it; phone: +390554574261

Claudio Luchinat: claudioluchinat@cerm.unifi.it; phone: +390554574296

Enrico Ravera: ravera@cerm.unifi.it; phone: +390554574240

ABSTRACT: Bacterial L-asparaginases injected intravenously are widely used in acute leukemia treatment, to decrease L-asparagine levels and induce cancer cells autophagy. However, the immune response against protein-based biological drugs is an important adverse reaction. This adverse effect would be prevented by avoiding the contact with the patient's immune system. We here report the design and extensive characterization of a bioinspired hydroxyapatite-L-asparaginase composite, which is able to hydrolyze L-asparagine in serum. L-Asparaginase is expressed as a chimera carrying a hydroxyapatite-promoting peptide. We expect that this new biomaterial will be a candidate for extracorporeal processing in leukemia. The chimeric gene design is easily adaptable to embed other enzymes in hydroxyapatite, with possible applications in different diseases.

Graphical Abstract:

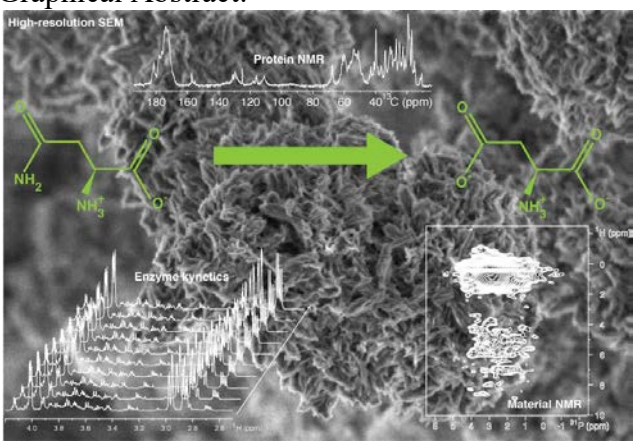

Keywords: extracorporeal therapy, solid-state NMR, biomaterials, biologics, mineral embedded enzymes

Abbreviations: NMR, Nuclear Magnetic Resonance; EM, Electron Microscopy; XRD, X-ray diffractometry; EDS, Energy dispersive X-ray spectroscopy; HA, Hydroxyapatite; HABP, Hydroxyapatite binding peptide; ALP, alkaline phosphatase; ANSII, type-II bacterial asparaginase; ALL, acute lymphoblastic leukemia

Highlights:

1. Hypothesis driven design of an inorganic-enzyme composite yields an active biomaterial for selectively remove L-asparagine in acute lymphoblastic leukemia;
2. Structural characterization at different levels allows for rationalization of the reactivity;
3. The modular design of the enzyme engineering will ease portability to other enzymes for other therapeutic applications.

1. Introduction

Biological drugs (biologics [1]) are the fastest-growing category of approved therapeutics, with most biologics being proteins.[2] One of the earliest examples of biologics are L-asparaginases, a family of proteins of bacterial origin that catalyze the hydrolysis of L-asparagine to L-aspartate. The depletion of L-asparagine in the blood circulation induces autophagy in acute lymphoblastic leukaemia (ALL) cells, which lack the L-asparagine synthetase enzyme. L-asparaginase has also been used to treat acute myeloid leukaemia (AML) in patients who cannot or do not wish to receive blood derivatives.[3,4] The most common L-asparaginases in therapy are type-II bacterial L-asparaginases (ANSII), in particular from *E. coli* and *E. chrisantemi. E.coli* ANSII is in clinical use since 1967[5] and, more recently the PEGylated form of ANSII has substituted native ANSII, because it exhibits a lower immunogenicity and prolonged *in vivo* lifetime.[6]

Different strategies have been proposed to reduce the immunogenicity of L-asparaginases. One suggested strategy, was to extract them from plantae, fungi[7] and higher vertebrates.[8] Yet, a different strategy would be to avoid contact with the immune system of the patient, rather than to try to trick it. Extracorporeal processing of blood has been proposed almost fourty years ago.[9] Because of the advancements in biomaterials research, highly biocompatible composites are now available for the preparation of new biomedical devices. In particular hydroxyapatite (HA)-based biomaterials exhibit an excellent biocompatibility and are widely used as bone substitute, in tissue engineering and for biocompatible devices.[10] They are also being considered as potential drug and vaccine carriers with tunable release times and low toxicity.[11–16]

In this manuscript, we describe the rational design of a biomaterial that embeds an L-asparaginase chimera into a hydroxyapatite support, and which is able to clear L-asparagine from serum *in vitro*. Since it is clear that enzyme-containing composites need to be studied by several techniques,[17,18] we have characterized the system by NMR spectroscopy of both the material and the enzyme and by electron microscopy.

2. Materials and methods

2.1 Construction of expression vector pET21-HABP - To endow any target enzyme with the ability of hydroxyapatite templating and binding, we have created an expression vector that hosts two copies of the W6p. W6p is an acidic analog of the amino-terminal 15-residues fragment of salivary statherin and core motif of dentin matrix protein 1, an acidic protein that can trigger CaP formation *in vitro* by binding calcium ions.[19] In order to generate pET21-HABP, the multiple cloning site of the pET21a vector between XhoI and XbaI was removed, and sequentially replaced by a) the coding nucleotides of a His6 tag, b) a TEV protease cleavage site, c) the nucleating peptide W6p

(RWRLEGTDDKEEPESQRRIGRFG) followed by a thrombin protease cleavage site, d) a multiple cloning site (containing restriction sites NdeI and BamHI), e) a second W6p nucleating peptide. The correct cDNA sequences of the expression clones were confirmed by DNA sequencing. The multiple cloning site between the thrombin protease cleavage site and the second W6p nucleating peptide permits the insertion of the gene encoding the protein of interest. Therefore, the chimeric protein can be co-expressed with one or two W6p at the amino or carboxyl-terminal. The cleavage sites permit the post-purification removal of the His6-tag using the TEV protease or the removal of the amino terminal W6p using thrombin protease.

2.2 Expression of E. coli L-Asparaginase II (ANSII) HABP- The DNA encoding the ANSII was cloned between NdeI and BamHI into the pET21-HABP vector. The ANSII was expressed as a fusion protein with an HABP peptide at the C-terminus. The His6-W6p peptide of the N-terminal domain is not present post-expression due to the removal of the protein's pro-domain during the secretion into the periplasmic space.

The gene encoding ANSII HABP in pET-21a-HABP was transformed into Escherichia coli *BL21(DE3)C41* cells which were subsequently cultured in rich (LB) medium containing ampicillin (0,1 mg/mL). Cells were grown at 310 K, until A_{600nm} reached a value of 0.6-0.8, and subsequently induced with IPTG (0.75 mM final concentration). Cells were further grown at 298 K overnight and then harvested by centrifugation at 6500 rpm (JA-10 Beckman Coulter) for 20 min at 277 K. All the purification procedures were carried out at 277 K. The pellet was resuspended in 20 mM Tris-HCl, pH 9.5, 15 mM EDTA, 20% sucrose buffer (60 mL per liter of culture) and then kept for 20 min under magnetic stirring. The suspension was centrifuged at 10000 rpm (F15-6x100y Thermo Scientific) for 30 min and the supernatant discarded. The pellet was re-suspended in H_2O Milli-Q (60 mL per liter of culture) and then kept for 20 min under magnetic stirring. The suspension was centrifuged again at 10000 rpm (F15-6x100y Thermo Scientific) for 30 min. The supernatant was treated with ammonium sulfate from 30% to 90% to precipitate the ANSII HABP protein. Then the protein was re-dissolved in minimal amount of 20 mM Tris-HCl buffer at pH 9.5 and dialyzed extensively against the same buffer. The ANSII HABP was further purified by Q-Sepharose column using 20 mM Tris-HCl buffer at pH 9.5 with a linear 0-1 M NaCl gradient. Fractions containing pure ANSII HABP were identified by Coomassie staining 13.5% SDS-PAGE gels. The ANSII was further purified by gel filtration using a Superdex 75 26/60 column in 25 mM Tris-HCl buffer at pH 7.4 and concentrated with Amicon ultrafiltration device to a final concentration of 0.4 mM. The overall yield of purified protein was 35 mg/L. The purified protein was analyzed on native PAGE gel (BioRad Mini-PROTEAN Precast Gel) to estimate the molecular mass of the protein assemblies and on a 13.5% SDS-PAGE gel to estimate the molecular mass of the monomeric protein.

2.3 Dynamic Light Scattering (MALS-QELS) — Purified protein samples were analyzed by size exclusion chromatography connected to a multiangle light scattering (MALS) equipped with QELS module (quasielastic light scattering) for R_H measurements. 100 µL samples were loaded on a Superdex 10/30 column (GE Health-care) equilibrated in 25 mM Tris-HCl buffer at pH 7.4. A constant flow rate of 0.5 mL/min was applied. Elution profiles were detected by an Optilab rEX interferometric refractometer and a Dawn EOS multiangle laser light-scattering system at 690 nm (Wyatt Technology Corp.). Data acquisition and processing were carried out using ASTRA 5.1.9.1 software (Wyatt Technology). Determination of molecular masses and hydrodynamic radii are reported as mean values ± S.D. of duplicate experiments.

2.4 Biomineralization Reaction - To assess the mineralization capabilities of the chimeric proteins co-expressed with the peptides, a mineralization model based on an alkaline phosphatase (ALP) solution was used.[20] The ALP is added to the protein solution to allow the diffusion of Ca^{2+} and the enzymatic hydrolysis of the β-glycerophosphate ions to the protein. ALP then releases the PO_4^{3-} groups, which react with the calcium ions to form HA.

The protocol for a successful biomineralization proposed by Gungormus et al.[21] requires a protein concentration of 0.4 mM in 25 mM Tris-HCl buffer at pH 7.4 supplied with 24 mM Ca^{2+} and 14.4 mM of β-glycerophosphate, with a final concentration of alkaline phosphatase at 1.4 µg/mL. The reaction mixture was then incubated at 310 K for 24 h, and finally centrifuged at 10000 rpm (Hettich Mikro 200R) for 15 min at 273 K. Then, the supernatant of the reaction was removed and the pellet was washed with MilliQ water until all free protein was removed.

2.5 Enzymatic Activity Assay – The analysis of the enzymatic activity of ANSII and ANSII HABP was performed according to the Sigma Aldrich protocol with slight modifications. The protocol comprises the following steps. A 2 mL solution containing 10 mM of L-asparagine, solubilized in 25 mM Tris-HCl buffer at pH 8.6, is incubated at 37 °C for 10 minutes. Then, an enzyme solution of known concentration or 0.5-6 mg or entrapped enzyme is added to the solution containing L-asparagine and the mixture is incubated for 30 minutes at 37 °C. The reaction is then stopped by adding trichloroacetic acid (TCA) to a final concentration of 68 mM. Then 0.2 mL of the reaction were added to 4.3 mL of deionized water and the sample was treated with 1 mL of Nessler's reagent. After 1 minute of incubation the optical density was measured at 436 nm using a UV/VIS spectrophotometer. The activity values of samples were average of three repeated measurements.

2.6 NMR experiments - Protein solid-state NMR spectra were acquired using a Bruker Avance II NMR spectrometer operating at 700 MHz ^{1}H Larmor frequency, equipped with a 3.2 mm HCN MAS probe with a λ/4 insert. Samples were packed into 3.2 mm zirconia rotors (Bruker), center packed

with a silicon insert. The 90° radio-frequency (RF) pulse widths were 2.6 μs for ^{1}H, 3.5 μs for ^{13}C and 7 μs for ^{15}N. An optimal inter scan delay was found to be 1.3 s. During ^{13}C evolution/detection SW_fTPPM[22–25] was applied to decouple protons with a 90 kHz RF field, an optimal RF power was chosen based on $^{13}C'$ T_2 measured by echo decay.[26] The sample spinning frequency was regulated to 10 kHz. Sample temperature was regulated to 255 K at the stator outlet, corresponding to 280 K in the sample, and temperature was calibrated by measuring the PEG-H_2O chemical shift difference on a different sample.[27,28] The spectrum of the PEGylated asparaginase (red, bottom trace in Figure 10) was acquired on a Bruker Avance III NMR spectrometer operating at 850 MHz ^{1}H Larmor frequency, as described in reference [29].

NMR experiments for characterization of the biomineral were carried out using a Bruker Avance III spectrometer operating at 500 MHz ^{1}H Larmor frequency, equipped with a 4 mm MAS VTN probe, and the spinning frequency was adjusted to 10 kHz. 1D ^{1}H Bloch decay and window phase-modulated-Lee-Goldburg (wPMLG)[30] experiments were carried out using ^{1}H 90° pulse of 2.55 μs. 8 scans with a recycle delay of 2 s were used in the Bloch decay measurement. In the wPMLG measurement, 6 s recycle delay and 528 repetitions were used. 1D ^{31}P cross polarization (CP) measurements by varying the contact time for polarization transfer were carried out using TPPM heteronuclear proton decoupling during acquisition.[31] Each experiment employed a 5 s recycle delay and 256 repetitions. 2D ^{1}H-^{31}P heteronuclear correlation (HETCOR) measurements employed 505 t_1 increments, CP contact times of either 500 μs or 5 ms, PMLG5 scheme[32] for ^{1}H homonuclear decoupling during t_1 and a TPPM pulse scheme for heteronuclear proton decoupling during acquisition. A recycle delay of 1 s and 128 repetitions per each t_1 point were used.

Solution NMR experiments for the evaluation of the enzymatic activity were carried out at 310 K on Bruker AVANCE NMR spectrometers equipped with triple-resonance cryoProbes and operating at the ^{1}H Larmor frequency of 700 and 900 MHz. A Carr-Purcell-Meiboom-Gill (CPMG) spin echo sequence was applied in the case of the protein in bovine serum, to suppress signals arising from high molecular weight molecules. CPMG spectra were acquired using 8 scans, 16 k data points, 14005 Hz spectral width, 584 ms acquisition time, 4 s recycle delay and 77 ms mixing time.

2.7 Electron Microscopy - Sample morphology analysis was carried out on FEI Magellan 400L high-resolution SEM instrument using accelerating voltage of 5 kV. HABP was suspended in absolute ethanol and sonicated for 10 min. About 4 μL of suspension were dropped on a piece of silicon that was adhered by a double-sided carbon tape to a special grid. The sample was left overnight for complete solvent evaporation before EM measurements. Morphology and elemental composition of samples were also investigated by FESEM (Field Emission Scanning Electron Microscope) and EDS

(Energy Dispersive Spectroscopy), using a ZEISS MERLIN - GEMINI 2 Equipped With an X-Max 50 (Oxford) EDS detector. The secondary electron micrographs were obtained at 1,7 mm of working distance (WD), at 0.7 kV of acceleration voltage (EHT) using in lens detector, whereas for chemical analysis the parameter were 8.5 mm WD and 10 kV of EHT. A special Charge Compensator allowed us to analyze the sample without any kind of preparation or coating, so the sample was directly adhered by double-sided carbon tape to the grid.

3. Results and Discussion

In its native, therapeutically active form ANSII constitutes a homotetrameric assembly of about 140 kDa with D_2 symmetry which is also described as a dimer of two intimate dimers.[33] Two active sites are present at the interface between the two monomers forming each dimeric subunit, for a total of four catalytic sites per tetramer. From the native and SDS-PAGE gels performed on the wild-type and chimeric ANSII-HABP constructs it is apparent that the protein monomers bearing HABP at the C-terminal do not associate to form fully the homotetrameric assembly, but rather a smaller assembly, that can be identified as the dimer of about 80 kDa. This qualitative finding is supported by the size-exclusion chromatography (SEC) and light scattering measurements that show a major fraction corresponding to the dimer with a shoulder corresponding to the tetramer, which increases with increasing concentration (Figure 1).

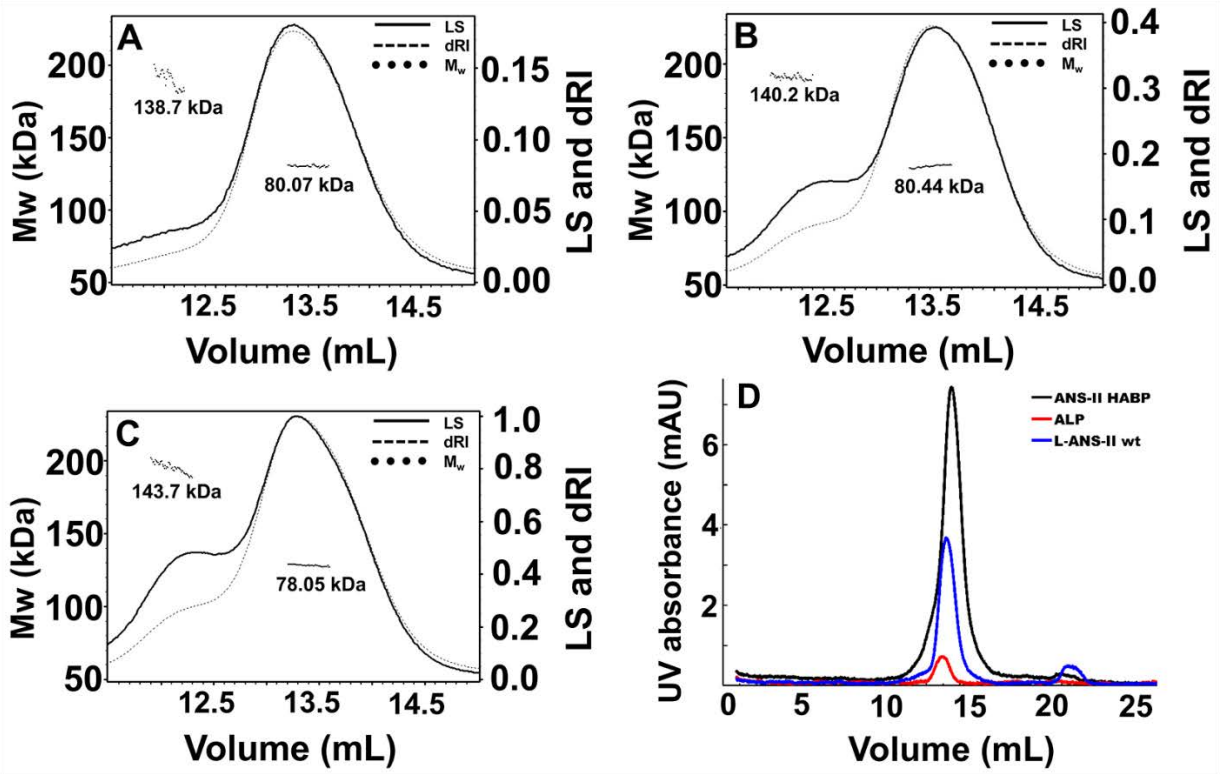

Figure 1. SEC-LS profiles, showing the simultaneous presence of the dimer and of the tetramer of ANSII-HABP.

As previously reported by others, the lack of the native quaternary structure does not abolish the catalytic activity of the enzyme,[34] however, in our system it is reduced by about a factor 4, as shown in Figure 2.

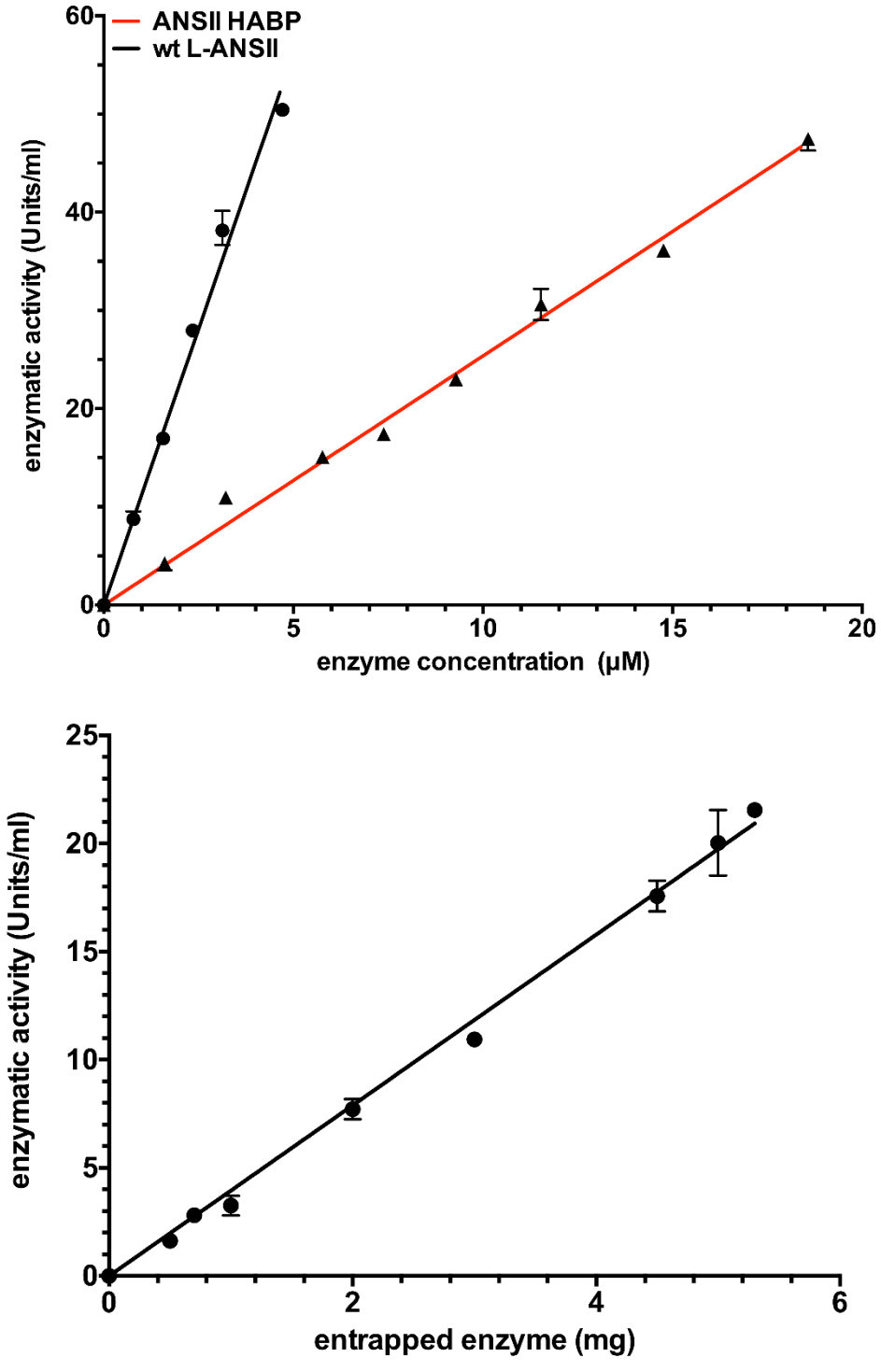

Figure 2. Concentration/activity profiles for free wt ANSII, free ANSII-HABP and HA/ANSII-HABP. For the free wt ANSII (on the top) the regression describing the activity is Y=11.25x with R^2 =0.9898, while the regression describing the activity of ANSII - HABP is Y=2.537x with R^2 =0.9926. The activity of HA/ANSII-HABP (on the bottom) is described by the following regression Y=3.947x with R^2 =0.9965

To further investigate the loss of activity, we measured the enzymatic activity by NMR, analyzed the results in the framework of the Schnell-Mendoza equation,[35,36] and compared the results with literature values for wt ANSII.[37] The kinetic measurements (Figure 3, top panel) show that the k_{cat} is sizably decreased on passing from the wt enzyme to the ANSII-HABP construct (29 ± 1 s^{-1} against 2.1 ± 0.2 s^{-1} for the wt and the mutant enzymes respectively). Conversely, the introduction of the HABP in the protein does not alter the affinity and accessibility of the active site to the substrate: K_M equals $1.3 \cdot 10^{-4}$ M^{-1} and $3.0 \cdot 10^{-5} \pm 1.0 \cdot 10^{-5}$ M^{-1} for the wt enzyme and the mutant enzyme, respectively. The decrease of k_{cat} can be explained by the loss of the quaternary structure that probably slightly alters also the structure of the dimeric subunit and affects the enzyme turnover. Actually, a factor 4 difference in K_M, combined with a factor ~14 in k_{cat}, yields a factor ~3÷4 difference in total enzyme turnover k_{cat}/K_M.

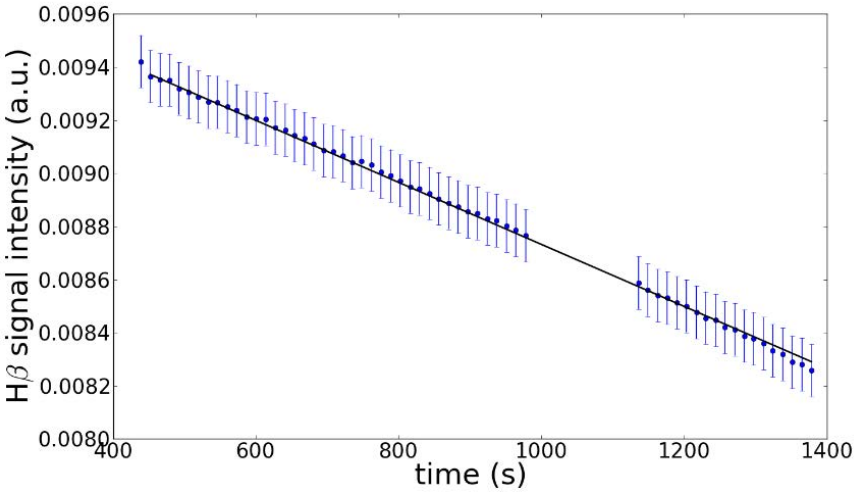

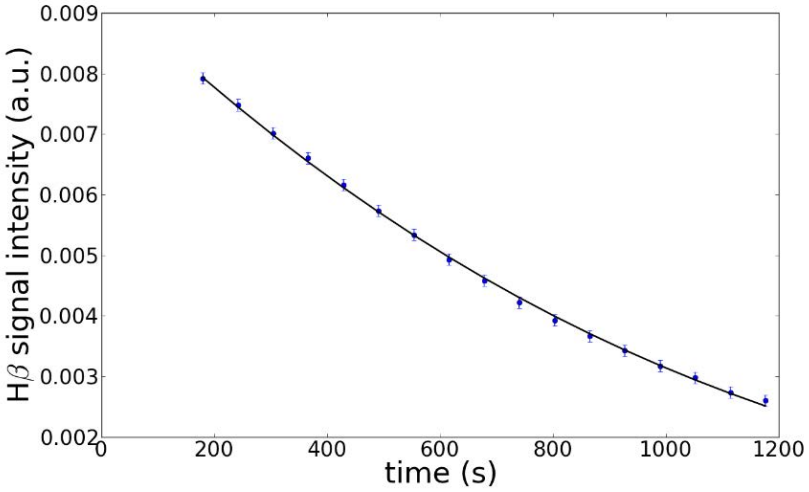

Figure 3. Kinetic measurement of free ANSII-HABP activity (top panel) and HA/ANSII-HABP composite activity (bottom panel). The decrease in the Hβ signal intensity is measured (1% error assumed), represented as blue points, and fitted (black) to the Schnell-Mendoza equation.

The enzymatic activity of the composite was assayed by NMR also in bovine serum (Figure 4), by monitoring the disappearance of the L-asparagine Hα and $H\beta_{2,3}$ signals. The measurements were performed under the conditions usually applied for NMR-based metabolomic profiling of serum,[38] upon spiking of the serum solution with 50 mM L-asparagine, and filtering out the high molecular weight components of the serum by application of a CPMG spin echo sequence. The composite is found to remain active.

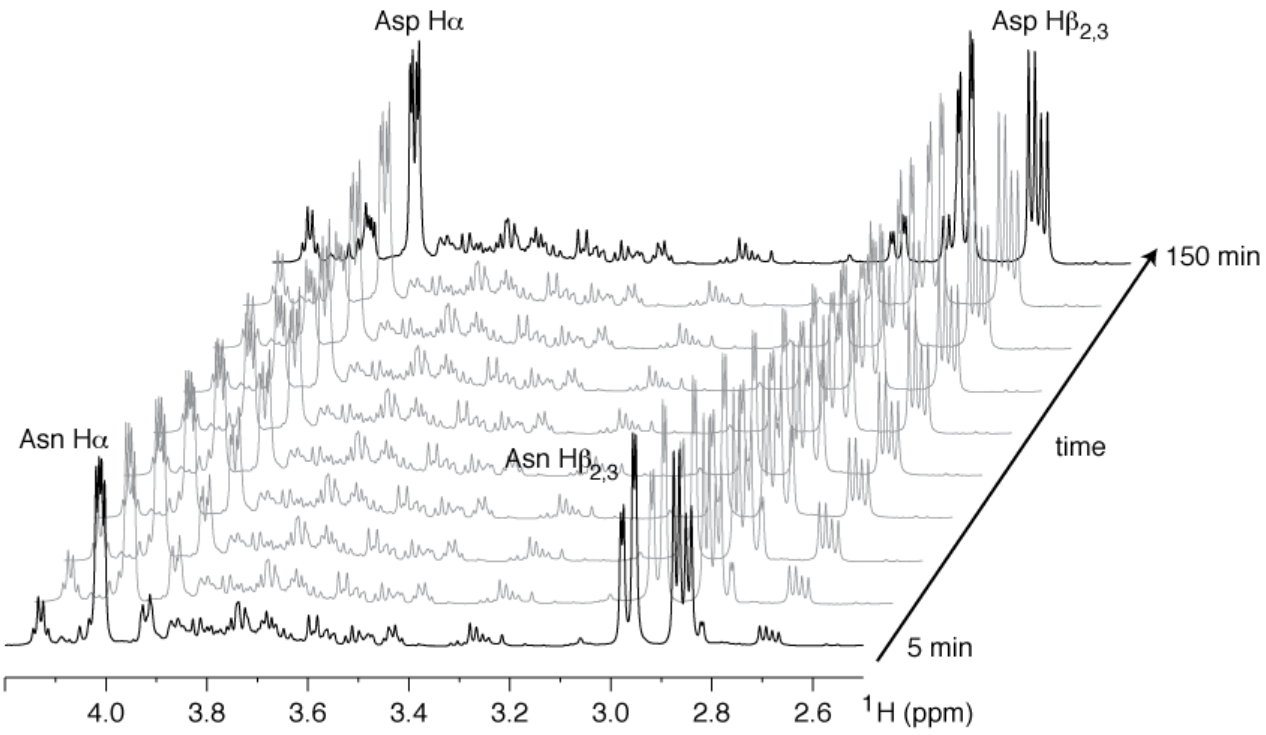

Figure 4. A portion of the CPMG-filtered ^{1}H spectrum of bovine serum, in the presence of the composite (8 mg), and upon spiking with 50 mM L-asparagine. The L-asparagine Hα and $H\beta_{2,3}$ signals, which are apparent in the initial spectrum are sizably reduced in about 2.5 h.

Even though the HABP seems to hamper the formation of the dimer of dimers, nevertheless it maintains the biomineralization activity. The biomineralization process catalyzed by ALP in the presence of β-glycerophosphate provided the biocomposite material. The material thus formed was analyzed by X-ray powder diffraction (XRD), electron microscopy and NMR measurements. The XRD (Figure 5) profile shows the typical reflections of hydroxyapatite (HA).[39] The reflections are sizably broad, in line with the small size of the crystallites formed. The reflection at low 2θ angle (~ 10°) may suggest that some octacalcium phosphate (OCP) has also formed.[40]

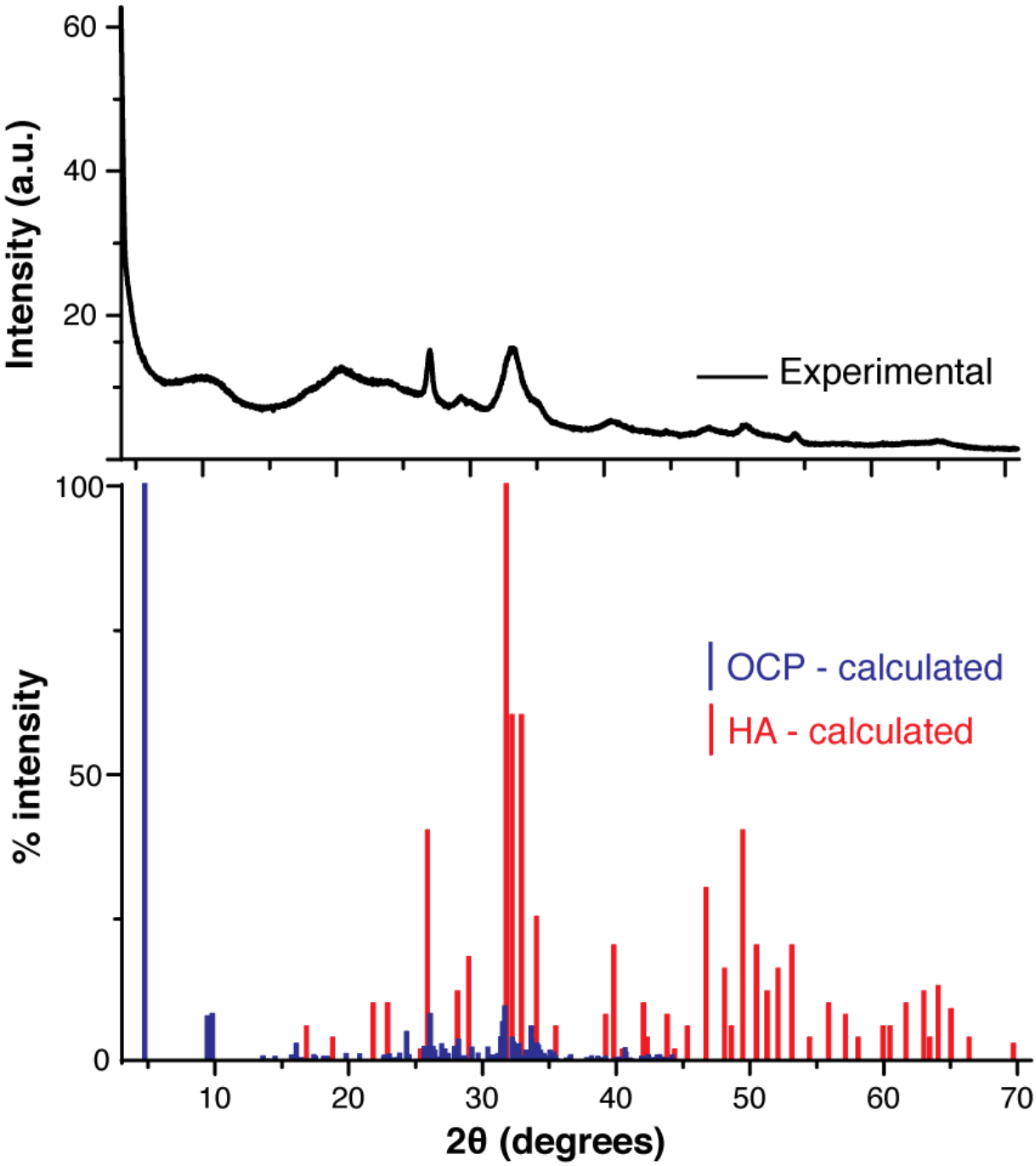

Figure 5. XRD profiles of HA/ANSII-HABP composite (black line), hydroxyapatite (red) and octacalcium phosphate (blue) stick plots.

Elemental analysis performed on the biomineralized material provided the elemental composition and a quantitative determination of the protein content, found to be of the order of 40 ± 1% in the dried material. After reacting 1 mL of mixture, and rinsing it several times, about 28 mg of wet material are obtained. Assuming that only HA will form, with a 40% w/w protein content in the material, 4 mg of composite should precipitate. If, on the contrary, only OCP is formed, about 2 mg of composite

will precipitate. Thus, in the wet material, we can estimate that 6.7% to 13% will consist of the biocomposite material. These numbers are key to the analysis of the kinetic profile of the entrapped enzyme. With these concentrations, K_M= 0.017 ± 0.002 and k_{cat}^{HA}=1.5 ± 0.2 s^{-1} or k_{cat}^{OCP}=2.9 ± 0.2 s^{-1} can be obtained. Assuming that the activity is unaffected, an enzyme weight concentration of 10% in the wet material would be obtained. In any case, the turnover rate is unaffected, whereas the affinity of the substrate is markedly reduced, as usual.[41] Interestingly, even in the worst-case scenario (i.e. assuming that the whole material is HA) the k_{cat} would be reduced to about 70% of its free enzyme value. Considering the approximations taken to obtain this number, we find it strikingly close to the 80% protein loading on the surface observed by EDS with low penetration depth (*vide infra*).

A detailed analysis of the morphology of the biomineralized material was obtained from the SEM micrographs that show fused structures that are homogeneous in shape and size (Figure 6). These structures more closely resemble hydroxyapatite nanosheets,[42] rather than octacalcium phosphate, which usually yields spherical particles.

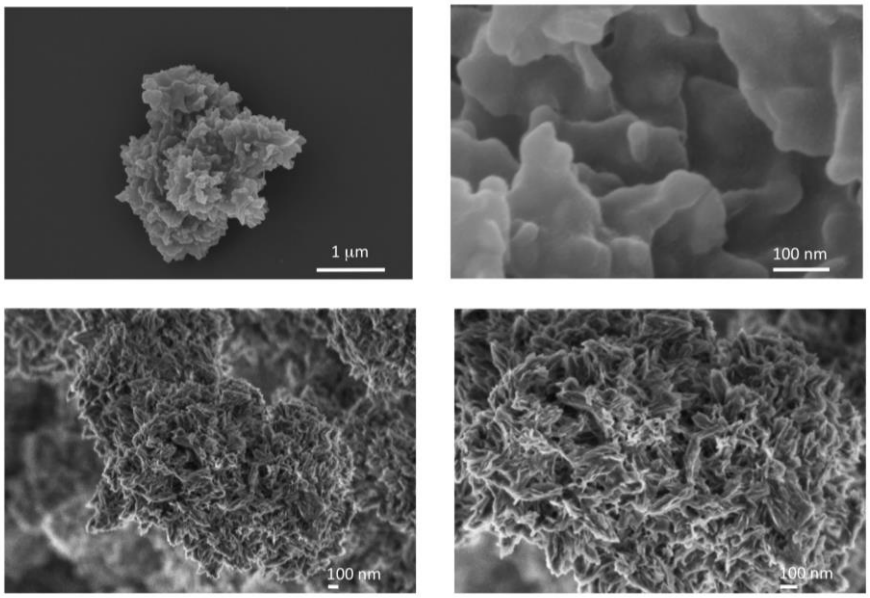

Figure 6. SEM images of the HA/ANSII-HABP composite, taken with (upper panels) and without (lower panels) conductive staining. The high protein loading at the surface (vide infra) reduces the achievable resolution.

Biomineralized samples were further characterized in terms of elemental composition, by energy dispersive X-ray spectroscopy (EDS) and Inductively coupled plasma (ICP) emission was used for elemental analysis of the total Ca and P content in the sample. The ICP measurement shows a Ca/P ratio of 1.78, a value slightly higher than the theoretical HA value of 1.67. Phosphate depletion from the mineral phase had been observed[43] for hydroxyapatite prepared synthetically in the presence of a mineral binding peptide and was attributed to the existence of a disordered phase in addition to

ordered HA phase.[43] The following NMR analysis of the phosphate species in the sample will examine their origin.

Table 1. Secondary electron emission analysis of the composite.

Element	Average wt %	Std %	average atom count	Std
C	23	3	1.9	0.2
N	10	3	0.7	0.2
Ca	26	4	0.7	0.1
P	14	2	0.44	0.06

Table 2. Summary of the elemental composition of the composite, compared with expected values.

Ratio	measured – EDS	measured - ICP	expected for HA	expected for OCP
Ca/P	1.6 ± 0.3	1.78	1.67	1.33
Ratio	measured	expected for current protein chimeric construct		
C/N	2.8 ± 0.9	3.57		
Protein %	47 ± 7			

A Bloch decay (BD), a homonuclear decoupled ^{1}H spectrum of HA/ANSII-HABP and a BD spectrum of HA are shown in Figure 7. The BD spectrum of HA/ANSII-HABP (red) shows a broad intense water resonance at 5.3 ppm, showing the appreciable water content in HA/ANSII-HABP, however as will be shown, these water molecules are not necessarily residing at the enzyme-mineral interface. The most up field line at 0.2 ppm is due to the hydroxyl protons of the mineral. Similar OH^- line is observed in the BD spectrum of HA (green) in the Figure. The peak at 1.3 ppm is associated with aliphatic side-chain protons of the protein chimera but may include some contribution from HA as can be seen by comparing to the mineral spectrum. In the homonuclear decoupled wPMLG spectrum (blue) of HA/ANSII-HABP, the water line is extensively attenuated, exposing three clear bands at 1.3 ppm, at 4.5 ppm and at 7.2 ppm from ANSII-HABP protons. These three bands are grossly associated with the protein chimera's sidechain, Hα and amide protons respectively.

Though the wPMLG experiment is intended to enhance resolution by ^{1}H-^{1}H decoupling, in this biomaterial sample we find that it improves the capability to observe the protein proton lines by

simple line suppression mechanism. Exposing the protons to a strong effective field tilted at the magic angle causes exclusive broadening of the water signal beyond detection due to coincidental matching of water motional time scale with the field's decoupling cycle period (15 μs). The motions experienced by ANSII-HABP are quite different and therefore are not affected similarly by the homonuclear decoupling. The widths of ANSII-HABP proton lines are 3-6 ppm and they result from immobile protein molecules.

The ^{31}P CP spectrum of HA/ANSII-HABP is shown in Figure 8a (blue). The peak observed is composed of two resonances at 2.6 ppm (fwhm 3 ppm) and at 2.9 ppm (fwhm 1.2 ppm) as judged by deconvolution performed using DMFIT[42]. Similar analysis using automated deconvolution to deduce the components of the phosphate line in HA by the DMFIT program was shown before[41]. The best fit was obtained using DMFIT. It uses frequency, intensity, width and Gaussian/Lorentzian ratio of each spectral line. It also reports a standard deviation value (stdev) between experimental and fitted lines in DMFIT which confirms the best fit in the minimization process. A single-line fitting resulted in a higher stdev than two-line fitting (see Figure S5). The peak at 2.9 ppm is the typical phosphate resonance in HA crystals (denoted here as pHA) and the peak at 2.6 ppm, a phosphate in a slightly shielded environment, (denoted hereafter as pS), can be associated with a shielded hydrogen phosphate ions (HPO_4^{2-}) which reside at HA/ANSII-HABP interface. This peak cannot be attributed to beta-glycerophosphate which exhibits a higher chemical shift.[45] Such mono-acid phosphates were shown to adopt a large range of chemical shifts, depending on the surroundings ions. In HA/ANSII-HABP this is reflected in the significant width of the pS peak at 7 ppm (FWHM).[46]

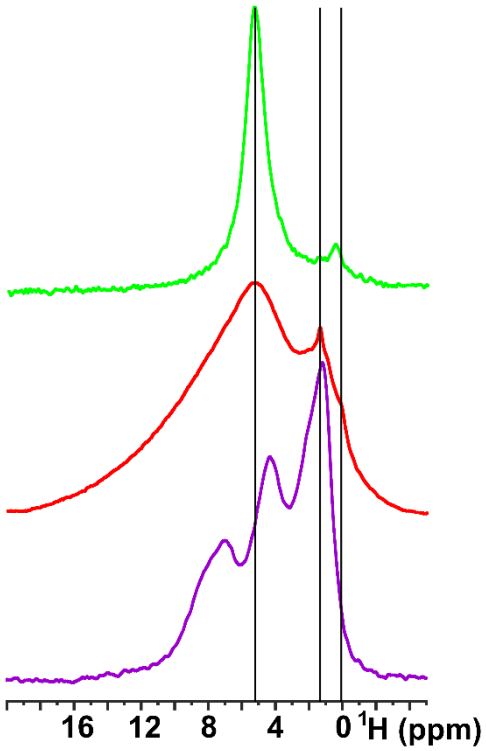

Figure 7. ^{1}H NMR spectra of ANSII-HABP acquired using wPMLG for homonuclear-decoupling (blue) and a simple 90°-acquisition (i.e. a Bloch decay) (red). ^{1}H Bloch decay spectrum (green) of synthetic hydroxyapatite prepared without calcination is also shown for comparison.

^{31}P CP measurements were carried out by varying the contact time from 100 μs to 10 ms, and the intensities of the pHA (black) and pS (red) peaks were plotted against the contact time (see Figure 8b). Recently, similar magnetization build-up curves were used to isolate magnetization transfers between interfacial protons and phosphates and bulk protons and phosphates in apatite samples prepared with a bone protein binding peptide which displays similar properties of having a crystalline phase of HA and a disordered phase containing calcium phosphate ions and the biomolecule[39]. Here, we follow a similar strategy.

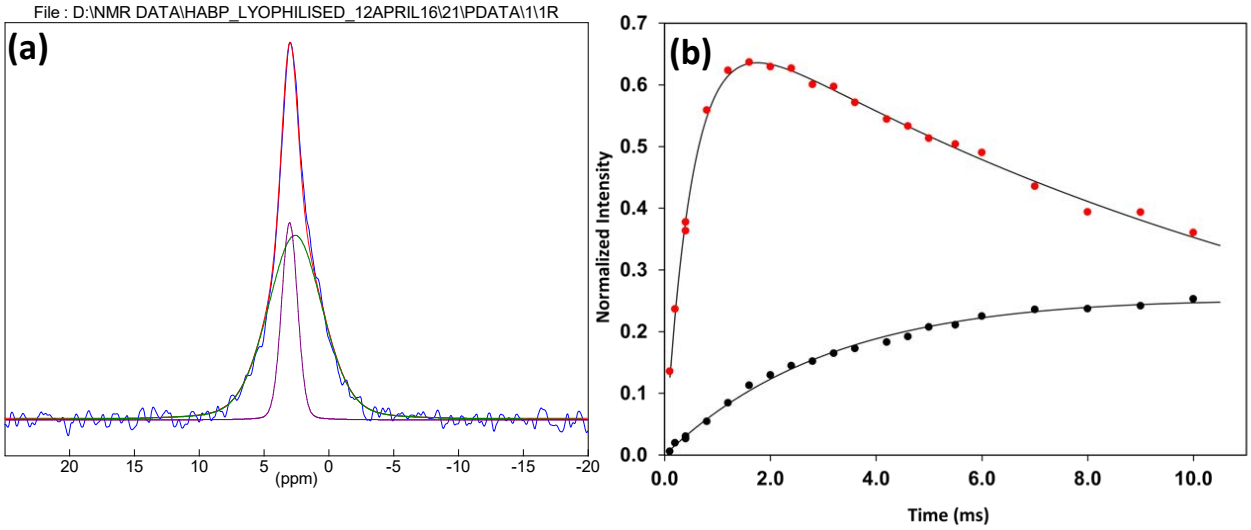

Figure 8. (a) An example of the ^{31}P CP spectrum of HA/ANSII-HABP obtained using 3.6 ms contact time deconvoluted using the DMFIT program. The experimental spectrum (blue) is shown with the sum of simulated peaks (red) and individual lines at 2.6 ppm (green) and 2.9 ppm (purple). (b) ^{31}P intensity buildup with increasing CP contact time of pHA phosphates (black) and pS phosphates (red).

These intensity buildup curves show the rate of magnetization transfer from adjacent protons to the two phosphate species. Relative line intensity in the Table 3 is derived from the fit to the experimental phosphate line, in figure 8 as follows:

The integral (integrated intensity) of experimental phosphate peak for each contact time point was calculated and the values were normalized to the highest integral to obtain the buildup normalized to 1. Each spectrum was then deconvoluted into the two phosphate contributions and the calculated area under each deconvolved peak was taken as a fraction of one. Therefore, the intensity per phosphate peak and per contact point was overall normalized to the fractional intensity of that phosphate species within each contact time spectrum and to the intensity of the highest signal in the CP buildup curve. The curve of pHA was fitted using Eq. 1 and that of pS was fitted using the extended Eq. 2 which accounts for relaxation processes which further influence transfer.

(1) $$I(t) = I_0 \times \left[1 - e^{\left(-\frac{t}{\tau_{CP}}\right)}\right]$$

(2) $$I(t) = \frac{I_0}{\left(1-\frac{\tau_{CP}}{T_{1\rho}^H}\right)} \times \left[e^{\left(-\frac{t}{T_{1\rho}^H}\right)} - e^{\left(-\frac{t}{\tau_{CP}}\right)}\right]$$

In these equations, I_o is the overall intensity of phosphate magnetization, τ_{cp} is the typical cross polarization time and $(T^H_{1\rho})$ is the longitudinal rotating frame relaxation time of the protons.
The kinetic parameters, summarized in Table 3, were deduced from best fitted curves calculated by minimizing the deviations of signal intensity I_o, the magnetization transfer time constant (τ_{cp}) and the ^{1}H rotating frame relaxation time ($T^H_{1\rho}$) in calculations and in experiments.

Table 3. Kinetic parameters of ^{31}P magnetization buildup of phosphates in HA/ANSII-HABP

Peak position (ppm)	Peak identity	Width (ppm)	τ_{cp} (ms)	$T_{1\rho}$ (ms)	Normalized area
2.9	pHA	1.4	3.1	*	0.27
2.6	pS	5.0	0.5	13.1	0.73

The relatively low normalized pHA intensity, 0.27, is indicative of the low content of crystalline HA in ANSII-HABP. This line typically has an intensity > 0.6 in other co-precipitation procedures of proteins with HA [39]. The extracted magnetization transfer time of pHA, 3.1 ms (Table 3), closely resembles the value for synthetic HA[39] (see also Figure S4 in the supporting information), and is somewhat intermediate between hydroxyl-to-phosphate transfer time in apatite crystals grown with an osteonectin binding peptide and interfacial transfer time from protons outside the crystals to crystalline phosphates in that same sample[39]. This finding suggests that either water or protein molecules are located close to the faces of the HA crystal and transfer magnetization to ordered (crystalline) phosphate ions in exposed crystal surfaces. The transfer rate of the pS line, 0.5 ms, is similar to the magnetization transfer observed for interfacial phosphates in the aforementioned apatite grown with osteonectin binding peptide.
Two-dimensional ^{1}H-^{31}P heteronuclear correlation (HETCOR) spectra in Figure 9 show magnetization transfers from individual protons along their chemical shift axis (F1) to phosphates along F2, their chemical shift axis. During the ^{1}H magnetization evolution under the chemical shift in t_1, PMLG decoupling sequence was used to suppress ^{1}H-^{1}H dipolar couplings. Figure 9 (left panel) shows an intense cross peak between HA hydroxyl protons at 0.2 ppm and phosphates at 2.9 ppm (i.e. pHA). It also shows a group of narrower cross peaks correlating ^{1}H at 1.3 ppm, 4.0-6.5 and 7.0-8.5 ppm along F1 with pS phosphates. These resonances are attributed to protein protons that transfer magnetization to proximal pS phosphates in the mineral. The homonuclear decoupling employed in t_1 effectively removed water proton excitation, and therefore no correlations are observed between water and phosphate species. This is quite different from other preparations of apatite minerals[39,44], whereby a strong correlation of water protons with phosphates in a disordered calcium phosphate

layer on HA crystallites was observed. The absence of the water resonance in the 2D HETCOR measurements is further demonstrated in the ^{1}H projections (taken along the phosphate maximal intensity) of these measurements as compared to similar measurements in synthetic HA where the relative intensity is much different (see Figure S6 in the supporting information). Similar 2D ^{1}H-^{31}P HETCOR measurements without PMLG decoupling (data not shown) did not show any water cross peaks with phosphates, so it is evident that water molecules are distantly located from phosphates. The HETCOR spectrum at the longer CP mixing time (Figure 9, right panel), shows a significantly broadened HA cross peak indicating that transfers from OH^- protons to phosphates cover now a wider distribution including pS phosphates. The protein protons, interestingly, do not show more extensive cross peak patterns and do not show clear transfers to pHA phosphates. This suggests that only pS phosphates are in close proximity to the protein and that the bulk mineral phase is in fact quite distant from the biomolecule. So, it is not unreasonable to conclude that ANSII-HABP is surrounded by a significant layer of interfacial phosphates probably of the mono-acid type and therefore has no close interactions with HA crystallites.

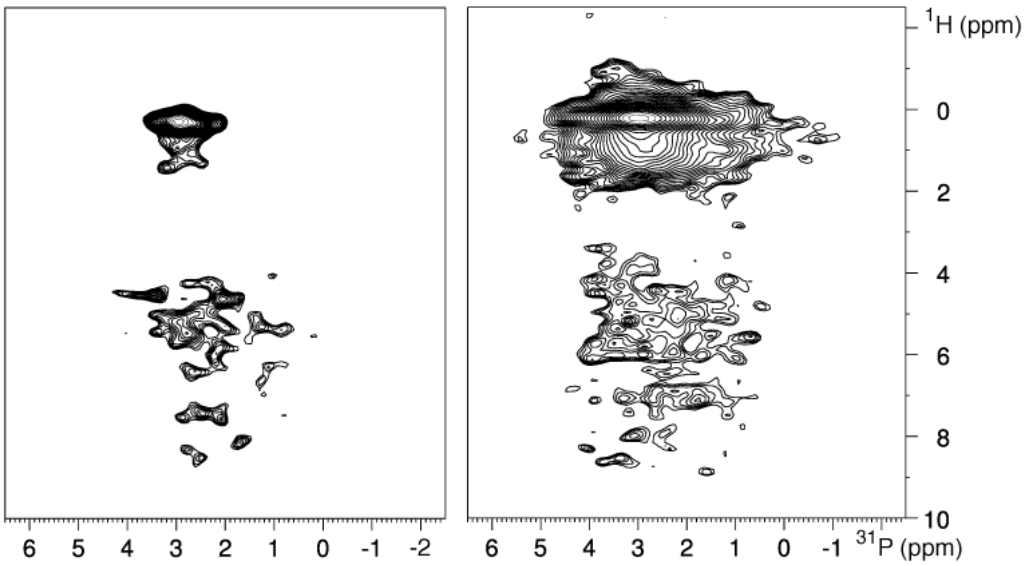

Figure 9. ^{1}H-^{31}P heteronuclear correlation (HETCOR) spectra of ANSII-HABP using contact times of 0.5 ms (left) and 5 ms (right).

Comparing the mineralization protocol employed here with other protocols,[40,43,47] the ^{31}P and ^{1}H NMR data overall suggest that hydroxyl and phosphate chemical shifts in the bulk HA crystallites precipitated with ANSII-HABP preserve the typical shift of synthetic HA. The main difference is seen in the pHA ^{31}P magnetization buildup, which is characterized by intermediate τ_{cp} (3.1 ms) that is closer to HA prepared alone rather than with proteins.[43,47] Interfacial phosphates (pS) are

slightly more shielded than the crystalline ones, exhibiting an opposite trend than observed for amorphous layer phosphates on HA, which typically resonate at 3.1-3.2 ppm.[40,47] Polarization buildup from interfacial protons to pS occurs overall at a similar rate. However, a much longer rotating frame relaxation time is observed, suggesting that polarizing protons may be experiencing different (probably faster) motions in ANSII-HABP than in the calcium phosphate layers on HA crystals. For the interfacial protons arising from the protein chimera, this may be related to their appearance as relatively sharp cross peaks in the HETCOR spectra. The $T^{H}_{1\rho}$ is similar to the relaxation time measured for carbonated HA,[48] suggesting that the factors governing this relaxation mechanism, including e.g. possible motions in the mineralized HA/ANSII-HABP phase, may be similar to the motions in the carbonated hydroxyapatite.

To obtain high-resolution structural information on the protein embedded into the biocomposite material, solid-state NMR experiments have been carried out under magic angle spinning (MAS) conditions. MAS NMR spectroscopy provides high resolution spectra for most types of non-soluble molecular aggregates including multimeric assemblies[49–52], crystalline materials of pure protein,[53,54] complex bone materials,[55] proteins embedded in silica matrix[56–60] or coated with PEG[29]. Here, the spectra of HA/ANSII-HABP have been compared with that obtained for the PEGylated wt ANSII.[29] Two different types of MAS experiments were employed to obtain ^{13}C NMR spectra of these samples. In one of the experiments, the commonly used cross-polarization[61] with ramped ^{1}H amplitude (ramp-CP[62]) pulse sequence was used to transfer the proton magnetization to ^{13}C nuclei for detection with enhanced sensitivity. In the second type of experiments, the magnetization transfer from protons to ^{13}C nuclei via both ramp-CP and nuclear Overhauser effect (NOE) were combined to enhance the sensitivity of ^{13}C detection.[63] The resulting spectra for the HA/ANSII-HABP composites are shown in black in Figure 10, and compared to the CP spectrum of the PEGylated wt ANSII from reference [29]. The HA/ANSII-HABP composite turned out to be a peculiar sample from the solid-state NMR standpoint: the first observation is that the overall spectral resolution of the CP spectrum is low (Figure 10, middle row). The second remarkable feature is that a significant share of the protein is not responsive to the dipolar-based ramp-CP experiment (Figure 10, middle row), whereas it appears in a sedimented sample of wt L-asparaginase (Figure 10, bottom row). On the other hand the ^{13}C spectra obtained via the combination of ramp-CP and NOE exhibited many additional ^{13}C peaks. Most of these additional peaks appear in the aliphatic region (0 to 75 ppm) and some peaks from aromatic side chains also appear (110 to 140 ppm). Moreover, some new peaks can be observed also in the carbonyl region (150-180 ppm). The observed peaks around 153 ppm belong to the C_Z of the L-arginine side-chains, while those around 178 ppm relate to the Cγ or

Cδ of the L-aspartate and L-asparagine or L-glutamate and L-glutamine side-chains, respectively (Figure 11). These observations suggest that the additional peaks, observed via NOE, originate from those chemical groups or amino acid residues that undergo significant motion on the milliseconds (or faster) timescale, and are therefore not detectable by the dipolar-coupling based cross-polarization (Figure 10, middle spectrum). One needs to consider the hypothesis of a substantial water-protein magnetization transfer (either through intermolecular NOE, which is prevailing at high spinning rates and low temperature, or through chemical exchange followed by spin diffusion, which is most probably dominant under the present experimental conditions [64]) at the time of the NOE mixing, plus the contribution due to direct ^{13}C excitations which is intrinsic for the pulse sequence applied.[63] Either of the two mechanisms do not detract from the idea, but rather corroborates it, that a large share of the protein is sizeably exposed to water.

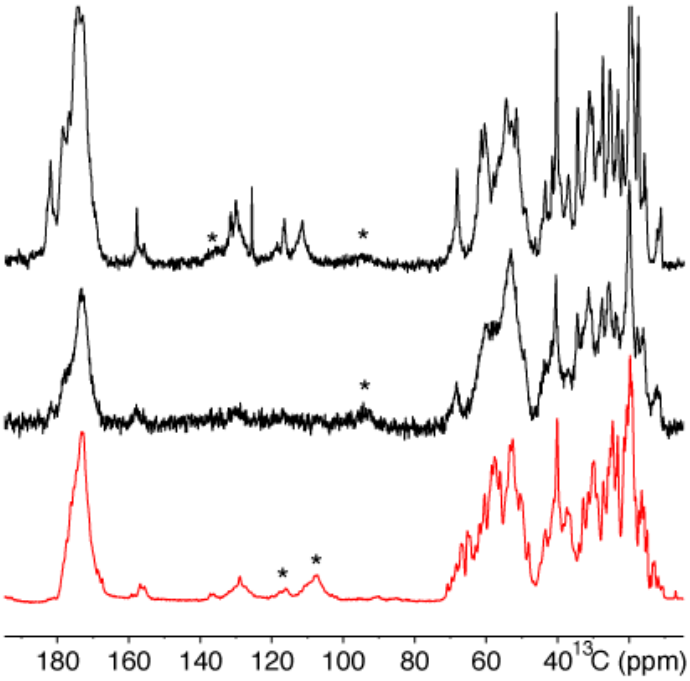

Figure 10. ^{13}C NMR spectra of HA/ANSII-HABP (black) and PEGylated wt ANSII (red) obtained under MAS using cross-polarization only (middle and bottom spectra) or cross-polarization hybridized with NOE pumping (topmost).[63] The spinning sidebands are marked as *. NOE mixing was set to 1.3 s and the CP contact time was 1.2 ms.

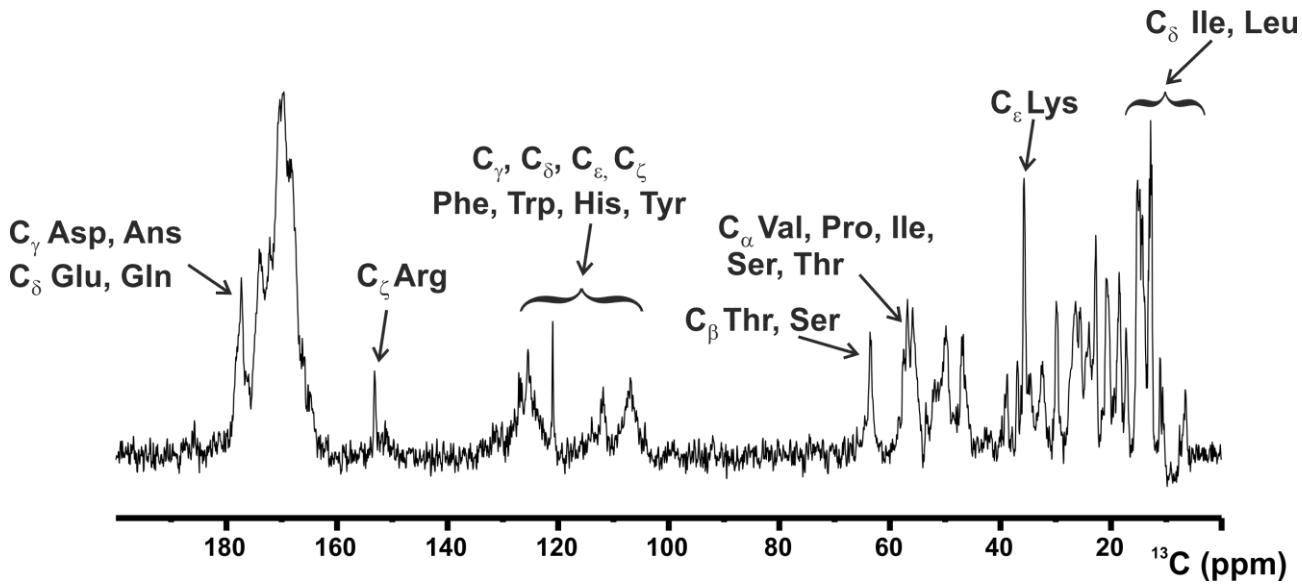

Figure 11. Difference ^{13}C NMR spectra of HA/ANSII-HABP between CPNOE experiment (Figure 10, top) and CP experiment (Figure 10, middle), showing the largest deviation between the two spectra, with the indication of the chemical shift regions for amino acid side-chains.

Therefore, the solid-state NMR results indicate that the enzyme is not completely immobile in the material, but undergoes motions on the milliseconds (or faster) time scale. This is in line with the observation that the protein is mainly sitting at the surface of the particles, rather than being entrapped into the material. Despite the preserved mobility, the observed chimeric ANSII-HABP is stably linked to the HA particles; the weakly bound protein was previously removed by multi-step washing procedure, monitored by UV spectroscopy: at the first wash, the protein concentration was 3 μM, at the second wash the protein concentration was 1 μM and no enzyme was detected at the third wash.

4. Conclusions

We have described a hypothesis-driven design of a functional biomaterial, i.e.: L-asparaginase immobilized on hydroxyapatite, with the aim of depleting L-asparaginase from biological fluids without direct contact of L-asparaginase with the immune system, with the perspective of clinical application to acute leukemias. We have demonstrated that a large array of experimental approaches based on different techniques is needed to understand the properties of this inorganic-biologic composite. NMR measurements of the protein-apatite complex have shown that the ANSII-HABP is strongly water-exposed, but at the same time experiences negligible interactions with HA crystals. The enzyme is held in the mineral phase through interactions with a disordered calcium phosphate phase that is depleted from water and does not allow for facile release of the enzyme from the mineral. We have also proven that the material is active in serum. The construction of the chimera is readily

portable to other enzymes, making the biomolecular/biomaterial engineering of general use. We also expect that the multimethodological characterization approach, which is applicable to any enzyme-mineral composite, will represent the starting point of a new protocol for biomaterials characterization.

Acknowledgements

XRD measurements (courtesy of Samuele Ciattini and Laura Chelazzi) have been taken at the CRIST of the University of Florence. Elementary analysis data were taken at the microanalysis laboratory of the University of Florence (courtesy of Stefania Pucci). Ms. Shani Hazan is acknowledged for help with the analysis and fitting of the ^{31}P CP buildup curves. SEM measurements on FEI-Magellan have been collected at the Bar-Ilan University Nanotechnology Center. Gigliola Lusvardi (Università degli Studi di Modena e Reggio Emilia) is acknowledged for fruitful discussion of the SEM and XRD data. Guido Pintacuda is acknowledged for fruitful discussion of the NOE-pumped spectra.

Funding: This work has been supported by Ente Cassa di Risparmio di Firenze, MIUR PRIN 2012SK7ASN, EC Contracts pNMR No. 317127, IDPbyNMR No. 264257, and the ESFRI Infrastructure Instruct through its Core Centre CERM, Italy. This work has been also supported by the University of Florence CERM-TT and by the "Piano di Internazionalizzazione di Ateneo" of the University of Florence. CERTEMA is supported by Regione Toscana e Provincia di Grosseto. ER holds a FIRC triennial fellowship "Guglielmina Locatello e Gino Mazzega". AR acknowledges the Hans Fischer senior fellowship from Cofund.

Author Information

Author contributions: MF, CL and ER conceived the project; MF, GG, CL, AR and ER designed the experimental work; AL and SG performed the molecular biology research; LC, GG, IM, AR and ER performed the NMR measurements; AC, GG and IM acquired the EM data; all authors analyzed the data and wrote the manuscript.

Conflict of interest: None.

References

[1] R.A. Rader, (Re)defining biopharmaceutical, Nat. Biotechnol. 26 (2008) 743–751. doi:10.1038/nbt0708-743.

[2] B. Leader, Q.J. Baca, D.E. Golan, Protein therapeutics: a summary and pharmacological classification, Nat. Rev. Drug Discov. 7 (2008) 21–39. doi:10.1038/nrd2399.

[3] J.H. Parmentier, M. Maggi, E. Tarasco, C. Scotti, V.I. Avramis, S.D. Mittelman, Glutaminase activity

determines cytotoxicity of l-asparaginases on most leukemia cell lines, Leuk. Res. 39 (2015) 757–762. doi:10.1016/j.leukres.2015.04.008.
[4] A. Emadi, N.A. Bade, B. Stevenson, Z. Singh, Minimally-Myelosuppressive Asparaginase-Containing Induction Regimen for Treatment of a Jehovah's Witness with mutant IDH1/NPM1/NRAS Acute Myeloid Leukemia, Pharmaceuticals. 9 (2016) 12. doi:10.3390/ph9010012.
[5] J.M. Hill, J. Roberts, E. Loeb, A. Khan, A. MacLellan, R.W. Hill, L-asparaginase therapy for leukemia and other malignant neoplasms. Remission in human leukemia, JAMA. 202 (1967) 882–888.
[6] M.L. Graham, Pegaspargase: a review of clinical studies, Adv. Drug Deliv. Rev. 55 (2003) 1293–1302.
[7] A. Shrivastava, A.A. Khan, M. Khurshid, M.A. Kalam, S.K. Jain, P.K. Singhal, Recent developments in l-asparaginase discovery and its potential as anticancer agent, Crit. Rev. Oncol. Hematol. (2015). doi:10.1016/j.critrevonc.2015.01.002.
[8] A.M. Schalk, H.-A. Nguyen, C. Rigouin, A. Lavie, Identification and structural analysis of an L-asparaginase enzyme from guinea pig with putative tumor cell killing properties, J. Biol. Chem. 289 (2014) 33175–33186. doi:10.1074/jbc.M114.609552.
[9] J.A. Jackson, H.R. Halvorson, J.W. Furlong, K.D. Lucast, J.D. Shore, A new extracorporeal reactor-dialyzer for enzyme therapy using immobilized L-asparaginase, J. Pharmacol. Exp. Ther. 209 (1979) 271–274.
[10] X. Wang, H.C. Schröder, M. Wiens, H. Ushijima, W.E. Müller, Bio-silica and bio-polyphosphate: applications in biomedicine (bone formation), Curr. Opin. Biotechnol. 23 (2012) 570–578. doi:10.1016/j.copbio.2012.01.018.
[11] Y. Mizushima, T. Ikoma, J. Tanaka, K. Hoshi, T. Ishihara, Y. Ogawa, A. Ueno, Injectable porous hydroxyapatite microparticles as a new carrier for protein and lipophilic drugs, J. Controlled Release. 110 (2006) 260–265. doi:10.1016/j.jconrel.2005.09.051.
[12] B. Palazzo, M. Iafisco, M. Laforgia, N. Margiotta, G. Natile, C.L. Bianchi, D. Walsh, S. Mann, N. Roveri, Biomimetic Hydroxyapatite–Drug Nanocrystals as Potential Bone Substitutes with Antitumor Drug Delivery Properties, Adv. Funct. Mater. 17 (2007) 2180–2188. doi:10.1002/adfm.200600361.
[13] G. Wang, X. Li, L. Mo, Z. Song, W. Chen, Y. Deng, H. Zhao, E. Qin, C. Qin, R. Tang, Eggshell-Inspired Biomineralization Generates Vaccines that Do Not Require Refrigeration, Angew. Chem. Int. Ed. 51 (2012) 10576–10579. doi:10.1002/anie.201206154.
[14] K. Tomoda, H. Ariizumi, T. Nakaji, K. Makino, Hydroxyapatite particles as drug carriers for proteins, Colloids Surf. B Biointerfaces. 76 (2010) 226–235. doi:10.1016/j.colsurfb.2009.10.039.
[15] C. Kojima, K. Watanabe, Adsorption and Desorption of Bioactive Proteins on Hydroxyapatite for Protein Delivery Systems, J. Drug Deliv. 2012 (2012) 1–4. doi:10.1155/2012/932461.
[16] C. Liao, J. Zhou, Replica-exchange molecular dynamics simulation of basic fibroblast growth factor adsorption on hydroxyapatite, J. Phys. Chem. B. 118 (2014) 5843–5852. doi:10.1021/jp501463r.
[17] U. Roessl, S. Leitgeb, S. Pieters, T. De Beer, B. Nidetzky, In Situ Protein Secondary Structure Determination in Ice: Raman Spectroscopy-Based Process Analytical Tool for Frozen Storage of Biopharmaceuticals, J. Pharm. Sci. 103 (2014) 2287–2295. doi:10.1002/jps.24072.
[18] J.M. Bolivar, I. Eisl, B. Nidetzky, Advanced characterization of immobilized enzymes as heterogeneous biocatalysts, Catal. Today. 259 (2016) 66–80. doi:10.1016/j.cattod.2015.05.004.
[19] G. Wang, R.-Y. Cao, R. Chen, L. Mo, J.-F. Han, X. Wang, X. Xu, T. Jiang, Y.-Q. Deng, K. Lyu, S.-Y. Zhu, E.-D. Qin, R. Tang, C.-F. Qin, Rational design of thermostable vaccines by engineered peptide-induced virus self-biomineralization under physiological conditions, Proc. Natl. Acad. Sci. 110 (2013) 7619–7624. doi:10.1073/pnas.1300233110.
[20] M.P. Ferraz, F.J. Monteiro, C.M. Manuel, Hydroxyapatite nanoparticles: A review of preparation methodologies, J. Appl. Biomater. Biomech. JABB. 2 (2004) 74–80.
[21] M. Gungormus, H. Fong, I.W. Kim, J.S. Evans, C. Tamerler, M. Sarikaya, Regulation of in vitro Calcium Phosphate Mineralization by Combinatorially Selected Hydroxyapatite-Binding Peptides, Biomacromolecules. 9 (2008) 966–973. doi:10.1021/bm701037x.
[22] R.S. Thakur, N.D. Kurur, P.K. Madhu, Swept-frequency two-pulse phase modulation for heteronuclear dipolar decoupling in solid-state NMR, Chem. Phys. Lett. 426 (2006) 459–463. doi:10.1016/j.cplett.2006.06.007.
[23] R.S. Thakur, N.D. Kurur, P.K. Madhu, An experimental study of decoupling sequences for multiple-

quantum and high-resolution MAS experiments in solid-state NMR, Magn. Reson. Chem. 46 (2008) 166–169. doi:10.1002/mrc.2153.
[24] R.S. Thakur, N.D. Kurur, P.K. Madhu, An analysis of phase-modulated heteronuclear dipolar decoupling sequences in solid-state nuclear magnetic resonance, J. Magn. Reson. 193 (2008) 77–88. doi:10.1016/j.jmr.2008.04.024.
[25] P.K. Madhu, Heteronuclear Spin Decoupling in Solid-State Nuclear Magnetic Resonance: Overview and Outlook, Isr. J. Chem. 54 (2014) 25–38. doi:10.1002/ijch.201300097.
[26] W.P. Rothwell, J.S. Waugh, Transverse relaxation of dipolar coupled spin systems under rf irradiation: Detecting motions in solids, J. Chem. Phys. 74 (1981) 2721–2732. doi:10.1063/1.441433.
[27] M. Fragai, C. Luchinat, G. Parigi, E. Ravera, Practical considerations over spectral quality in solid state NMR spectroscopy of soluble proteins, J. Biomol. NMR. 57 (2013) 155–166. doi:10.1007/s10858-013-9776-0.
[28] A. Böckmann, C. Gardiennet, R. Verel, A. Hunkeler, A. Loquet, G. Pintacuda, L. Emsley, B.H. Meier, A. Lesage, Characterization of Different Water Pools in Solid-State NMR Protein Samples, J. Biomol. NMR. 45 (2009) 319–327.
[29] E. Ravera, S. Ciambellotti, L. Cerofolini, T. Martelli, T. Kozyreva, C. Bernacchioni, S. Giuntini, M. Fragai, P. Turano, C. Luchinat, Solid-State NMR of PEGylated Proteins, Angew.Chem.Int.Ed. 55 (2016) 2446–2449. doi:10.1002/anie.201510148.
[30] E. Vinogradov, P.K. Madhu, S. Vega, Proton spectroscopy in solid state nuclear magnetic resonance with windowed phase modulated Lee–Goldburg decoupling sequences, Chem. Phys. Lett. 354 (2002) 193–202.
[31] A.E. Bennett, C.M. Rienstra, M. Auger, K.V. Lakshmi, R.G. Griffin, Heteronuclear Decoupling in Rotating Solids, J. Chem. Phys. 103 (1995) 6951–6958.
[32] E. Vinogradov, P.K. Madhu, S. Vega, A bimodal Floquet analysis of phase modulated Lee–Goldburg high resolution proton magic angle spinning NMR experiments, Chem. Phys. Lett. 329 (2000) 207–214.
[33] A.L. Swain, M. Jaskólski, D. Housset, J.K. Rao, A. Wlodawer, Crystal structure of Escherichia coli L-asparaginase, an enzyme used in cancer therapy, Proc. Natl. Acad. Sci. U. S. A. 90 (1993) 1474–1478.
[34] S. Verma, R.K. Mehta, P. Maiti, K.-H. Röhm, A. Sonawane, Improvement of stability and enzymatic activity by site-directed mutagenesis of E. coli asparaginase II, Biochim. Biophys. Acta BBA - Proteins Proteomics. 1844 (2014) 1219–1230. doi:10.1016/j.bbapap.2014.03.013.
[35] S. Schnell, C. Mendoza, Closed Form Solution for Time-dependent Enzyme Kinetics, J. Theor. Biol. 187 (1997) 207–212. doi:10.1006/jtbi.1997.0425.
[36] F. Exnowitz, B. Meyer, T. Hackl, NMR for direct determination of Km and Vmax of enzyme reactions based on the Lambert W function-analysis of progress curves, Biochim. Biophys. Acta BBA - Proteins Proteomics. 1824 (2012) 443–449. doi:10.1016/j.bbapap.2011.10.011.
[37] C. Derst, J. Henseling, K.H. Röhm, Engineering the substrate specificity of Escherichia coli asparaginase. II. Selective reduction of glutaminase activity by amino acid replacements at position 248, Protein Sci. Publ. Protein Soc. 9 (2000) 2009–2017. doi:10.1110/ps.9.10.2009.
[38] P. Bernini, I. Bertini, C. Luchinat, P. Nincheri, S. Staderini, P. Turano, Standard operating procedures for pre-analytical handling of blood and urine for metabolomic studies and biobanks, J. Biomol. NMR. 49 (2011) 231–243. doi:10.1007/s10858-011-9489-1.
[39] J.D. Hanawalt, H.W. Rinn, L.K. Frevel, Chemical Analysis by X-Ray Diffraction, Ind. Eng. Chem. Anal. Ed. 10 (1938) 457–512. doi:10.1021/ac50125a001.
[40] Y.-H. Tseng, C.-Y. Mou, J.C.C. Chan, Solid-state NMR study of the transformation of octacalcium phosphate to hydroxyapatite: a mechanistic model for central dark line formation, J. Am. Chem. Soc. 128 (2006) 6909–6918. doi:10.1021/ja060336u.
[41] L. Cao, Carrier-bound Immobilized Enzymes: Principles, Application and Design, John Wiley & Sons, 2006.
[42] X.-Y. Zhao, Y.-J. Zhu, F. Chen, B.-Q. Lu, J. Wu, Nanosheet-assembled hierarchical nanostructures of hydroxyapatite: surfactant-free microwave-hydrothermal rapid synthesis, protein/DNA adsorption and pH-controlled release, CrystEngComm. 15 (2013) 206–212. doi:10.1039/C2CE26315G.
[43] T. Iline-Vul, I. Matlahov, J. Grinblat, K. Keinan-Adamsky, G. Goobes, Changes to the Disordered Phase and Apatite Crystallite Morphology during Mineralization by an Acidic Mineral Binding Peptide from

Osteonectin, Biomacromolecules. (2015). doi:10.1021/acs.biomac.5b00465.
[44] D. Massiot, F. Fayon, M. Capron, I. King, S. Le Calvé, B. Alonso, J.-O. Durand, B. Bujoli, Z. Gan, G. Hoatson, Modelling one- and two-dimensional solid-state NMR spectra, Magn. Reson. Chem. 40 (2002) 70–76. doi:10.1002/mrc.984.
[45] L.C. Gatiboni, G. Brunetto, D. dos S. Rheinheimer, J. Kaminski, C.M. Pandolfo, M. Veiga, A.F.C. Flores, M.A.S. Lima, E. Girotto, A.C.C. Copetti, Spectroscopic quantification of soil phosphorus forms by 31p-nmr after nine years of organic or mineral fertilization, Rev. Bras. Ciênc. Solo. 37 (2013) 640–648. doi:10.1590/S0100-06832013000300010.
[46] P. Conte, D. ŠMejkalová, A. Piccolo, R. Spaccini, Evaluation of the factors affecting direct polarization solid state 31P-NMR spectroscopy of bulk soils, Eur. J. Soil Sci. 59 (2008) 584–591. doi:10.1111/j.1365-2389.2008.01043.x.
[47] I. Matlahov, T. Iline-Vul, M. Abayev, E.M.Y. Lee, M. Nadav-Tsubery, K. Keinan-Adamsky, J.J. Gray, G. Goobes, Interfacial Mineral–Peptide Properties of a Mineral Binding Peptide from Osteonectin and Bone-like Apatite, Chem. Mater. 27 (2015) 5562–5569. doi:10.1021/acs.chemmater.5b01696.
[48] A. Kaflak-Hachulska, A. Samoson, W. Kolodziejski, 1H MAS and 1→ 31P CP/MAS NMR Study of Human Bone Mineral, Calcif. Tissue Int. 73 (2003) 476–486. doi:10.1007/s00223-002-2111-5.
[49] A. Loquet, B. Habenstein, A. Lange, Structural Investigations of Molecular Machines by Solid-State NMR, Acc. Chem. Res. 46 (2013) 2070–2079. doi:10.1021/ar300320p.
[50] A. Loquet, N.G. Sgourakis, R. Gupta, K. Giller, D. Riedel, C. Goosmann, C. Griesinger, M. Kolbe, D. Baker, S. Becker, A. Lange, Atomic model of the type III secretion system needle, Nature. 486_ _ (2012) 276–279.
[51] S. Yan, C.L. Suiter, G. Hou, H. Zhang, T. Polenova, Probing Structure and Dynamics of Protein Assemblies by Magic Angle Spinning NMR Spectroscopy, Acc. Chem. Res. 46 (2013) 2047–2058. doi:10.1021/ar300309s.
[52] Y. Han, G. Hou, C.L. Suiter, J. Ahn, I.-J.L. Byeon, A.S. Lipton, S. Burton, I. Hung, P.L. Gor′kov, Z. Gan, W. Brey, D. Rice, A.M. Gronenborn, T. Polenova, Magic Angle Spinning NMR Reveals Sequence-Dependent Structural Plasticity, Dynamics, and the Spacer Peptide 1 Conformation in HIV-1 Capsid Protein Assemblies, J. Am. Chem. Soc. 135 (2013) 17793–17803. doi:10.1021/ja406907h.
[53] F. Castellani, B. van Rossum, A. Diehl, M. Schubert, K. Rehbein, H. Oschkinat, Structure of a protein determined by solid-state magic-angle-spinning NMR spectroscopy, Nature. 420 (2002) 98–102.
[54] E. Ravera, T. Schubeis, T. Martelli, M. Fragai, G. Parigi, C. Luchinat, NMR of sedimented, fibrillized, silica-entrapped and microcrystalline (metallo) proteins, J. Magn. Reson. 253 (2015) 60–70.
[55] K.H. Mroue, Y. Nishiyama, M. Kumar Pandey, B. Gong, E. McNerny, D.H. Kohn, M.D. Morris, A. Ramamoorthy, Proton-Detected Solid-State NMR Spectroscopy of Bone with Ultrafast Magic Angle Spinning, Sci. Rep. 5 (2015) 11991. doi:10.1038/srep11991.
[56] T. Martelli, E. Ravera, A. Louka, L. Cerofolini, M. Hafner, M. Fragai, C.F.W. Becker, C. Luchinat, Atomic level quality assessment of enzymes encapsulated in bio-inspired silica, Chem. - Eur. J. 4 (2016) 425–432.
[57] M. Fragai, C. Luchinat, T. Martelli, E. Ravera, I. Sagi, I. Solomonov, Y. Udi, SSNMR of biosilica-entrapped enzymes permits an easy assessment of preservation of native conformation in atomic detail, Chem. Commun. 50 (2013) 421–423. doi:10.1039/C3CC46896H.
[58] E. Ravera, L. Cerofolini, T. Martelli, A. Louka, M. Fragai, C. Luchinat, 1H-detected solid-state NMR of proteins entrapped in bioinspired silica: a new tool for biomaterials characterization, Sci. Rep. 6 (2016) 27851.
[59] E. Ravera, T. Martelli, Y. Geiger, M. Fragai, G. Goobes, C. Luchinat, Biosilica and bioinspired silica studied by solid-state NMR, Coord. Chem. Rev. (2016). doi:10.1016/j.ccr.2016.06.003.
[60] N.E. Fauré, P.J. Halling, S. Wimperis, A Solid-State NMR Study of the Immobilization of α-Chymotrypsin on Mesoporous Silica, J. Phys. Chem. C. 118 (2014) 1042–1048. doi:10.1021/jp4098414.
[61] A. Pines, M.G. Gibby, J.S. Waugh, Proton enhanced NMR of dilute spins in solids, J Chem Phys. 59 (1973) 569–590.
[62] G. Metz, X.L. Wu, S.O. Smith, Ramped-Amplitude Cross Polarization in Magic-Angle-Spinning NMR, J. Magn. Reson. A. 110 (1994) 219–227. doi:10.1006/jmra.1994.1208.
[63] R. Zhang, K.H. Mroue, A. Ramamoorthy, Hybridizing cross-polarization with NOE or refocused-INEPT

enhances the sensitivity of MAS NMR spectroscopy, J. Magn. Reson. San Diego Calif 1997. 266 (2016) 59–66. doi:10.1016/j.jmr.2016.03.006.
[64] A. Lesage, C. Gardiennet, A. Loquet, R. Verel, G. Pintacuda, L. Emsley, B.H. Meier, A. Böckmann, Polarization Transfer over the Water–Protein Interface in Solids, Angew. Chem. Int. Ed. 47 (2008) 5851–5854. doi:10.1002/anie.200801110.

SUPPORTING INFORMATION

L-ANSII HABP sequence post expression. In blue the HABP co-expressed at the C-terminus of the protein.

LPNITILATGGTIAGGGDSATKSNYTVGKVGVENLVNAVPQLKDIANVKGEQVVNIGSQDMNDNVWLTLAKKINTDCD
KTDGFVITHGTDTMEETAYFLDLTVKCDKPVVMVGAMRPSTSMSADGPFNLYNAVVTAADKASANRGVLVVMNDTV
LDGRDVTKTNTTDVATFKSVNYGPLGYIHNGKIDYQRTPARKHTSDTPFDVSKLNELPKVGIVYNYANASDLPAKALVD
AGYDGIVSAGVGNGNLYKSVFDTLATAAKTGTAVVRSSRVPTGATTQDAEVDDAKYGFVASGTLNPQKARVLLQLALT
QTKDPQQIQQIFNQYGSASLEGGMGGCGRWRLEGTDDKEEPESQRRIGRFG

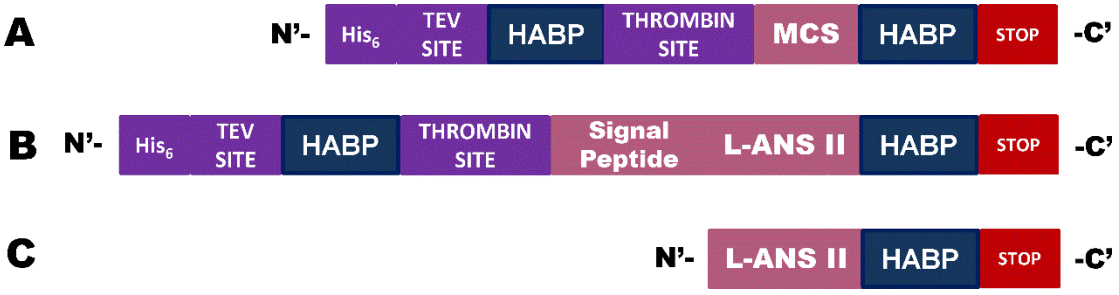

Figure S1: Schematic representation of the designed construct. A) Construction of expression vector *pET21-HABP*. MCS stands for multiple cloning site, where the gene encoding the protein of interest is cloned. B) Gene encoding L-ASNII with signal peptide targeting the protein to the periplasmic space C) L-ANSII expressed in *E.coli*.

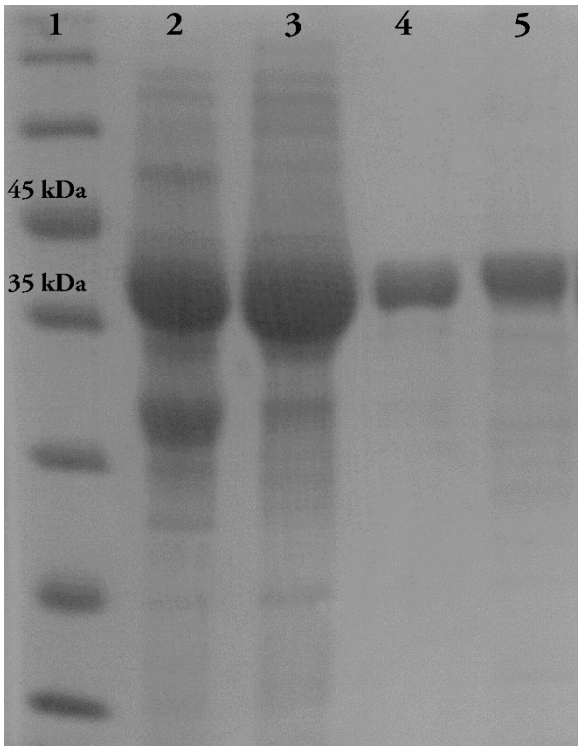

Figure S2. Coomassie-stained 13.5% SDS–PAGE showing expression, purification and immobilized ANSII HABP. Expected molecular weight 41kDa. Lane1: Low Molecular weight Marker Lane2: ANSII HABP *E.coli* crude. Lane3: ANSII HABP after 60% ammonium sulfate saturation. Lane3: ANSII HABP post purification. Lane 5: immobilized ANSII

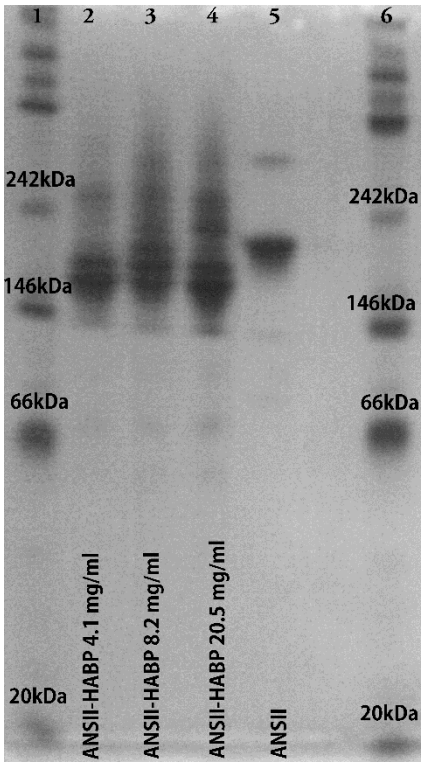

Figure S3. Native Page Gel

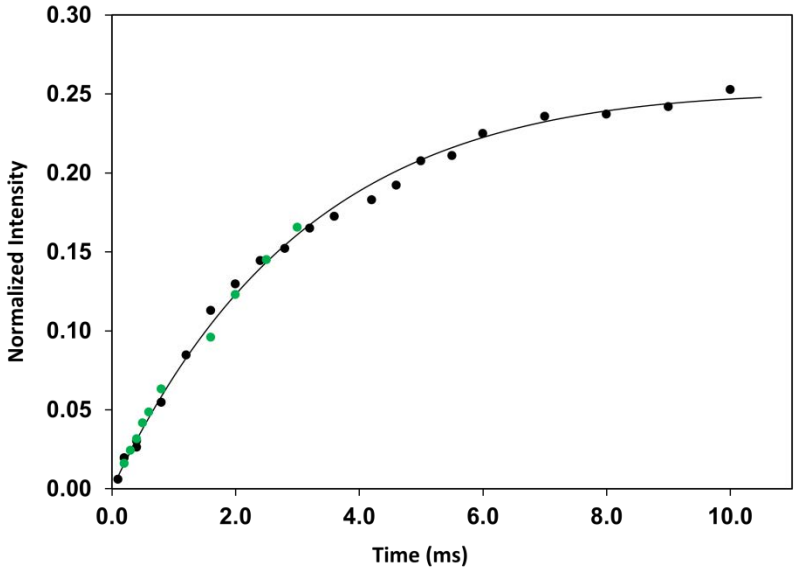

Figure S4. Similar plot as figure 10b, showing ^{31}P CP buildup curves of pHA (black) and of the HA phosphate line in hydroxyapatite prepared by titration method at 37°C (green, ref 31 in the main manuscript). It shows that the rate of magnetization buildup of pHA in ANSII-HABP is similar to that of HA suggesting that this line represents a ^{31}P nucleus experiences a similar ^{1}H environment as in previously measured crystallites.

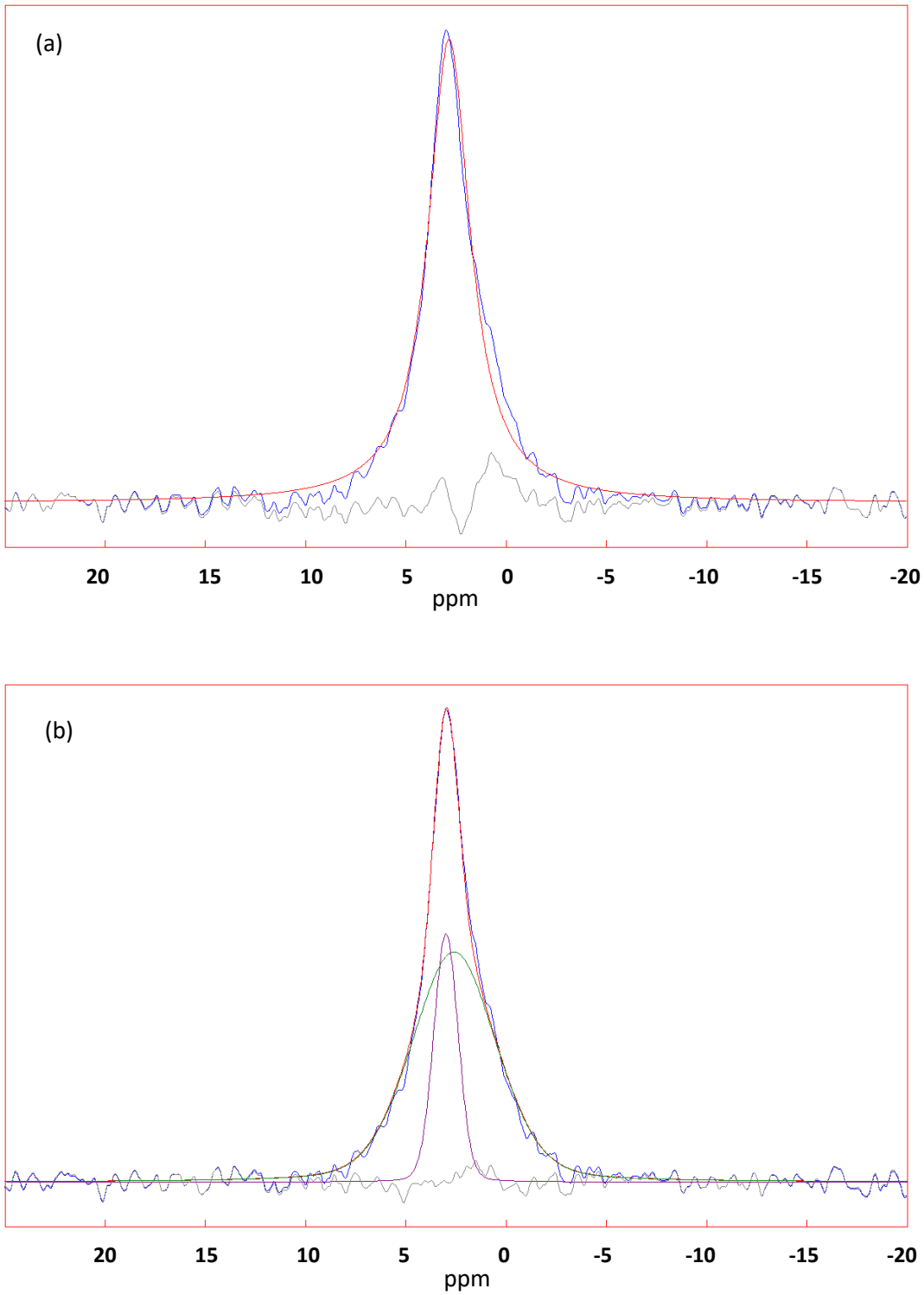

Figure S5. Automatic fitting comparison in DMFIT program. (a) A fit using single peak produced a line located at 2.85 ppm with a linewidth of 2.54 ppm and stdev of 0.46. (b) A fit using two peaks produced two lines at 2.9 and 2.6 ppm with a stdev of 0.29. The experimental spectrum is ^{31}P CP recorded with a contact time of 3.6 ms. Gray lines in both spectra represent subtraction spectra (delta) between the experimental signal (blue) and the computed signal (red).

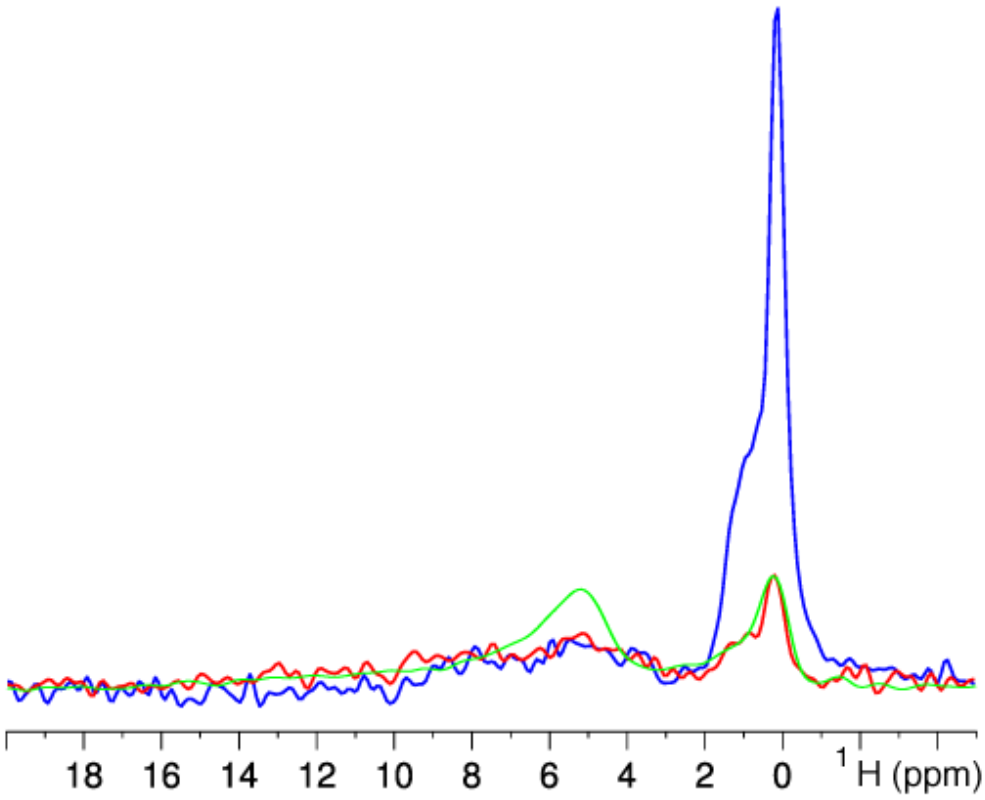

Figure S6. 1D ^{1}H projections from 2D ^{1}H-^{31}P HETCOR spectra of HABP with CP contact times of 0.5 ms (red), 5 ms (blue) and of synthetic hydroxyapatite with contact time of 0.4 ms (green) for comparison.

4. CONCLUSIONS - PERSPECTIVES

Bio-minerals are hybrid materials consisting of organic and inorganic constituents. Understanding the molecular structure of the interface between organic and inorganic constituents of bio-minerals is a main goal in biomineralization research. The interactions between organic and inorganic components are assumed to be of key importance for the formation of the remarkable structures of biominerals as well as their outstanding materials properties. In this study, I have used bio-silica and HA as solid matrices to immobilize enzymes/proteins, to synthesize hybrid biomaterials for potential medical application.

Solid-state NMR spectroscopy is very well suited to investigate biomaterials, their organic-inorganic interface, and to obtain structural information on the immobilized proteins/enzymes and on the inorganic matrices.

We have studied the encapsulation of proteins/enzymes in the biosilica matrix obtained with different external promoters, such as poly-L-Lysine and R5 peptide, and with the fusion peptide R5. Biosilicified cMMP12 obtained by using poly-L-Lysine or the fusion peptide R5, retains its catalytic activity. However, the entrapment yield for the chimeric protein co-expressed with the R5 promoter is 2-3 times higher than that obtained for wild type enzyme entrapped using the external promoter poly-L-Lysine. The high protein content inside biosilica matrix obtained with the fusion peptide R5 has provided the opportunity to characterize both the enzyme and the inorganic matrix at atomic resolution through high resolution ssNMR. The presence of the R5 peptide does not alter the structure of the protein embedded in the silica matrix, as revealed by 2D ^{13}C-^{13}C correlation spectra, since cMMP12 and cMMP12-R5 are almost completely superimposable.

^{1}H-^{15}N HSQC experiments are usually applied in solution state NMR in order to obtain information for the structure of the investigated biomolecule. Small changes in the environment around the nuclei of the studied biomolecule can result in chemical shift perturbation. We have performed ssNMR 2D ^{1}H-^{15}N HSQC in order to determine if the protein maintained its structural features after encapsulation in the biosilica matrix. Through this experiment we have observed that most of the resonances do not experience a sizable chemical shift variation after biosilification, confirming that both cMMP12-R5 and GFP-R5 preserve their structural integrity in the silica matrix. Some resonances of both proteins experience heterogeneous broadening due to static disorder caused by possible interactions with the silica matrix or due to conformational freezing of loops induced by the presence of amorphous matrix.

Furthermore, some resonances clustering close to loops or charged residues, as well as the residues of R5 peptide are missing due to heterogeneity or mobility that does not permit efficient dipolar based polarization transfer.

During this project, I have developed a new functional biomaterial containing *E.coli* L-asparaginase to remove L-asparagine from biological fluids without a direct contact of the enzyme with the immune system. The results we have obtained may open new perspective for the use of L-asparaginase-containing biomaterials to treat acute leukemias. We have also shown that an integrated approach consisting of a large array of different techniques can be applied to investigate the properties of this inorganic-biologic composite. In particular, NMR measurements on the L-asparaginase -apatite complex have shown that the ANSII-HABP is strongly water-exposed, but at the same time experiences negligible interactions with HA crystals. The enzyme is held in the mineral phase through interactions with a disordered calcium phosphate phase that is depleted from water and does not allow for facile release of the enzyme from the mineral. We have also proven that the material is active in serum. The same strategy based on the use of the fusion peptide HABP is readily portable to other enzymes, making the described biomolecular/biomaterial engineering of general use. We also expect that the multi-methodological characterization approach, which is applicable to any enzyme-mineral composite, will represent the starting point of a new protocol for biomaterials characterization.

Finally, we have designed and tested a new PAMAM based bivalent dendron inhibitor of MMPs for the treatment of dry eyes syndrome (DES). This water soluble molecule inhibits MMP9 with a nanomolar affinity, and it is able to bind simultaneously two catalytic domains of MMPs or Carbonic anhydrases at the same time. Moreover, this PAMAM inhibitor is not selective for MMP9, but has an increased residence time, a good corneal penetration in animal models, and it can be used topically. The *in vivo* effectiveness and therapeutic potential of this inhibitor have been clearly demonstrated by treating DES on rabbits, in an experimental model of DES accompanied with increased MMP9 expression.

ACKNOLEDGEMENTS

I am sincerely grateful to Professor Lucia Banci, Professor Rolf Boelens who gave me the opportunity to carry out my PHD in Structural Biology here in CERM. I am deeply grateful to Professor Claudio Luchinat for the great opportunity he gave me to work with his research group on challenging and most importantly interesting research projects. The countless scientific discussions we had were precious to me. Moreover, I would like to thank my tutor, Prof. Marco Fragai, for his guidance throughout all these challenging projects and for his brilliant ideas, but more importantly for his constant support throughout all my doctorate. I would also like to thank Dr Vito Calderone for his collaboration for the crystallography part. I would like to thank Professor Cristina Nativi for the collaboration on the MMP inhibitors projects, Professor Gil Goobes and Professor Ayyalusamy Ramamoorthy for the collaboration on the Hydroxyapatite project. I am grateful also to my postdocs Dr Enrico Ravera, Dr Linda Cerofolini and Dr Tommaso Martelli for their constant support and collaboration.

Last but not least, I would like to thank all the people in the lab of chemistry and all the cermians, the old ones and the new ones, for these wonderful three years that we worked together.

Finally, I would like to dedicate this doctorate to my family and Pantelis because they were there for me at all times, supportive and patient every step of the way.

This thesis was financially supported by:

C.I.R.M.M.P.
Consorzio Interuniversitario
Risonanze Magnetiche di
Metallo Proteine

GIOTTOBIOTECH
www.giottobiotech.com

IDPbyNMR

MARIE CURIE ACTIONS

SEVENTH FRAMEWORK PROGRAMME

REPORT OF SCIENTIFIC ACTIVITIES :

During my doctorate I have worked on the expression, purification and crystallization of the catalytic domains of MMP12 and MMP14. After successful isolation I have characterized the interaction of both enzymes with different MMPIs (i.e. bivalent PAMAM inhibitor) through fluorescent assays, X-Ray diffraction and NMR spectroscopy. Furthermore, I have designed and cloned MT1-MMP full length with the transmembrane domain (TMB) and ΔCAT MT1-MMP TMB. For both constructs I have developed protocols for expression in *E.coli* and successful purification and refolding. In order to further study these proteins through ssNMR I have used bicelles and liposomes in order to approach physiological conditions.

I have also worked on **NOD** (**N**ucleotide-binding **O**ligomerization **D**omain) proteins **1** and **2.** These proteins are intracellular, cytosolic signaling host pattern recognition receptors. They operate as microbial sensors, being involved in the recognition of specific peptidoglycan **(PG)** moieties from Gram-positive and Gram-negative bacteria. Both of them are important components of the innate immune system and are involved in the same signaling pathways. In particular, I have designed and cloned the full length NOD1 (1-953 a.a) and NOD2 (1-1040 a.a.), as well as the C-terminal domain of the two proteins, i.e. NOD1-LRR (626-953 a.a.) and NOD2-LRR (789-1040 a.a.). The C-terminal part of both proteins is pivotal for the recognition of PGs and thus is called ligand recognition domain. I have successfully expressed and purified NOD1-LRR from *E.coli* for the characterization of the interaction with PG moieties.

Moreover, I have also worked on the cloning, expression, purification of chimeric proteins for the development of hybrid biomaterials. In particular, I have cloned the catalytic domain of MMP12, Green Fluorescent Protein, L-Asparaginase II, Superoxide dismutase, Carbonic Anhydrase II in an expression vector that offers the possibility to co-express any protein with the R5 peptide fused at the C-terminal of the protein sequence. Then I expressed, purified and characterized cMMP12-R5 and GFP-R5 pre- and post- silification, as well as their wild type constructs for comparison. Moreover, I have expressed and purified Carbonic anhydrase II for structural assignment using solution state NMR and entrapped the protein in biosilica using poly-L-lysine for solid state NMR experiments.

I have also designed and created an expression vector hosting two HydroxyApatite Binding Peptides and a multiple cloning site between them that permits the cloning of any protein of interest in the expression vector. Afterwards, I cloned L- ANSII, CAII and GFP in between the two HABP peptides. I have successfully expressed, purified and characterized all three chimeric proteins. Then, I characterized the free chimeric enzymes through biophysical and biochemical methods by comparing them with the wild type enzymes. Moreover, I have developed the protocol for the biomineralization reaction in order to create the HA protein-biomineral. Finally, I studied the enzymatic activity of free ANS-HABP and immobilized ANSII HABP (HA/ANSII-HABP).

Publications

1. Atomic-Level Quality Assessment of Enzymes Encapsulated in Bioinspired Silica. Martelli T, Ravera E, Louka A, Cerofolini L, Hafner M, Fragai M, Becker CF, Luchinat C.* Chemistry. 2016 Jan 4;22(1):425-32. doi: 10.1002/chem.201503613. Epub 2015 Dec 2.
2. A Divalent PAMAM-Based Matrix Metalloproteinase/Carbonic Anhydrase Inhibitor for the Treatment of Dry Eye Syndrome. Richichi B, Baldoneschi V, Burgalassi S, Fragai M, Vullo D, Akdemir A, Dragoni E, Louka A, Mamusa M, Monti D, Berti D, Novellino E, De Rosa G, Supuran CT, Nativi C*. Chemistry. 2016 Jan 26; 22(5): 1714-21. doi: 10.1002/chem.201504355. Epub 2015 Dec 22.
3. ^{1}H-detected solid-state NMR of proteins entrapped in bioinspired silica: a new tool for biomaterials characterization. Ravera E,* Cerofolini L, Martelli T, Louka A, Fragai M, Luchinat C*. Sci Rep. 2016 Jun 9;6:27851. doi: 10.1038/srep27851.
4. Biomaterial-embedded asparaginase removes asparagine from serum: a route to treat childhood leukemia. Louka A, Matlahov I, Giuntini S, Cerofolini L, Cavallo A., Ravera E*, Fragai M*, Ramamoorthy A, Goobes G, Luchinat C* (Submitted)

Teaching report

Attended Seminars: I year: (Total credits=6,75) (34 hours)

Attended Seminars: II year: 6.5 credits (37 hours)
Internal speakers: 3.5 credits (28 hours) + own seminar: 1 credit (1 hour)
External speakers: 2.0 credits (8 hours)

Attended Seminars: III year: 7.0 credits (39 hours)
Internal speakers: 3.5 credits (28 hours) + own seminar: 1 credit (1 hour)
External speakers: 2.5 credits (10 hours)

Attended Courses: I year: (Total credits=8,5) (34 hours)

1. **Bioinformatics (2 Credits)**
2. **Drug Discovery (2 Credits)**
3. **Advanced Molecular Biology (2 Credits)**
4. **IDP: State of the art and perspectives (1,5 Credits)**
5. **Metabolomics (1 Credit)**

Attended Courses: II year: 20.5 credits

1. **X-ray spectroscopy applications on biomolecules (2 credits)**
2. **Dynamic nuclear polarization (2 credits)**
3. **Paramagnetic NMR (2 credits)**
4. **Integrated structural biology (2 credits)**
5. **Structure di biomolecole *semestral course undergraduate (6 credits)**
6. **Computational tools in structural biology (2 credits)**
7. **X-ray molecular structure determination (1.5 credits)**
8. **Case study: The influenza virus and the discovery of sialidase inhibitors (1 credit)**
9. **Solid state biological NMR (2 credits)**

Attended Courses: III year: 10.5 credits

1. **Solid state biological NMR (0.5 credits)**
2. **Improving the NMR culture (2 credits)**
3. **X-ray crystallography of proteins (2 credits)**
4. **Protein structure determination through NMR (2 credits)**
5. **Paramagnetic molecules: Relaxometry and NMR parameters (2 credits)**
6. **NMR of large molecular assemblies (2 credits)**

Attended Schools -
Attended Conferences or workshops:
I year (poster presentation)
IDP by NMR final meeting :" High resolution tools to understand the functional role of protein intrinsic disorder."**,** Riva del Sole**,** Castiglione della Pescaia, Grosseto, Italy (21-26 September 2014).

***poster presentation:** **"NOD-LRR1 and NOD-LRR2: The challenge of expression in *E. coli* ." Louka A.**, Molinaro A., Silipo A., Fragai M., Luchinat C.

II year (one poster presentation and one poster participation)
Instruct Biennial Structural Biology Meeting 2015: Convitto Della Calza, Florence, Italy, (20 - 22 May 2015).
***poster presentation:** **"Expression, purification and characterization of the full length Membrane Type 1 Matrix Metalloproteinase (MT1-MMP)." Louka A.**, Martelli T., Cerofolini L., Fragai M., Luchinat C.
"ssNMR of encapsulated and auto-encapsulated proteins." Martelli T., Ravera E., **Louka A**., Cerofolini L., Fragai M. Luchinat C.

III year (one poster presentation and two poster participations).
Chianti Workshop: Magnetic Resonance for Cellular Structural Biology, Principina Terra (Grosseto), Italy, (5-10 June 2016)
***poster presentation:** **"Enzyme immobilization through Ca/P Biomineralization" Louka A.**, Ravera E., Fragai M., Ramamoorthy A., Goobes G., Luchinat C.

“NMR for biomaterials” Ravera E., Martelli T., Cerofolini L., Michaelis V.K., Ong T. C., Keeler E.G., Giuntini S., **Louka A**., Hafner M., Goobes G., Fragai M., Becker C.F.W., Ramamoorthy A., Griffin R.G, Luchinat C.

EUROMAR 2016: Aarhus, Denmark (July 3-7 2016)
“**NMR for biomaterials (and vice versa?)”** Ravera E., Martelli T., Cerofolini L., Michaelis V.K., Ong T. C., Keeler E.G., Giuntini S., **Louka A.**, Hafner M., Goobes G., Fragai M., Becker C.F.W., Griffin R.G., Luchinat C.

Total credits: I year=15.25
Total credits: II year=27
Total credits: III year=17.5
Total credits all 3 years = 59.75